THE UNIVERSITY OF
WARWICK

University of Warwick institutional repository: http://go.warwick.ac.uk/wrap

A Thesis Submitted for the Degree of PhD at the University of Warwick

http://go.warwick.ac.uk/wrap/77250

This thesis is made available online and is protected by original copyright.

Please scroll down to view the document itself.

Please refer to the repository record for this item for information to help you to cite it. Our policy information is available from the repository home page.

Design of novel monomers for applications in hydrolytically degradable thermoplastic elastomers

Ruairí P. Brannigan

A thesis submitted in partial fulfilment

of the requirements for the degree of:

Doctor of Philosophy in Chemistry

June 2015

THE UNIVERSITY OF
WARWICK

Tá an obair seo tiomnaithe do mo mháthair agus m’athair Pat agus Ann Brannigan.

Cé go bhfuil siad imithe, riamh go bhfuil siad le dearmad.

Acknowledgements

Firstly I would like to thank my supervisor and mentor Prof. Andrew Dove for allowing me the opportunity to work within his group. Thank you for your continued belief in my ability, no matter how bleak it looked at times, without your guidance, encouragement and 'colourful' critiques, I would not be the scientist I am today. Of course I would like to thank Lubrizol for their continued funding which without none of this would have been possible.

To ALL my Dove and ROR peeps, from the sincerest place possible, thank you for making my time here truly awesome, I wouldn't have had it any other way! Special mentions to Craig, Ian, Vinh, Big Ch'Edda, Annette, Team France (Guillaume and Anne), Dafni and Becky, you're all sound and deadly craic. I would especially like to thank James Wilson (AKA Dr Chuckles), for all the laughs, boozing, science-ing and for helping me through the tough times, you aren't that bad for a veggie. Also thanks to Dan for taking the weight off me at times…. literally.

I would not be here today if it wasn't for the encouragement, love and support from my parents Pat and Ann, to whom this work is dedicated. Although they aren't here to see the results, their unwavering belief in me kept me going. I love you and you are sadly missed. I would like to thank my family, especially my big brothers Ciarán, Patrick and Anthony, for their continual love and support, even with my poor explanation as to what I was actually doing for 3 and a half years they kept the faith that at least one of us had to be smart. To Niall- howya bai?

Emma, thank you for being you! For picking me up when I was down and for being there to share the laughs and adventure. You have helped me more than you'll ever know. Cé go bhfuil an todhchaí neamhchinnte, tá a fhios agam go mbeidh tú a bheith i gcónaí ar mo thaobh, a stór mo chroí.

Table of Contents

Table of Figures

Table of Tables

Table of Schemes

List of Abbreviations

δ	Chemical shift (nuclear magnetic resonance spectroscopy)
δ	Phase angle (dynamic mechanical thermal analysis)
ΔHf	Heat of fusion
ΔHf^{θ}	Heat of fusion of 100% crystalline sample
ε	Strain
ε_{break}	Elongation at break
σ	Bending stress
%HS	Percentage hard segment
1,4-BDI	1,4-Butanediisocyanate
1,4-BDO	1,4-Butanediol
2θ	Bragg's angle
AIBN	Azobisisobutyronitrile
API	Active pharmaceutical ingrediant
APT	Attached proton test
bis-MPA	Bis(hydroxylmethyl)propionic acid
C_{3c}	Ethyl (1,3-dihydroxypropan-2-yl)carbamate
C_{3u}	1-(1,3-dihydroxypropan-2-yl)-3-ethylurea
C_{4u}	1-(1,4-dihydroxybutan-2-yl)-3-ethylurea
C_{5u}	1-(1,5-dihydroxypentan-2-yl)-3-ethylurea
CL	ε-Caprolactone
C_{Nb}	(2-(norbornene)-1,3-dioxane-5,5-diyl)dimethanol
C_{Ph}	(2-phenyl-1,3-dioxane-5,5-diyl)dimethanol

DA_{inv}	Inverse electron demand Diels-Alder
DBU	1,8-Diazabicyclo[5.4.0]undec-7-ene
DCM	Dichloromethane
DI H_2O	Deionised Water
DLA	D-Lactide
DLS	Dynamic Light scattering
$Đ_M$	Dispersity
DMF	Dimethyl formamide
DMSO	Dimethyl sulfoxide
DMTA	Dynamic mechanical thermal analysis
DP	Degree of polymerisation
DPP	Diphenyl phosphate
DRI	Differential refractive index
DSC	Differential scanning calorimetry
D_T	Diffusion at time T_e
E	Young's modulus
E'	Storage modulus
E''	Loss modulus
FT-IR	Fourier-transform infrared
GPC	Gel permeation chromatography
H_{12}MDI	4,4-Methylenebis(cyclohexyl isocyanate)
HGH	Human growth hormone
HMW	High moecular weight
iROP	"Immortal" ring opening polymerisation
LA	Lactide

LLA	L-Lactide
LMW	Low molecular weight
M_0	Initial mass
MAC	5-Methyl-5-allyloxycarbonyl-1,3-dioxan-2-one
MALDI-ToF MS	Matrix-assisted laser desorption ionisation time-of-flight mass spectrometry
MDO	2-Methylene-1,3-dioxepane
M_n	Number-averaged molecular weight
mPEG	Methoxypolyethylene glycol
MSL	Micro-stereolithography
M_t	Mass at given time
MTBD	7-Methyl-1,5,7-triazabicyclo[4.4.0]dec-5-ene
M_w	Weight-averaged molecular weight
NCA	*N*-Carboxyanhydride
NMR	Nuclear magnetic resonance
NTC	9-norbornene-2,4,8,10-tetraoxaspiro[5,5]undecan-3-one
NTD	(2-(norbornene)-1,3-dioxane-5,5-diyl)dimethanol
NVP	*N*-vinyl-2-pyrrolidone
OCA	*O*-Carboxyanhydride
PCC	Poly(9,9-dimethyl-2,4,8,10-tetraoxaspiro[5.5]undecan-3-one)
PCL	Poly(ε-caprolactone)
PDLA	Poly(D-lactide)
PDLLA	Poly(D,L-lactide)
PDMS	Poly(dimethylsiloxane)
PEG	Poly(ethylene glycol)
PEU	Poly(ester-urethane)

PGA	Poly(glycolide)
PHA	Polyhydroxyalkanoates
PHB	Poly(hydroxybutyrate)
PHBV	Poly(hydroxybutyrate-co-valerate)
PLA	Poly(lactide)
PLGA	Poly(lactide-co-glycolide)
PLLA	Poly(L-lactide)
PMAC	Poly(5-Methyl-5-allyloxycarbonyl-1,3-dioxan-2-one)
PMMA	Poly(methyl methacrylate)
PNTC	Poly(9-norbornene-2,4,8,10-tetraoxaspiro[5,5]undecan-3-one)
PPTO	Poly(9-phenyl-2,4,8,10-tetraoxaspiro[5,5]undecan-3-one)
PS	Poly(styrene)
PTD	(2-phenyl-1,3-dioxane-5,5-diyl)dimethanol
PTMC	Poly(trimethylene carbonate)
PTO	9-Phenyl-2,4,8,10-tetraoxaspiro[5,5]undecan-3-one
PTSA	Para-toluenesulfonic acid
PU	Poluyurethane
PVL	Poly(δ-valerolactone)
R	Ratio of diisocyanate to polyol
R^2	Coefficient of determination
rac-LA	Racemic lactide
rac-PLA	Poly(*rac*-lactide)
RAFT	Radical addition-fragmentation transfer
ROP	Ring opening polymerisation
SFF	Solid free-form fabrication

SL	Stereolithography
SLS	Static light scattering
TBD	1,5,7-Triazabicyclo[4.4.0]dec-5-ene
T_c	Crystallisation temperature
T_e	Time taken to hydrolyse surface polymer chains
TEM	Transmission electron microscopy
T_g	Glass transition temperature
THF	Tetrahydrofuran
TIPS	Thermally-induced phase separation
T_m	Melting transition temperature
TMC	Trimethylene carbonate
TPE	Thermoplastic plastic elastomer
TPEU	Thermoplastic poly(ester-urethane)
TPEUU	Thermoplastic poly(ester-urethane-urea)
TPU	Thermoplastic polyurethane
TU	1-(3,5-Bis(trifluoromethyl)phenyl)-3-cyclohexylthiourea
UTS	Ultimate tensile strength
UV	Ultraviolet
VL	δ-Valerolactone
WAXD	Wide angle x-ray diffraction
W_S	Width of sample
X_c	Percentage crystallinity

Publications

Block Copolymer Materials from the Organocatalytic Ring-Opening Polymerization of a Pentaerythritol-Derived Cyclic Carbonate, R. P. Brannigan, A. Walder, A. P. Dove, *J. Polym. Sci. A. Polym. Chem.*, 2014, **52**, 2279-2286.

(**Chapter 3**)

Declaration of authorship

Experimental work contained within this thesis is original research carried out by the author, unless otherwise stated, in the Department of Chemistry at the University of Warwick, between October 2011 and June 2015. No material contained herein has been submitted for any other degree, or at any other institution.

Analysis conducted by other authors are detailed as followed; elemental analysis (Chapter 2) conducted by Warwick Analytical Services, multi-angle light scattering analysis (Chapter 2) conducted by Dr Daniel Wright, MALDI-ToF analysis (Chapter 2) conducted by Dr Dafni Moatsou, wide angle x-ray diffraction analysis (Chapters 3 and 4) conducted by Cathrin Kirchhoefer.

Signed: _____ Date: _____

Ruairí Brannigan

Abstract

This thesis explores the synthesis of novel monomers in the design of hydrolytically degradable materials with defined physical and chemical properties using a selection of coupling and polymerisation techniques. Chapter 1 introduces the concept of hydrolytically degradable polymers, namely polyesters, and exhibits the dynamic range of biomedical applications in which they might be utilised.

In Chapter 2, the organocatalysed ROP of a previously synthesised spirocyclic carbonate monomer bearing pendant benzyl-acetal functionality (PTO) and a novel spirocyclic carbonate monomer bearing pendant norbornene-acetal functionality (NTC) are described. The successful post-polymerisation modification of the norbornene functionality is demonstrated utilising a variety of addition reactions; the 1,3-dipolar cycloaddition of azides, inverse electron demand Diels-Alder reaction with tetrazines and the radical thiol-ene addition. Furthermore, the synthesis, self-assembly and pH-triggered degradation of graft copolymers, prepared by the thiol-ene addition of a thiol-terminated hydrophilic polymer to the hydrophobic polycarbonate backbone, is also described.

Chapter 3 describes the synthesis of A-B-A triblock copolyester-carbonates *via* the ROP of PTO (described in Chapter 2) initiated from an α,ω-dihydroxy poly(caprolactone) (PCL) macroinitiator, with varying molecular weights, yielding thermoplastic materials with superior tensile properties (elongation and Young's modulus) to that of the PCL homopolymer. Furthermore, the alteration of PCLs thermal and degradation properties, as a consequence of the chain extension PTO, was also described.

In Chapter 4, the utilisation of the diol precursors to PTO and NTC (described in Chapter 2) as chain extenders for the organocatalysed synthesis of novel PCL-based thermoplastic polyester-urethanes (TPEUs) is reported. The successful post-polymerisation modification of the norbornene functionality is demonstrated utilising addition reactions optimised from Chapter 2. Furthermore, the mechanical, surface hydrophilicity and degradation properties of the TPEUs, before and after modification, are also described.

Chapter 5 describes the synthesis of novel diol chain extenders derived from natural amino acids, modified with carbamate and urea pendant groups, and their utilisation in the organocatalysed synthesis of novel PCL-based TPEUs. The modulation of physical and degradation properties by varying polymer composition and extender type were also described.

Chapter 6 provides a summary of the key findings of Chapters 2 – 5 and Chapter 7 provides the experimental methods of this thesis.

1 Introduction

1.1 Introduction to biomaterials and degradable polymers

Arguably, the most rapidly evolving area in materials science in the past century has been the development of biodegradable polymers for medical applications.[1,2] A wide range of naturally occurring polymeric materials have been employed as biomaterials such as proteins (collagen[3], elastin[4], silk fibroin[5]), calcium phosphates[6] (hydroxyapatite[7]), polysaccharides (chitosan[8], hyaluronate[9]), polyhydroxyalkanoates[10] (PHAs) (poly(hydroxybutyrate)[11] (PHB), poly(hydroxybutyrate-*co*-valerate)[12] (PHBV)) *etc*. Although the utilisation of natural polymers offers advantages, such as proteolytic degradation and enhanced cell viability, the range of applications and criteria for which biomaterials are required has become too vast for natural polymers to endure (*e.g.* controlled/sustained pharmaceutical delivery in varying environments, degradable textiles, wound dressings, site-specific regenerative medicine/tissue engineering *etc.*).[13,14]

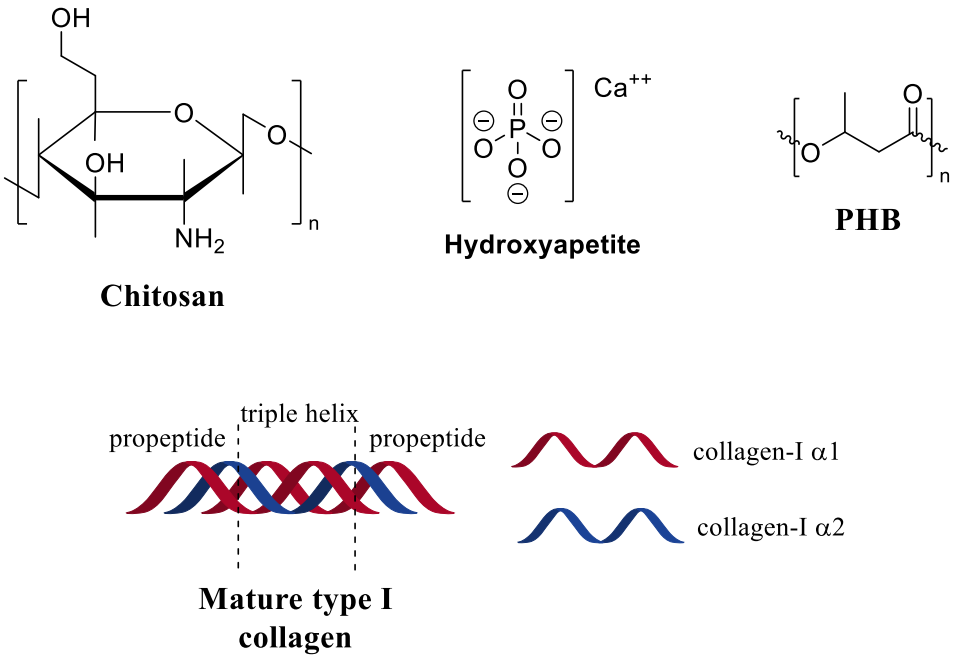

Figure 1.1 Naturally occurring polymeric materials used as biomaterials.

The development of novel synthetic materials, which undergo bio-degradation, have been at the forefront of biomaterials research as a consequence of the issues surrounding common 'biostable' materials *e.g.* long-term incompatibility and invasive revision surgeries.[15,16] Furthermore, synthetic biomaterials not only allow for the development of modulus-matched polymeric materials with 'site-specific' degradation profiles, they negate certain disadvantages found with their natural counterparts such as immunogenic responses, difficult purification and processability.[17]

In general terms, there are 4 prolific mechanisms of biomaterial degradation; hydrolytic degradation (scission of susceptible bonds by water), enzymatic degradation (enzyme catalysed scission of bonds), oxidative degradation (radical attack supported by peroxide producing inflammatory reactions) and physical degradation (*i.e.* mechanical loading and wear, swelling-deswelling *etc*.). Natural polymeric materials tend to be highly susceptible to enzymatic and oxidative degradation, and as a consequence of varying enzymatic and macrophage levels from patient-to-patient, uniform degradation profiles may be unachievable. Conversely, the uniformity of degradation and thermo-mechanical properties achieved with synthetic biodegradable biomaterials, which generally undergo hydrolytical degradation, is unprecedented.[18-20]

1.2 Hydrolytic degradation

Hydrolysis is defined as the reaction of water with susceptible bonds of a compound to form two or more products.[21] When discussing bulk polymer degradation there are several factors determining the rate of hydrolysis-induced mass loss of a material; susceptibility of bonds and reactivity of hydrolysable bonds, diffusion rates of hydrolysis-contributing chemicals (*i.e.* water, ions, degradation products/small polymer

chains *etc*.) and thermodynamics of polymer-water interactions. In order to define the rate of hydrolysis of polymer bonds, polymer solutions have been employed to negate the effects of polymer-water interactions and diffusion rates.[22]

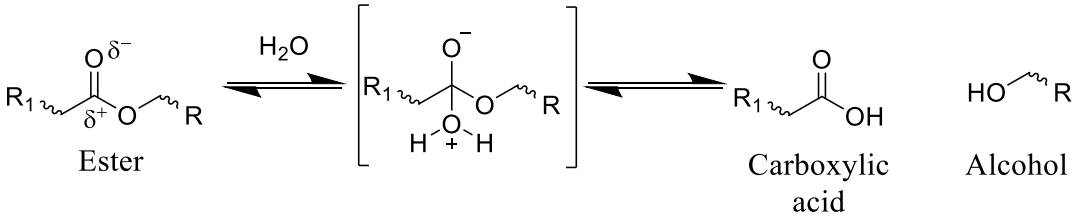

Scheme 1.1. A simplified example of cleavage of hydrolysable ester bond and products.

1.2.1 Hydrolytic degradation of polymers in solution

In solution, the hydrolysis of susceptible polymeric bonds proceeds *via* 2nd order reaction kinetics, meaning the rate of hydrolysis is proportional to the concentration of water and hydrolysable bonds. The susceptibility of a chemical bond to undergo hydrolysis is primarily dependant on the charge value of the reacting carbon atoms (Scheme 1.1).

Extensively demonstrated in literature, chemical functionalities with charge values >0.3 generally exhibit a higher susceptibility to hydrolysis (*i.e.* esters, amides, carbonates, carbamates, ureas, anhydrides, orthoesters *etc*.).[23] Secondary to charge effects, steric effects and conjugate structures have a substantial effect on the rate of hydrolysis of chemically susceptible bonds.

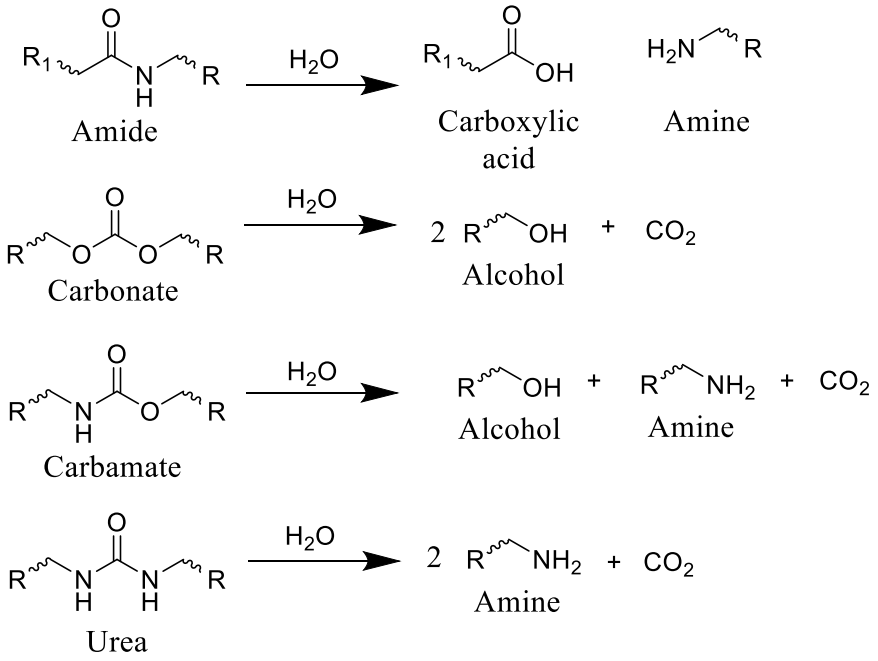

Scheme 1.2. Example of cleavage of hydrolysable bonds and products.

Although exhibiting high charge values (0.45-0.72), amide, carbonate, carbamate, urea and aromatic ester-based polymers exhibit lower rates of hydrolysis owing to conjugate structures. Furthermore, steric effects exhibited by substituted reactants can drastically reduce the rate of hydrolysis as a consequence of bond inaccessibility. An excellent example of steric effects can be seen in the reduced rate of hydrolysis of polydimethylsiloxane (PDMS), where the two methyl substituents significantly protect the silicon atoms from hydrolysis irrespective of its high charge value (0.62). Importantly, it has been shown that the hydrolytic degradation of polymers, both in solution and in bulk, proceeds by a random scission of hydrolysable bonds *e.g.* all chemically identical hydrolysable bonds in a polymer are equally reactive irrespective of chain position (*i.e.* chain end *vs* mid-block).[22]

1.2.2 Hydrolytic degradation of polymers in bulk

As may be obvious, the most significant difference between polymers in solution and polymers in bulk is the molecular mobility. The restrictions in molecular mobility mean, when in bulk, the diffusion of water and reactants are limited. Therefore, hydrolytic degradation in polymeric systems in bulk can be defined as a combination of the diffusion of water into a polymer network and subsequent random cleavage of hydrolysable bonds.[20,14] The diffusion of water into a bulk polymer network of a given composition (*i.e.* poly(lactic acid) (PLA)) is constant and is relatively independent of morphology *i.e.* amorphous poly(D,L-lactic acid-*co*-L-lactic acid) (PDLLA-*co*-PLLA). Although this diffusion coefficient may affect the macroscopic degradation of a material, degradation kinetics are still determined by the hydrolysis reaction on a molecular scale. In simplistic terms, hydrolytic degradation of synthetic materials can be split into two modes; bulk degradation and surface erosion, however, both mechanisms are not necessarily independent of each other.[24,25]

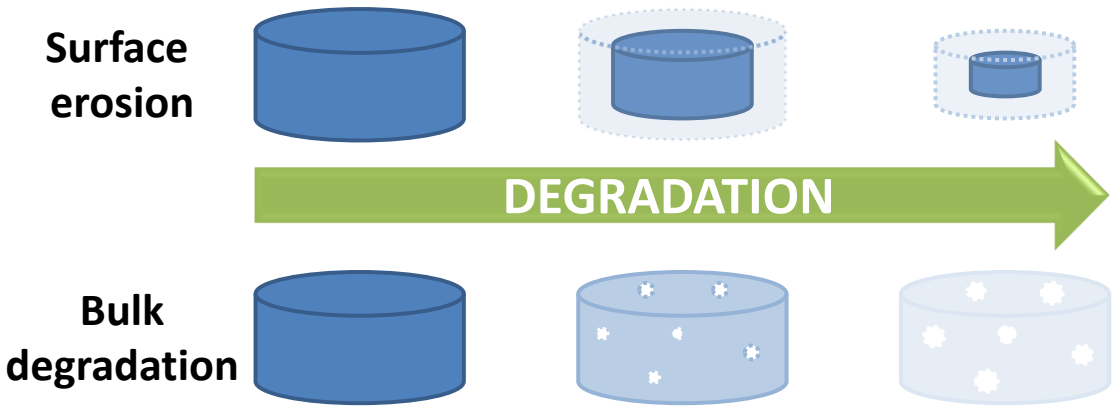

Figure 1.2. Degradation mechanisms; surface erosion versus bulk degradation

The dominant mode of degradation may be predicted by examining the relationship between the time taken for hydrolysis of surface polymer chains into small soluble components (T_e), dependent on quantum chemical effects mentioned earlier, and water diffusion into a polymer within this given time (D_T), an intrinsic property of a polymer defined by the physico-chemical properties of the material (*i.e.* polymer density, hydrophobicity, phase behaviour *etc.*).

Bulk degradation is characterised by a higher rate of water diffusion to hydrolysis ($D_T >> T_e$), leading to sample saturation by the degradation media, and a non-linear mass loss over time (Figure 1.3). Bulk degradation is the dominant mechanism in most polyester-based polymers *i.e.* poly(lactide) (PLA), poly(glycolide) (PGA), poly(ε-caprolactone) (PCL) *etc.*[20,25] A further important characteristic of bulk degradation is the presence of autocatalytic effects as a consequence of the accumulation of degradation products.

In the case of surface degradation, degradation products are free to diffuse away from the polymer matrix, however in bulk degradation, degradation products which may partake in the hydrolysis reaction (*i.e.* hydroxyl and carboxylic acid groups formed during ester cleavage) have reduced diffusivity through the polymer matrix leading to accumulation.[22] This accumulation results in areas of accelerated degradation and leads to the loss of structural integrity and mechanical stability and ultimately leads to the collapse and disintegration of the polymer matrix. As a result, autocatalysis is an important consideration when designing medical devices which undergo bulk degradation.

Some functionalities such as polyorthoesters and certain polyanhydrides and polycarbonates (poly(trimethylene carbonate) (PTMC)), however, undergo mainly surface erosion. Surface erosion is characterised by a faster rate of hydrolysis than water diffusion ($D_T \leq T_e$) and generally expresses a linear loss in mass over time.[26-28]

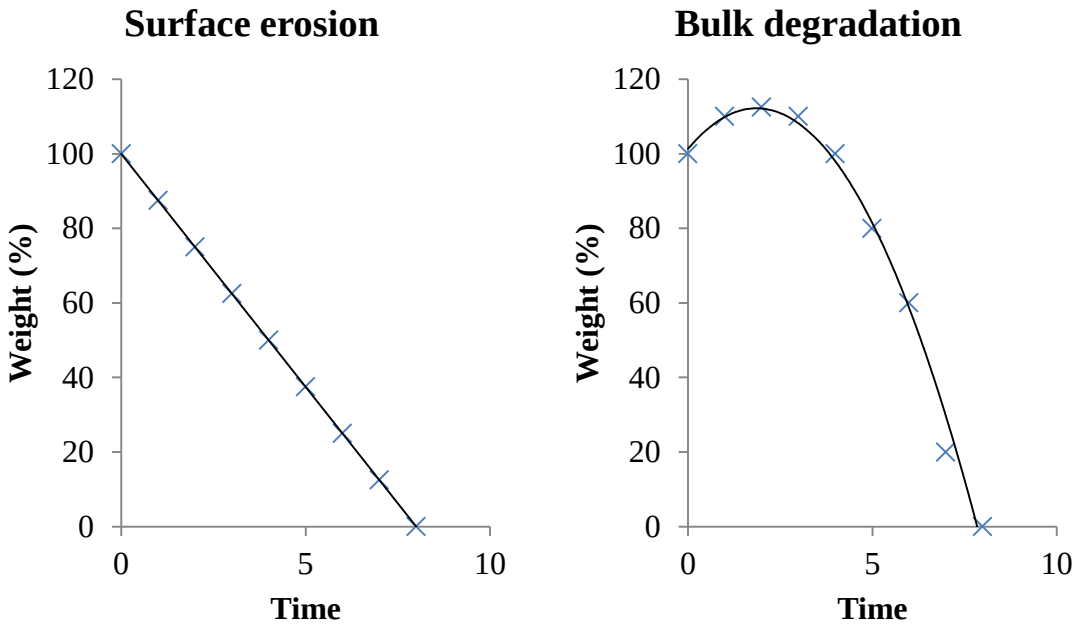

Figure 1.3. Example of a degradation profile exhibiting surface erosion (left) and bulk degradation (right).

It is important to note that as diffusion of water into a polymer network is a function of distance over time, the mode of degradation may also be determined by sample size. For example, if a sample has a width (W_s) much greater than D_T ($W_s >> D_T$) then the sample would degrade by surface erosion. Additionally, as the sample width is reduced, the degradation mode will approach a bulk degradation mechanism.

1.3 Other mechanisms of degradation

1.3.1 Enzymatic degradation

Enzymatic degradation is defined as the enzyme catalysed scission of bonds of a compound to form two or more products.[21] Owing to the versatility of nature, a wide range of enzyme catalysed degradation reactions are available, however, the most common mechanism of enzyme catalysed polymer degradation is hydrolysis.[22] Unlike standard hydrolytic degradation, enzymatic degradation is not common in synthetic polymers as a consequence of the substrate specific nature of many enzymes.[29]

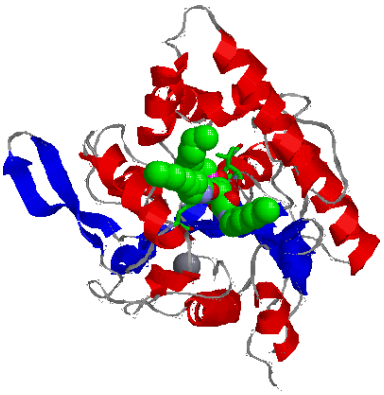

Figure 1.4. Example of a lipase; Pseudomonas triacylglycerol hydrolase

Furthermore, enzymatically degradable polymers may exhibit drastic alterations in their degradation rate dependant on the innate enzyme concentration of the site. Akin to hydrolytic degradation, the physical properties of the polymer (*i.e.* crystallinity, molecular weight, chemical composition *etc*.) can affect the rate of degradation, however, the inherent specificity of enzymes and their 3D confirmation (as a consequence of environmental factors such as temperature and pH) may render them inaccessible to catalyse the hydrolysis reaction.[19,29]

1.3.2 Oxidative degradation

As mentioned previously, oxidative degradation occurs as a result of the scission of susceptible bonds by radical attack supported by peroxide producing inflammatory reactions.[14] Consequent to implantation and acceptance of a synthetic or natural material, owing to acute inflammatory responses, implants are encapsulated in a matrix chiefly consisting of fibroblasts, collagens, foreign body giant cells (FBGCs) and varying levels of macrophages.[22] In order to facilitate the clearing of degradable implanted devices, FBGCs and macrophages produce peroxides at the surface of the implant to illicit degradation.[30] These latent peroxides are readily degraded by naturally occurring or process induced free radicals which in turn proliferate and partake in oxidative degradation of susceptible bonds of the implanted device. Although the vast majority of polymer bonds are susceptible to oxidative reactions, structures which can facilitate the proliferation of free radicals with adequate lifetime, such as polyolefins, polyethers vinyl polymers and polyamines, are generally more susceptible.[22,31]

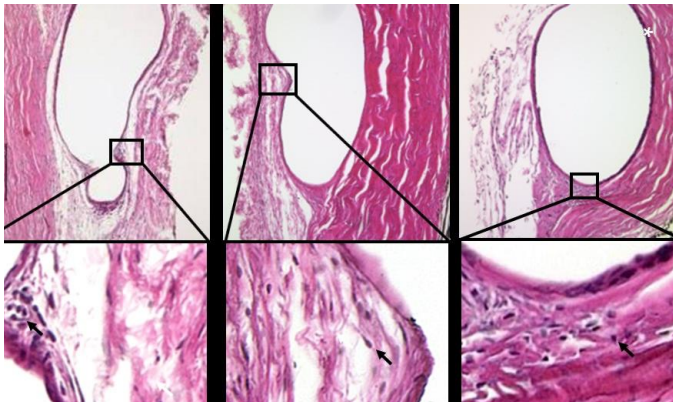

Figure 1.5. Encapsulated polymer fibrils after 1, 4 and 8 weeks (*left to right*) implantation in ocular tissue and expansions.[32]

1.3.3 Physical degradation

Physical degradation is considered as the scission of bonds, both physical and chemical, within a polymer chain as a consequence of the application of mechanical stresses upon the material.[33] As with other forms of degradation, physical or mechanical degradation is dependent on a number of physical properties such as molecular weight, molecular composition and viscosity, however, external factors such as applied shear stress, temperature and water-induced plasticisation also need to be considered, especially when considering modulus-matched degradable biomaterials.[34] Typically, high molecular weight polymers with high viscosities exhibit a higher mechanical deterioration when appropriate shear stresses are applied to them. This is a consequence of reduced chain mobility allowing for the polymer chains to experience the full extent of the shear force applied.[35] Conversely, polymers with low viscosities are able to dissipate shear stress through enhanced chain mobility and multilateral translations. Furthermore, application of shear stress on low viscosity polymers may induce increased amounts of chain entanglement and recombination negating or 'masking' the effects brought on by mechanical degradation (*i.e.* reduction in mechanical strength, permeability *etc*.).[34] Although low viscosity polymers exhibit a better resistance to mechanical stresses, they are subject to other adverse characteristics such as reduced creep resistance and viscous deformation.[35]

Another key factor in the mechanical degradation of biomaterials is the effect of plasticisation and delamination induced by the uptake of water. Water-induced plasticisation of polymers manifests itself by a reduction in the glass transition (T_g) leading to increased chain mobility.[22] As with inherently low viscosity polymers, the reduction in the T_g leads to a reduction in creep resistance and possible mechanical

deformation (*i.e.* unrecoverable plastic deformation, viscous flow *etc*.) and structural failure (*i.e* micro-fractures, reduced load-bearing capabilities *etc*.).

In the case of phase separated polymers, which often require synergistic interactions of each component phase, absorption of water may leads to disruption or delamination of the phases with loss of synergistic interactions, and ultimately, mechanical failure. It is important to note that delamination of phases tends only to occur in materials in which each component phase are relatively hydrophilic.[36,37]

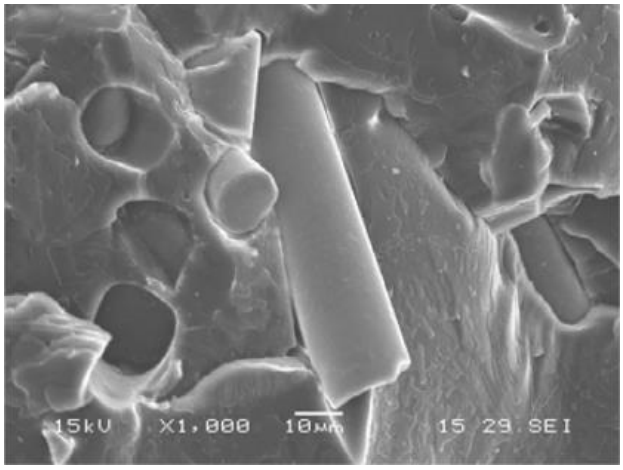

Figure 1.6. SEM of delamination of a polyurethane composite reinforced with glass fibres.[22]

1.4 Polyesters for use in biomaterials

Owed to their synthetic versatility and diverse properties, in conjunction with their historic and regulatory compliance, polyesters have been the most widely investigated synthetic polymer for biomedical applications. Although all polyesters may undergo degradation, aliphatic polyesters with relatively short chain lengths possess suitable

degradation profiles for biomedical applications.[25] As mentioned earlier in this chapter, the degradation of the majority of polyesters proceeds by bulk degradation which, characteristically, results in the accumulation of acidic degradation products. The accumulation of leachable acidic by-products, and low molecular weight degradants, in degradable medical devices has been found to be a key contributor in inflammatory responses in tissue.[38,39] As such, implantation sites which exhibit low metabolic activity or vascularity, and therefore low ability to eliminate by-products, may be unsuitable for polyester-based materials and should be met with great consideration.[38,40]

Aliphatic polyesters may be synthesised by the condensation of diacids/diacid chlorides with diols (A + B)[41,42], self-condensation of hydroxyacids (AB monomer)[43], ester interchange reaction (transesterification)[44] or, more recently, by dehydrogenation polymerisation of diols.[45] Although these methods offer a simplistic route to the synthesis of aliphatic polyesters, molecular weight control and low dispersities are often unachievable.

Figure 1.7. Commercially developed polyester-based all-inside meniscal repair devices. (left to right) Lactosorb® Meniscal Staple, Lactosorb® Meniscal Screw, Clearfix® Meniscal Screw, Biostinger®, Meniscal Dart®, Contour Meniscus Arrow®.[46]

Ring opening polymerisation (ROP) of cyclic lactones, carbonates and *O*-carboxyanhydrides (OCAs) allow for the synthesis of aliphatic polyesters and polycarbonates with excellent control over molecular weight, with high molecular weights achievable, while maintaining low dispersities (<1.1-1.2).[47-49] Furthermore, the ROP of these cyclic monomers require milder reaction conditions and shorter reaction times while negating the production of unwanted condensation by-products (*i.e.* HCl, H_2 *etc*.).

Although ROP of lactones had previously been limited to relatively small cyclic species (C_4-C_7), recent reports have successfully shown the controlled 'immortal' ROP (iROP) of macrolactones (C_8-C_{17}), however, their use as biomaterials has been limited as a consequence of their slow degradation profiles.[50-52] Owing to these distinct advantages, the ROP of lactones and cyclic carbonates has become the most industrially relevant methodology in the synthesis of aliphatic polyesters and polycarbonates for biomedical applications.

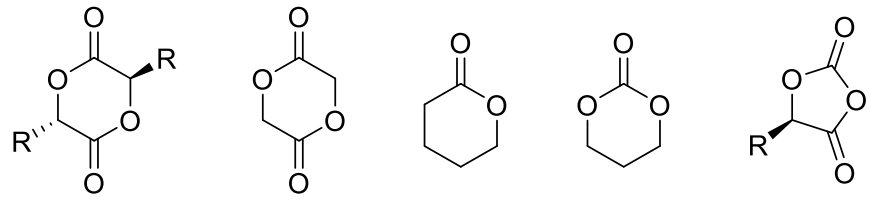

Figure 1.8. Cyclic monomers for the synthesis of polyesters by ROP.

1.4.1 Introduction to poly(glycolide) (PGA)

Poly(glycolide) (PGA) is the simplest of the aliphatic polyesters and was used in the development of the first biodegradable synthetic polymer (DEXON®) investigated in medical applications by Frazza *et al.* (American Cyanamid Company).[53] PGA is synthesised *via* the ROP of glycolide, a cyclic diester comprising of two units glycolic acid, and is a highly crystalline polymer (46-52%).[54] PGA displays a glass transition temperature (T_g) between 35-40 °C and a melting temperature (T_m) range of 225-230 °C, with low solubility in most organic solvents.[55] As a consequence of its thermal and morphological characteristics, PGA has a high Young's modulus (E) (E = 12.8 GPa) and is an excellent candidate for bone internal fixation devices (*i.e.* Biofix®).[14]

However, PGA undergoes mass loss by hydrolytic degradation within 12 months with loss of tensile strength after just 1-2 months. This, in combination with its poor solubility, limits the applications of PGA homopolymers for soft tissue implants. As a result, several PGA containing copolymers have been developed (*i.e.* poly(glycolide/lactide) (Vicry®), poly(glycolide/caprolactone) (MONOCRYL®), poly(glycolide/trimethylene carbonate) (MAXON®) *etc*.).

1.4.2 Introduction to poly(lactide)(PLA)

In order to improve the range of biomedical applications of PGA, a number of copolymers have been synthesised. The most extensively researched of these materials are copolymers with poly(lactide) (PLA) (Scheme 1.3).[56,57,58]

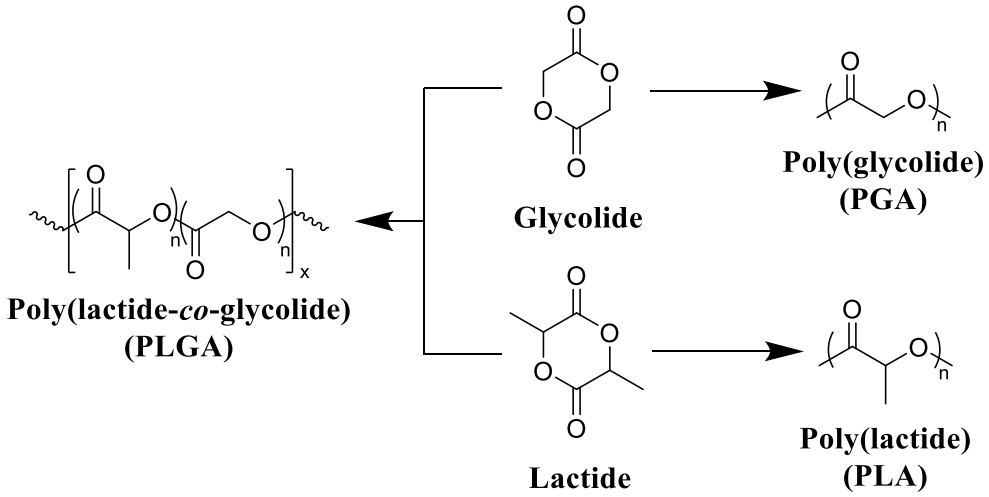

Scheme 1.3. Structure of glycolide and lactide monomers and corresponding homopolymers and copolymer, poly(lactide-*co*-glycolide) (PLGA).

Like glycolide, lactide is a cyclic diester, however comprises of two units of lactic acid, which differs from glycolic acid by a methyl group As a consequence of the chiral centre of lactic acid, lactide is present as three isomers, *SS* (*L*-lactide), *RR* (*D*-lactide) and *RS* (*meso*-lactide), with *L*-lactide being the naturally occurring isomer (Figure 1.6). Stereo-pure poly(*L*-lactide) (PLLA) homopolymers are considered crystalline polymers (30-35% dependant on molecular weight and processing) with relatively high T_g's (57-60 °C), a high *E* (~4.8 GPa) and low strains before mechanical failure (~6%).[55]

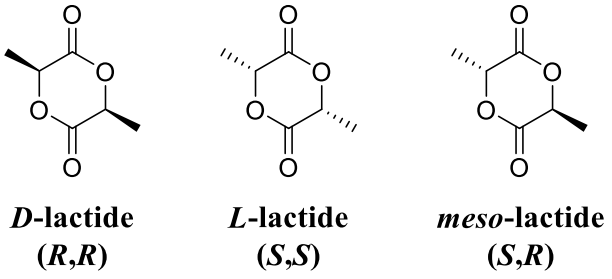

Figure 1.9. Isomers of lactide

As a consequence of steric factors, mentioned earlier in the chapter, PLA exhibits a reduction in hydrolytic activity, compared to PGA, which manifests in reabsorption times ranging from months to decades dependant on polymer processing (*i.e.* crystallinity, orientation, specimen type *etc*.), polymer purity (*e.g.* tacticity), molar mass and distributions.[59,56] PLLA degradation products (*e.g. L*-lactic acid) is easily eliminated from the body by the Cori cycle (later by the Krebs cycle) as glucose (*via* pyruvate). Owing to this enhanced hydrolytic durability and mechanical strength, PLLA has been successfully employed in the development of several commercially available medical devices for meniscal repair (Lactosorb® Meniscal Staple, Bionx Meniscal Arrow®, Linvatec BioStinger™ *etc*.). Furthermore, copolymerisation of PLLA and PGA has resulted in numerous medical devices with adjustable reabsorption time dependent on the incorporation of PGA such as the multifilament sutures Vicryl® and Vicryl Rapid® (fast degrading).[57]

As a consequence of stereo-irregularities in the polymer microstructure, the non-selective ROP of racemic lactide (*rac*-lactide) results in atactic polymers which are amorphous with a reduced T_g (50-53 °C). Owing to its amorphous nature, poly(*rac*-lactide) exhibits a higher susceptibility to hydrolytic degradation (<5 months) as a consequence of enhance permeability.[60] More recently, the effects of stereocomplexation of PLLA/PDLA blends on the physical, mechanical and degradation properties have been investigated. As discussed by Tsuji, the stereocomplexation of PLLA and PDLA result in materials with superior mechanical durability, $E \approx 8.6$ GPa and elongation at break of 30%. Furthermore, stereocomplexed materials exhibited a drastic change in T_g (PLLA = 57-60 °C, stereocomplex = 65-72 °C), T_m (PLLA = 170-190 °C, blend = 220-230 °C), and percentage crystallinity, (PLLA = 35%, blend = 70%).[61]

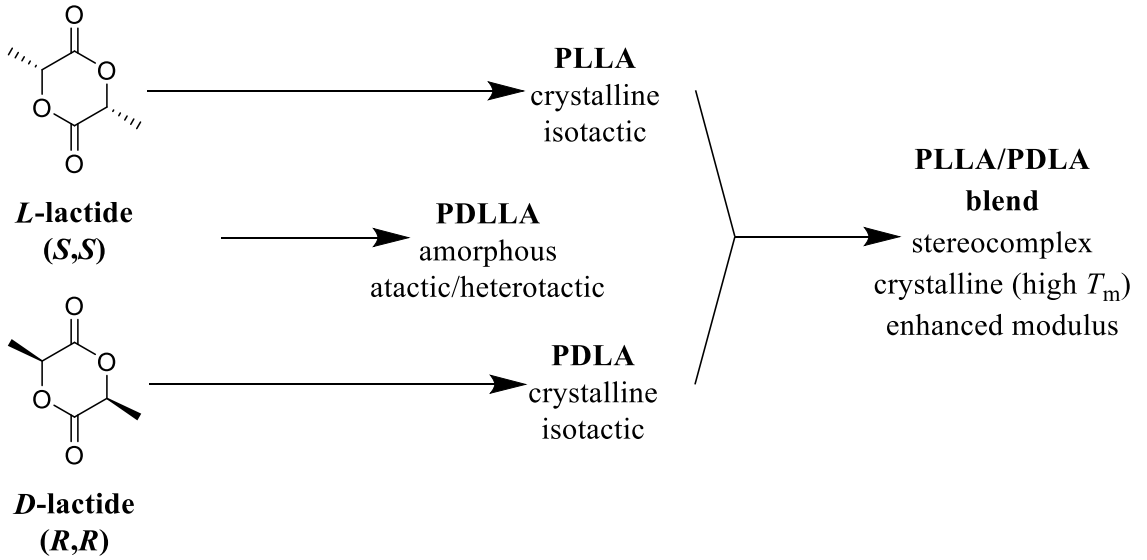

Scheme 1.4. Resultant polymer properties from homo- and copolymerisation of *D*- and *L*-lactide and isotactic stereocomplexation of homopolymers.

As a consequence of the high crystallinity, and therefore low permeability/mobility, stereocomplexed PLLA/PDLA blends exhibit a lower susceptibility to hydrolytic degradation.[60-62] Furthermore, Tsuji *et al*. demonstrated that stereocomplexed blends were found to retain their tensile strength at extended periods of degradation (16 months) compared to PLLA homopolymers under the same conditions (4 months).[61, 62] Although stereocomplexation allow for a vast improvement in the mechanical strength PLA materials, PLLA/PDLA blends still exhibit relatively low extensions before mechanical failure. As a result, PLLA-based copolyesters have been developed (*i.e.* poly(LLA-*co*-caprolactone), poly(LLA-trimethylene carbonate-LLA)).

1.4.3 Introduction to poly(ε-caprolactone) (PCL)

Poly(ε-caprolactone) (PCL) is a semi-crystalline linear aliphatic polyester comprising of an ester-linked C_5 hydrocarbon repeat unit. Traditionally, PCL is synthesised by the alcohol initiated ROP of ε-caprolactone (CL), however, more recently PCL has been prepared through the free radical or xanthate-mediated radical addition-fragmentation chain-transfer (RAFT) polymerisation by the ring-opening of 2-methylene-1,3-dioxepane (MDO)(Scheme 1.5).[63,64] It is important to note, however, although the controlled radical ROP of MDO has seen great advancements in recent times, adverse side-reactions such as branching and ring-retention result in polyesters with poorly defined molecular weights and physical properties.[65] Furthermore, well-defined high molecular weight PCL is only achievable through the ROP of ε-caprolactone.[64]

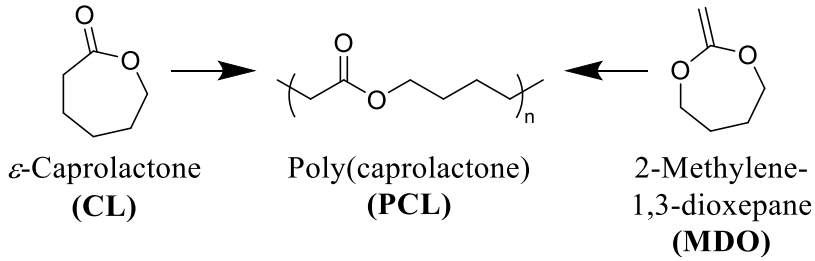

Scheme 1.5. ROP of ε-caprolactone (*left*) and the xanthate-mediated RAFT ring-opening polymerisation of 2-methylene-1,3-dioxepane (*right*).

In comparison to PLA and PGA-based materials, PCL exhibits quite low mechanical strength (E = 0.4 GPa), however, owing to relatively good elongation at break (ε_{break} = 300-500%), in conjunction with its reasonable processing temperatures (T_m = 59-60 °C, $T_g \approx$ -60 °C), solubility, permeability and blend compatibility, PCL has gained much

attention for its potential use in biomedical applications (*i.e.* active pharmaceutical ingredient (API) blended composites, elastomeric copolymers, bioactive scaffolds *etc*.).[55,66] Furthermore, PCLs slow degradation time (~2 years), compared to PGA and PDLA, owed to increased hydrophobicity, and ability to be resorbed and eliminated through the citric acid cycle as 6-hydroxyl caporic acid/acetyl coenzyme A, offers a further point of interest for its application as a degradable biomaterial.[67]

As a consequence of the poor load bearing capabilities of PCL homopolymers its use in commercially viable biomedical applications has been hindered, however recent advancements in biomedical and processing technologies has allowed for a resurgence in PCL-centred materials research.[67] In more commercial areas, PCL copolymers, composites and blends were investigated as long term (>1 year) drug delivery sutures owing to their tailorable degradation times (Capronor, Ethicon Inc: MONOCRYL®).

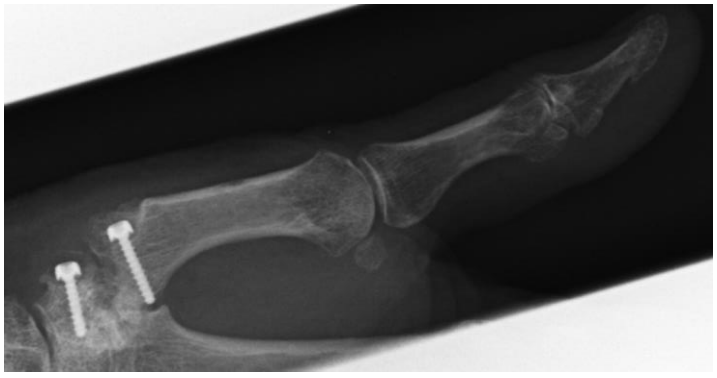

Figure 1.10. Implanted PCL-based Artelon® reinforcement screw

However, PCL-based materials have found applications in nerve regeneration (NEUROLAC®, PDLLA-*co*-PCL),[68] oral surgery (Resilon™, bioactive glass/bismuth

oxychloride/barium sulphate/PCL composite),[69] tissue reinforcement/torn tendon replacement patches (Artelon® Sportmesh™, PCL-based polyester-urethane-urea),[70] anti-adhesives (Mesofol®, PCL-*co*-PLLA)[71] and wound dressings.[72,73] Arguably the most prolific area of poly(ε-caprolactone) copolymers is in the synthesis of degradable segmented thermoplastic polyester-urethanes (TPEUs) which will be discussed later.

1.4.4 Introduction to poly(trimethylene carbonate) (PTMC)

First reported by Carothers and Van Natta in 1930, poly(trimethylene carbonate) (PTMC), similar to PCL, remained relatively unused in biomedical applicable research until the 1970's.[74,75] PTMC is an amorphous polymer with a low T_g (-17 °C), low Young's modulus (~3 MPa) and relatively good strain at break (~160%).[55] Commercially, as a consequence of their low Young's modulus, PTMC-based devices have been limited to copolymers, generally with glycolides, for applications as flexible sutures (Biosyn™) tissue fixation devices (Suretac™) and orthopaedic screws (Acufex®). However, owing to its elastic properties as a consequence of increased molecular mobility, high molecular weight (HMW) PTMC is an excellent candidate, and has been extensively researched, in the fabrication of currently non-commercial devices for soft tissue regeneration.[76,77] Furthermore, low molecular weight (LMW) PTMC/poly(ethylene glycol) (PEG) triblock copolymers have been used for the sustained release of corticosteroids.[78]

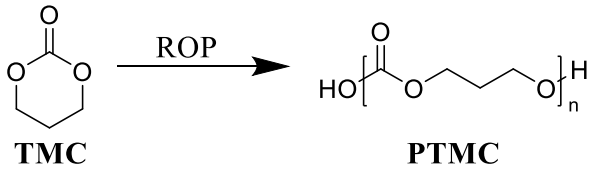

Scheme 1.6. ROP of trimethylene carbonate

Unlike all of the polyesters mentioned previously, PTMC degrades by surface erosion, retaining its structural form until late onset degradation, making it ideal for applications in regenerative medicine.[26] Furthermore, unlike PLA or PGA-based polymers, PTMC does not produce acidic moieties upon degradation responsible for tissue necrosis and autocatalytic degradation.

Interestingly, it was found that the hydrolytic degradation of PTMC was extremely slow (>4 years), however samples exhibited rapid degradation *in vivo*. Feijen *et al.* hypothesised that changes in the pH of the implants environment, subsequent to biological responses, may contribute to increased hydrolytic degradation, however studies have concluded that pH has no effect and that enzymatic interactions are important to the rapid surface erosion *in vivo*.[26]

Furthermore, extensive studies have shown that molecular weight has a dramatic effect on the *in vivo* degradation of PTMC.[79] Contrary to intuition, HMW PTMC exhibited a greater rate of mass loss than the low molecular weight equivalent. This has been attributed to the 'interfacial activation' of lipases at the more hydrophobic HMW PTMC surface.[26]

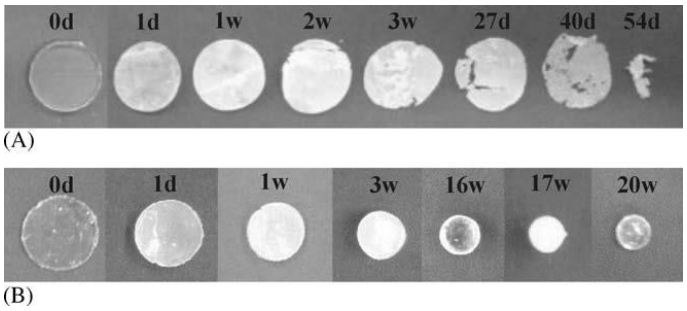

Figure 1.11. Degradation specimens of high molecular weight PMTC (A) and low molecular weight PMTC (B) at different time points.[26]

Another application of PTMC is the synthesis of thermoplastic elastomeric materials based on phase-separable block copolymers. Kim *et al*. first reported the synthesis of PLLA/PTMC ABA triblock copolymers and their subsequent use as thermoplastic elastomers.[80,81] Consequently, PTMC has been extensively reported as effective 'soft' segments in triblock block copolymers in conjunction with high T_g or highly crystalline copolymers.[82,83,84,85] Like PLA, PGA and PCL, PTMC has been effectively utilised in the synthesis of highly elastic degradable thermoplastic polyester-urethanes for applications ranging from textiles to biomedical devices.

1.5 Application of polyesters in the synthesis of thermoplastic polyester-urethanes and polyester-urethane-urea elastomers

Thermoplastic polyester-urethanes (TPEUs) and thermoplastic polyester-urethane-ureas (TPEUUs) are a class of segmented degradable multiblock copolymers, traditionally synthesised by the step-growth polymerisation of telechelic polyester macrodiols, diisocyanates and small diol (urethane) or diamine (urea) extenders *via* the nucleophilic addition of the terminal hydroxyl/amine groups to the diisocyanate (Scheme 1.8).[86,87]

Characterised by their vast range of mechanical, thermal and degradation properties, determined by polymer composition, block lengths and ratios, TPEUs and TPEUUs have been extensively used in the development of devices for use in medical applications such as tissue fixation, wound dressings, regenerative medicine *etc*.[88]

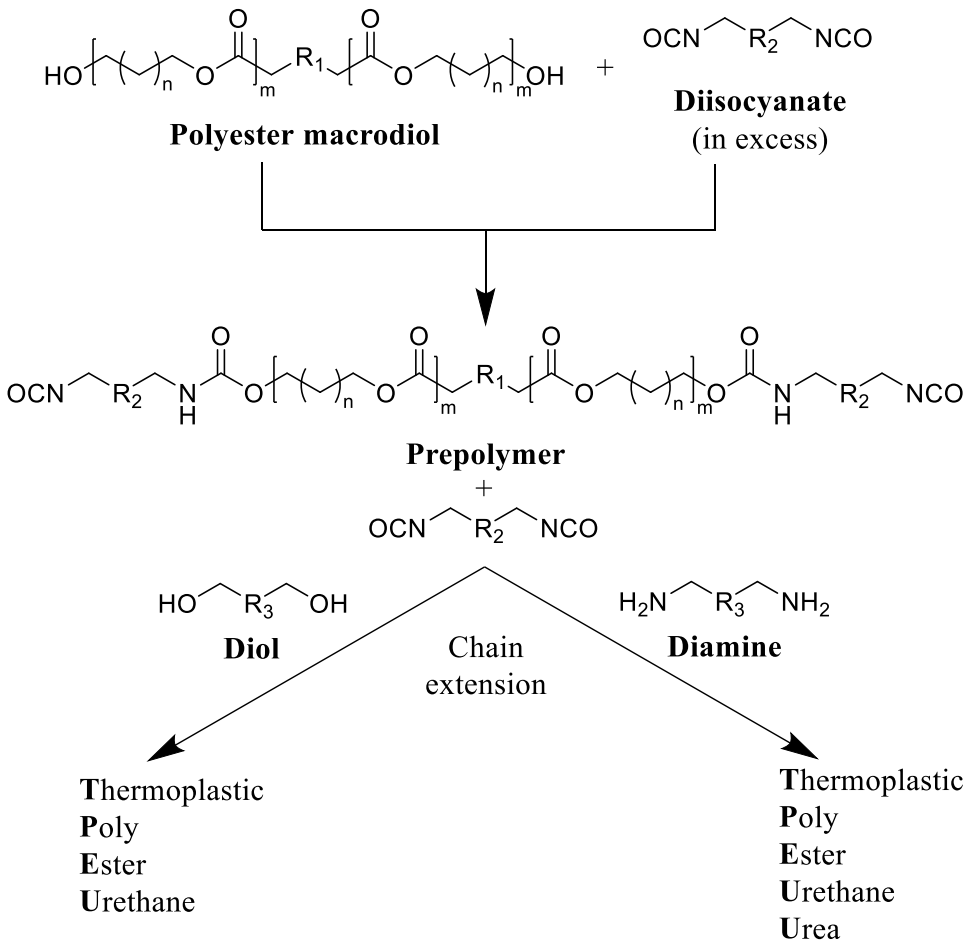

Scheme 1.7. Schematic for the prepolymer formationand chain extension for the synthesis of TPEU/TPEUUs.

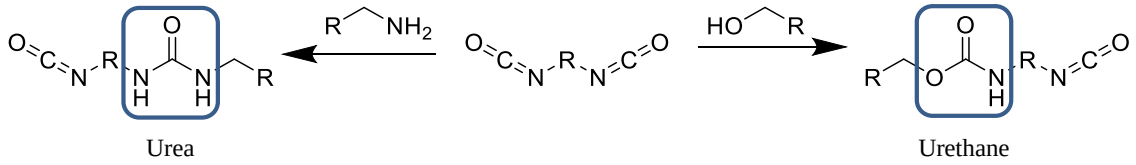

Scheme 1.8. Synthesis of urea (*left*) or urethane (*right*) bond from reaction of a diisocyanate with an amine or alcohol respectively.

TPEU/TPEUUs derive their mechanical versatility as a consequence of their phase separated and highly segmented nature (Figure 1.9).[36] While the implementation of flexible 'soft' blocks provide excellent elongations, highly ordered 'hard' blocks provide rigidity and strength through physical crosslinks.[37] This combination allows for the development and modulation of viscoelastic properties of the resultant materials.[89] Although the phase separation of segmented polyurethanes allows access to a wide range of mechanical properties, the compartmentalisation of phases can lead to heterogeneous degradation profiles throughout the polymer matrix leading to severe loss of mechanical integrity.[76,36] This occurs as a consequence of differences in diffusivity of degradation media and autocatalytic inducing degradation products, hydrolysis rates of esters/carbonates *vs.* urethanes/ureas, and topology of the 'hard-soft' phase separated polymer network.[37] Although a range of polyurethane and urea-based materials have been developed since their inception, only the synthesis of PLGA, PCL and PTMC-based TPEU/TPEUUs and their applications will be discussed herein.

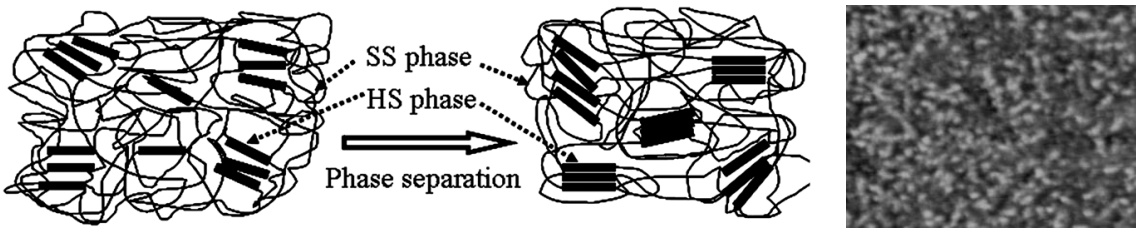

Figure 1.12. Schematic of phase separation in TPEU/TPEUUs (*left*)[90] and an AFM image of a phase separated TPEU (*right*).[91]

1.5.1 PLA and PLGA TPEUs

As mentioned previously, owing to the rapid degradation of PGA and the brittle nature of PLLA, the use of poly(glycolide)s and poly(lactide)s as macrodiols in the synthesis of TPEU/TPEUUs has been relatively limited. However, both PLA and PLA/PGA copolymers (PLGA) have been investigated owed there improved mechanical properties and tunable degradation times.

In agreement with the degradation of the homopolyesters previously discussed, Storey and Hickey demonstrated the vastly increased degradation of PGA-based TPEUs (8% weight loss after 13 days) over PLA-based TPEUs (1.3% weight loss after 13 days). Furthermore it was observed that PLA-based TPEUs exhibited a superior Young's modulus (767 MPa) and ultimate tensile strength (UTS) (41 MPa) than the PGA-based materials (E = 2.14 MPa, UTS = 9.22 MPa), coinciding with the trends observed in the mechanical analysis of the homopolyesters.[92] In a separate study conducted by Storey *et al*., PLGA (50:50 mol% PLA:PGA statistical copolymer) was incorporated into a poly(butylene adipate) (PBA) thermoplastic polyurethane (TPU) in order to introduce enhanced degradability.[93]

As predicted, PLGA-based TPEUs exhibited enhanced degradation however, interestingly, PLGA containing TPEUs also exhibited an increase in *E* (27 MPa) in comparison to PBA TPEUs (13 MPa) with no significant variance in UTS (~20 MPa) or percentage strain at break (~600 %). Furthermore, the degradation of the PLGA-containing TPEUs was further enhanced by the utilisation of a more hydrophilic initiator (2,2-bis-(hydroxymethyl)butanoic acid) for the ROP of lactide/glycolide, consequently increasing the water uptake capability of the material.

Unlike the previous examples, Adhikari *et al*. designed injectable degradable polyurethane systems for orthopaedic applications utilising a mix of both PGA and PDLLA macrodiols in the same TPEU.[94] It was found, as expected, that PDLLA-based TPEUs exhibited a slight reduction in mechanical strength when copolymerised with PGA macrodiols, with an inversely proportional change in degradation times. Furthermore, it was found that the onset of degradation was retarded by the addition of a β-tricalcium phosphate, owing to its quenching of acidic degradation products.

1.5.2 PCL TPEU/TPEUUs

For reasons analogous to the properties of the homopolyester (*i.e.* increased flexibility, biocompatibility, reduced autocatalytic degradation *etc*.), PCL-based TPEU/TPEUUs have been the most extensively examined and commercially utilised macrodiols in the synthesis of degradable polyurethane materials.[95] Furthermore, as has been previously mentioned in the synthesis of polyesters for biomedical applications, Kylmä and Seppälä employed PCL in order to reduce hydrolytic susceptibility and improve the viscoelasticity of PLA-containing TPEUUs.[86]

In order to investigate the effect of molecular weight of the macrodiols on the mechanical properties and morphology of the resultant TPEUs, Schouten *et al.* used telechelic PCL initiated from 1,4-butanediol (1,4-BDO) with molecular weights ranging from 750 to 2800 g mol^{-1}.[96] The PCL macrodiols were end-capped with excess 1,4-butanediisocyanate (1,4-BDI) and chain extended with 1,4-BDO to yield high molecular (100-160 kg mol^{-1}) weight TPEUs. Schouten *et al.* noted at higher molecular weight PCL, TPEUs exhibited an enhanced elastic behaviour with a reduced plastic deformation and an enhanced percentage strain at break (>1200%). This was owed to the decrease in 'hard' block crystallinity as a consequence of reduced 'soft' block mobility at higher molecular weights, retarding 'hard' block association. The reduced mobility of the 'soft' block was characterised by an increase in the glass transition temperature of the incorporated PCL macrodiols, indicative of free volume in accordance with the Flory-Fox equation.[97] In addition to this, Watanabe and co-workers demonstrated the reduction in biodegradability of TPEUs with increasing molecular weight PCL macrodiols.[98] Parallel to previous results, this was attributed to poor diffusivity of degradation media through the polymer matrix as a consequence of low chain mobility at higher molecular weights. Furthermore, it was noted that the degradation was also retarded by the recrystallisation of low molecular weight PCL degradants further reducing diffusivity.[98]

In order to improve the mechanical rigidity and biocompatibility of PCL-based polyurethane materials, Guan *et al.* employed the use of the diamine chain extenders putrescine and lysine ethyl ester in the synthesis of TPEUUs.[99] It was found that upon biodegradation of the TPEUU 'hard' blocks, the biocompatible and excretable lysine ethyl ester, an amino acid derivative, or putrescine, a diamine essential for cell growth and differentiation, were released.

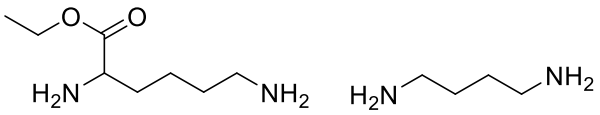

Lysine ethyl ester **Putrescine**

Figure 1.13. Natural diamine chain extenders for the synthesis of TPEUUs.

In addition to this, Guan *et al*. demonstrated the improved viability and proliferation of human umbilical vein endothelial cells (HUVECs) when seeded on the putrescine-containing TPEUUs. Furthermore, the choice of chain extender was also found to significantly affect the mechanical properties of the PCL-based TPEUUs. It was found that putrescine-containing TPEUUs exhibited a higher *E* (78 MPa), UTS (11.9 MPa) and a reduced plastic deformation over its lysine counterpart (*E* = 38 MPa, UTS = 4.7 MPa). This was attributed to the enhanced hydrogen bonding of the lysine-containing TPEUUs through the ester side group causing rigid plastic-like properties.

1.5.3 PTMC TPEU/TPEUUs

Although homo-PTMC exhibits an enhanced elasticity in comparison with other polyesters, it has been relatively under-utilised exclusively as a macrodiol in the synthesis of TPEU/TPEUU elastomers.[100,101,102] Similar to studies discussed previously, Wagner *et al.* synthesised a series of PTMC macrodiols with varying molecular weights (1.5-5.4 kg mol^{-1}) and utilised them in the synthesis of TPEUUs employing 1,4-BDI and putrescine as the diisocyanate and extender respectively.[100] Although each TPEUU exhibited comparable strains at break (~750%), it was noted at low strains (50%), TPEUUs comprised of higher molecular weight PTMC macrodiols exhibited a reduction in unrecoverable deformation through hysteresis (<5%). This trend continued

at higher strains (400%), however the degree of deformation increased by an order of magnitude (50-80%). In conjunction to this, it was found that PTMC-based TPEUUs exhibited excellent cell viability and proliferation with very low susceptibility to hydrolysis (>80% mass remaining after 28 days), similar to the PTMC homopolymer discussed earlier. Furthermore, utilising an extender free methodology, Hilborn *et al.* reported the synthesis of highly elastic TPEUUs which exhibited high strains at break, in excess of 1900%, UTS (>30 MPa) and reasonable Young's moduli (~4.5 MPa).[101]

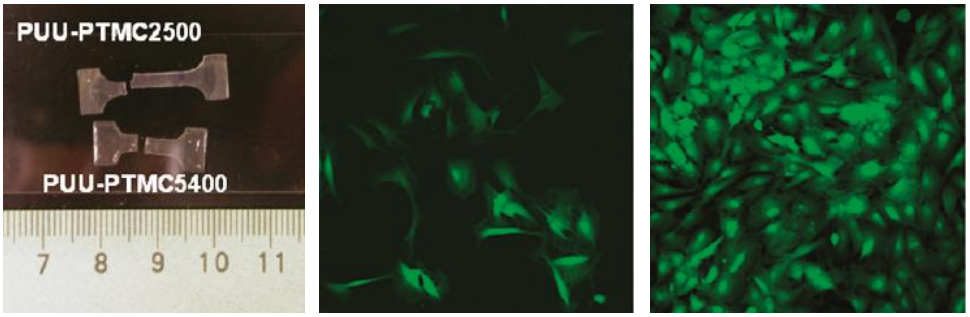

Figure 1.14. PTMC-based TPEUUs with improved elasticity with higher molecular weight diols (*right*), good cell viability (*middle*) and excelent cell proliferation (*right*).[100]

In a comprehensive analysis of hydrolytic stability, cytotoxicity and mechanical robustness after partial degradation of PTMC-based TPEUs, Sobczak *et al.*[102] reported that after 5 weeks under accelerated degradation conditions (10% aq.HCl at 70 °C), PTMC-TPEUs retained greater than 85% of their original mass by gravimetric analysis. Furthermore, these materials were reported to retain between 78-80% of their initial strain at break and UTS. In addition to this Sobczak and co-workers found that PTMC-based TPEUs exhibited no significant cytotoxic effect when evaluated with luminescent bacteria (*V. fischeri*) or ciliated protozoans (*S. ambiguum* and *T. thermophila*).

1.6 Conclusion

In conclusion, the development and production of synthetic hydrolytically degradable polymers for applications as biomaterials is of upmost importance for the advancement of effective biomedical therapeutics such as tissue regeneration, sustained API release, degradable implants *etc.* As is evident, even from the small selection of polymers discussed, aliphatic polyesters offer a facile route to a plethora of materials with a variety of thermal, degradation and mechanical properties. Furthermore, these properties can be precisely defined through stereo-chemistry, copolymerisation, initiating species chosen, targeted molecular weight and morphology.

1.7 References

1. M. Okada, *Prog. Polym. Sci.*, 2002, 27, 87-113.
2. R. Chandra and R. Rustgi, *Prog. Polym. Sci.*, 1998, 23, 1273-1335.
3. C. H. Lee, A. Singla and Y. Lee, *Int. J. Pharm.*, 2001, 221, 1-22.
4. L. Buttafoco, N. G. Kolkman, P. Engbers-Buijtenhuijs, A. A. Poot, P. J. Dijkstra, I. Vermes and J. Feijen, *Biomaterials*, 2006, 27, 724-734.
5. B. Kundu, R. Rajkhowa, S. C. Kundu and X. Wang, *Adv. Drug Deliv. Rev.*, 2013, 65, 457-470.
6. R. Z. LeGeros, *Clin. Orthop. Relat. Res.*, 2002, 395, 81-98.
7. W. Suchanek and M. Yoshimura, *J. Mater. Res.*, 1998, 13, 94-117.
8. H. W. T. Matthew and J. K. F. Suh, *Biomaterials*, 2000, 21, 2589-2598.
9. Y. Luo, K. R. Kirker and G. D. Prestwich, *J. Control. Release*, 2000, 69, 169-184.
10. G. Q. Chen and Q. Wu, *Biomaterials*, 2005, 26, 6565-6578.
11. T. Freiera, C. Kunzea, C. Nischana, S. Kramera, K. Sternberga, M. Sab, U. T. Hoptb and K.-P. Schmitza, *Biomaterials*, 2002, 23, 2649-2657.
12. G. T. Köse, H. Kenar, N. Hasırcı and V. Hasırcı, *Biomaterials*, 2003, 24, 1949-1958.
13. J. A. Hubbell, *Nat. Biotechnol.*, 1995, 13, 565-576.
14. L. S. Nair and C. T. Laurencin, *Prog. Polym. Sci.*, 2007, 32, 762-798.
15. J. R. Lentino, *Clin. Infect. Dis.*, 2003, 36, 1157.
16. A. van Ooij, S. M. Kurtz, F. Stessels, H. Noten and L. van Rhijn, *Spine*, 2007, 32, 223-229.
17. N. Goonoo, A. Bhaw-Luximon, G. L. Bowlin and D. Jhurry, *Polym. Int.*, 2013, 62, 523-533.

18. G. H. Altman, F. Diaz, C. Jakuba, T. Calabro, R. L. Horan, J. Chen, H. Lu, J. Richmond and D. L. Kaplan, *Biomaterials*, 2003, 24, 401-416.

19. H. S. Azevedo, F. M. Gama and R. L. Reis, *Biomacromolecules*, 2003, 4, 1703-1712.

20. D. S. Katti, S. Lakshmi, R. Langer and C. T. Laurencin, *Adv. Drug Deliv. Rev.*, 2002, 54, 933-961.

21. A. Göpferich, *Biomaterials*, 1996, 17, 103-114.

22. S. Lyu and D. Untereker, *Int. J. Mol. Sci.*, 2009, 10, 4033-4065.

23. R. A. Larson and E. J. Weber, *Reaction Mechanisims in Environmental Chemistry*, CRC Press 1994.

24. K. E. Uhrich, S. M. Cannizzaro, R. S. Langer and K. M. Shakesheff, *Chem. Rev.*, 1999, 99, 3181-3198.

25. C. G. Pitt, M. M. Gratzl, G. L. Kimmel, J. Surles and A. Schindler, *Biomaterials*, 1981, 2, 215-220.

26. Z. Zhang, R. Kuijer, S. K. Bulstra, D. W. Grijpma and J. Feijen, *Biomaterials*, 2006, 27, 1741-1748.

27. J. Heller, J. Barr, S. Y. Ng , K. S. Abdellauoi and R. Gurny, *Adv. Drug Deliv. Rev.*, 2002, 54, 1015-1039.

28. D. S. Muggli, A. K. Burkoth and K. S. Anseth, *J. Biomed. Mater. Res. A*, 1999, 46.

29. H. S. Azevedo and R. L. Reis, *Understanding the Enzymatic Degradation of Biodegradable Polymers and Strategies to Control Their Degradation Rate*, CRC Press, 2005.

30. J. Casas, Q. Zhao, M. Donovan, P. Schroeder, K. Stokes and D. Untereker, *J. Biomed. Mater. Res. Symp.*, 1999, 46, 475-484.

31. M. C. Sobieraj and C. M. Rimnac, *J. Mech. Behav. Biomed. Mater.*, 2009, 2, 433-443.

32. M. Kropp, K.-M. Morawa, G. Mihov, A. Salz, N. Harmening, A. Franken, A. Kemp, A. Dias, J. Thies, S. Johnen and G. Thumann, *Polymers*, 2014, 6, 243-260.

33. C. Booth, *Polymer*, 1963, 4, 471-478.

34. F. Bueche, *J. Appl. Polym. Sci.*, 1960, 4, 101-106.

35. A. A. Hamouda, C. Eliassen, C. Idsoe and T. Jacobsen, *Annu, Trans. Nord. Rheo. Soc.*, 2005, 13, 65-71.

36. K. Stokes, R. McVenes and J. M. Anderson, *J. Biomater. Appl.*, 1995, 9, 321-353.

37. P. Krol, *Prog. Mater. Sci.*, 2007, 52, 915-1015.

38. O. Bostman, E. Hirvensalo, J. Makinen and P. Rokkanen, *J. Bone Joint Surg. Br.*, 1990, 72, 592-596.

39. M. Vert, *Prog. Polym. Sci.*, 2007, 32, 755-761.

40. J. E. Bergsma, W. C. de Bruiju, F. R. Rozema, R. R. M. Bos and G. Boering, *Biomaterials*, 1995, 16, 25-31.

41. P.-J. Roumanet, F. Laflèche, N. Jarroux, Y. Raoul, S. Claude and P. Guégan, *Eur. Polym. J.*, 2013, 49, 813-822.

42. H. W. Gibson, S. Liu, C. Gong, Q. Ji and E. Joseph, *Macromolecules*, 1997, 30, 3711-3726.

43. M. Kolitz, N. Cohen-Arazi, I. Hagag, J. Katzhendler and A. J. Domb, *Macromolecules*, 2009, 42, 4520-4530.

44. Z. Zhang, X. Lou, Y. Lu and D. Ma, *Eur. Polym. J.*, 2001, 37, 99-104.

45. D. M. Hunsicker, B. C. Dauphinais, S. P. Mc Ilrath and N. J. Robertson, *Macromol. Rapid. Commun.*, 2012, 33, 232-236.

46. D. J. King and M. J. Matava, *Oper. Techn. Sport Med.*, 2004, 12, 161-169.

47. O. Dechy-Cabaret, B. Martin-Vaca and D. Bourissou, *Chem. Rev.*, 2004, 104, 6147-6176.

48. R. J. Pounder and A. P. Dove, *Biomacromolecules*, 2010, 11, 1930–1939.

49. S. M. Guillaume, *Eur. Polym. J.*, 2013, 49, 768-779.

50. I. van der Meulen, M. de Geus, H. Antheunis, R. Deumens, E. A. J. Joosten, C. E. Koning and A. Heise, *Biomacromolecules*, 2008, 9, 3404-3410.

51. I. van der Meulen, Y. Li, R. Deumens, E. A. Joosten, C. E. Koning and A. Heise, *Biomacromolecules*, 2011, 12, 837-843.

52. K. S. Bisht, L. A. Henderson, R. Gross, D. L. Kaplan and G. Swift, *Macromolecules*, 1997, 30, 2705-2711.

53. E. J. Frazza and E. E. Schmitt, *J. Biomed. Mater. Res. Symp.*, 1971, 1, 43-58.

54. D. K. Gilding and A. M. Reed, *Polymer*, 1980, 22, 494-498.

55. I. Engelberg and J. Kohn, *Biomaterials*, 1990, 12, 292-304.

56. A. Södergård and M. Stolt, *Prog. Polym. Sci.*, 2002, 27, 1123-1163.

57. C. C. Chu, *Polymer*, 1985, 26, 591-594.

58. R. A. Kenley, M. Ott Lee, R. T. Mahoney and L. M. Sanders, *Macromolecules*, 1987, 20, 2398-2403.

59. C. A. P. Joziasse, D. W. Grijpma, J. E. Bergsma, F. W. Cordewener and A. J. Pennings, *Colloid Polym. Sci.*, 1998, 276, 968-975.

60. S. Li and S. McCarthy, *Biomaterials*, 1999, 20, 35-44.

61. H. Tsuji, *Macromol. Biosci.*, 2005, 5, 569-597.

62. S. Li and M. Vert, *Polym. Int.*, 1994, 33, 37-41.

63. F. J. Natta, J. W. Hill and W. H. Carothers, *J. Am. Chem. Soc*, 1934, 56, 455-457.

64. G. G. Hedir, C. A. Bell, N. S. Ieong, E. Chapman, I. R. Collins, R. K. O'Reilly and A. P. Dove, *Macromolecules*, 2014, 47, 2847-2852.

65. S. Agarwal, *Polym. Chem.*, 2010, 1, 953-964.

66. J. C. Middleton and A. J. Tipton, *Biomaterials*, 2000, 21, 2335-2346.

67. M. A. Woodruff and D. W. Hutmacher, *Prog. Polym. Sci.*, 2010, 35, 1217-1256.

68. A. L. Luis, J. M. Rodrigues, J. V. Lobato, M. A. Lopes, S. Amado, A. P. Veloso, P. A. S. Armada-da Silva, S. Raimondo, S. Geuna, A. J. Ferreira, A. S. P. Varejao, J. D. Santos and A. C. Maurício, *Bio-Med. Mater. Eng.*, 2007, 17, 39-52.

69. A. Elzubair, C. N. Elias, J. C. Suarez, H. P. Lopes and M. V. Vieira, *J. Dent.*, 2006, 34, 784-789.

70. K. Gissefalt, B. Edberg and P. Flodin, *Biomacromolecules*, 2002, 3, 951-958.

71. L. S. Klopp, B. J. Simon, J. M. Bush, M. R. Enns and S. A. Turner, *Spine*, 2008, 33, 1518-1526.

72. K. W. Ng, H. N. Achuth, S. Moochhala, T. C. Lim and D. W. Hutmacher, *J. Biomater. Sci., Polym. Ed.*, 2007, 18, 925-938.

73. D. S. Jones, J. Djokic, C. P. McCoy and S. P. Gorman, *Biomaterials*, 2002, 23, 4449-4458.

74. W. H. Carothers and F. J. Van Natta, *J. Am. Chem. Soc*, 1930, 52, 314-325.

75. B. Amecke, D. Bendix and G. Entenmann, in *Encyclopedia handbook of biomaterials and bioengineering, Part A: Materials, Vols 1 and 2*, eds. D. L. Wise, D. J. Trantolo, D. E. Altobelli, M. J. Yaszemski, J. D. Gresser and E. R. Schwartz, Marcel Dekker Inc., 1995, pp. 97-1007.

76. E. Bat, B. H. Kothman, G. A. Higuera, C. A. van Blitterswijk, J. Feijen and D. W. Grijpma, *Biomaterials*, 2010, 31, 8696-8705.

77. A. P. Pêgo, A. A. Poot, D. W. Grijpma and J. Feijen, *J. Control. Release*, 2003, 87, 69-79.

78. Z. Zhang, D. W. Grijpma and J. Feijen, *J. Control. Release*, 2006, 111, 263-270.

79. A. Albertsson and M. Eklund, *J. Appl. Polym. Sci.*, 1995, 57, 87-103.

80. J. H. Kim, S. Y. Lee and D. J. Chung, *Polym. J.*, 2000, 32, 1056-1059.

81. J. H. Kim and J. H. Lee, *Polym. J.*, 2002, 34, 203-208.

82. S. Dai, L. Xue and Z. Li, *ACS Catal.*, 2011, 1, 1421-1429.

83. Z. Zhang, D. W. Grijpma and J. Feijen, *Macromol. Chem. Phys.*, 2004, 205, 867-875.

84. L. K. Widjaja, J. F. Kong, S. Chattopadhyay, V. T. Lipik, S. S. Liow, M. J. Abadie and S. S. Venkatraman, *J. Mech. Behav. Biomed. Mater.*, 2012, 6, 80-88.

85. R. Shi, D. Chen, Q. Liu, Y. Wu, X. Xu, L. Zhang and W. Tian, *Int. J. Mol. Sci.*, 2009, 10, 4223-4256.

86. J. Kylma and J. V. Seppala, *Macromolecules*, 1997, 30, 2876-2882.

87. A. Lendlein and S. Kelch, *Angew. Chem., Int. Ed.*, 2002, 41, 2034-2057.

88. N. M. K. Lamba, K. A. Woodhouse and S. L. Cooper, *Polyurethanes in Biomedical Applications*, CRC Press LLC, 1997.

89. T. O. Ahn, S. U. Jung, H. M. Jeong and S. W. Lee, *J. Appl. Polym. Sci.*, 2003, 51, 43-49.

90. Z. Wu, H. Wang, X. Tian, P. Cui, X. Ding and X. Ye, *Phys. Chem. Chem. Phys.*, 2014, 16, 6787-6794.

91. E. Tocha, H. Janik, M. Debowski and G. J. Vancso, *J. Macromol. Sci., Part B: Phys.*, 2002, 41, 1291-1304.

92. R. F. Storey and T. P. Hickey, *Polymer*, 1994, 35, 830-838.

93. S. J. Moravek, M. K. Hassan, D. J. Drake, T. R. Cooper, J. S. Wiggins, K. A. Mauritz and R. F. Storey, *J. Appl. Polym. Sci.*, 2010, 115, 1873-1880.

94. R. Adhikari, P. A. Gunatillake, I. Griffiths, L. Tatai, M. Wickramaratna, S. Houshyar, T. Moore, R. T. Mayadunne, J. Field, M. McGee and T. Carbone, *Biomaterials*, 2008, 29, 3762-3770.

95. C. J. Bettinger, *Macromol. Biosci.*, 2011, 11, 467-482.

96. R. G. Heijkants, R. V. van Calck, T. G. van Tienen, J. H. de Groot, P. Buma, A. J. Pennings, R. P. Veth and A. J. Schouten, *Biomaterials*, 2005, 26, 4219-4228.

97. G. Odian, *Principles of Polymerization, Fourth Edition*, John Wiley & Sons, Inc., 2004.

98. A. Watanabe, Y. Takebayashi, T. Ohtsubo and M. Furukawa, *J. Appl. Polym. Sci.*, 2009, 114, 246-253.

99. J. Guan, M. S. Sacks, E. J. Beckman and W. R. Wagner, *J. Biomed. Mater. Res. A*, 2002, 61, 493-503.

100. Z. Ma, Y. Hong, D. M. Nelson, J. E. Pichamuthu, C. E. Leeson and W. R. Wagner, *Biomacromolecules*, 2011, 12, 3265-3274.

101. B. Asplund, T. Bowden, T. Mathisen and J. Hilborn, *Biomacromolecules*, 2007, 8, 905-911.

102. M. Sobczak, C. Dębek, E. Olędzka, G. Nałęcz-Jawecki, W. L. Kołodziejski and M. Rajkiewicz, *J. Polym. Sci., Part A: Polym. Chem.*, 2012, 50, 3904-3913.

2 Organocatalysed ring-opening polymerisation and post-polymerisation modification of spirocyclic carbonate monomers derived from pentaerythritol

2.1 Introduction:

As described in chapter 1, the ring opening polymerisation (ROP) of cyclic monomers in the synthesis of novel materials has been of great interest in recent years. The utilisation of ROP allows for the precise control of molecular weights, polymer composition, end-group fidelity and low polydispersities.[1-3] This method of polymerisation also allows for the facile synthesis of biodegradable and biocompatible materials through utilisation of an ever expanding palette of degradable cyclic monomers (*e.g.* cyclic lactones/lactams, *O*-carboxyanhydrides (OCAs), *N*-carboxyanhydrides (NCAs), cyclic carbonates *etc.*).[4-7]

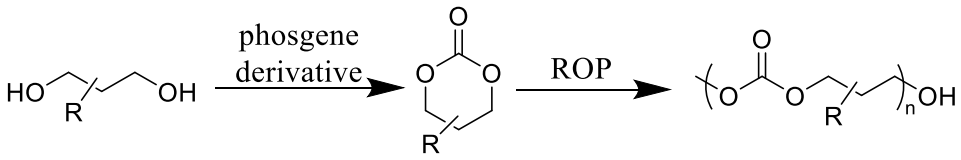

Scheme 2.1. Ring closure synthesis of cyclic carbonate and subsequent ROP

Polycarbonates are of particular interest in both biomedical and commercial applications not only as a result of their low toxicity, biocompatibility and tunable degradability, but also to the fact that a wide variety of diol precursors can be inexpensively sourced.[7,8] A further reason for a recent interest in these materials is the ease in which functionality can be incorporated into the polymer *via* synthesis of monomers with specific functionalisations or post-polymerisation modifiable sites.[9-11]

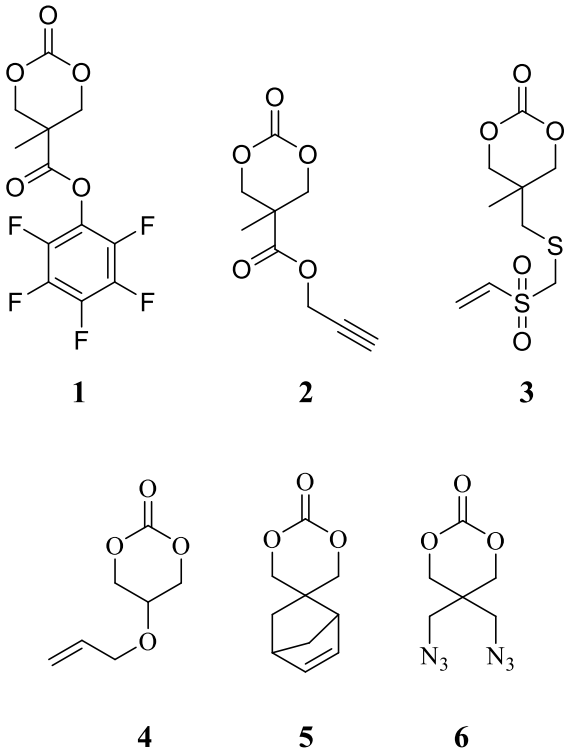

Figure 2.1. A range of functional carbonates; 1. pentafluorophenol,[12] 2. alkyne,[13] 3. allyl sulfonyl,[14] 4. allyl,[15] 5. norbornene,[16] 6. azide.[17]

Although the synthesis of functionalised monomers allow for the utilisation of more efficient small molecule-type reactions and purification, incorporation of certain modifications may hinder or even prevent polymerisation. In contrast, recent developments in coupling chemistries such as 'click' chemistry has allowed for the synthesis of a range of polymers which can incorporate otherwise unachievable functionalities such as multi-functional polymers for orthogonal modifications.[18] A wide range of efficient post-polymerisation modifications have been reported including the post-polymerisation modification of pentafluorophenyl ester, allyl, allyl sulfone, alkyne, azide and norbornene functionalised carbonates.

Herein we describe the synthesis and organocatalysed ROP of a spirocyclic carbonate monomer derived from pentaerythritol, containing a cleavable benzylidene pendant group.[19,20] Utilising the synthetic strategy employed in the synthesis of this previously synthesised monomer, we describe the synthesis and ROP of a novel norbornene-functional carbonate monomer and its potential for the synthesis of modifiable biomaterials *via* post-polymerisation modification.

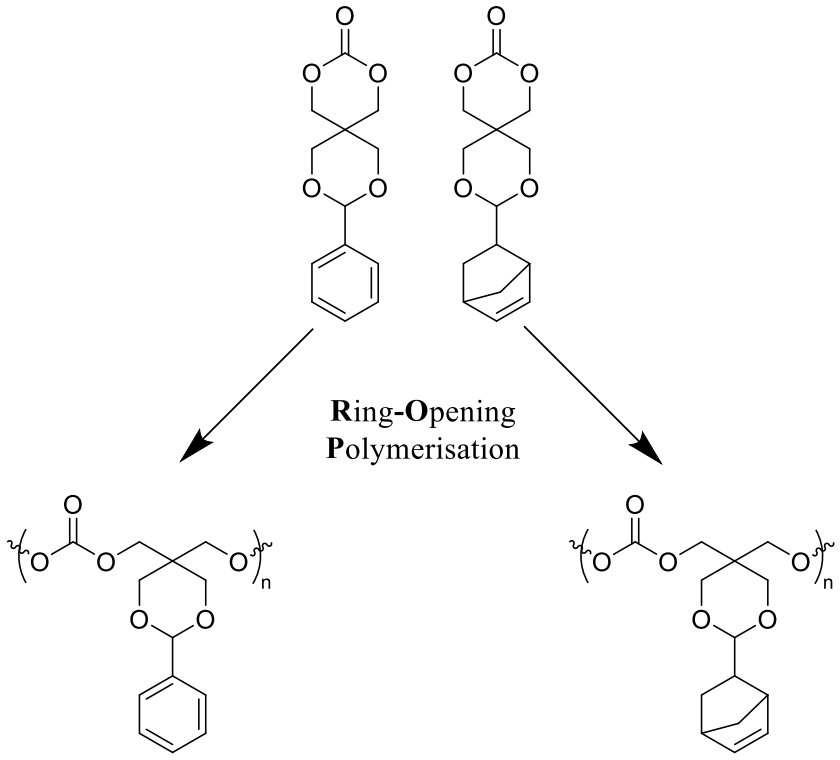

Scheme 2.2. Pentaerythritol-derived spirocyclic carbonate monomers: 9-phenyl-2,4,8,10-tetraoxaspiro[5, 5]undecan-3-one (PTO) (*left*), 9-norbornene-2,4,8,10-tetraoxaspiro[5, 5]undecan-3-one (NTC) (*right*) and corresponding homopolymers.

2.2 Results and Discussion

2.2.1 Synthesis and organocatalysed ROP of 9-phenyl-2,4,8,10-tetraoxaspiro[5, 5]undecan-3-one (PTO):

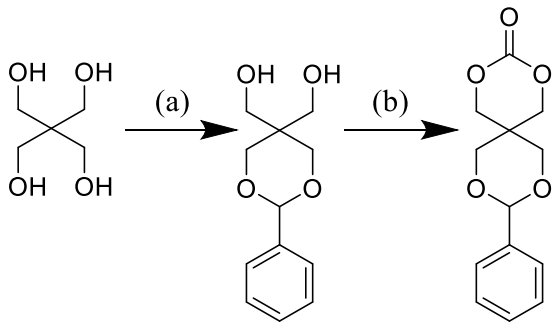

Scheme 2.3. Synthesis of PTO from pentaerythritol. (a) Benzaldehyde, HCl, deionised H_2O, 80 °C to 25 °C (b) Ethyl chloroformate, Et_3N, THF, 0 °C to 25 °C.

As has been previously reported, the acid-catalysed acetal formation between benzaldehyde and pentaerythritol and subsequent ring-closure of the resultant diol with ethyl chloroformate offers a facile and good yielding route to achieve functional cyclic carbonate monomers.[20,21] The use of deionised water (DI H_2O) as the reaction solvent allows for the synthesis of the mono-functionalised product exclusively. This is owed to the increased hydrophobicity of (2-phenyl-1,3-dioxane-5,5-diyl)dimethanol causing the diol to precipitate from solution at room temperature and preventing any further reaction. The diol was filtered and recrystallised from hot toluene to remove any excess benzaldehyde before the subsequent ring-closure with ethyl chloroformate. The conversion of the benzylidene acetal functional diol to the spirocyclic monomer was monitored by ^{1}H and ^{13}C NMR spectroscopy.

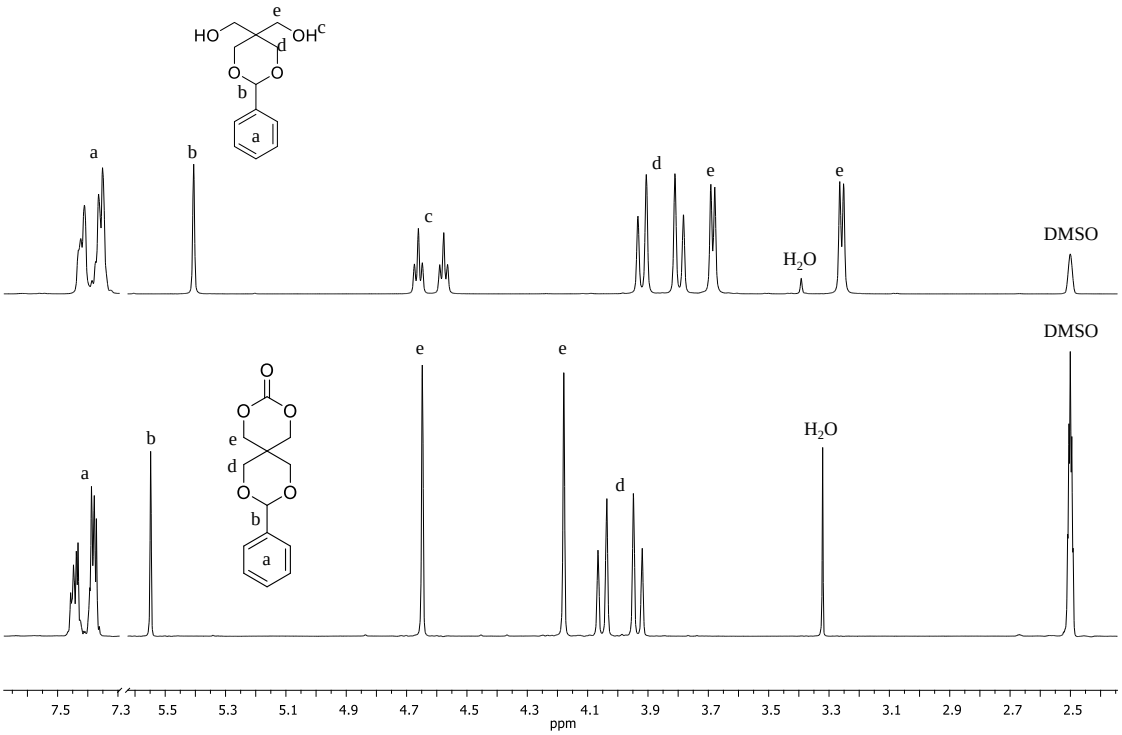

Figure 2.2. ^{1}H NMR spectra of the (2-phenyl-1,3-dioxane-5,5-diyl)dimethanol (*top*) and resultant PTO monomer (*bottom*). (400 MHz, 298 K, DMSO-d_6.)

The evolution of a multiplet at δ = 7.45–7.31 ppm and a singlet at δ = 5.40 ppm, attributed to the benzyl functionality and the methine adjacent to the acetal respectively, verify the successful modification of the pentaerythritol. This is further confirmed by the presence of two triplets at δ = 4.57 and 4.66 ppm attributed to the protons of the diol hydroxyl groups. The conversion of the diol to the cyclic carbonate monomer was verified by the shift and collapse of two doublets into singlets, attributed to the methylene groups adjacent to the hydroxyl functionality, from δ = 4.68 and 3.25 ppm to δ = 4.64 and 4.17 ppm. This shift is attributed to the conversion from a diol to carbonate functionality. In conjunction with the retention of the benzylidene acetal signals and the loss of the triplets attributed to the diol, this is indicative of the monomer formation (Figure 2.2).

The complete conversion of the diol to the monomer can also be determined by ^{13}C NMR spectroscopy through the shift of the signals attributed to the carbons adjacent to the diol from δ = 59.48 and 60.97 ppm to δ = 69.88 and 70.61 ppm when converted to the carbonate. Furthermore, the appearance of a singlet at δ = 147.63 ppm attributed to the carbonyl carbon is indicative of successful monomer synthesis.

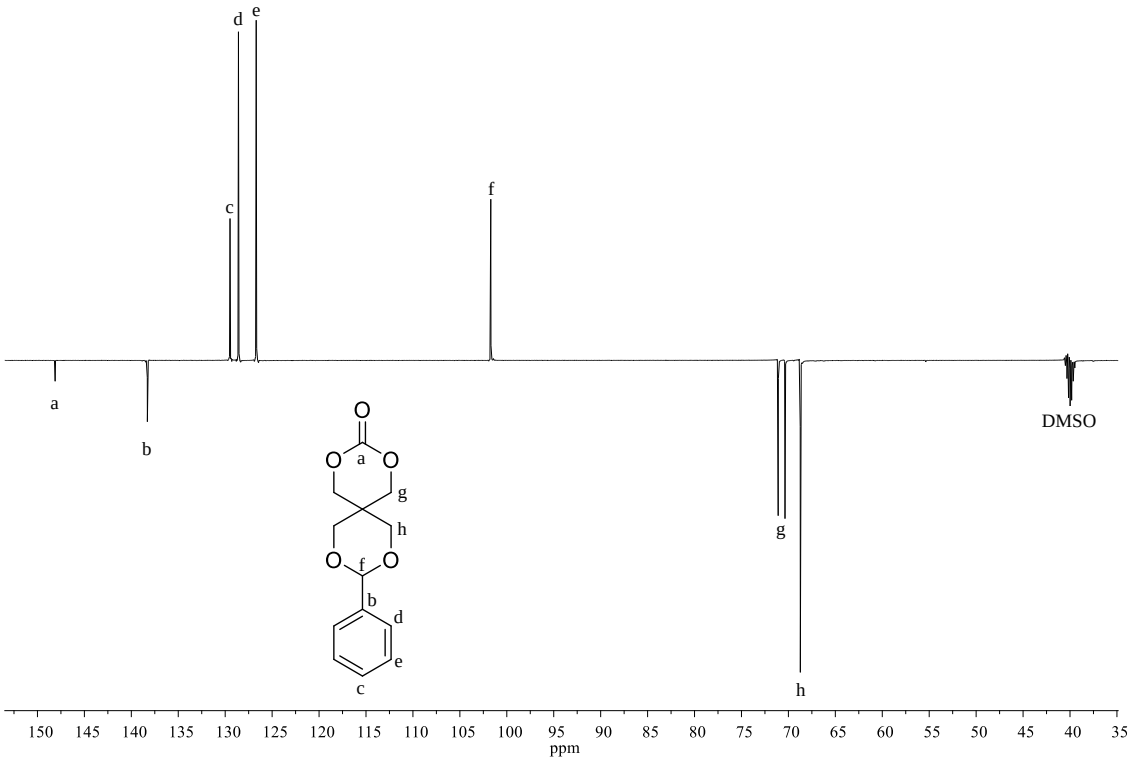

Figure 2.3. ^{13}C APT (attached proton test) NMR spectrum of PTO. (125 MHz, 298 K, DMSO-d_6.)

The ROP of PTO, initiated from benzyl alcohol (BnOH) in deuterated chloroform ($CDCl_3$) at ambient temperature (25 °C), was catalysed utilising the previously reported binary organocatalytic system of 1,8-diazabicyclo[5.4.0]undec-7-ene (DBU) and 1-(3,5-bis(trifluoromethyl)phenyl)-3-cyclohexylthiourea (TU) at catalyst loadings of 1 and 5 mol% respectively. This allowed for the synthesis of well-defined linear polycarbonates which displayed low dispersities ($Đ_M$ = 1.09-1.19) at a range of degrees of

polymerisation (DP) (10, 20, 50 100, 250), indicative of minimal side reactions, such as transesterification, occurring during the ROP (Table 2.1, Figure 2.4).

The conversion of the monomer to polymer (PPTO) was monitored by ^{1}H NMR spectroscopy exploiting the shift from δ = 5.42 to 5.35 ppm of the proton adjacent to the acetal when polymerised (Figure 2.5). The number-average molecular weight (M_n), obtained by size exclusion chromatography (SEC), was plotted against percentage monomer conversion, determined by ^{1}H NMR spectroscopy, and was found to progress in a linear fashion which is indicative of 'living' chain growth (Figure 2.4). Furthermore, the ring-opening polymerisation of PTO was found to exhibit first order kinetics, characteristic of this polymerisation technique (Figure 2.6).

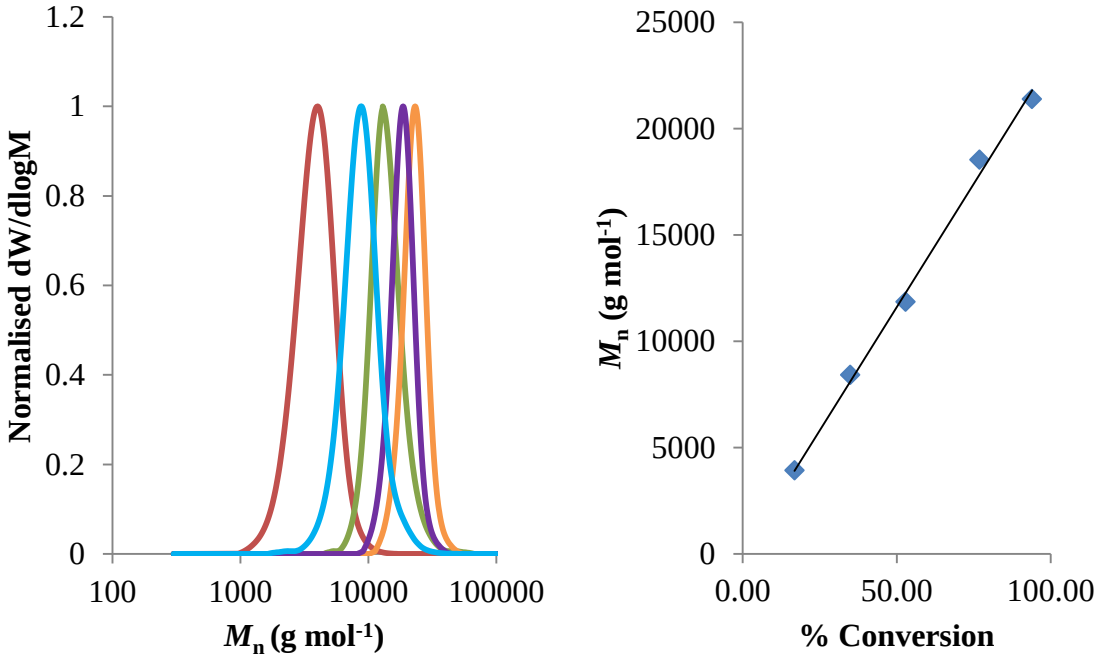

Figure 2.4. SEC RI chromatograms of PPTO in $CHCl_3$ against poly(styrene) (PS) standards, initiated from benzyl alcohol ($[M]_0/[I]_0$ = 100), conversion over time (*left*). Percentage conversion, obtained *via* ^{1}H NMR spectroscopy, versus molecular weight (M_n), obtained *via* SEC (*right*).

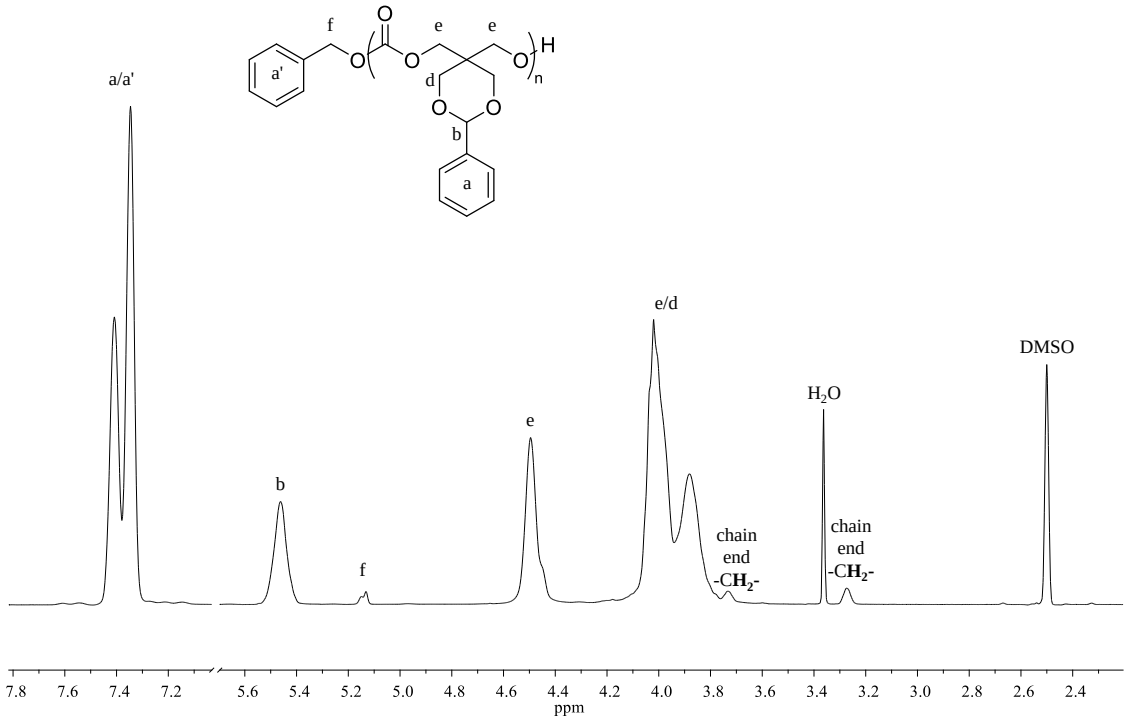

Figure 2.5. ^{1}H NMR spectrum of PPTO (DP20) initiated from benzyl alcohol. (400 MHz, 298 K, DMSO-d_6.)

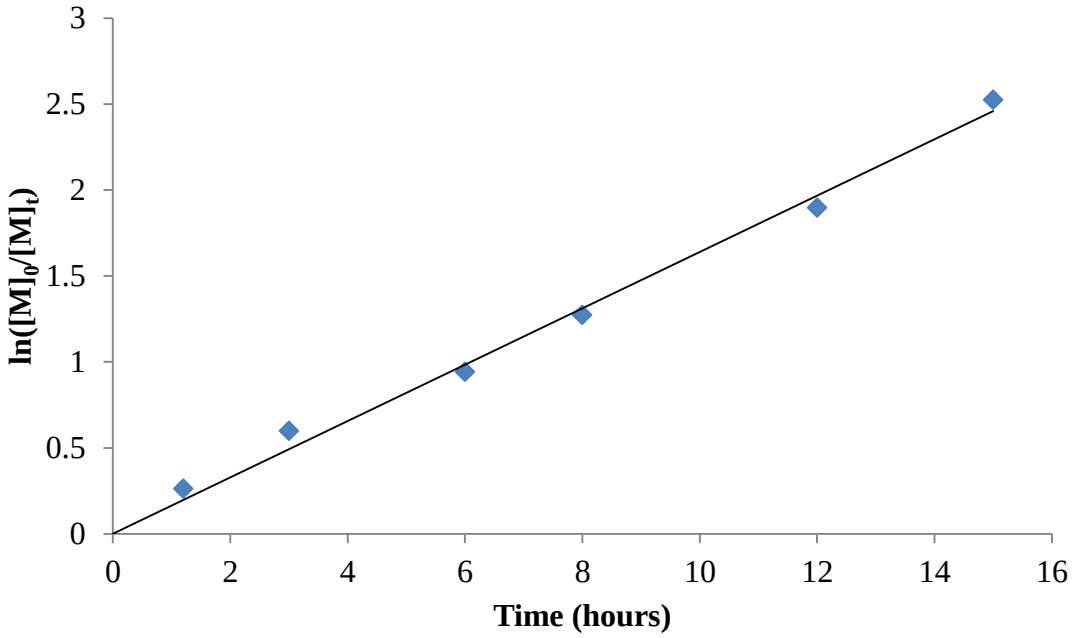

Figure 2.6. First-order linear fits of the kinetic data for the DBU/TU catalysed ROP of PTO initiated from benzyl alcohol ($[M]_0/[I]_0 = 100$).

The utilisation of a silica 'plug' for polymer purification offered a facile method for the complete removal of the basic organocatalysts and residual monomer without acid-quenching which may catalyse acetal-cleavage. The polymer was loaded onto the silica using CH_2Cl_2 as the eluent, removing residual monomer and TU (R_f = 0.8 and R_f = 0.9 respectively), before switching the eluent to ethyl acetate to recover the polymer (R_f = 0.9) whilst the DBU remained on the silica (R_f = 0). The polymer was recovered from solution *in vacuo* and displayed no observable degradation or acetal cleavage. (Figure 2.5).

Table 2.1. PPTO homopolymer data as determined by SEC and ^{1}H NMR spectroscopy

$[M]_0/[I]_0$	Monomer Conversion[a] (%)	$M_{n\text{-theory}}$ (kg mol^{-1})	$M_{n\text{-NMR}}$[a] (kg mol^{-1})	$M_{n\text{-SEC}}$[b] (kg mol^{-1})	$Đ_M$[b]
10	98	2.6	2.5	2.1	1.19
20	94	5.1	4.8	4.2	1.17
50	91	12.6	11.5	10.5	1.12
100	93	25.1	23.4	21.1	1.09
250	89	62.6	55.7	50.8	1.10

[a] Determined by ^{1}H NMR spectroscopy [b] Determined by SEC analysis in $CHCl_3$ against PS standards

2.2.2 Synthesis and organocatalysed ROP of 9-norbornene-2,4,8,10-tetraoxaspiro[5, 5]undecan-3-one (NTC):

Employing the method described in the synthesis of PTO, 5-norbornene-2-carboxaldehyde was utilised in the synthesis of a norbornene functional spirocyclic carbonate monomer. As previously demonstrated, the mono functionalised pentaerythritol was obtained as a precipitate from DI H_2O and recrystallized from hot toluene. The synthesis of (2-(norbornene)-1,3-dioxane-5,5-diyl)dimethanol (NTD) was verified by ^{1}H NMR spectroscopy by the presence of a series of signal between δ = 3.00 ppm and 0.60 ppm, attributed to the saturated norbornene hydrocarbons. Furthermore, the presence of two multiplets at δ = 6.17 ppm and 5.94 ppm confirms the retention of the norbornene alkene functionality (Figure 2.7).

As noted in the synthesis of PTO, the successful ring closure of (2-(norbornene)-1,3-dioxane-5,5-diyl)dimethanol was verified by the shift of the methylene signals adjacent to the hydroxyl functionalities from δ = 3.12 and 3.54 ppm to δ = 4.06 and 4.50 ppm in conjunction with the complete loss of the triplets at δ = 4.40 and 4.52 ppm attributed to the hydroxyl proton (Figure 2.5). Synonymously to PTO, utilising ^{13}C NMR spectroscopy, a singlet attributed to the carbonyl carbon of the carbonate functionality can be observed at δ = 147.63 ppm, in conjunction with a shift of the signals attributed to the carbons adjacent to the hydroxyl groups, from δ = 59.57 ppm and 61.02 ppm to δ = 69.86 ppm and 70.7 ppm, upon conversion to the carbonate. Furthermore, the formation of the spirocyclic carbonate monomer can be verified by Fourier-transform infra-red (FT-IR) spectroscopy, through the loss of the hydroxyl absorbance band at ~ 3300 cm^{-1} in conjunction with the evolution of an absorbance band at ~ 1730 cm^{-1} attributed to the carbonate carbonyl absorbance frequency (Figure 2.8).

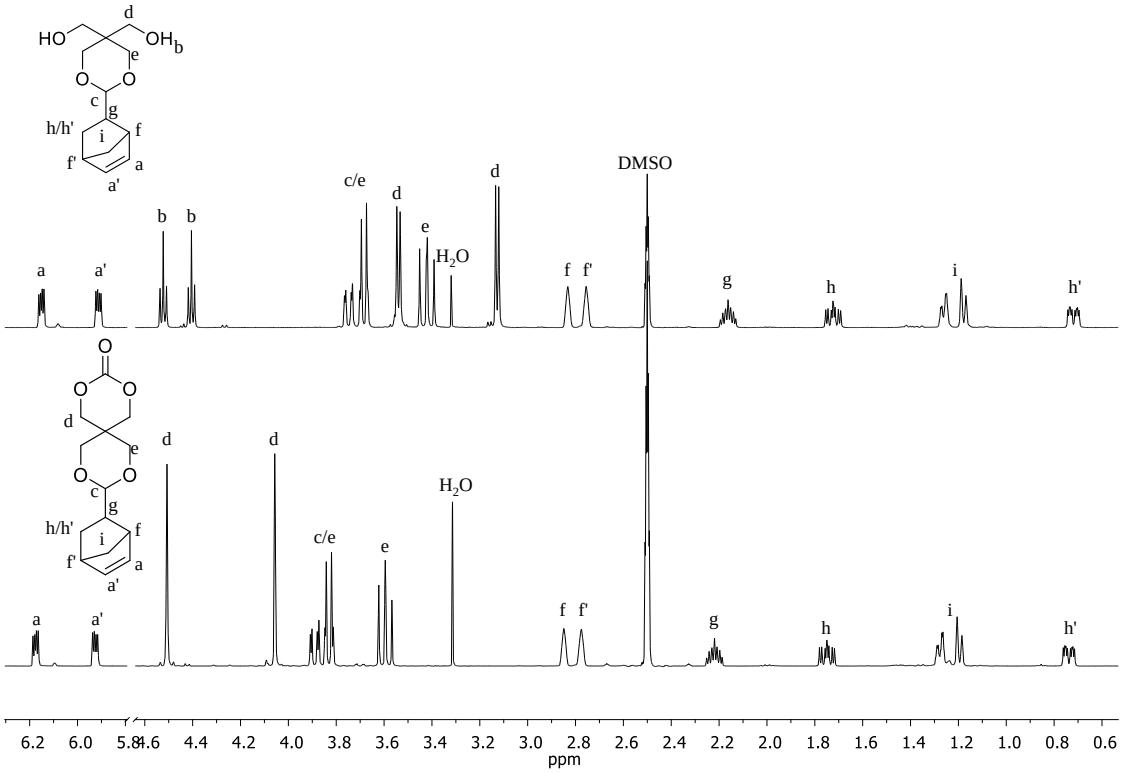

Figure 2.7. ^{1}H NMR spectrum of (2-(norbornene)-1,3-dioxane-5,5-diyl)dimethanol (NTD) (*top*) and 9-norbornene-2,4,8,10-tetraoxaspiro[5,5]undecan-3-one (NTC) (*bottom*). (400 MHz, 298 K, DMSO-d_6.)

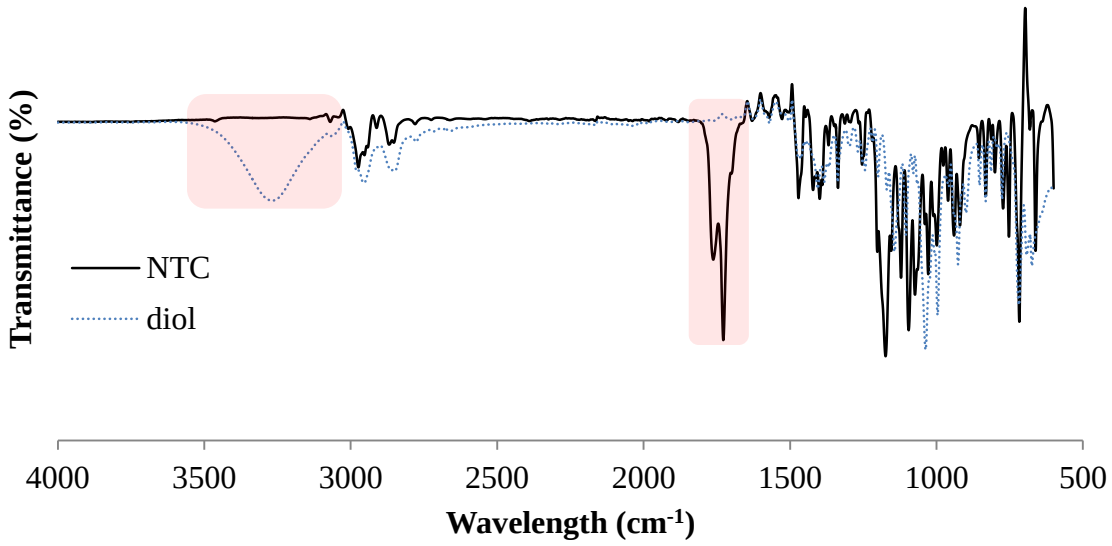

Figure 2.8. FT-IR spectrum of NTC and NTD.

The organocatalysed ROP of NTC was conducted using the conditions described in the synthesis of PPTO. It was found that the M_n *vs* percentage monomer conversion followed a linear trend and the resultant polymers displayed low dispersities ($Đ_M$ = 1.09-1.19) at a range of degrees of polymerisation (DP) (10, 20, 50 100, 250) (Table 2, Figure 2.9). Furthermore, as seen with PTO, the ring-opening polymerisation of NTC exhibited first order kinetics (Figure 2.10). The presence of the side-group functionality after polymerisation was verified by ^{1}H NMR spectroscopy by the retention of the characteristic norbornene alkene peaks at δ = 5.94 and 6.17 ppm in conjunction with a series of signals between δ = 0.60 and 3.00 ppm (Figure 2.11).

Table 2.2. PNTC homopolymer data as determined by SEC and ^{1}H NMR spectroscopy

$[M]_0/[I]_0$	Monomer Conversion[a] (%)	$M_{n\text{-theory}}$ (kg mol^{-1})	$M_{n\text{-NMR}}$[a] (kg mol^{-1})	$M_{n\text{-SEC}}$[b] (kg mol^{-1})	$Đ_M$[b]
10	98	2.8	2.7	2.5	1.20
20	95	5.4	5.2	4.9	1.14
50	92	13.4	12.4	11.5	1.10
100	91	26.7	24.3	22.4	1.08
250	87	66.6	58.0	52.2	1.05

[a] Determined by ^{1}H NMR spectroscopy [b] Determined by SEC analysis in $CHCl_3$ against PS standards

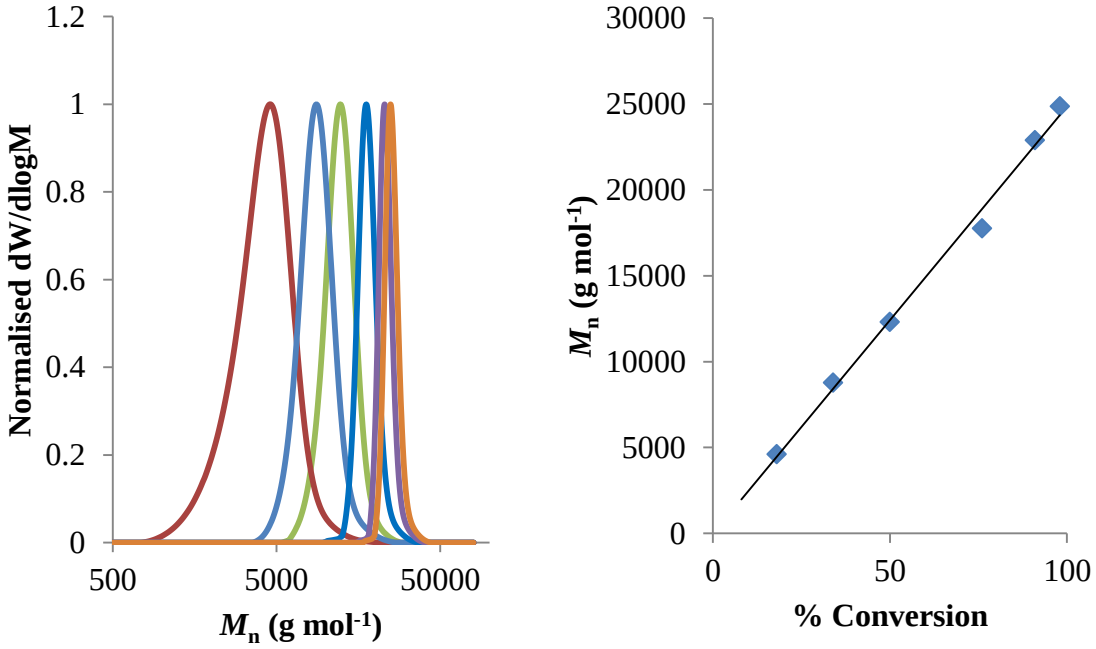

Figure 2.9. SEC RI chromatograms of PNTC in $CHCl_3$ against PS standards, initiated from BnOH ($[M]_0/[I]_0$ = 100), conversion over time (*left*). Percentage conversion, obtained *via* ^{1}H NMR spectroscopy, versus molecular weight (M_n), obtained *via* SEC (*right*).

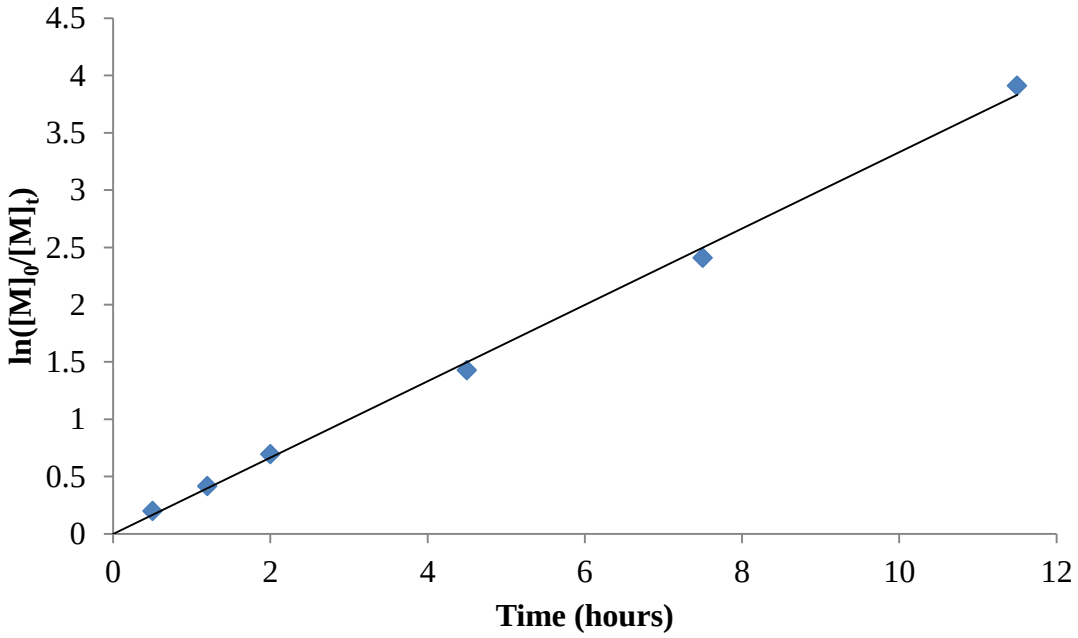

Figure 2.10. First-order linear fits of the kinetic data for the DBU/TU catalysed ROP of NTC initiated from benzyl alcohol ($[M]_0/[I]_0 = 100$).

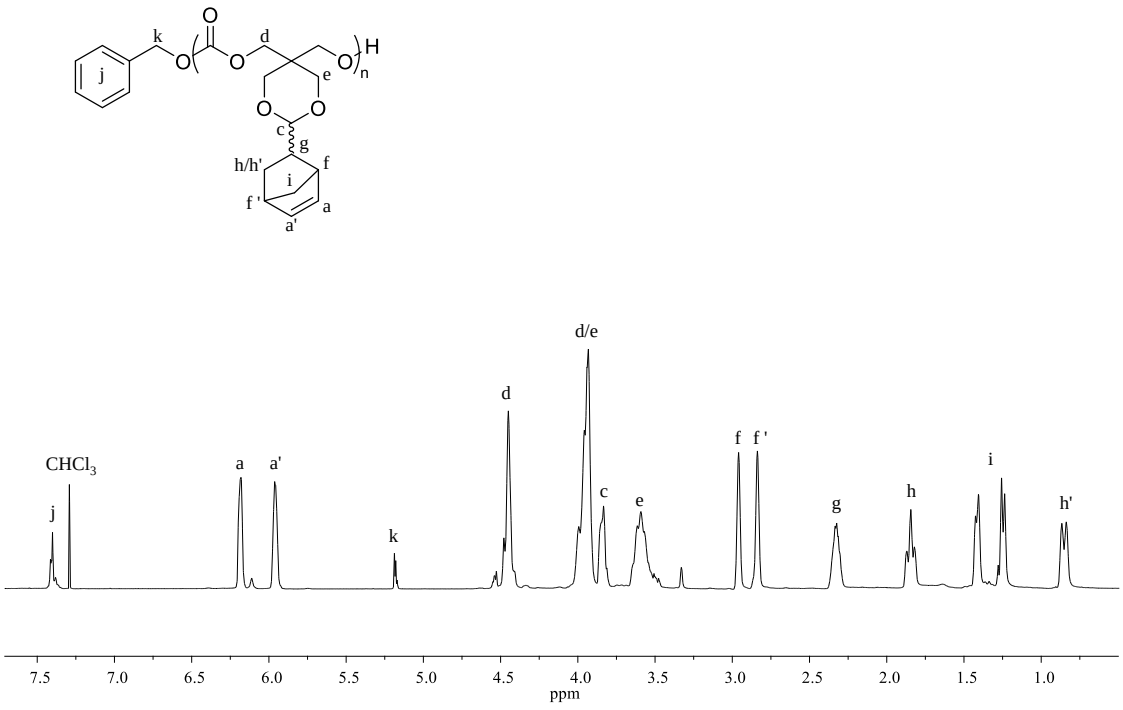

Figure 2.11. ^{1}H NMR spectrum of poly(NTC) (PNTC) (DP10) initiated from benzyl alcohol. (400 MHz, 298 K, $CDCl_3$).

Analysis of PNTC (DP10) by matrix assisted laser desorption ionisation time-of-flight mass spectrometry (MALDI-ToF MS) was also employed to confirm the retention of the norbornene functionality (Figure 2.12). It was noted that only a single distribution, with a spacing of m/z = 266.12 between neighbouring peaks, was observed. This distribution corresponds to the benzyl alcohol initiated PNTC exclusively without any cleavage of the acetal side group.

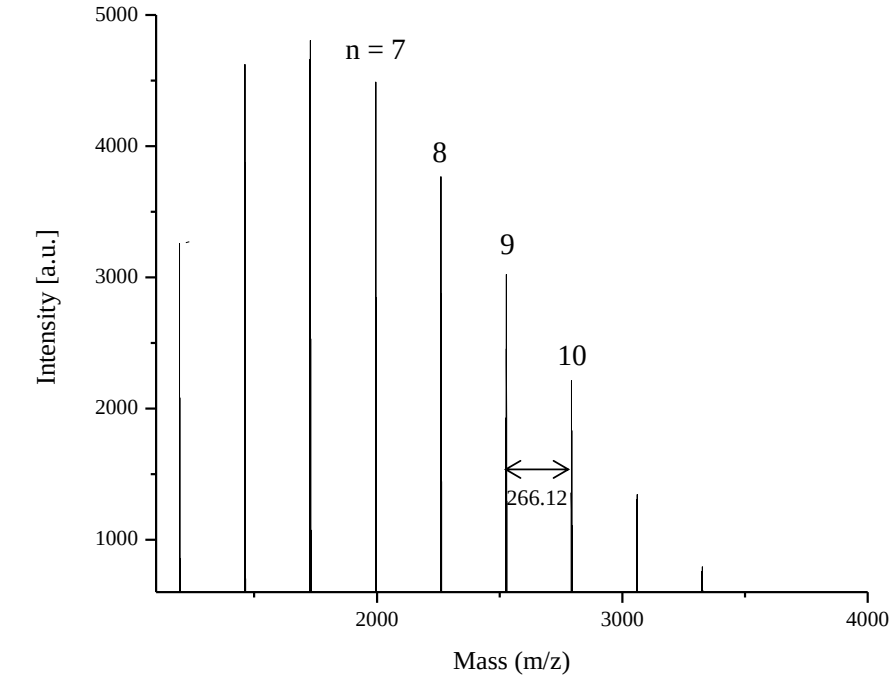

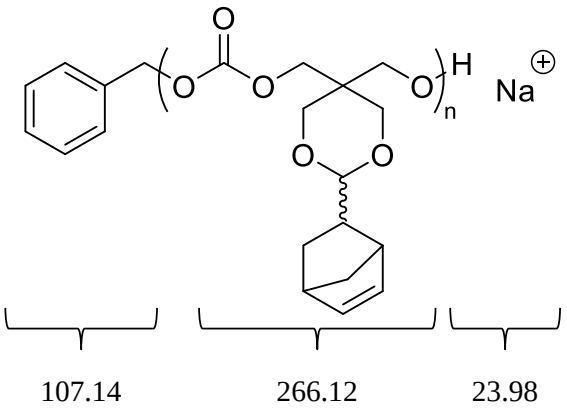

n	Calc. m/z	Exp. m/z
7	1992.96	1992.80
8	2259.08	2259.90
9	2526.20	2525.91
10	2791.32	2791.55

Figure 2.12. MALDI-ToF mass spectrum of PNTC (DP10) initiated from benzyl alcohol.

2.2.3 Post-polymerisation modification of PNTC:

As has been extensively reported, norbornene moieties are prone to a number of conjugation reactions such as halide addition, cycloadditions, thiol-ene additions, hetero Diels−Alder reactions *etc*.[22,23,24]

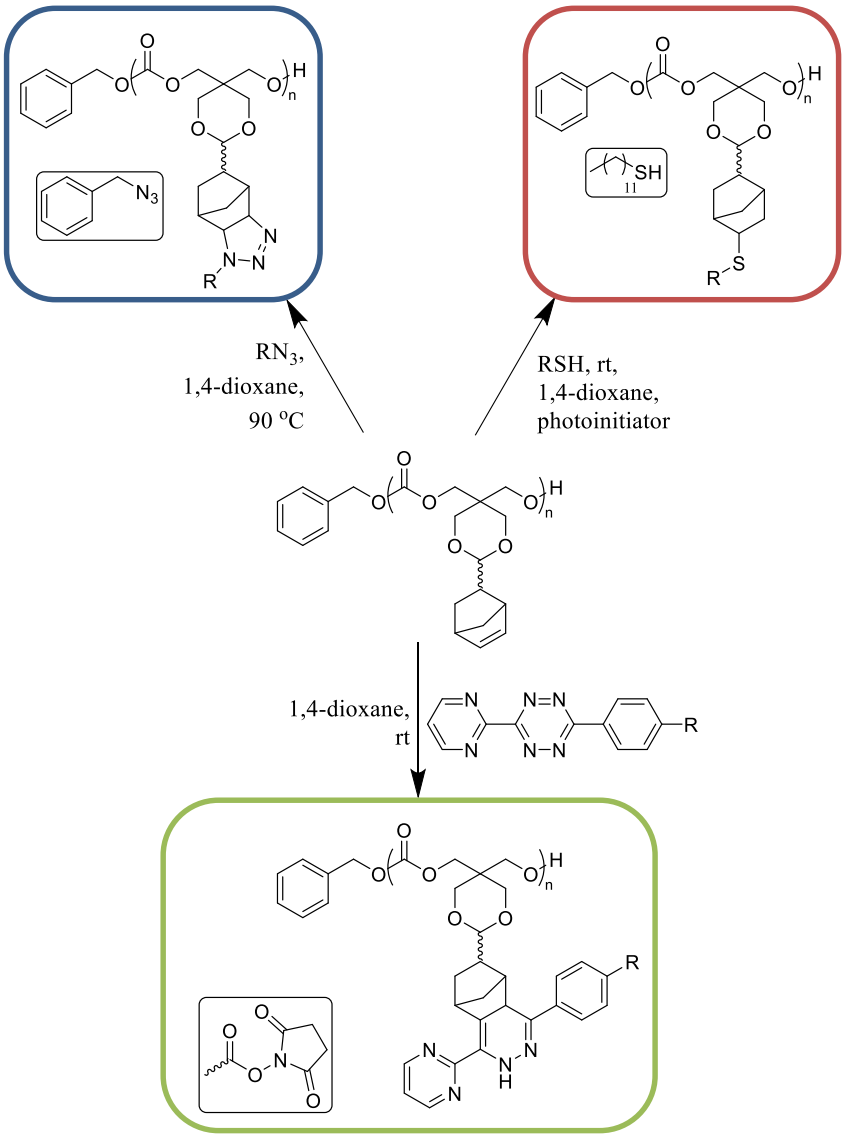

Scheme 2.4. Post-polymerisation modification of PNTC; 1,3-dipolar cycloaddition (*blue*), radical thiol addition (*red*), DA_{inv} (*green*).

As such, the post-polymerisation modification of norbornene containing polymers has been of great interest recently. In order to exhibit its versatility, PNTC (DP20) was modified *via* a 1,3-dipolar cycloaddition with benzyl azide, an inverse electron demand Diels−Alder (DA_{inv}) reaction with 2,5-dioxopyrrolidin-1-yl 6-(6-(pyrimidin-2-yl)-1,2,4,5-tetrazin-3-yl)benzoate and the photoinduced radical thiol addition with 1-dodecanethiol (Scheme 2.4). Owing to its efficiency and mild conditions, 2,2-dimethoxy-2-phenylacetophenone photoinitiator was used as the radical source for the radical thiol addition in place of thermal initiators (*i.e.* azobisisobutyronitrile (AIBN)). The 1,3-dipolar cycloaddition and the DA_{inv} proceeded with no catalyst or initiator required.

Subsequent to functionalisation, each polymer was precipitated in triplicate to remove any unreacted small molecules before being analysed by SEC and ^{1}H NMR spectroscopy. ^{1}H NMR spectroscopy revealed the complete consumption of the norbornene alkene functionality at δ = 5.94 and 6.17 ppm and the appearance of characteristic signals attributed to each modification (*Benzyl azide*; δ = 7.34 and 4.90 ppm. *Dodecanethiol*; δ = 1.35 and 0.85 ppm. *Tetrazine*; δ = 9.37-7.12 and 2.88 ppm) indicative of the successful modification of PNTC (Figure 2.13).

In agreement with previous results, it was found that the number average molecular weight by SEC of each modified polymer was found to increase with no significant change in the dispersities ($Đ_M$ = 1.14-1.12). This is indicative of the controlled nature of the modifications with minimal to no adverse side reactions *i.e.* backbone degradation, chain-chain coupling *etc.* (Figure 2.16). It was noted, however, that there were some variances in the $M_{n\text{-theory}}$ and the M_n by SEC. It is hypothesised that this is owed to changes in the hydrodynamic volume of the functionalised polymers through interactions with the $CHCl_3$ eluent (Table 3).

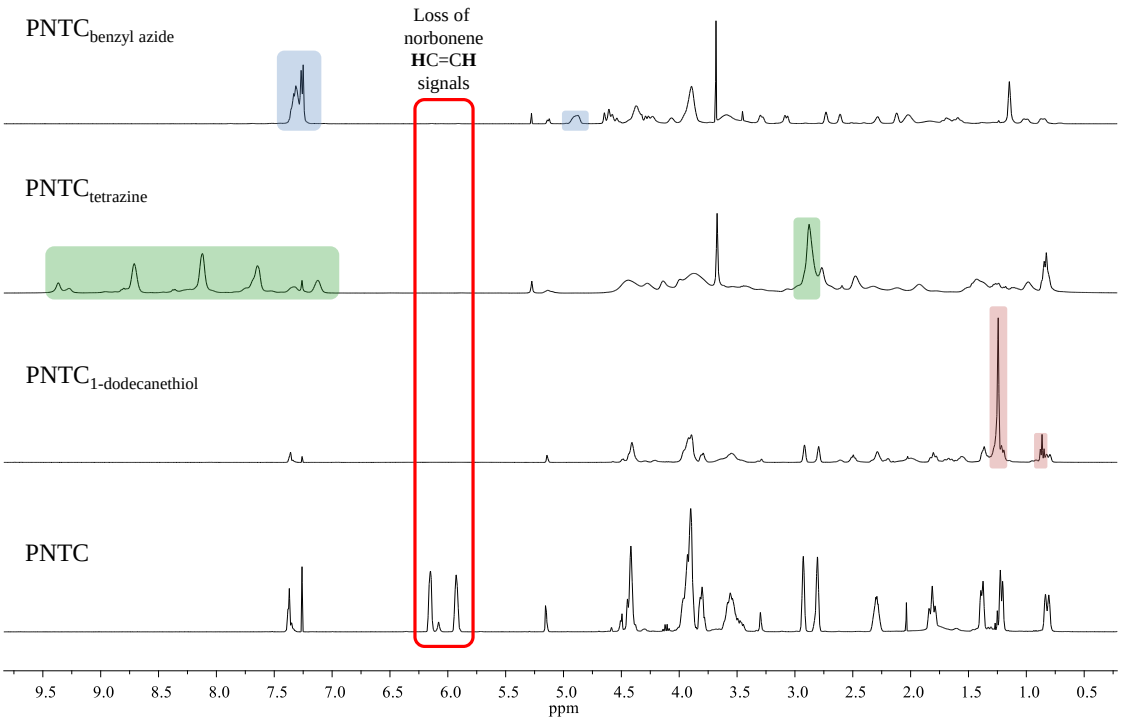

Figure 2.13. ^{1}H NMR spectra PNTC (DP20) (*bottom*), thiol functionalised (*red*), tetrazine functionalised (*green*) and azide functionalised (*blue*) PNTCs (DP20). (400 MHz, 298 K, $CDCl_3$)

Table 2.3. Comparison of molecular weights of modified PNTC (DP20).

Modification	$M_{n\text{-theory}}$ (kg mol^{-1})	$M_{n\text{-SEC}}$[a] (kg mol^{-1})	$M_{n\text{-NMR}}$[b] (kg mol^{-1})	$Đ_M$[a]
-	5.4	5.2	5.2	1.14
Benzyl azide	8.1	6.5	8.0	1.14
1-dodecanethiol	9.4	7.3	-	1.12
Tetrazine	12.9	6.9	12.8	1.13

[a] Determined by SEC analysis in $CHCl_3$ against PS standards. [b]Determined by ^{1}H NMR spectroscopy.

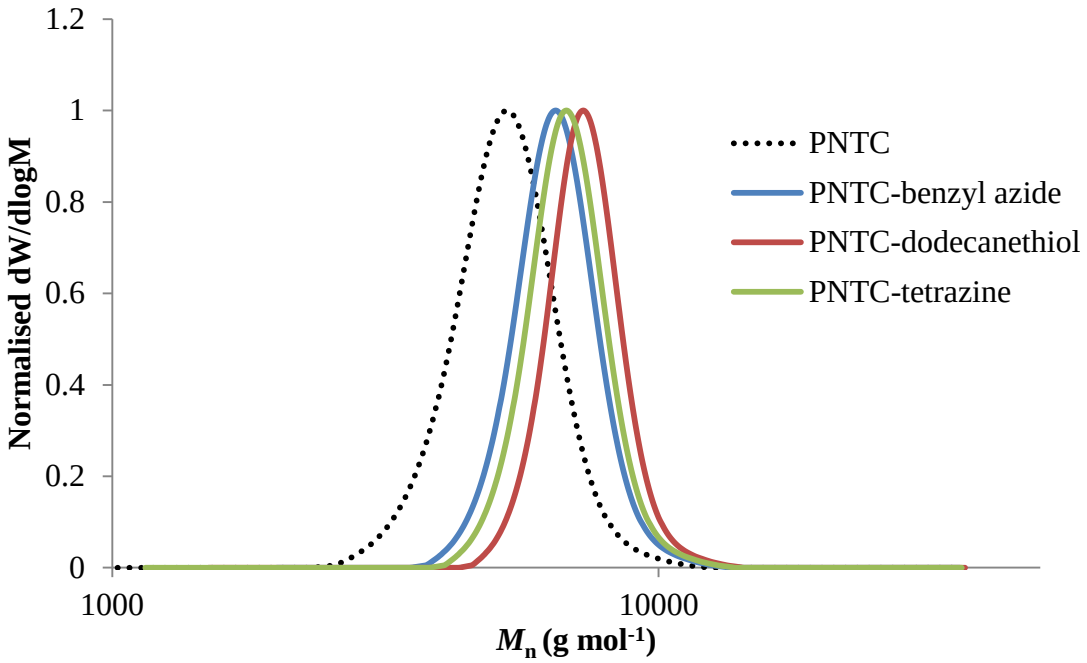

Figure 2.14. RI SEC chromatograms of functionalised PNTC (DP20) in $CHCl_3$ against PS standards.

As has been extensively reported in literature,[25-27] the susceptibility of acetal bonds to acid catalysed scission has been employed in synthesis of degradable/stimuli responsive polymers. As such, modified PNTCs were subjected to acidic conditions (pH 5) overnight in order to determine the 'release' capabilities of these functional polycarbonates. As expected, the SEC chromatograms revealed a significant reduction in the molecular weight (M_n) of each modified polymer with an increase in the dispersities ($Đ_M$ = 1.23-1.27). Interestingly, however, it was noted the cleaved polymers exhibited comparable molecular weights (M_n = 4.1-4.7 kg mol^{-1}), which may be indicative of complete cleavage (Figure 2.15).

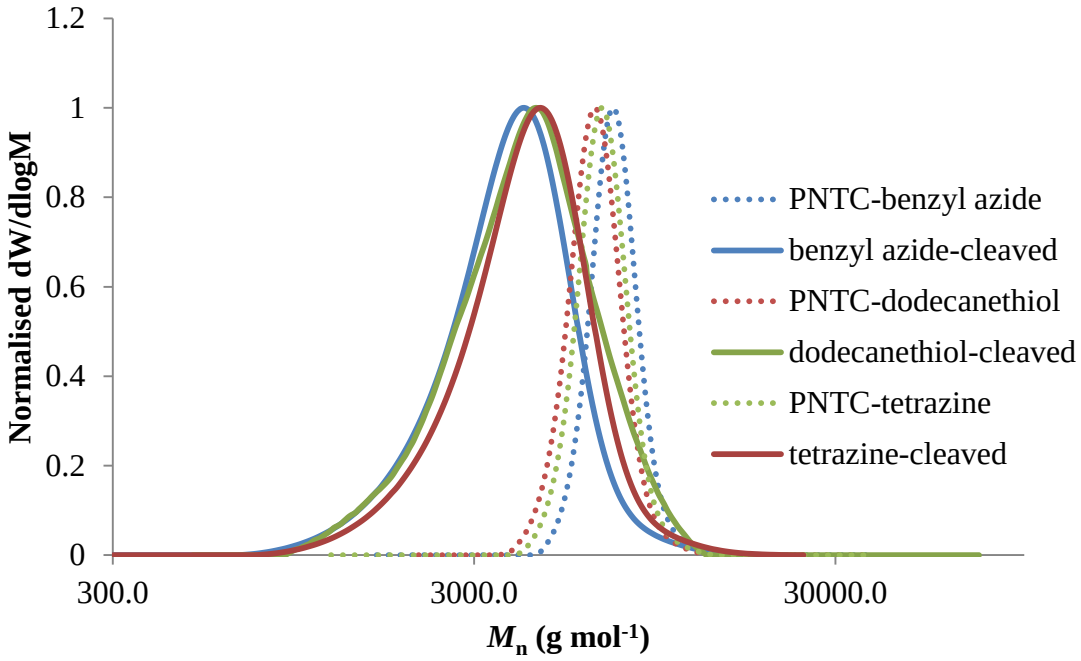

Figure 2.15. RI SEC chromatograms of modified PNTCs and resultant polymers after being subjected to acidic conditions. SEC experiments in $CHCl_3$ against PS standards.

2.2.4 Synthesis and self-assembly of PNTC-based graft copolymers:

In order to further assess the acid catalysed acetal cleavage, in conjunction with exhibiting the versatility of PNTC, 3-mercaptopropionate functionalised poly(ethylene glycol) monoether (M_n = 550 g mol^{-1}) (PEG_{550}-SH) was grafted to PNTC (DP20) using the method described in the radical thiol addition of 1-dodecanethiol. As with the 1-dodecanthiol addition, it was found by ^{1}H NMR spectroscopy and SEC that full grafting was achieved (Figure 2.16-2.17). The amphiphilic graft copolymer PNTC-*g*-PEG_{550} was subsequently self-assembled *via* direct dissolution in DI H_2O and analysed by multi-angle light scattering (static light scattering (SLS) and dynamic light scattering (DLS)) and transmission electron microscopy (TEM).

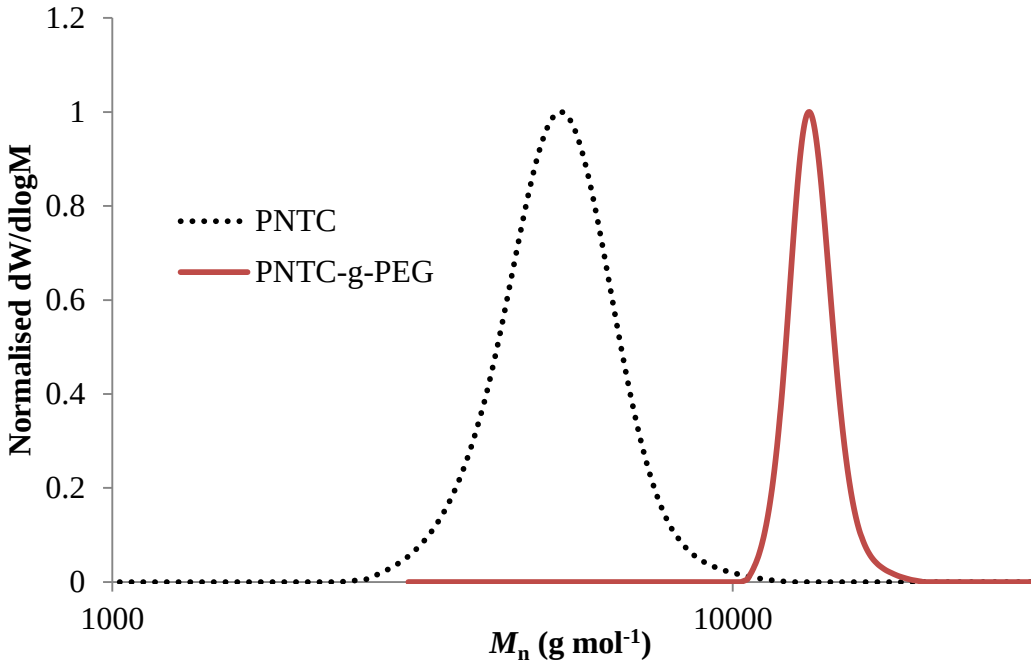

Figure 2.16. RI SEC chromatograms of PNTC (DP20) and resultant graft copolymer PNTC-*g*-PEG$_{550}$ in $CHCl_3$ against PS standards.

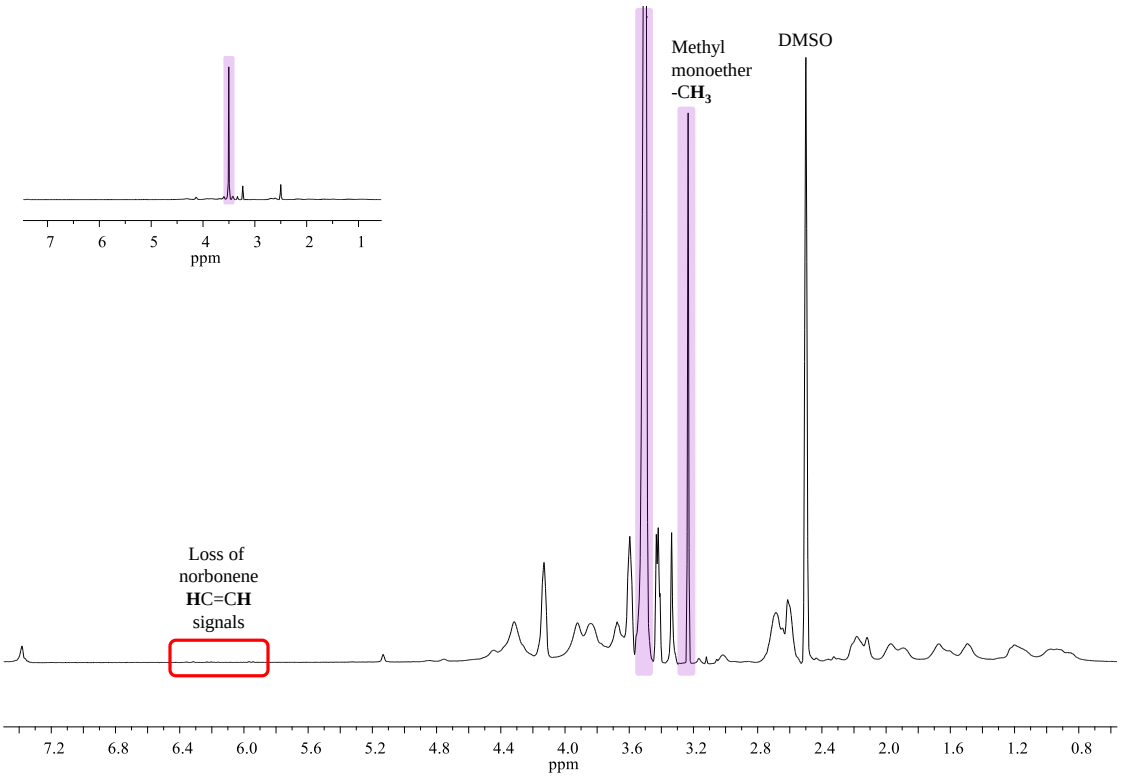

Figure 2.17. ^{1}H NMR spectrum and expansion of PNTC-*g*-PEG$_{550}$. (400 MHz, 298 K, DMSO-d_6).

The combination of DLS and SLS indicated the formation of polymeric particles with a hydrophobic core of PNTC and a hydrophillic PEG_{550} corona. It was found by DLS that the PNTC-*g*-PEG_{550} copolymers self-assembled into nano-structures, by direct dissolution in DI H_2O at a concentration of 1 mg/mL, with a diameter of 5.8 nm, while SLS revealed an aggregation number of approximately 30. Furthermore, it is important to note that a second minor distribution attributed to a larger species was also present. However, as has been previously reported, this is an artefact of particle-particle interactions (*i.e.* spurious aggregates) rather than the formation of larger structures.[28] This was demonstrated by the addition of a salt (NaCl, 2 mg/mL), in order to act as a buffer, which resulted in the complete removal of the larger structures with no effect on the size of the smaller nano-structures (Fig. 2.19).

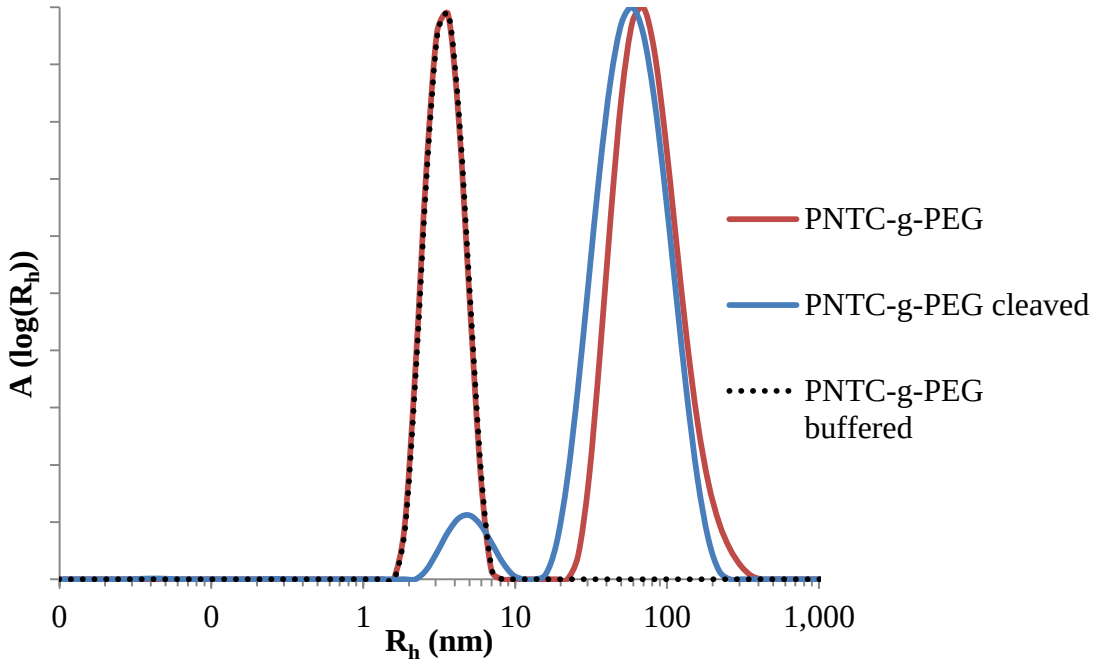

Figure 2.18. Representative size distributions of self-assembled PNTC-*g*-PEG_{550} in H_2O at a concentration of 1 mg mL^{-1} from SLS (θ = 130°).

In agreement with the DLS data, the TEM analysis of the particles revealed the presence of particles with a diameter of 9 nm. Furthermore, the absence of larger aggregates confirms the anomalies found in DLS being attributed to spurious aggregate artefacts.

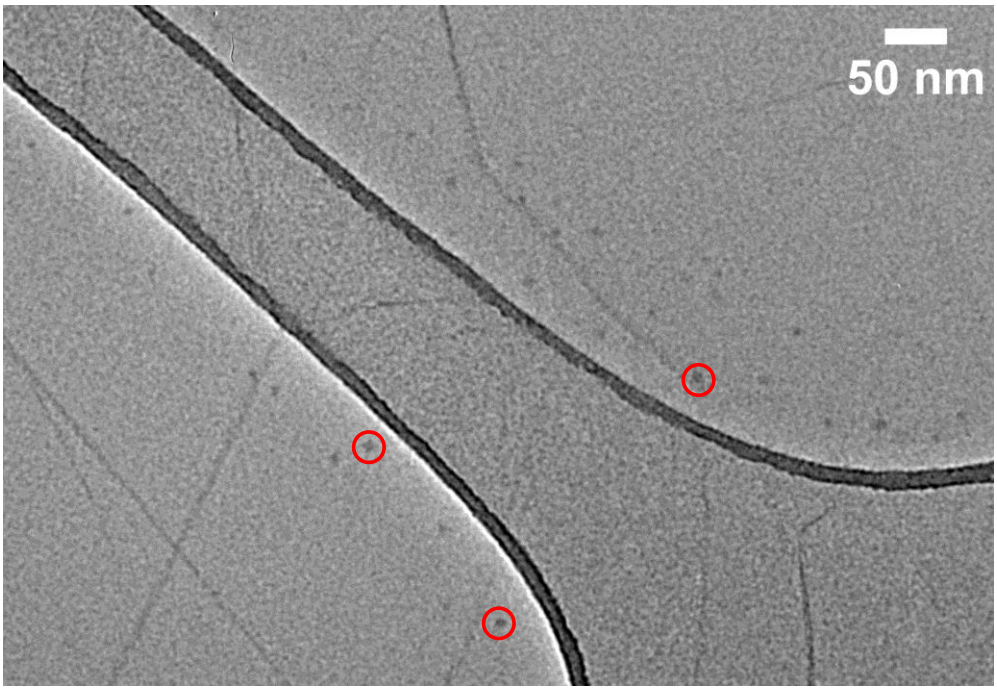

Figure 2.19. Representative TEM image of PNTC-PEG$_{550}$ nano-structures on a graphene oxide grid. (Scale bar: 50 nm)

After self-assembly in DI H_2O, PNTC-*g*-PEG$_{550}$ nano-structure solutions were acidified to pH 5 and analysed by SLS (θ = 130°) in order to determine structural decay of the nano-strucure during acid catalysed acetal scission. It was found after 12 h, that the diameter of the particles remained relatively unchanged (d = 7.0 ±0.7 nm), however, there was a severe reduction in the aggregation number ($N_{agg} \approx 4$). This is indicative of the reduction in molecular weight of the self-assembled structure by through the acid-catalysed cleavage of the PEGylated norbonene acetal (Figure 2.18).

2.3 Conclusion

In conclusion, pentaerythritol, through the acid catalysed acetal formation and subsequent ring closure reaction with ethyl chloroformate, was shown to be an excellent platform in the synthesis of novel functional spirocyclic carbonate monomers. Furthermore, the binary organocatalyst system of DBU/TU could be employed in the ROP of these monomers to produce well-defined polycarbonates with no adverse side reactions. As demonstrated from the study, PNTC offers an elegant route to decorated polymeric structures with potential stimuli responsive release applications. Furthermore, grafted copolymers of PNTC offer a facile method to produce nano-structure with triggered release applications.

2.4 References

1. O. Dechy-Cabaret, B. Martin-Vaca and D. Bourissou, *Chem. Rev.*, 2004, 104, 6147-6176.
2. R. J. Pounder and A. P. Dove, *Biomacromolecules*, 2010, 11, 1930–1939.
3. S. M. Guillaume, *Eur. Polym. J.*, 2013, 49, 768-779.
4. R. J. Pounder and A. P. Dove, *Polym. Chem.*, 2010, 1, 260.
5. Q. Yin, R. Tong, Y. Xu, K. Baek, L. W. Dobrucki, T. M. Fan and J. Cheng, *Biomacromolecules*, 2013, 14, 920-929.
6. J. Rodriguez-Hernández, M. Gatti and H. A. Klok, *Biomacromolecules*, 2003, 4, 249-258.
7. S. Dai, L. Xue and Z. Li, *ACS Catal.*, 2011, 1, 1421-1429.
8. Z. Zhang, R. Kuijer, S. K. Bulstra, D. W. Grijpma and J. Feijen, *Biomaterials*, 2006, 27, 1741-1748.
9. R. J. Williams, I. A. Barker, R. K. O'Reilly and A. P. Dove, *ACS Macro Lett.*, 2012, 1, 1285-1290.
10. S. Tempelaar, L. Mespouille, P. Dubois and A. P. Dove, *Macromolecules*, 2011, 44, 2084-2091.
11. S. Venkataraman, N. Veronica, Z. X. Voo, J. L. Hedrick and Y. Y. Yang, *Polym. Chem.*, 2013, 4, 2945-2948.
12. A. C. Engler, J. M. W. Chan, D. J. Coady, J. M. O'Brien, H. Sardon, A. Nelson, D. P. Sanders, Y. Y. Yang and J. L. Hedrick, *Macromolecules*, 2013, 46, 1283-1290.
13. T. h. Li, X. b. Jing and Y. b. Huang, *Polym. Adv. Technol.*, 2011, 22, 1266-1271.
14. R. Wang, W. Chen, F. Meng, R. Cheng, C. Deng, J. Feijen and Z. Zhong, *Macromolecules*, 2011, 44, 6009-6016.

15. P. G. Parzuchowski, M. Jaroch, M. Tryznowski and G. Rokicki, *Macromolecules*, 2008, 41, 3859-3865.

16. T. Takata, K. Amachi, K. Kitazawa and T. Endo, *Macromolecules*, 1989, 22, 3188-3190.

17. X. Zhang, Z. Zhong and R. Zhuo, *Macromolecules*, 2011, 44, 1755-1759.

18. R. K. Iha, K. L. Wooley, A. M. Nystrom, D. J. Burke, M. J. Kade and C. J. Hawker, *Chem. Rev.*, 2009, 109, 5620-5686.

19. Z. Xie, C. Lu, X. Chen, L. Chen, Y. Wang, X. Hu, Q. Shi and X. Jing, *J. Polym. Sci., Part A: Polym. Chem.*, 2007, 45, 1737-1745.

20. J. Xu, Z.-L. Liu and R.-X. Zhuo, *J. Appl. Polym. Sci.*, 2006, 101, 1988-1994.

21. L.-L. Mei, G.-P. Yan, X.-H. Yu, S.-X. Cheng and J.-Y. Wu, *J. Appl. Polym. Sci.*, 2008, 108, 93-98.

22. R. M. Desai, S. T. Koshy, S. A. Hilderbrand, D. J. Mooney and N. S. Joshi, *Biomaterials*, 2015, 50, 30-37.

23. C. C. Lin, C. S. Ki and H. Shih, *J. Appl. Polym. Sci.*, 2015, 132.

24. P. Espeel and F. E. Du Prez, *Macromolecules*, 2015, 48, 2-14.

25. E. M. Bachelder, T. T. Beaudette, K. E. Broaders, J. Dashe and J. M. J. Fréchet, *J. Am. Chem. Soc*, 2008, 103, 10494-10495.

26. K. Miao, W. Shao, H. Liu and Y. Zhao, *Polym. Chem.*, 2014, 5, 1191-1201.

27. A. E. Neitzel, M. A. Petersen, E. Kokkoli and M. A. Hillmyer, *ACS Macro Lett.*, 2014, 3, 1156-1160.

28. C. Chassenieux, T. Nicolai and D. Durand, *Macromolecules*, 1997, 30, 4952-4958.

3 Block copolymer thermoplastic materials from the organocatalysed ROP of pentaerythritol-derived spirocyclic carbonates

3.1 Introduction

As a result of their low toxicity, tunable biodegradability and biocompatibility, in conjunction with their versatile mechanical properties, both aliphatic polyester and polycarbonate homopolymers and copolymers have been of recent interests in the field of renewable biomaterials.[1-4] As a consequence of these distinct advantages over conventional aliphatic hydrocarbon-based polymers, these materials are excellent candidates in the production of biodegradable thermoplastics elastomers (TPEs) for biomedical applications.[5-9]

The utilisation of ring-opening polymerisations (ROP) of cyclic ester/carbonate monomers to achieve precisely-defined polymers employing organocatalysts, such as diphenyl phosphate (DPP), 1,5,7-triazabicyclo[4.4.0]dec-5-ene (TBD) or the dual-catalytic system of 1-(3,5-bis(trifluoromethyl)phenyl)-3-cyclohexylthiourea (TU) and 1,8-diazabicyclo[5.4.0]undec-7-ene (DBU) have been extensively studied in recent years.[10-14] As a consequence of their relatively low toxicity, mild reaction conditions, facile removal and reduced propensity for adverse side reactions in comparison to traditional metal-based catalysts, organocatalysts have facilitated the advancement of ROP for the synthesis of well-defined polyester-carbonates for biomedical applications.[15-19]

As has been described in chapter 1, aliphatic polyesters have been extensively synthesised from the ROP of a vast range of readily available cyclic esters such as lactide (LA), ε-caprolactone (ε-CL), δ-valerolactone (δ-VL) *etc*. Whilst this range of monomers allows for the modulation of physio-chemical properties such as phase transition temperatures, toughness, stiffness and degradability, homopolyesters have

been shown to display relatively poor mechanical properties *i.e.* low percentage elongations, inelasticity, brittleness *etc*.[20,21]

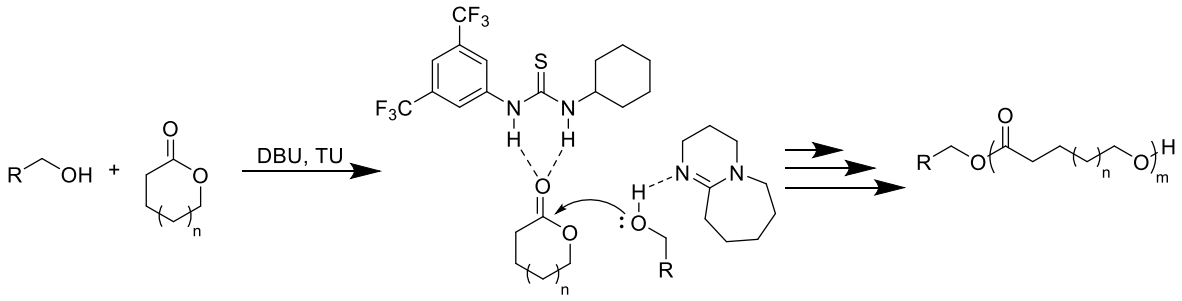

Scheme 3.1. Organocatalysed (DBU/TU) ROP of lactones initiated from a primary alcohol.

In more recent studies, the introduction of low T_g polycarbonates, such as trimethylene carbonate, into polyester-based materials has been shown to yield biomaterials with improved mechanical properties and degradability *i.e.* higher degrees of flexibility, higher elongation/elasticity, tunable degradation profiles *etc*.[22,23] These materials may be produced either by the copolymerisation of cyclic(ester/carbonate) monomers or through chain extension from homopolymer macro-initiators to yield block copolymer-type structures.[24-26] The synthesis of cyclic carbonate monomers is therefore of great interest, as these compounds offer a facile route to the evolution of novel biomaterials with superior mechanical properties.[27-30]

As shown in chapter 2, cyclic carbonates can be prepared by the ring-closure of diol precursors and as a consequence of the wide range of diol precursors available, a plethora of novel carbonate monomers with varied functionalities can be synthesised

through the ring-closure of functional or modified diols.[31-33] These functionalities can in turn be employed to dictate the physio-chemical properties of the resultant materials such as glass transition (T_g), crystallisation/melting temperatures (T_c/T_m), tensile properties *etc*.[34,35]

The premise for the utilisation of an A-B-A system in the synthesis of TPEs is based on the concept of an amorphous-crystalline or 'hard-soft' phase separated system.[36-39] In these A-B-A systems the interior block typically comprises of a low T_g (< 25 °C) amorphous polymer (e.g. poly(oxyethylene glycol), poly(siloxane), poly(hexamethylene adipate glycol) *etc*.) which are flexible at ambient temperatures. The terminal blocks, in contrast, generally comprise of high T_g polymers which display a higher order of crystallinity and self-association (*e.g.* poly(α-methylene-γ-butyroactone), poly(styrene) *etc*.). In more recent times the incorporation of renewable materials into these TPE systems, as either a single component or as a complete composite, has been of great interest in fields such as regenerative medicine[6,40-43] however few studies have focused on degradable, high T_g polycarbonate-based hard blocks.[44,45]

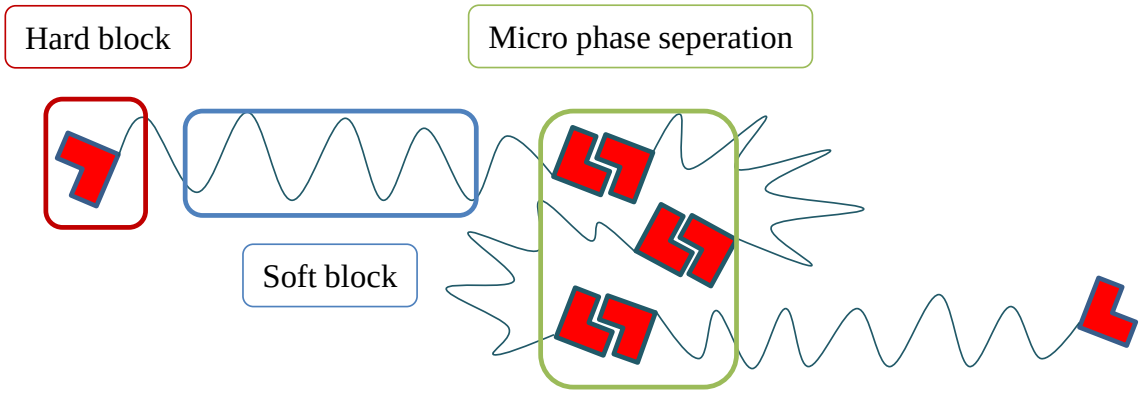

Scheme 3.2. Representation of bulk microphase separation within A-B-A triblock copolymers.

Herein, using the conditions developed for the homopolymerisation of 9-phenyl-2,4,8,10-tetraoxaspiro[5, 5]undecanone (PTO) outlined in chapter 2, the organocatalysed ROP of PTO, initiated from a poly(caprolactone) (PCL) α,ω-dihydroxy macro-initiator to synthesise an A-B-A triblock copolymer as a novel method to improve the mechanical properties of PCL through the introduction phase separation from a high T_g polycarbonate hard block is reported. Subsequently, the compilation of an A-B-A triblock copolymer library based on varying molecular weights of A and B blocks in order to assess the effect of molecular structures on the physio-chemical, thermal and mechanical properties of the resultant materials (*i.e.* glass transition temperature (T_g), percentage crystallinity (X_c), Young's modulus (E), elongation at break *etc.*) is reported.

3.2 Results and discussion

3.2.1 Synthesis of A-B-A triblock copolymers

The DPP catalysed ROP of ε-CL in toluene, previously reported by Kakuchi *et al.*[12], was initiated from 1,4-butanediol (1,4-BDO) at ambient temperature (25 °C) to yield α,ω-dihydroxy PCL (Scheme 3.3) ranging in molecular weights ($M_{n\ NMR}$ = 14 kg mol^{-1} – 30 kg mol^{-1}) with low dispersities ($Đ_M$ = 1.1-1.3, Table 3.1; polymers **1**, **3** and **5**). The use of Amberlyst A21^{TM} basic resin offered a facile method of catalyst quenching and removal and was found to have no adverse effect on the resultant polymers.

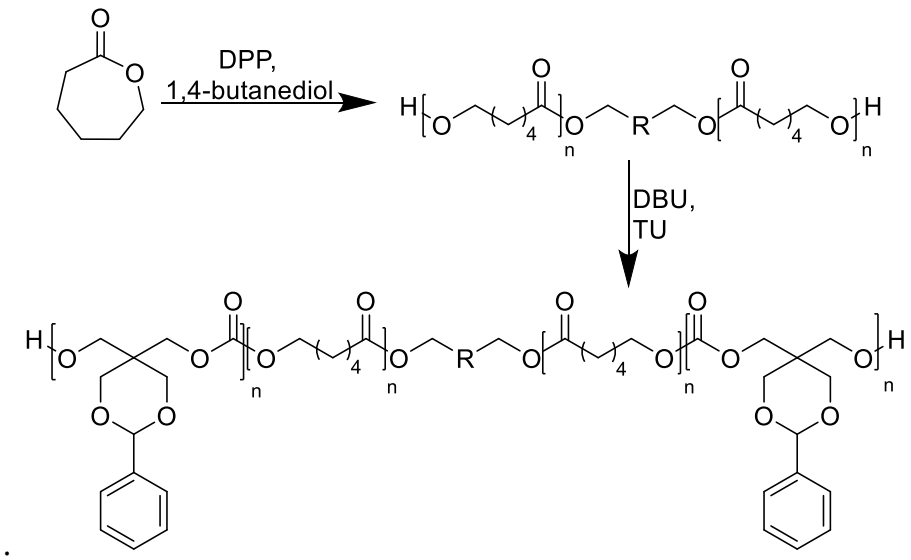

Scheme 3.3. A-B-A triblock copolymer synthesis. (a) 1,4-BDO, DPP, toluene, room temp.; (b) PTO, DBU, TU, CH_2Cl_2, room temp.

The α,ω-dihydroxy PCLs were dissolved in CH_2Cl_2 and dried over 3Å molecular sieves and used as a macro-initiator for the ROP of PTO using the DBU/TU dual-organocatalytic system as described previously for the homopolymerisation of PTO (chapter 2). The system allowed for the synthesis of well-defined A-B-A triblock copolymers, with narrow dispersities (Table 3.1, Figure 3.2), displaying the versatile and selective nature of the dual-catalytic system in regards to the usage of ester-containing macroinitiators with no observable adverse side reactions. The purification of the resultant materials *via* a silica 'plug', optimised for the PPTO homopolymers, again allowed for the facile removal of residual monomer and catalyst without the use of strong acidic conditions which may cleave the benzylidene acetal side group. This was verified by ^{1}H NMR spectroscopy. (Figure 3.1)

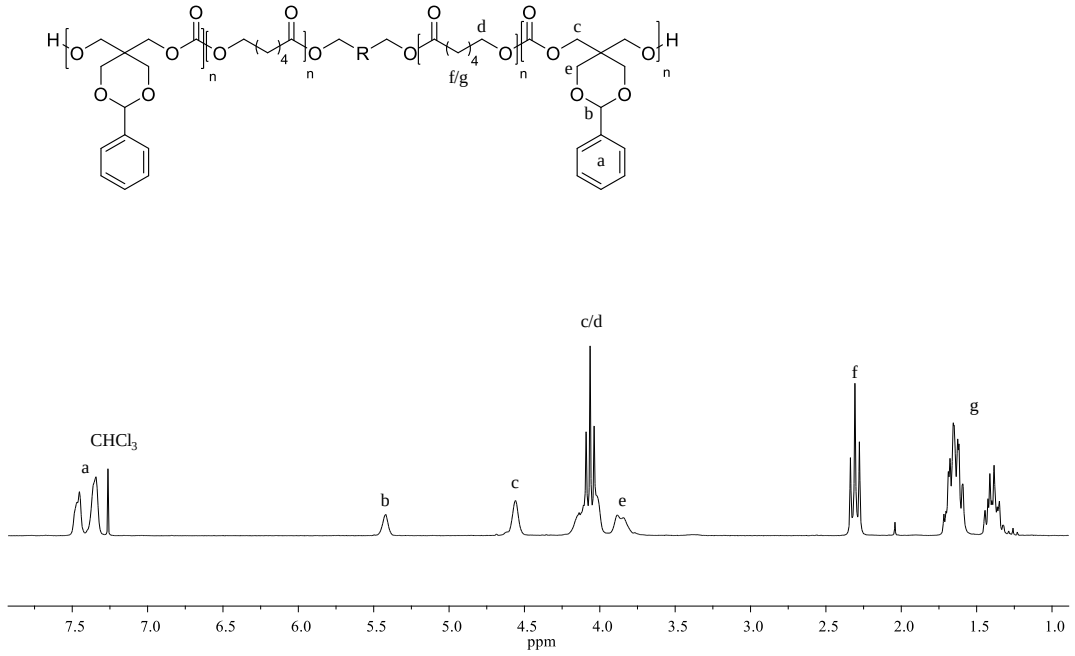

Figure 3.1. ^{1}H NMR Spectrum of PPTO-PCL-PPTO triblock copolymer **7** (Table 3.1). (400 MHz, 298 K, DMSO-d_6).

In order to determine the structure-property relationship of the A-B-A triblock materials, a library was constructed with varying weights of PCL 'soft' midblock and PPTO 'hard' terminal blocks (Table 3.2). In each case the ROP chain extension allowed for the formation of well-defined polymers with decreasing dispersities with increasing weights of hard block added.

Table 3.1. Comparison of PCL/PPTO A-B-A triblock copolymers.

Polymer	PCL $M_{n\ NMR}$[a]	PPTO $M_{n\ NMR}$[a,b]	Wt% PPTO[c]	M_n GPC (kg mol^{-1})[d]	$Đ_M$[b]
1	14,000	0	0	24.2	1.10
2	14,000	5,000	41.7	27.7	1.09
3	22,000	0	0	43.0	1.30
4	22,000	5,000	31.3	46.3	1.19
5	30,000	0	0	52.7	1.32
6	30,000	4,250	22.0	56.1	1.30
7	30,000	14,000	48.3	68.9	1.14
8	30,000	16,500	52.4	72.1	1.13

[a] Determined by ^{1}H NMR spectroscopy. [b] Total M_n of PTO component. [c] Weight% of PPTO calculated from M_n values determined by ^{1}H NMR spectroscopy [d] Determined by GPC analysis in DMF against poly (methyl methacrylate) (PMMA) standards.

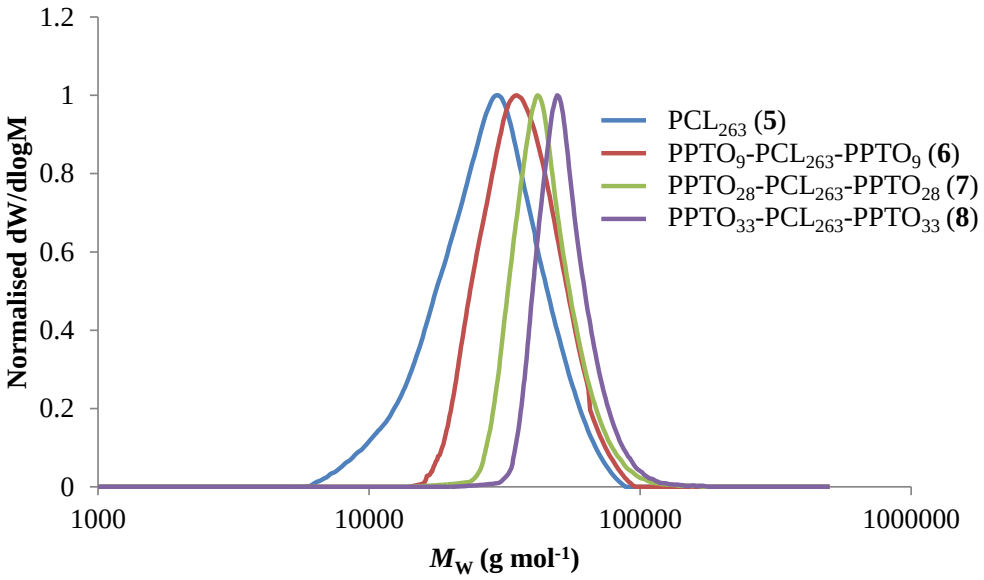

Figure 3.2. GPC RI traces of PCL ($M_{n\ NMR}$ = 30 kg mol^{-1}) based A-B-A triblock copolymers. (Table 3.1)

3.2.2 Thermal and mechanical analysis of A-B-A triblock copolymer library

The triblock copolymers were analysed by DSC with the thermal cycles being performed consecutively in triplicate between -100 and 150 °C at a rate of +/-10 °C min^{-1}. The percentage crystallinity (X_c) of the poly(caprolactone) (PCL) 'soft-block' was determined by the STARe V11.00a (build 4393) software according to equation 3.1 (**eq 3.1**);

$$X_c = \frac{\Delta Hf}{\Delta Hf^0} \times 100 \qquad (\mathbf{3.1})$$

Where ΔHf^0 is the heat of fusion of a 100% crystalline sample of PCL quoted from literature (139.5 J/g).[46]

As has been previously reported by Albuerne *et al.*,[47] each of the PCL homopolymers was observed to display a high degree of crystallinity, with a $T_c \approx 34$ °C, attributed to the alignment of the PCL chains. Furthermore, it was noted that the percentage crystallinity of the PCL homopolymers significantly reduced with increasing molecular weight (Table 3.2) as a consequence of long-chain entanglement retarding the nucleation process, as is explained in reptation-nucleation theory.[48]

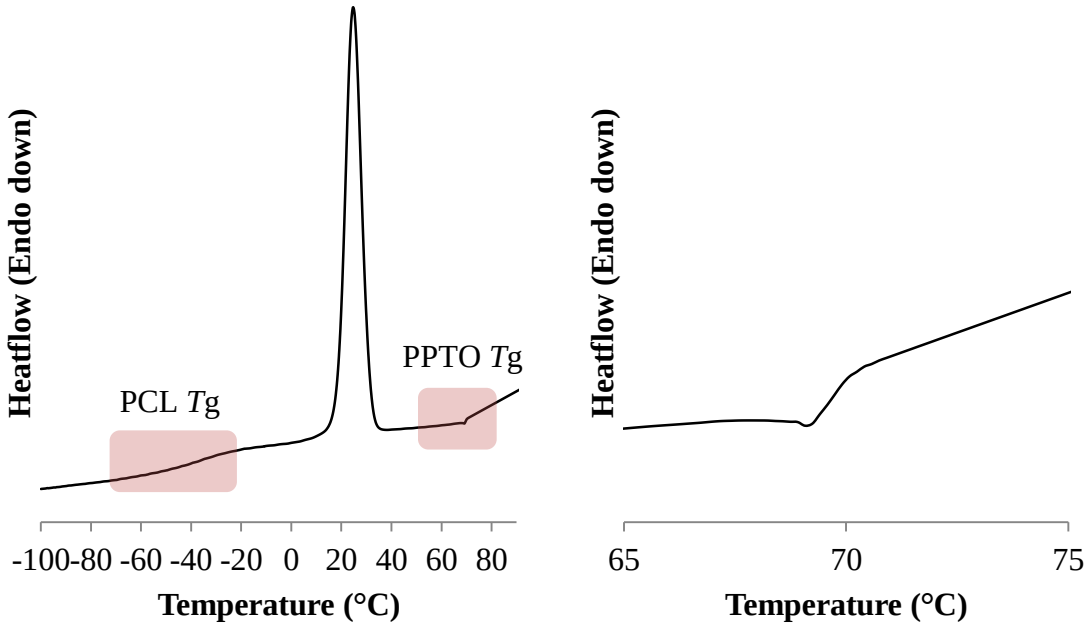

Figure 3.3. DSC thermograms. (*left*) PCL ($M_{n\ NMR}$ = 30 kg mol^{-1}) based A-B-A triblock **8** (Table 3.2, cooling cycle), (*right*) expansion of glass transition of PPTO hard-segment. Heatflow; endotherm down.

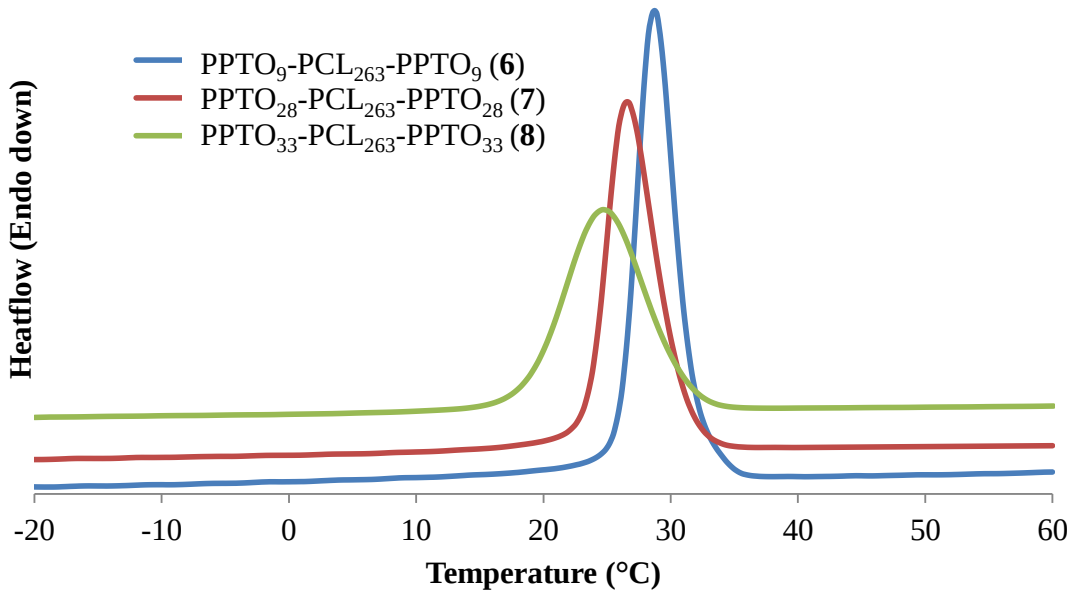

Figure 3.4. DSC thermogram of PPTO-PCL-PPTO triblock copolymers 6, 7, and 8 (Table 3.2) indicating the crystallisation temperature (T_c). (cooling cycle)

The presence of two glass transition temperatures in the DSC thermograms at -58 °C and 70 °C are attributed to the PCL and PPTO blocks respectively (Figure 3.3). The appearance of both glass transition temperatures is indicative of the bulk microphase separation of the A-B-A system. The DSC thermograms of the triblock copolymers also display a further reduction in the crystallinity of the PCL midblock which was found to be inversely proportionate to the PPTO chain length (Table 3.2, Figure 3.4).

Table 3.2. Comparison of crystallisation of PPTO-PCL-PPTO triblock copolymers.

Polymer	PCL T_c (°C)[a]	PCL Crystallinity (%)[a]
1	33.6	52.3
2	17.0	32.5
3	33.6	50.0
4	27.2	42.1
5	33.6	46.2
6	28.8	37.6
7	26.4	34.3
8	24.7	32.7

[a] Determined by DSC

This may be a result of the microphase separation of the A and B blocks further preventing the alignment and nucleation of the PCL midblock. The thermogravametric analysis of the triblocks further confirms the presence of 2 polymeric species through the presence of 2 discrete inflections at 318 and 389 °C which reveal that the PPTO

block degrades prior to that of the PCL block which under the same conditions begins thermal degradation at 389 °C (Figure 3.5).

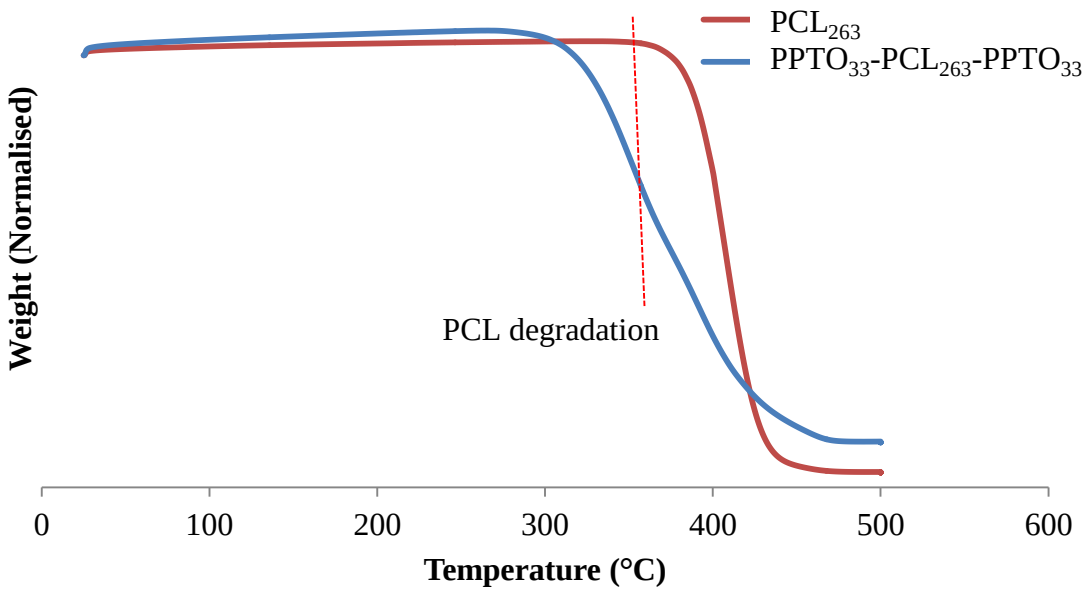

Figure 3.5. TGA thermogram of PPTO-PCL-PPTO triblock copolymer 8 and PCL (M_W = 30 kg.mol^{-1}) homopolymer 5 (Table 3.1).

The tensile properties of the A-B-A triblock copolymers and the PCL macroinitiators were investigated to deduce the effect of the reduction of the PCL crystallinity and the microphase separation within the material on the overall mechanical properties. As a consequence of their brittle nature, triblocks incorporating PCL macro-initiators in which $M_{n\ NMR}$ = 14 kg mol^{-1} were unable to be moulded for analysis. In the case of both PCL homopolymer (**5**, $M_{n\ NMR}$ = 30 kg mol^{-1}) and triblocks (Table 3.1, polymers **6**, **7**, **8**) consisting of PCL $M_{n\ NMR}$ = 30 kg mol^{-1}, at low strains, a linear response was observed on the stress-strain curves before deformation or 'necking' occurred (Figure 3.6). Consistent with previous reports,[49] the PCL homopolymer was observed to be a

relatively stiff material (E = 176.4 MPa) displaying poor elongation with a tendency towards 'necking' under low strain (<80%).

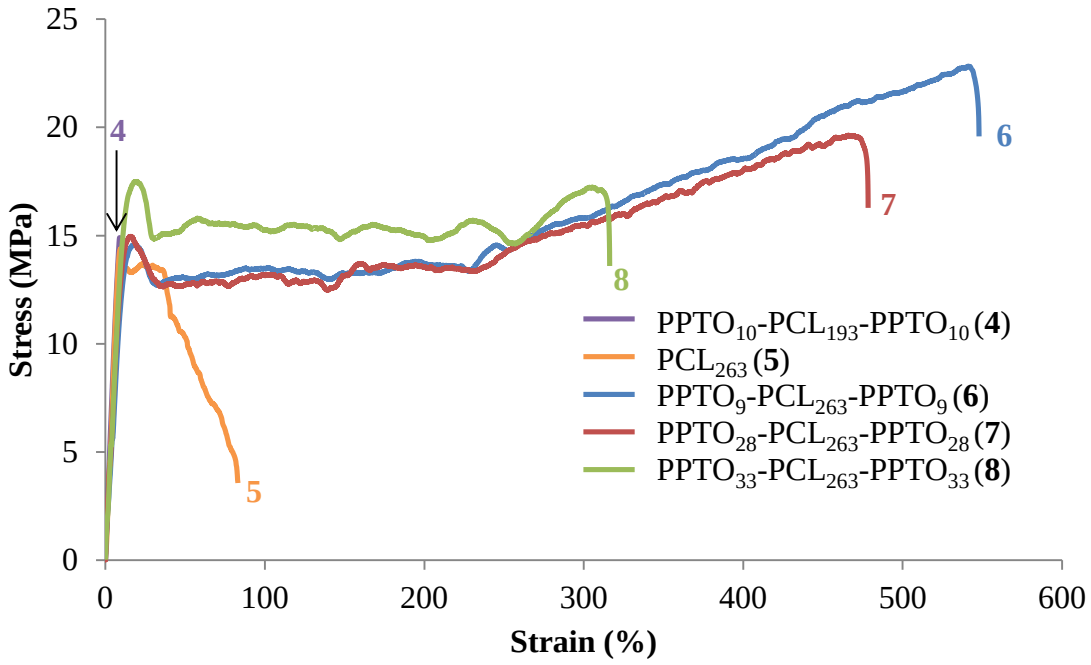

Figure 3.6. Stress-strain curves of PPTO-PCL-PPTO triblocks **4, 5, 6, 7, 8** (Table 3.3). Experiments were conducted at ambient temperature (25 °C) at an elongation rate of 5 mm.min^{-1} until failure.

Table 3.3. Comparison of tensile properties of PPTO-PCL-PPTO triblock copolymers

Polymer	Strain at Break (%)[a]	E (MPa)[a]
4	9.5 ± 21.5	190.3 ± 5.5
5	70.4 ± 26.2	176.4 ± 7.3
6	548.9 ± 37.0	151.8 ± 8.7
7	407.4 ± 59.7	162.1 ± 8.0
8	340.0 ± 22.7	193.9 ± 6.9

[a] Determined by tensiometric analysis (average of 10 samples, Figure 3.6).

The addition of PPTO terminal blocks led to a significant improvement in the elongation of the materials being observed. It was found that the addition of PPTO blocks with a $M_{n\ NMR}$ = 4.25 kg mol^{-1} (~12.5 wt% of the overall polymer composition) that the strain of the material increased from 70% to 549% (Figure 3.6, Table 3.3). It was also noted that the Young's modulus (*E*) of **6** was lower in comparison with the PCL homopolymer. It is postulated that this reduction in *E* is a result of the decreased crystallinity of the PCL midblock, while the improvement in elongation may be attributed to the microphase separation of the relatively small terminal block constituent creating an 'anchoring' effect for the amorphous region. Notably it was found that *E*, although initially reducing after the addition of PPTO in comparison to PCL homopolymer, was found to be proportional to molecular weight of the PPTO blocks (Table 3.3).

Furthermore, the strain at break of the materials was found to be inversely proportional to the molecular weight of the PPTO blocks. As a consequence of the PPTO segments constituting a higher weight percentage of the overall polymer composition, the mechanical properties become more dependent on the hard block. Comparison of the wt% PPTO block to both strain at break and Young's modulus for materials with at 30 kg mol^{-1} PCL block (Figure 3.6) confirms this observation, demonstrating that increasing PPTO wt% leads to decreasing strain at break. It was also observed that A-B-A triblock **7** (Table 3.3) displayed a comparable Young's modulus to the PCL homopolymer but with a vastly superior elongation before failure with no observable 'necking'. The point of plastic deformation of triblock **8** (17 MPa) was also found to be superior to that of the PCL homopolymer (14 MPa) (Table 3.3).

3.2.3 Accelerated degradation studies of A-B-A triblock copolymer library

Accelerated degradation of A-B-A triblock copolymers were conducted and analysed until degraded disks were irrecoverable from the degradation medium.

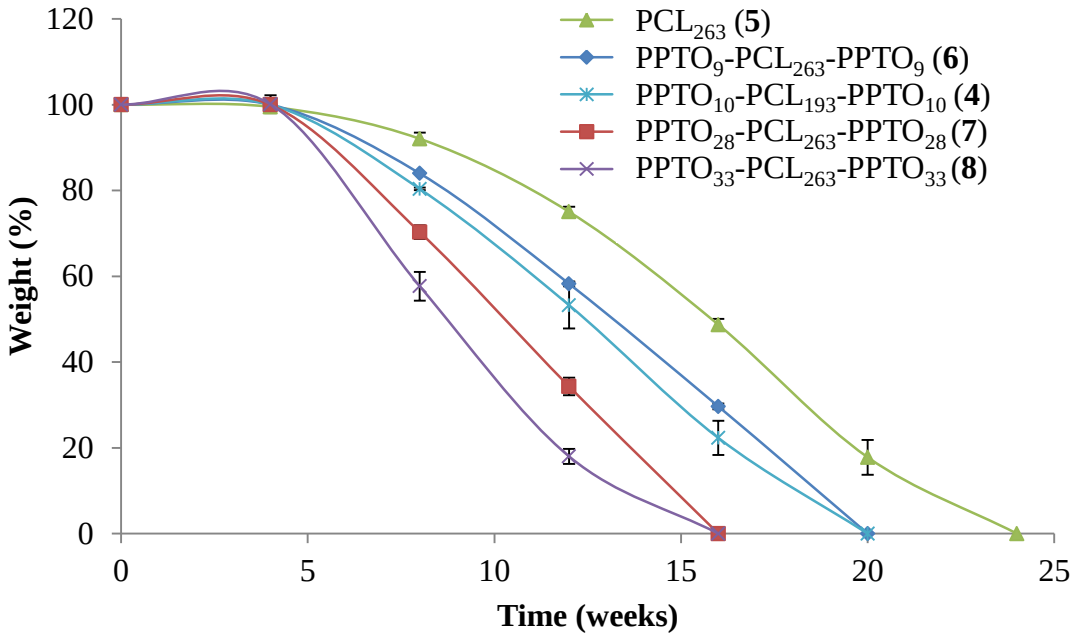

Figure 3.7. Degradation of A-B-A triblock copolymers 5, 6, 7 and 8 (Table 3.1) in accelerated conditions.

The percentage of mass loss was calculated using equation 3.2 (**eq 3.2**)[50];

$$\%\ mass\ loss\ = \left[\frac{(M_0 - M_t)}{M_0}\right] \times 100 \qquad (\mathbf{3.2})$$

Where M_0 is the initial weight of the degradation disk and M_t is the mass at a given time point. It was found that these materials underwent bulk degradation, typical of polyester-based materials, and the degradation rate was inversely proportional to the percentage of crystallinity of the PCL content. As has been previously reported, this is due to the increased uptake of degradation media into the amorphous regions over crystalline regions, leading to the accelerated scission of ester bonds *via* hydrolysis.[50,51]

3.3 Conclusions

In conclusion, it was found that the utilisation of the bifunctional organocatalytic system of DBU/TU in the ROP of PTO, described in chapter 2, could be used to synthesise high T_g polycarbonates which could be further used in degradable biomaterials. The synthesis of A-B-A triblock co-polymers, in which PTO was initiated from PCL macro-initiators, were investigated and shown to yield a thermoplastic 'hard-soft' material. These micro-phase separated materials were found to display superior tensile properties to the corresponding PCL homopolymers while retaining PCLs low thermal processing temperatures. The ROP of pentaerythritol-based cyclic carbonates offers a simple synthetic route into degradable high T_g polymers for utilisation in improving the tensile properties of low T_g polyesters through micro-phase separation.

3.4 References

1. O. Coulembier, P. Degée, J. L. Hedrick and P. Dubois, *Prog. Polym. Sci.*, 2006, 31, 723-747.
2. S. A. Gurusamy-Thangavelu, S. J. Emond, A. Kulshrestha, M. A. Hillmyer, C. W. Macosko, W. B. Tolman and T. R. Hoye, *Polym. Chem.*, 2012, 3, 2941-2948.
3. X. Wang, Y. Zhuang and L. Dong, *J. Appl. Polym. Sci.*, 2013, 127, 471-477.
4. Q. Li, W. Zhu, C. Li, G. Guan, D. Zhang, Y. Xiao and L. Zheng, *J. Polym. Sci., Part A: Polym. Chem.*, 2013, 51, 1387-1397.
5. D. Cohn and A. H. Salomon, *Biomaterials*, 2005, 26, 2297-2305.
6. M. T. Martello and M. A. Hillmyer, *Macromolecules*, 2011, 44, 8537-8545.
7. M. D. Harmon, R. James, N. B. Shelke and S. G. Kumbar, *J. Appl. Polym. Sci.*, 2013, 130, 3770-3777.
8. J. Fernandez, A. Etxeberria, J. M. Ugartemendia, S. Petisco and J. R. Sarasua, *J. Mech. Behav. Biomed. Mater.*, 2012, 12, 29-38.
9. W. Guerin, M. Helou, J.-F. Carpentier, M. Slawinski, J.-M. Brusson and S. M. Guillaume, *Polym. Chem.*, 2013, 4, 1095-1106.
10. R. C. Pratt, B. G. G. Lohmeijer, D. A. Long, R. M. Waymouth and J. L. Hedrick, *J. Am. Chem. Soc.*, 2006, 128, 4556-4557.
11. B. G. G. Lohmeijer, R. C. Pratt, F. Leibfarth, J. W. Logan, D. A. Long, A. P. Dove, F. Nederberg, J. Choi, C. Wade, R. M. Waymouth and J. L. Hedrick, *Macromolecules*, 2006, 39, 8574-8583.
12. K. Makiguchi, T. Satoh and T. Kakuchi, *Macromolecules*, 2011, 44, 1999-2005.

13. A. P. Dove, R. C. Pratt, B. G. G. Lohmeijer, R. M. Waymouth and J. L. Hedrick, *J. Am. Chem. Soc.*, 2005, 127, 13798-13799.

14. R. Todd, G. Rubio, D. J. Hall, S. Tempelaar and A. P. Dove, *Chem. Sci.*, 2013, 4, 1092-1097.

15. A. P. Dove, *ACS Macro Lett.*, 2012, 1, 1409-1412.

16. N. E. Kamber, W. Jeong and R. M. Waymouth, *Chem. Rev.*, 2007, 107, 5813-5840.

17. O. Dechy-Cabaret, B. Martin-Vaca and D. Bourissou, *Chem. Rev.*, 2004, 104, 6147-6176.

18. H. Urakami and Z. Guan, *Biomacromolecules*, 2008, 9, 592-597.

19. M. Helou, O. Miserque, J. M. Brusson, J. F. Carpentier and S. M. Guillaume, *Chemistry*, 2010, 16, 13805-13813.

20. J. M. Becker, R. J. Pounder and A. P. Dove, *Macromol. Rapid Commun.*, 2010, 31, 1923-1937.

21. M. L. Robertson, K. Chang, W. M. Gramlich and M. A. Hillmyer, *Macromolecules*, 2010, 43, 1807-1814.

22. M. Ryner and A.-C. Albertsson, *Biomacromolecules*, 2002, 3, 601-608.

23. T. Tyson, A. Finne-Wistrand and A.-C. Albertsson, *Biomacromolecules*, 2009, 10, 149-154.

24. S. Dai, L. Xue and Z. Li, *ACS Catal.*, 2011, 1, 1421-1429.

25. S. M. Guillaume, *Eur. Polym. J.*, 2013, 49, 768-779.

26. L. Mazzocchetti, M. Scandola and Z. Jiang, *Eur. Polym. J.*, 2012, 48, 1883-1891.

27. A. C. Engler, J. M. W. Chan, D. J. Coady, J. M. O'Brien, H. Sardon, A. Nelson, D. P. Sanders, Y. Y. Yang and J. L. Hedrick, *Macromolecules*, 2013, 46, 1283-1290.

28. R. J. Williams, I. A. Barker, R. K. O'Reilly and A. P. Dove, *ACS Macro Lett.*, 2012, 1, 1285-1290.

29. E. J. Vandenberg and D. Tian, *Macromolecules*, 1999, 32, 3613-3619.

30. R. Wang, W. Chen, F. Meng, R. Cheng, C. Deng, J. Feijen and Z. Zhong, *Macromolecules*, 2011, 44, 6009-6016.

31. S. Tempelaar, L. Mespouille, O. Coulembier, P. Dubois and A. P. Dove, *Chem. Soc. Rev.*, 2013, 42, 1312-1336.

32. S. Venkataraman, N. Veronica, Z. X. Voo, J. L. Hedrick and Y. Y. Yang, *Polym. Chem.*, 2013, 4, 2945-2948.

33. J. Feng, R.-X. Zhuo and X.-Z. Zhang, *Prog. Polym. Sci.*, 2012, 37, 211-236.

34. B. L. Dargaville, C. Vaquette, H. Peng, F. Rasoul, Y. Q. Chau, J. J. Cooper-White, J. H. Campbell and A. K. Whittaker, *Biomacromolecules*, 2011, 12, 3856-3869.

35. S. Tempelaar, L. Mespouille, P. Dubois and A. P. Dove, *Macromolecules*, 2011, 44, 2084-2091.

36. H. Fong and D. H. Reneker, *J. Polym. Sci., Part B: Polym. Phys.*, 1999, 37, 3488-3493.

37. J. Shin, Y. Lee, W. B. Tolman and M. A. Hillmyer, *Biomacromolecules*, 2012, 13, 3833-3840.

38. S. M. Lai and Y. C. Lan, *J. Polym. Res.*, 2013, 20, 1-8.

39. A. Asefnejad, M. T. Khorasani, A. Behnamghader, B. Farsadzadeh and S. Bonakdar, *Int. J. Nanomed.*, 2011, 6, 2375-2384.

40. S.-h. Hsu, S.-H. Chang, H.-J. Yen, S. W. Whu, C.-L. Tsai and D. Chanhen Chen, *Artif. Organs*, 2006, 30, 42-55.

41. S. H. Choi and T. G. Park, *J. Biomater. Sci., Polym. Ed.*, 2002, 13, 1163-1173.

42. A. Porjazoska, N. Kayaman-Apohan, O. Karal-Yilmaz, M. Cvetkovska, K. Baysal and B. M. Baysal, *J. Biomater. Sci., Polym. Ed.*, 2002, 13, 1119-1134.

43. S. S. Ray, *Acc. Chem. Res.*, 2012, 45, 1710-1720.

44. A. C. Fernandes, J. W. Barlow and D. R. Paul, *Polymer*, 1986, 27, 1788-1798.

45. G. Chatterjee, D. Dhara and M. Jegathesan,WO 2009050682 A2, 2009.

46. Q. Guo and G. Groeninckx, *Polymer*, 2001, 42, 8647-8655.

47. J. Albuerne, L. Ma´ rquez, A. J. Muller, J. M. Raquez, P. Degee and P. Dubois, *Macromolecules*, 2003, 36, 1633-1644.

48. M. J. Jenkins and K. L. Harrison, *Polym. Adv. Technol.*, 2006, 17, 474-478.

49. B. Lepoittevina, M. Devalckenaerea, N. Pantoustiera, M. Alexandrea, D. Kubiesc, C. Calbergb, R. Jérôme and P. Dubois, *Polymer*, 2002, 43, 4017-4023.

50. C. X. Lam, M. M. Savalani, S. H. Teoh and D. W. Hutmacher, *Biomed Mater*, 2008, 3, 034108.

51. S. Li, *Biomed. Mater.*, 1998, 48, 342-353.

4 Application of functional diols derived from pentaerythritol as chain extenders in the synthesis and post-polymerisation modification of novel thermoplastic polyester-urethanes elastomers

4.1 Introduction

Characterised by their enhanced ability to recover after incurring high strains and deformation, elastomeric materials have been of great interest in both biomedical and industrial applications.[1,2] Thermoplastic polyester-urethanes (TPEUs) are a category of degradable segmented elastomeric polymers which are generally synthesised *via* the step-growth polymerisation of telechelic poly diols (polyols) with diisocyanates and small diol chain-extenders.[3,4]

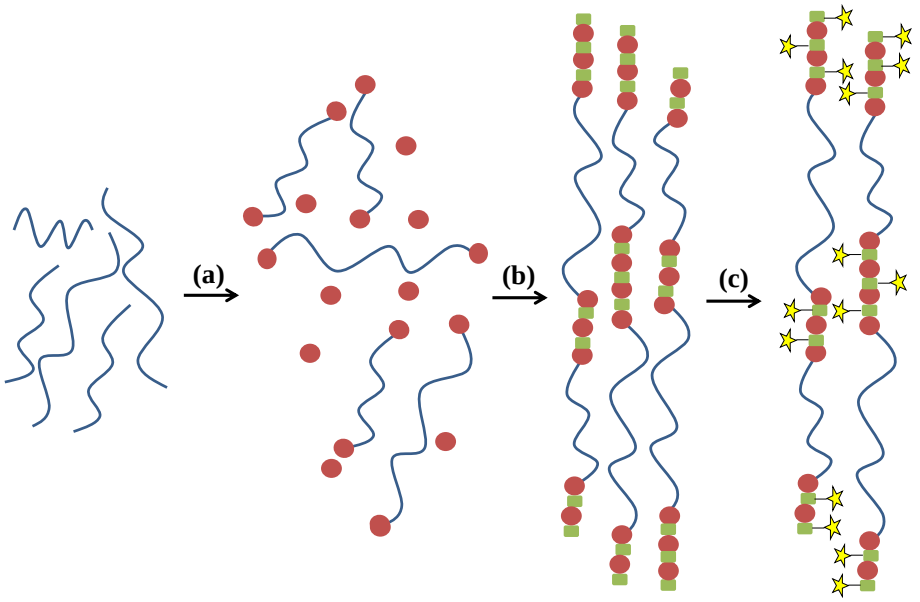

Scheme 4.1. Schematic of TPEU synthesis and post-polymerisation functionalisation; (a) polyol 'end-capping' by addition of excess diisocyanate, (b) chain extension with modifiable extender (c) post-polymerisation modification.

The success of elastomeric TPEUs is owed to their ability to access a vast range of thermal and mechanical properties through the mediation of their component parts.[5] In particular, the permutation of diol extenders is of great interest industrially owing to

their commercial availability and ease of synthesis and purification. The design of novel small diol extenders in order to control the physical properties of the resultant TPEUs has been extensively investigated since their inception, however, the application of extenders with post-polymerisation modifiable sites has been relatively overlooked until recent times.[6,7]

Herein, the application of (2-phenyl-1,3-dioxane-5,5-diyl)dimethanol and (2-(norbornene)-1,3-dioxane-5,5-diyl)dimethanol diols, synthesised in Chapter 2, as extenders in the synthesis of novel TPEUs is described. Furthermore, the post-polymerisation modification of norbornene containing TPUs to alter the physical properties of these materials is described.

4.2 Results and discussion

4.2.1 General synthesis of TPEUs from acetal-protected pentaerythritol

As has been reported in Chapter 2, (2-phenyl-1,3-dioxane-5,5-diyl)dimethanol and (2-(norbornene)-1,3-dioxane-5,5-diyl)dimethanol were synthesised *via* the acid-catalysed acetal formation between pentaerythritol and benzaldehyde and 5-norbonene-2-carboxaldehyde respectively. The extenders were purified by repetitive recrystallisation (×3) from hot toluene/THF and dried *in vacuo* to remove any trace solvents. The ^{1}H NMR spectra revealed the pure extenders as reported in Chapter 2 (Figure 4.1).

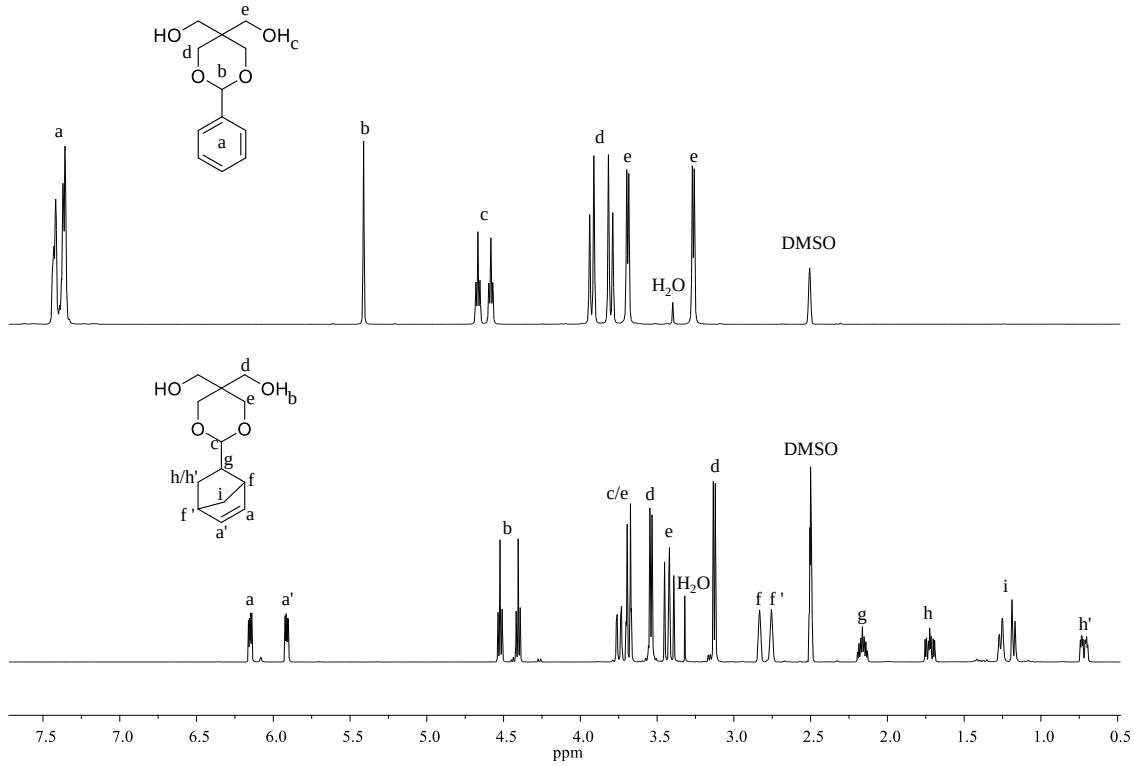

Figure 4.1. ^{1}H NMR spectra of (2-phenyl-1,3-dioxane-5,5-diyl)dimethanol (top) and 2-(norbonene)-1,3-dioxane-5,5-diyl)dimethanol (bottom). (400 MHz, 298 K, DMSO-d_6).

As a consequence of its ability to form highly segmented polyurethanes (PUs), the most common method employed in the synthesis of TPUs is the '2-shot' method.[8] This involves the formation of a 'pre-polymer' by the reaction of a polyol with an excess of diisocyanates; producing an isocyanate end-capped polyol. The pre-polymer is then polymerised in a step-growth fashion by the addition of a small diol extender. As such this method was employed in the synthesis of all TPEUs herein in which poly(caprolactone) (PCL, M_w = 2000 g mol^{-1} as determined GPC) was chosen as the polyol and 1-isocyanato-4-[(4-isocyanatocyclohexyl)methyl] cyclohexane (H_{12}MDI) was chosen as the diisocyanates.

The weight percentage of the overall TPU that is 'hard segment' (%HS) may be calculated based on the overall urethane content.[8] (eq. 4.1);

$$\%\mathrm{HS} = \frac{100(R-1)(M_{\mathrm{ex}} + M_{\mathrm{di}})}{(M_{\mathrm{po}} + R(M_{\mathrm{di}}) + (R-1)(M_{\mathrm{ex}})} \qquad (\mathbf{4.1})$$

Where, M_{ex}, M_{di} and M_{po} are the mole average molecular weights of the extender, diisocyanates and polyol respectively and R is the mole ratio of the diisocyanates to the polyol. TPEUs with a varying %HS of 30, 45 and 60% were selected and the mole ratio of diisocyanate to polyol was calculated by solving for R (Table 4.1). By altering the composition of the TPUs by varying the %HS and extender used, it is possible to tune the morphology of these segmented materials and in turn the mechanical properties.[9] Owing to its relatively low toxicity in comparison to conventional tin-based catalysts, 1,8-diazabicycloundec-7-ene (DBU) was employed as a catalyst for the step-growth polymerisation (5 mol% of polyol content). DBU facilitated the activation of the polyol/extender hydroxyl groups, aiding in the nucleophilic attack of the isocyanate bonds.

Table 4.1. Composition and molecular weight comparison of C_{Ph} and C_{Nb}-based TPUs.

Polymer	wt % 'hard block' (%HS)	H_{12}MDI/polyol ratio (R) [a]	M_w (kg mol^{-1})[b]	$Đ_M$[b]
$30C_{Ph}$	30	2.99	97.8	2.18
$45C_{Ph}$	45	4.80	97.0	2.23
$60C_{Ph}$	60	7.97	88.5	2.30
$30C_{Nb}$	30	2.93	99.0	2.19
$45C_{Nb}$	45	4.68	108.9	2.17
$60C_{Nb}$	60	7.75	90.1	2.38

[a] Determined by eq 4.1. [b] Determined by GPC analysis in DMF against poly(methyl metacrylate) (PMMA) standards.

The GPC chromatograms revealed that the C_{Ph} and C_{Nb}-based TPUs exhibited a unimodal distribution with polydispersities ($Đ_M$) close to 2 ($Đ_M \approx 2.1$-2.4). As described by Flory, this is characteristic of *A*-*B* and *A*-*A B*-*B* step growth polymerisations (Table 4.1, Figure 4.8).[10] Furthermore, it was noted that the disperities of the TPUs increased, while the M_w decreased, with increasing %HS. This is a consequence of the increased viscosity of the polymerisation reaction with higher molar ratios of diisocyanate/extender to polyol, reducing the availability of reactive chain ends.

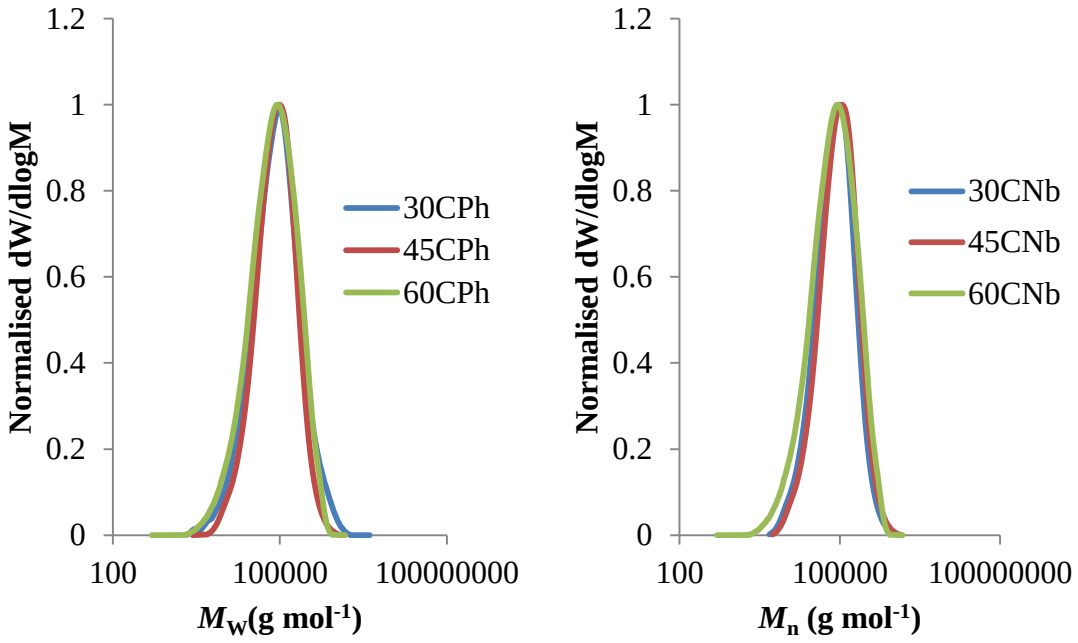

Figure 4.2. RI GPC chromatograms of C_{Ph} (*left*) and C_{Nb} (*right*)-based TPEUs in DMF against PMMA standards (Table 4.1).

The final composition of the C_{Ph} and C_{Nb}-based TPEUs, as calculated by eq 4.1, were verified by ^{1}H NMR and Fourier-transform infra-red (FT-IR) spectroscopy. Expectedly, it was found by ^{1}H NMR spectroscopy, for both C_{Ph} and C_{Nb}-based materials, that the signals attributed to the PCL 'soft' block (δ = 3.98, 2.27, 1.52 and 1.29 ppm) decreased with increasing %HS. In conjunction with this, the characteristic signals attributed to the functionalised pentaerythritol-derived extenders (C_{Ph}; δ = 7.36 and 5.45 ppm, δ = C_{Nb}; 6.30-5.80 ppm) were found to increase proportionally with increasing %HS, indicative of good extender incorporation into the final TPEUs (Figure 4.3).

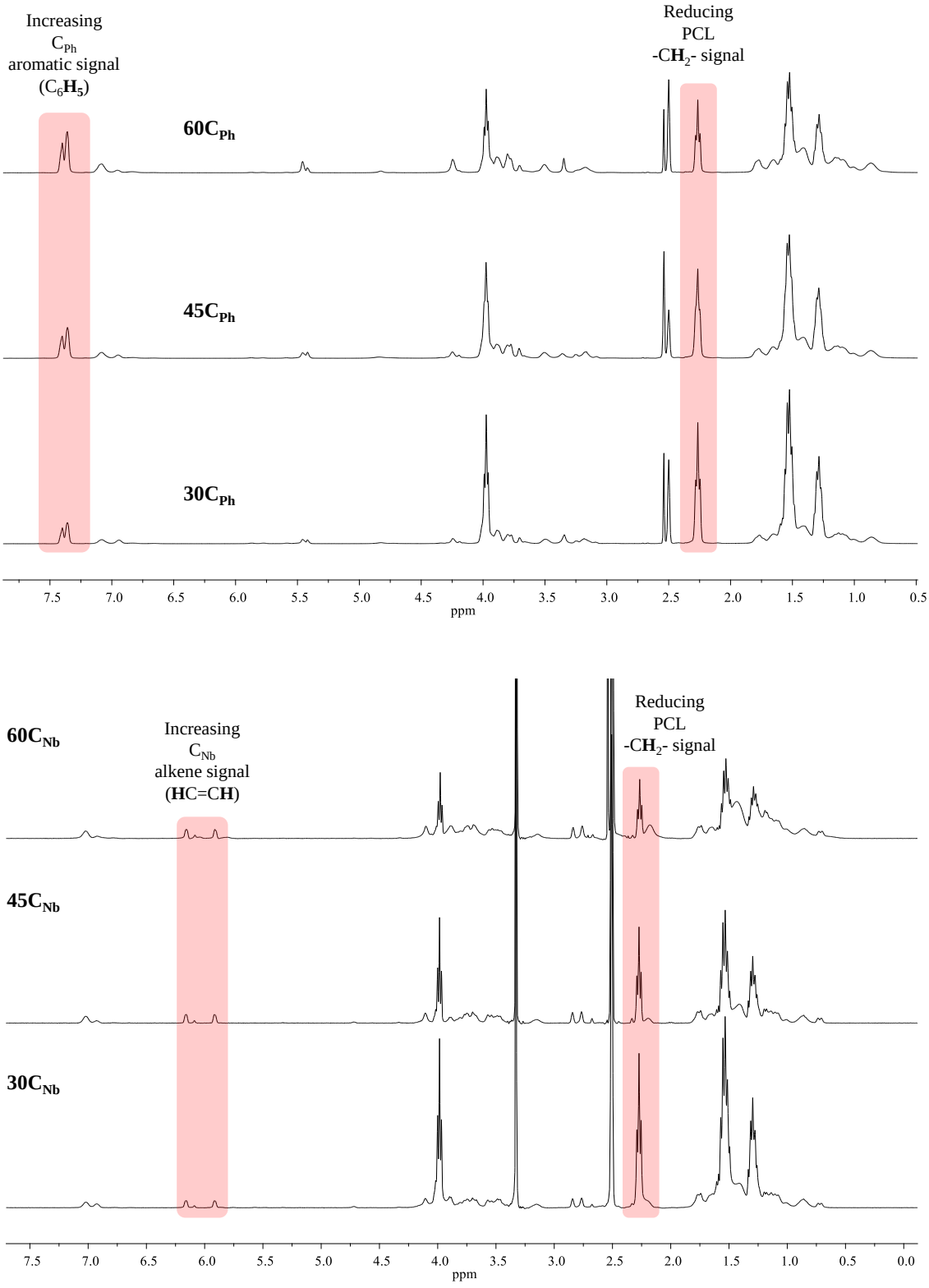

Figure 4.3. ^{1}H NMR spectra of C_{Ph}-based TPEUs (*top*) and C_{Nb}-based TPEUs (*bottom*) (Table 4.1). (400 MHz, 298 K, DMSO-d_6).

The FT-IR spectra of both the C_{Ph} and C_{Nb}-based TPEUs displayed absorption bands attributed to the urethane carbonyl stretching (amide I) and N-H bending (amide II) frequencies at ~1700 and ~1500 cm^{-1} respectively. Analogous to the trend observed in the ^{1}H NMR spectra, it was found that these absorptions increased proportional to the %HS as calculated by eq. 4.1. Furthermore, it was noted that the absence of an absorbance band between 2250 and 2275 cm^{-1}, attributed to the isocyanate cumulated double bonds, is indicative of complete reaction of the H_{12}MDI (Figure 4.4).

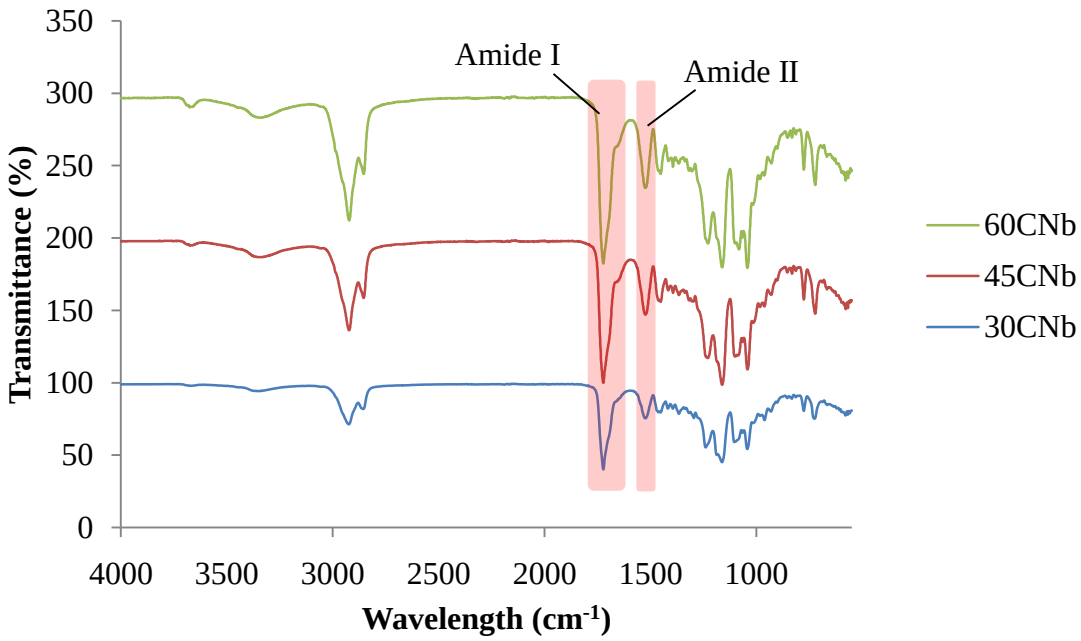

Figure 4.4. FT-IR spectra of C_{Nb}-based TPEUs.

In order to assess the morphology of the materials and verify their phase separation, the TPEUs were analysed using wide-angle x-ray diffraction (WAXD). All diffraction patterns were plotted as a function of Bragg's angle (2θ) (Figure 4.5).

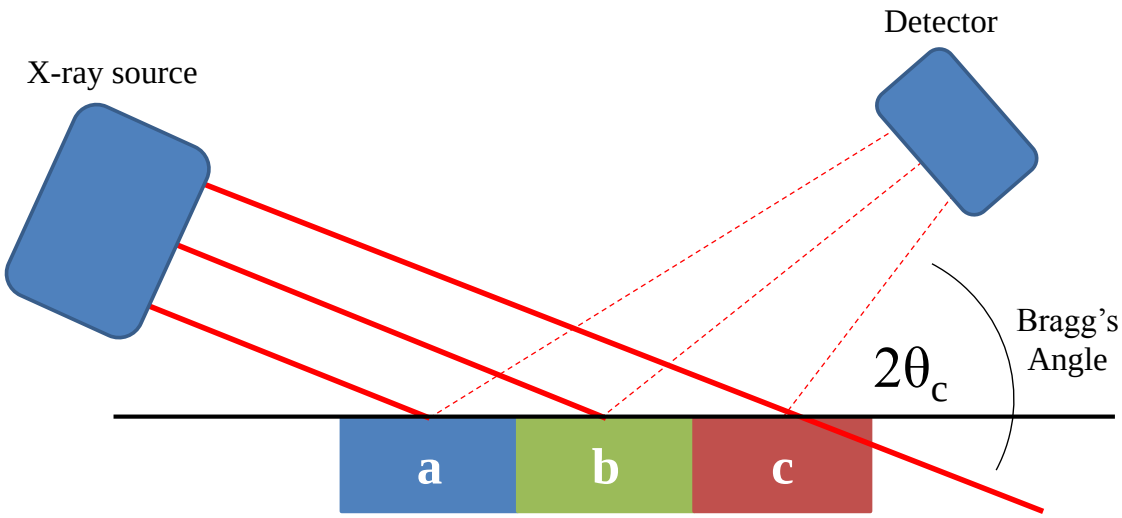

Scheme 4.2. Simplistic schematic of X-ray scattering of contrasting polymers in a segmented system.

As has been extensively reported, owing to differences in scattering patterns of contrasting polymers in segmented block copolymer-like systems, wide angle x-ray diffraction can be used to determine phase separation within a material.[11,12] For both C_{Ph} and C_{Nb} extenders, it was found that the x-ray diffraction patterns displayed a series of sharp crystalline peaks with a Bragg's angle (2θ) between 5-30°, however, the resultant TPEUs were found to display two broad undefined peaks at 2θ ≈ 20° and 2θ ≈ 44°, indicative of phase separated amorphous domains attributed to the 'hard' polyurethane segment and the 'soft' PCL segment respectively.[13,14]

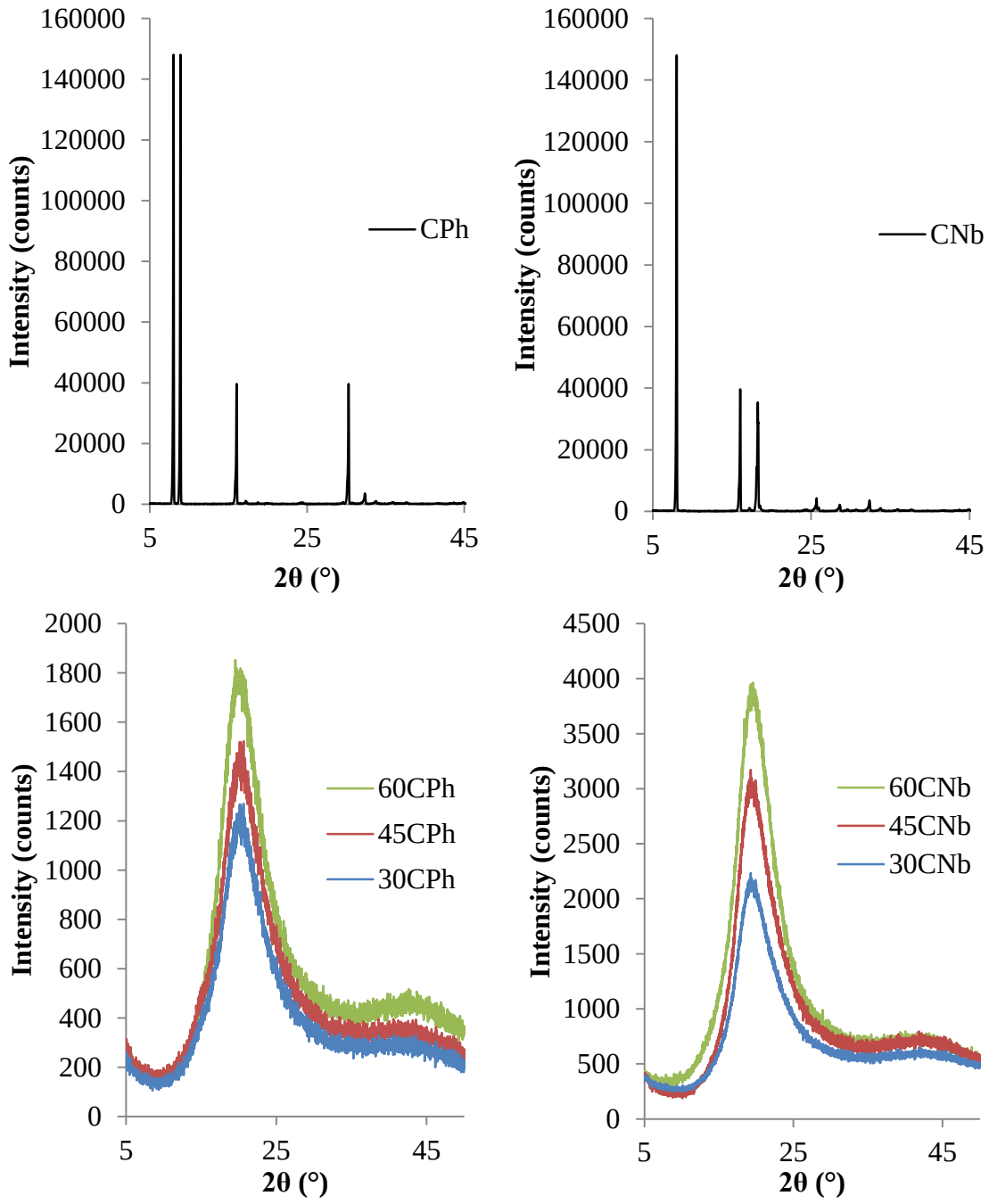

Figure 4.5. WAXD patterns of C_{Ph} extender and resultant TPEUs (*left*). C_{Nb} extender and resultant TPEUs (*right*).

4.2.2 Mechanical and degradation studies of TPEUs

The mechanical properties of the C_{Ph} and C_{Nb}-based TPEUs were assessed by tensiometric analysis, analogous to Chapter 3. For comparative reasons, each TPEU was annealed at 25 °C in an incubator for 5 days before testing in order to promote phase separation of the 'hard' and 'soft' segments. The TPEUs were subsequently subjected to axial loading at a constant crosshead speed, or rate of elongation, (5 mm min^{-1}) until failure. From an average of 10 comparable samples, the Young's modulus (*E*), elongation at break (ε_{break}) and ultimate tensile strength (*UTS*) of the materials were determined (Table 4.2).

Table 4.2. Comparison of tensile properties of C_{Ph} and C_{Nb}-based TPEUs.

Polymer	*E* (MPa)[a]	ε_{break} (%)[a]	*UTS* (MPa)[a]
$30C_{Ph}$	8.4 ± 1.4	757 ± 10	5.9 ± 0.16
$45C_{Ph}$	39.6 ± 2.8	424 ± 9	24.4 ± 0.44
$60C_{Ph}$	109.8 ± 5.6	41 ± 3	29.6 ± 1.01
$30C_{Nb}$	4.6 ± 0.9	1130 ± 19	2.2 ± 0.26
$45C_{Nb}$	40.2 ± 2.0	462 ± 12	25.3 ± 0.86
$60C_{Nb}$	110.3 ± 6.8	47 ± 2	30.5 ± 1.30

[a] Determined by tensiometric analysis (average of 10 samples, Figure)

The tensile analysis of the TPEUs revealed that both *UTS* and *E* increased proportionately with %HS, however, ε_{break} was found to be inversely proportional. As is evident from previous synonymous studies, this is owed to the increased brittle nature of the materials as the PU 'hard' segments becomes the major component of the bulk

material. This brittle nature is owed to the increased urethane content, and therefore increased hydrogen bonding sites, dictating the mechanical properties.

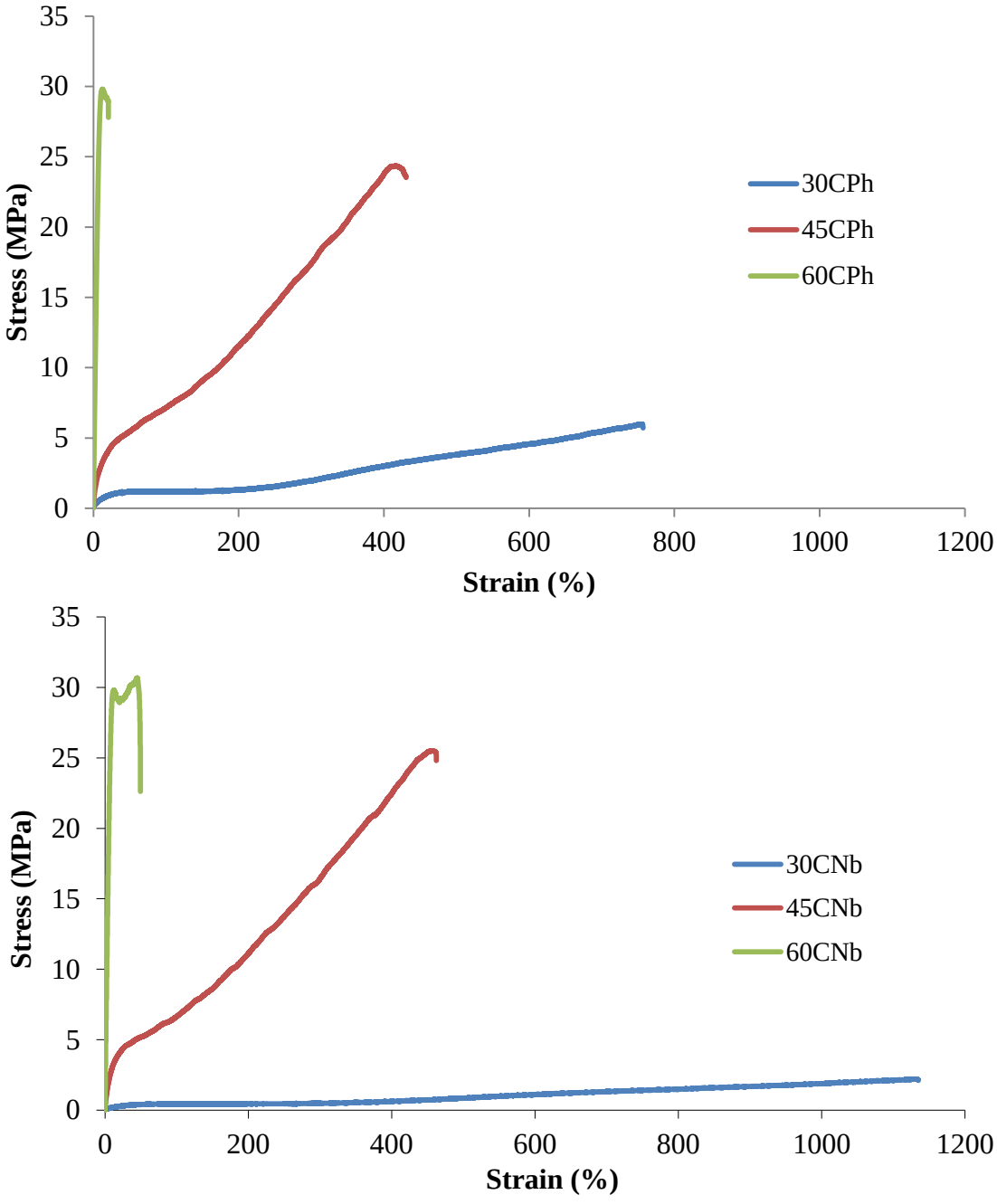

Figure 4.6. Exemplar stress-strain curves of C_{Ph}-based TPEUs (*top*) and C_{Nb}-based TPEUs (*bottom*). Experiments were conducted at ambient temperature (~ 25 °C) at an elongation rate of 5 mm min^{-1} until failure

It was noted that both the C_{Ph} and C_{Nb}-based TPEUs with a 45% 'hard-block' content ($45C_{Ph}$ and $45C_{Nb}$, Table 4.1), displayed nonlinear viscoelastic behaviour with relatively good elongation before mechanical failure (420-460% strain) and underwent recoverable deformation at 30-40 % strain. Furthermore, at high %HS (60%) it was found that the TPEUs underwent plastic deformation and mechanical failure at low strains (~ 40%) but exhibited a high *UTS* (~30 MPa), whereas at lower %HS (30%) TPEUs were found to have high elongations before mechanical failure (760-1130% strain) but exhibited extended recovery times after undergoing elastic deformation with low *E* (5-8 MPa) and *UTS* (2-6 MPa) (Figure 4.6).

In order to assess the hydrolytic degradability of the C_{Ph} and C_{Nb}-based TPEUs, the materials were subjected to accelerated degradation conditions. Each of the TPEUs were compression moulded into degradation 'disks' and placed into individual vials before being submerged in basic aqueous media (5 M aq. NaOH). The degradation samples were stored at 37 °C with constant agitation at 60 rpm and the weights of the dried disks were measured periodically with an analytical balance until they were unretrievable from the degradation media. This method was chosen to exhibit the hydrolytic degradation of the TPEUs as it allowed for the most rapid analysis and comparison of the degradation properties of the materials. The accelerated degradation was performed in triplicate and all results were reported as an average. For both C_{Ph} and C_{Nb}-based TPEUs, it was noted that differences in the overall percentage swelling and rate of degradation observed were found to be negligible, irrespective of the side group functionality (maximum swelling $60C_{Ph}$ = 14% ± 0.6%, $60C_{Nb}$ = 11% ± 0.8%, Figure 4.7-4.8). Furthermore, it was found that the percentage swelling increased slightly with increasing %HS owed to the decrease in the relatively organised and hydrophobic PCL domains, generating a more hydrophilic material.

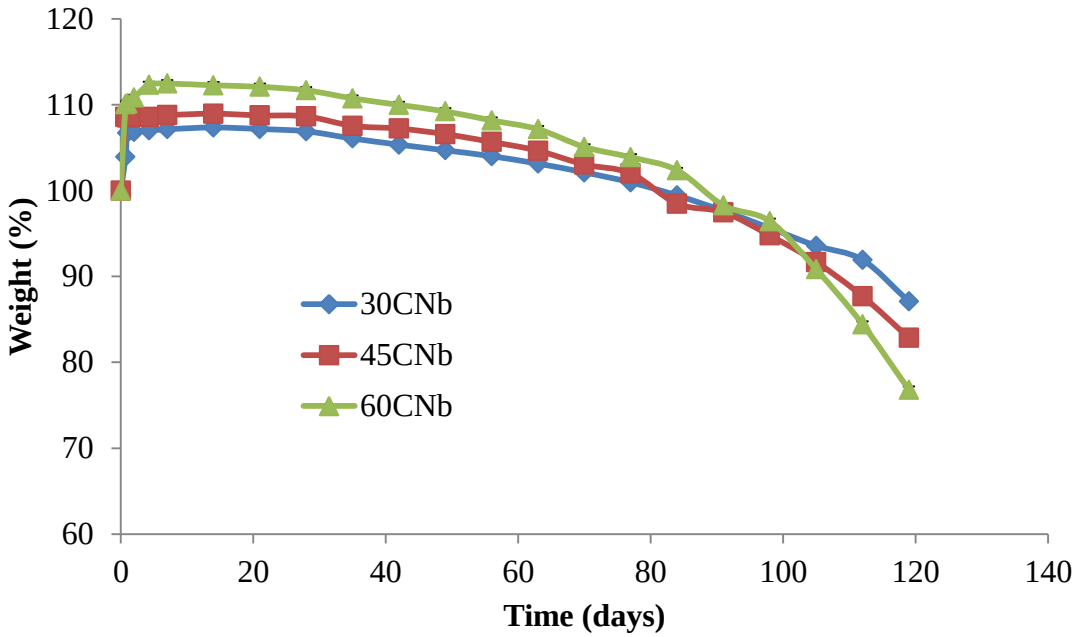

Figure 4.7. Percentage weight for C_{Ph}-based TPEUs, average of 3 samples.

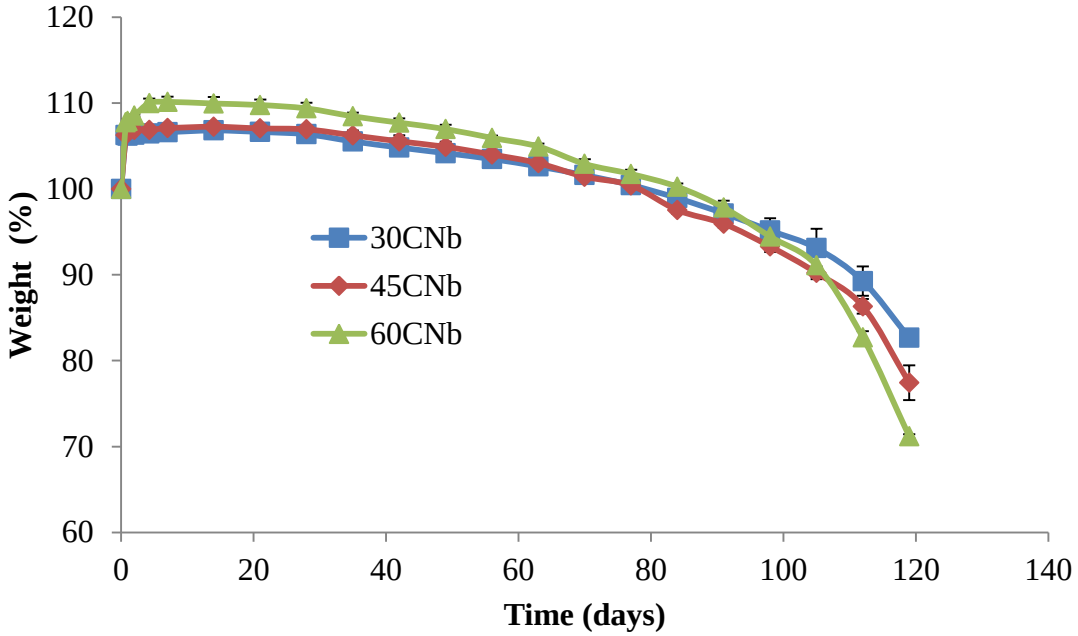

Figure 4.8. Percentage weight for C_{Nb}-based TPEUs, average of 3 samples.

The contact angle of a material is defined as the angle of a liquid/vapour interface when in contact with a solid surface. This angle can be used to define the hydrophilicity/hydrophobicity (when the liquid is H_2O) of a surface owing to differences in the interfacial tension caused by the surface composition. If the contact angle is greater than 90° the surface is said to be non-wetting (hydrophobic), whereas a contact angle of less than 90° denotes a surface which is said to be wettable (hydrophilic) with an angle of 0° indicating complete wetting (Scheme 4.3).[6]

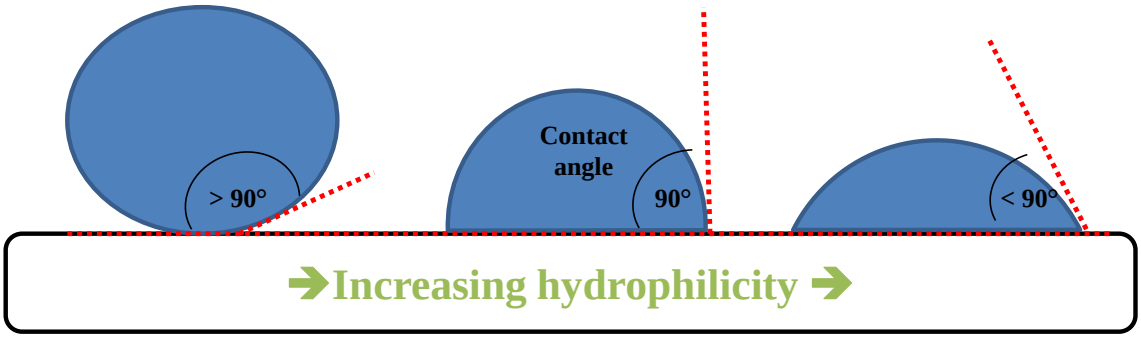

Scheme 4.3. Representative illustration of static contact angle measurements

The surface hydrophilicity of the TPEUs were analysed by static contact angle measurements in order to further assess the %HS and functionality on the wettability of the materials. Concurrent with the accelerated degradation study, it was found that the difference in contact angle measurements were relatively low when side-group functionality was changed from a phenyl to a norbornene acetal (Figure 4.9). Moreover, the contact angle measurements verified the increase in hydrophilicity with increasing %HS hypothesised in the accelerated degradation study.

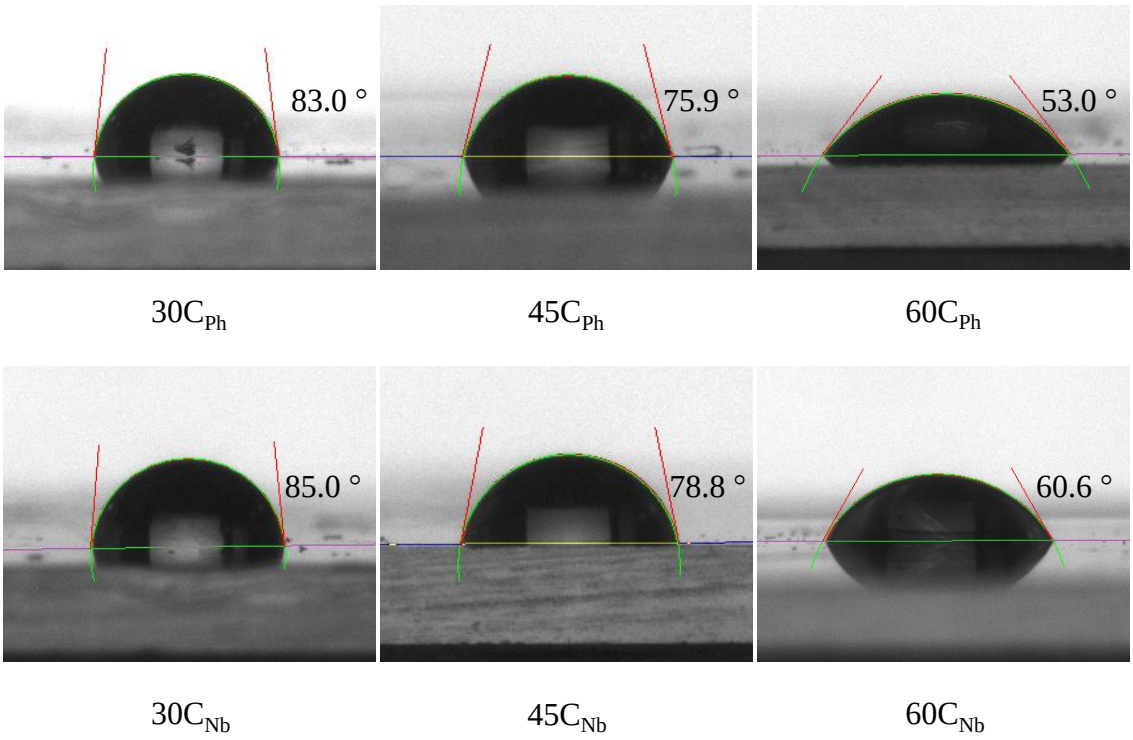

Figure 4.9. Static contact angle measurements for C_{Ph} and C_{Nb}-based TPEUs. Contact angle increases with increasing %HS (30>45>60 %HS).

4.2.3 Modification of C_{Nb}-based TPEUs

As has been demonstrated in Chapter 2, the post-polymerisation modification of norbornene containing polymers offers a unique method of creating novel materials with various properties and applications. As such, in order to assess the effect the modification of C_{Nb}-based TPEUs with hydrophilic small molecules has on the overall hydrophilicity and degradation profile of the TPEUs, C_{Nb}-based TPEUs were modified *via* a 1,3-dipolar cycloaddition with *O*-(2-Azidoethyl)-*O*′-methyl-triethylene glycol (TEG-azide) and the photoinduced radical thiol addition with 1-thioglycerol. Furthermore, C_{Nb}-based TPEUs were modified with the fluorophore, 7-Mercapto-4-

methylcoumarin (MMC), in order to demonstrate the efficiency of the modification process *via* ultraviolet-visible (UV-Vis) spectrophotometry.

The ^{1}H NMR spectra of the modified C_{Nb}-based TPEUs revealed, the complete consumption of the norbornene alkene functionality at δ = 5.94 and 6.17 ppm and the appearance of characteristic signals attributed to each modification (*TEG-azide*; δ = 3.50 ppm, *1-thioglycerol*; δ = 4.50-5.00 ppm, *7-mercapto-4-methylcoumarin*; 7.75-6.75 and 7.20 ppm, Figure 4.11), indicative of successful post-polymerisation modification.

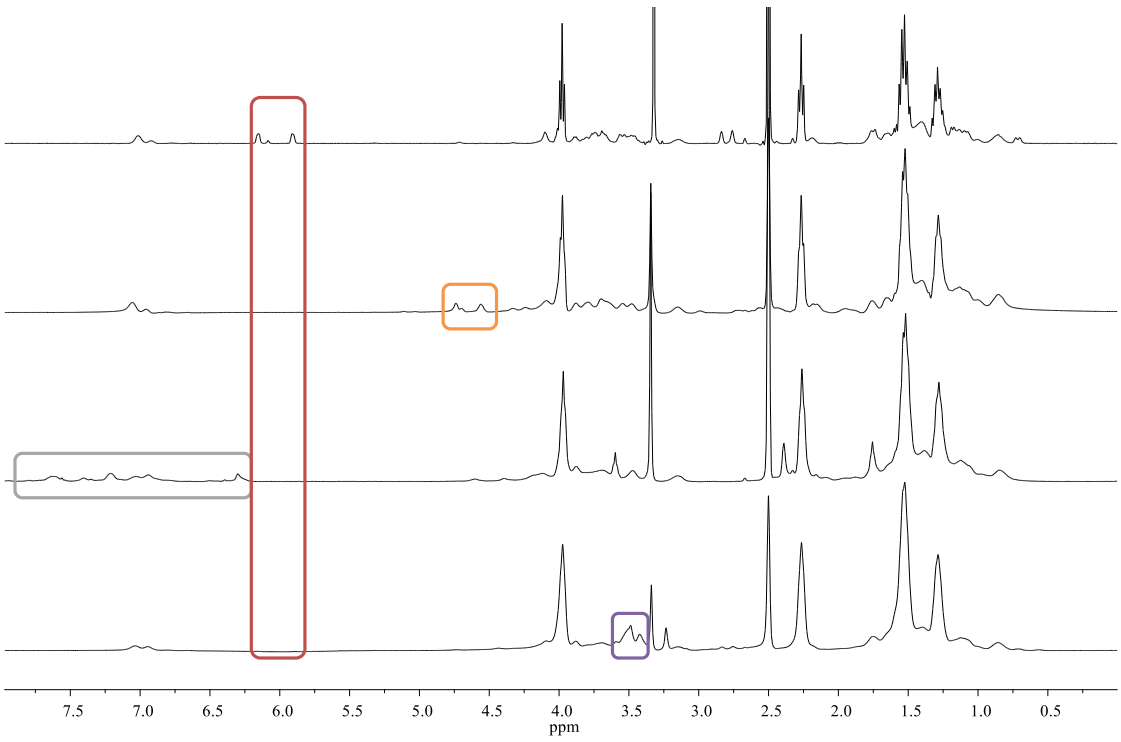

Figure 4.10. ^{1}H NMR spectra of 45C_{Nb}-based TPEUs (*top*), MMC funtionalised (g*rey*), TEG functionalised (*purple*) and thioglycerol functionalised (*orange*) TPEUs. (400 MHz, 298 K, DMSO-d_6).

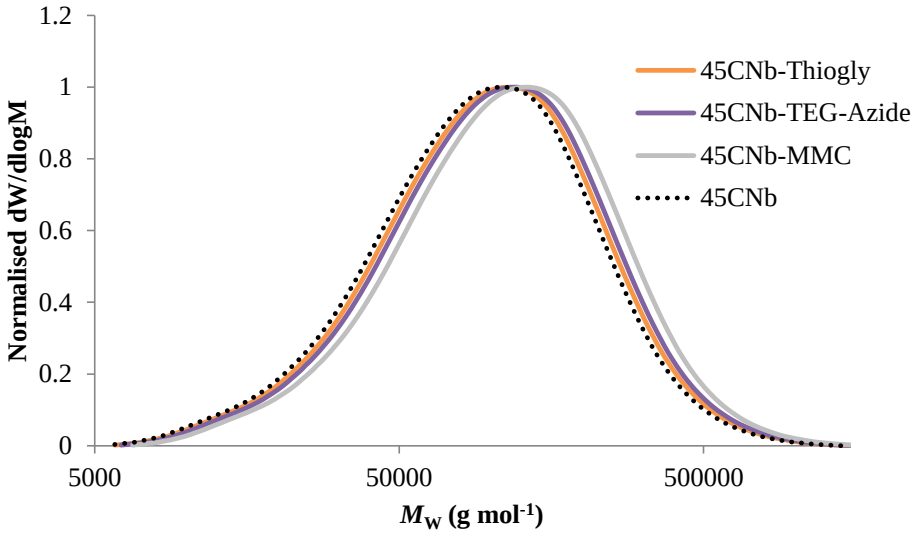

Figure 4.11. RI GPC chromatograms of modified TPEUs in DMF against PMMA standards.

The modified TPEUs were analysed by GPC and were found to increase in molecular weight with no significant effect on the dispersities, indicative of no adverse side reactions *i.e.* cross-linking, side-group cleavage *etc*. (Figure 4.11).

The successful modification of $45C_{Nb}$ with the fluorophore MMC was also verified by UV-vis spectrophotometry. It was found that the unmodified $45C_{Nb}$ exhibited no absorbance peak, however, after modification, a peak at λ = 388 nm was observed characteristic to the absorbance of 7-mercapto-4-methylcoumarin. Furthermore, it was noted that by reducing the equivalents of MMC used during the photoinduced thiol addition (1.1 eq. to 0.51 eq.) it was possible to control the incorporation of fluorophore into the molecule. This was denoted by a reduction in the intensity of absorbance observed, in accordance with the Beer-Lambert law (Figure 4.12).

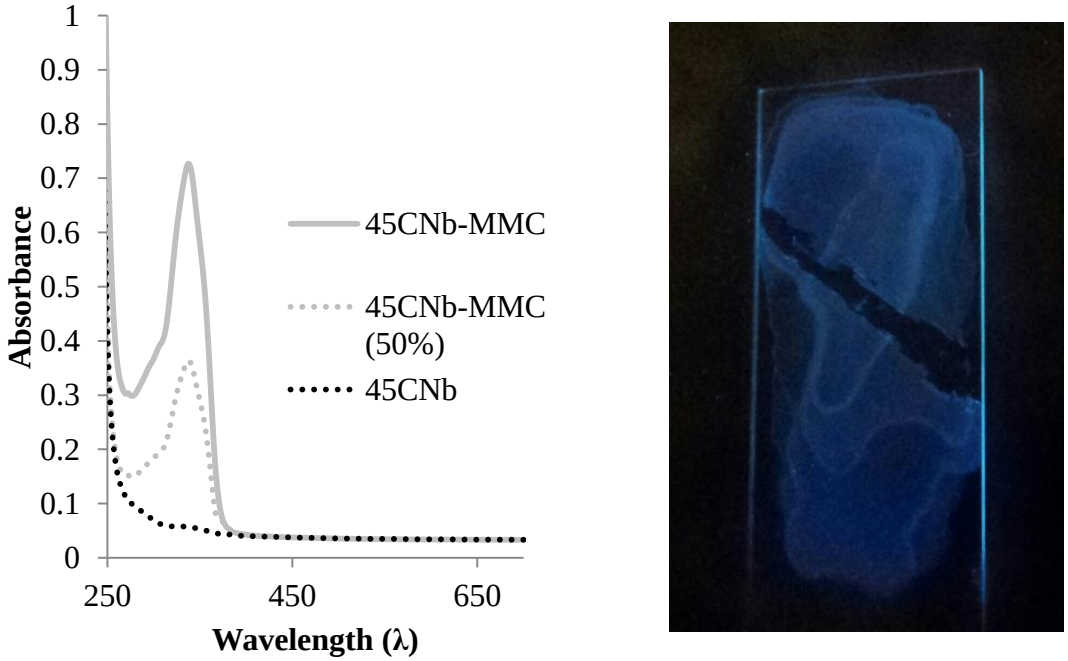

Figure 4.12. $45C_{Nb\text{-}MMC}$ TPEUs; UV-Vis absorption spectra at varying percentage modification (*left*) image of $45C_{Nb\text{-}MMC}$ and UV irradiation (*right*).

In order to assess the effect the modification of C_{Nb}-based TPEUs with hydrophilic small molecules has on the swelling/degradation profiles, as well as surface hydrophilicity of these materials, $45C_{Nb\text{-}Thiogly}$ and $45C_{Nb\text{-}TEG\text{-}azide}$ TPEUs were subjected to accelerated degradation studies and static contact angle measurements as previously mentioned. As anticipated, the incorporation of hydrophilic molecules into the 'hard' polyurethane segments lead to an increase in the surface hydrophilicity of the materials observable by a severe reduction in the static contact angle measurements (Figure 4.13).

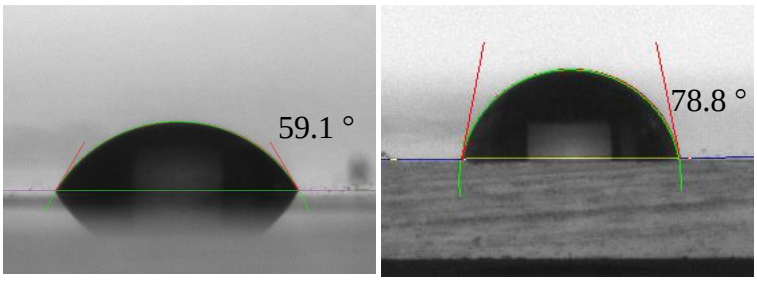

$45C_{Nb\text{-}Thiogly}$ $45C_{Nb}$

Figure 4.13. Static contact angle measurements for modified $45C_{Nb}$-based TPEUs. Contact angle increases with modification.

Furthermore, the accelerated degradation study revealed it that the percentage swelling of the modified TPEUs increased from 7% to 13% after modification, indicative of an increased ingression of degradation media into the TPEU network owed to increased hydrophilicity (Figure 4.16).

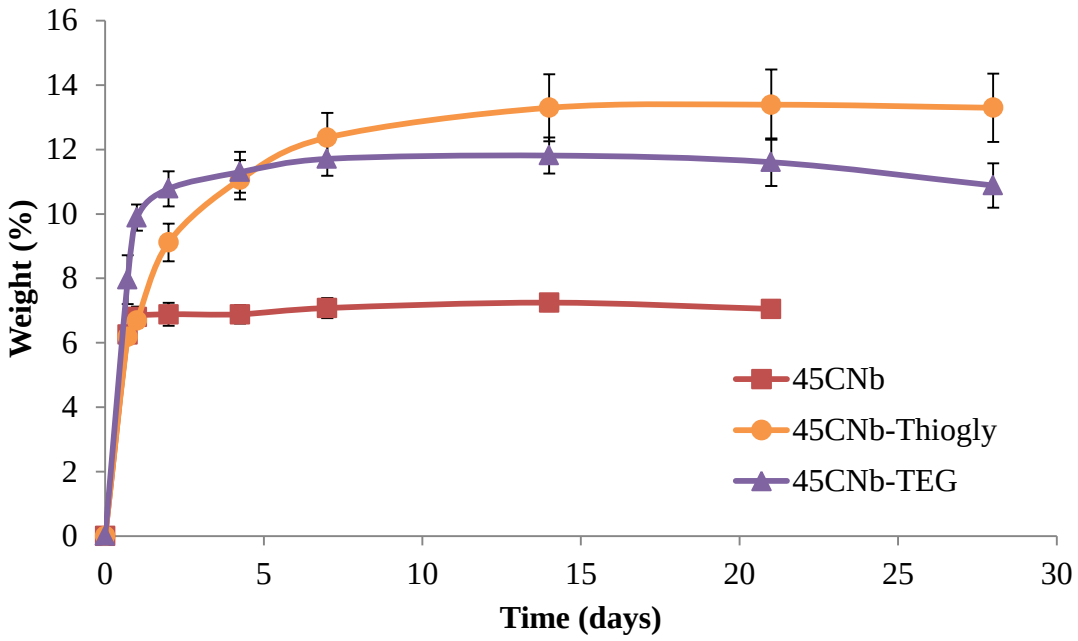

Figure 4.14. Percentage swelling for modified $45C_{Nb}$-based TPEUs, average of 3 samples.

In conjunction with the increase in percentage swelling, it was noted that a slightly higher rate of weight loss was also observed. The increased rate of weight loss is indicative of a higher hydrolytic degradation rate owed to the increased concentration of degradation media at hydrolysable bonds.

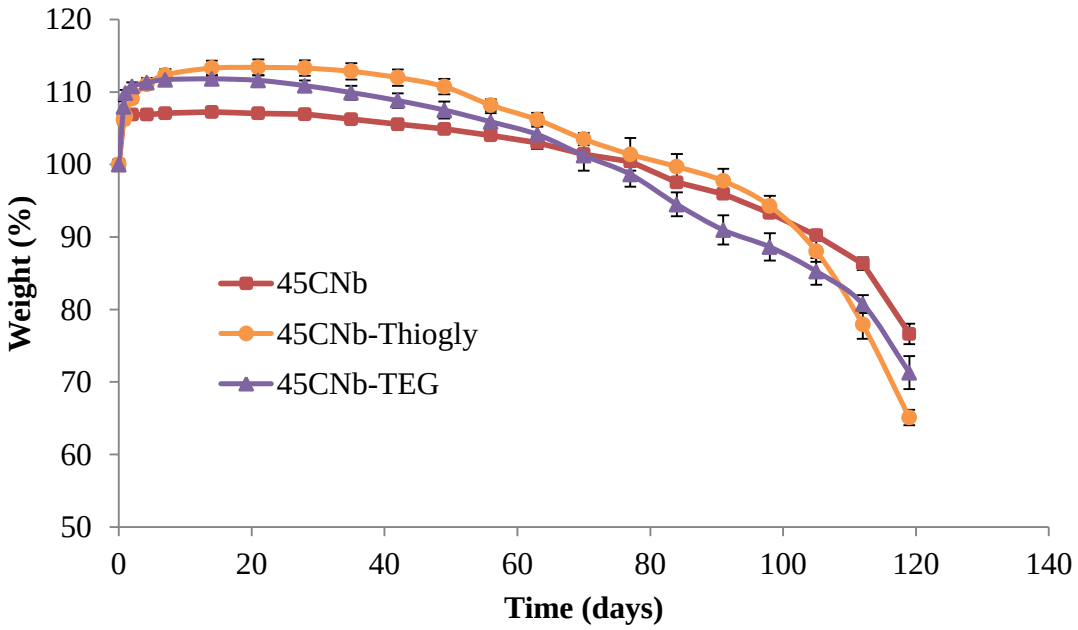

Figure 4.15. Percentage weight for modified $45C_{Nb}$-based TPEUs, average of 3 samples.

In order to assess the effect the post-polymerisation modifications had on the mechanical properties of the materials, C_{Nb}-based TPEUs were analysed by tensiometric analysis as previously reported. Furthermore, in order to generate consistent results, all of the modified TPEUs were processed, annealed and analysed under the same conditions.

Table 4.3. Comparison of tensile properties of modified C_{Nb}-based TPEUs.

Polymer	*E* (MPa)[a]	ε_{break} (%)[a]	*UTS* (MPa)[a]
$45C_{Nb}$	40.2 ± 2.0	462 ± 12	25.3 ± 0.86
$45C_{Nb\text{-}Thiogly}$	37.8 ± 2.7	474 ± 17	24.4 ± 1.33
$45C_{Nb\text{-}TEG}$	32.4 ± 1.8	519 ± 13	22.3 ± 0.98
$45C_{Nb\text{-}MMC}$	6.7 ± 1.8	165 ± 6	2.5 ± 1.10

[a] Determined by tensiometric analysis (average of 10 samples, Figure)

From tensiometric analysis, it was found that there was no significant change in the tensile properties of the $45C_{Nb\text{-}Thiogly}$ TPEU in comparison with the unmodified TPEU, whilst the $45C_{Nb\text{-}TEG}$ TPEU remained comparable with only minimal reduction in *E* and *UTS*. It was noted, however, that there was a significant increase in the ε_{break} of the $45C_{Nb\text{-}TEG}$ materials attributed to the associative behaviour of the mobile pendant TEG units. Interestingly, it was noted that the $45C_{Nb\text{-}MMC}$ polymers exhibited drastic reductions in *E*, *UTS* and ε_{break} owed to the disruptive nature of the bulky pendant groups on the phase separation of the TPEUs (Table 4.3, Figure 4.16).

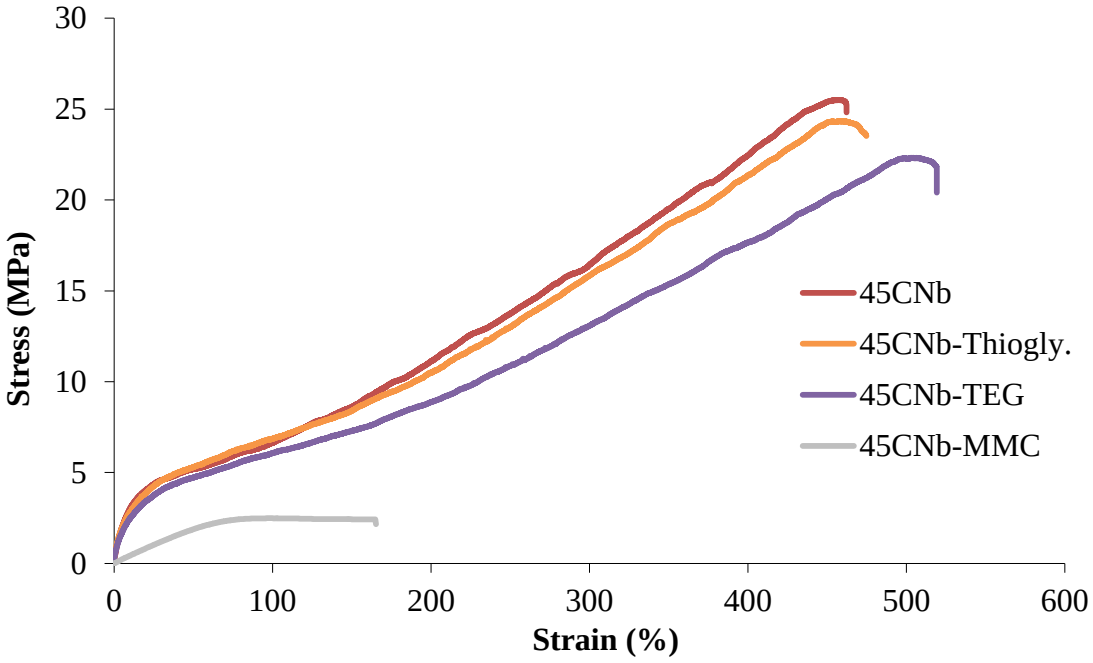

Figure 4.16. Exemplar stress-strain curves of modified C_{Nb}-based TPEUs. Experiments were conducted at ambient temperature (~ 25 °C) at an elongation rate of 5 mm min^{-1} until failure.

4.3 Conclusion

In conclusion, pentaerythritol, through the acid catalysed acetal formation described in Chapter 2, was shown to be an excellent platform in the synthesis of novel functional Thermoplastic polyester-urethanes with a range of mechanical properties determined by extender content.

Furthermore, as is evident from the study, norbornene-functional TPEUs (C_{Nb}) offer a unique route to decorated elastomeric materials which may be employed to control the hydrophilicity and degradation rate of the materials with minimal effect on the mechanical properties through post-polymerisation modifications.

4.4 References

1. R. Yoda, *J. Biomater. Sci., Polym. Ed.*, 1998, 9, 561-626.
2. A. Lendlein and S. Kelch, *Angew. Chem., Int. Ed.*, 2002, 41, 2034-2057.
3. J. Kylma and J. V. Seppala, *Macromolecules*, 1997, 30, 2876-2882.
4. A. Asefnejad, M. T. Khorasani, A. Behnamghader, B. Farsadzadeh and S. Bonakdar, *Int. J. Nanomed.*, 2011, 6, 2375-2384.
5. N. M. K. Lamba, K. A. Woodhouse and S. L. Cooper, *Polyurethanes in Biomedical Applications*, CRC Press LLC, 1997.
6. D. Fournier, B. G. De Geest and F. E. Du Prez, *Polymer*, 2009, 50, 5362-5367.
7. Z. Zhu, Q. Li, Q. Zeng, Z. a. Li, Z. Li, J. Qin and C. Ye, *Dyes Pigm.*, 2008, 78, 199-206.
8. M. J. O'Sickey, B. D. Lawrey and G. L. Wilkes, *J. Appl. Polym. Sci.*, 2002, 84, 229-243.
9. B. K. Kim, Y. J. Shin, S. M. Cho and H. M. Jeong, *J. Polym. Sci., Part B: Polym. Phys.*, 2000, 38, 2652-2657.
10. G. Odian, *Principles of Polymerization, Fourth Edition*, John Wiley & Sons, Inc., 2004.
11. K. Tashiro and S. Sasaki, *Prog. Polym. Sci.*, 2003, 28, 451-519.
12. Y. Nozue, Y. Shinohara and Y. Amemiya, *Polym. J.*, 2007, 39, 1221-1237.
13. V. Pistor, D. de Conto, F. G. Ornaghi and A. J. Zattera, *J. Nanomater.*, 2012, 2012, 1-8.
14. G. Trovati, E. A. Sanches, S. C. Neto, Y. P. Mascarenhas and G. O. Chierice, *J. Appl. Polym. Sci.*, 2010, 115, 263-268.

5 Application of modified amino acid-derived diols as chain extenders in the synthesis of novel thermoplastic polyester-urethane elastomers

5.1 Introduction

As a consequence of their low biodegradability and adverse effect on the environment, the utilisation of petroleum-based resources has been increasingly on the decline in the field of biomaterials.[1,2] Alternatively, in recent years, sustainable monomer feeds and bio-based materials have gained considerable interest owing to their low toxicity, biodegradability, biocompatibility and range of mechanical and chemical properties.[3,4,5]

As described in chapter 4, thermoplastic polyurethanes (TPUs) are a category of segmented polymers synthesised *via* the step-growth polymerisation of polyols with diisocyanates and small diol chain-extenders. In more recent times, both ester and carbonate-based polymers have been incorporated as the polyols in TPU synthesis (Thermoplastic polyester-urethanes (TPEUs)) in order to create degradability through increased hydrolytically degradable sites.[6,7] Furthermore, the utilisation of bio-derived small molecules as chain extenders allows for a more enzymatically degradable hard block.[8] An exemplary case which has been of great interest in recent years is the incorporation of amino acids as chain extenders in TPEUs, as they are anticipated not only to increase bio-degradability, but also to produce non-toxic and bio-absorbable degradation products.[9,10] However, as a consequence of the limited number of amino acids which contain appropriate functionality, the need for protection chemistries and the low solubility of amino acids in many organic solvents, advancements in this area have been somewhat limited.

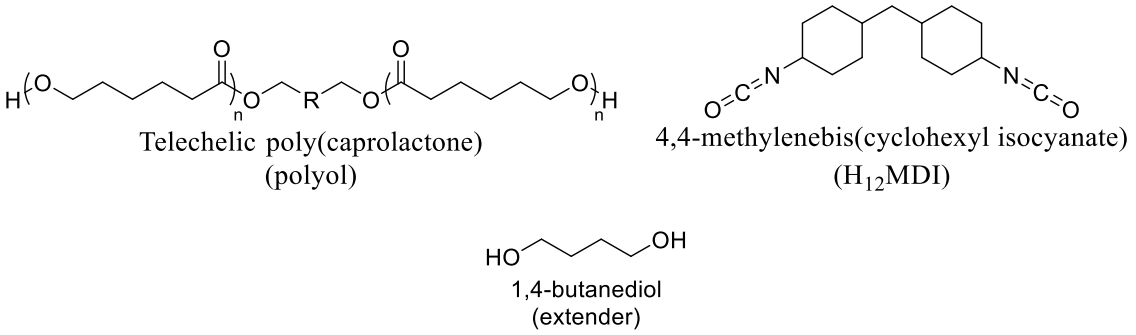

Figure 5.1. Exemplar polyol, diisocyanate and diol extender used in the synthesis of TPEUs.

Alternatively, reduced amino acid derivatives such as 2-amino-1,3-propanediol (serinol), may provide a route to bio-derived extenders, which can be chemo-selectively functionalised in order to control the thermal and mechanical behaviour of the resultant materials.[11] Herein we describe the synthesis of a series of diol extenders derived from the carboxylic acid functional amino acids, L-glutamic acid, L-aspartic acid and the alcohol functional L-serine, and their modification for application in the synthesis of novel TPEUs.

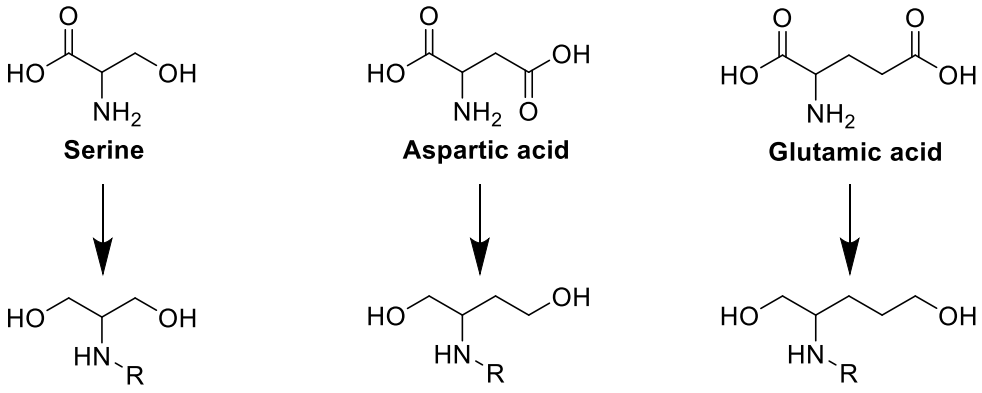

Scheme 5.1. Naturally occurring amino acids and their corresponding amine-protected diols.

5.2 Results and discussion

5.2.1 Synthesis of protected 2-amino-1,3-propanediol extenders (C_3)

Scheme 5.2. Modification of serinol (1) THF/DI H_2O, Na_2CO_3, ethyl chloroformate, room temp., ~ 14h. (2) Methanol/THF, ethyl isocyanate, room temp., 5h.

As described previously in literature by Hedrick *et al.*, the carbamate functionalised serine-derived extender (C_{3c}) was synthesised by reacting serinol with 1 equivalent of ethyl chloroformate (Scheme 2).[11] As a consequence of the poor solubility of serinol in organic solvents, the reaction was conducted in a mixture of tetrahydrofuran (THF) and deionised water (DI H_2O), however, owing to the increased reactivity of the amine group, the mono-functionalised C_{3c} extender was the major product and was easily isolated by liquid-liquid extraction, requiring no further purification and good yields (>80%).

In an analogous method to that used in the synthesis of the C_{3c} extender, the urea functionalised serine-derived extender (C_{3u}) was synthesised by reacting serinol with ethyl isocyanate, however, it was found that under the conditions described previously (THF/DI H_2O), yields were quite low (~60%). It was found that using methanol/THF as the reaction solvent, as described by Lacôte *et al*., yields up to and above 90% could be achieved.[12]

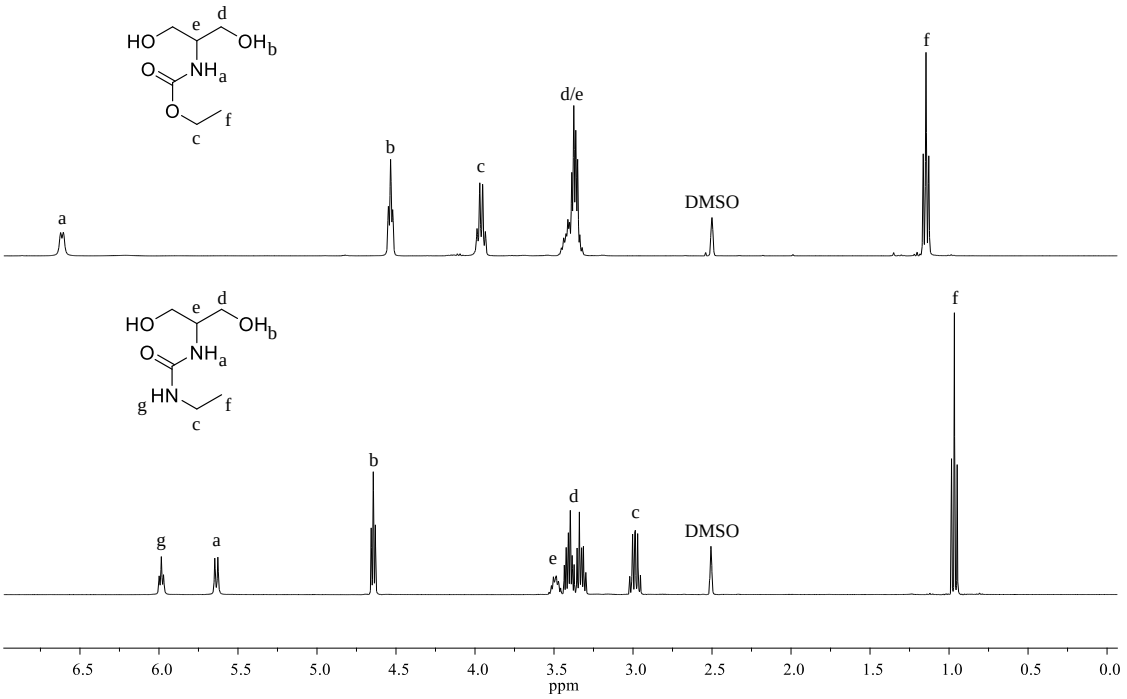

Figure 5.2. ^{1}H NMR spectrum of carbamate functionalised serinol (C_{3c}) (*top*) and urea functionalised serinol (C_{3u}) (*bottom*). (400MHz, 298 K, DMSO-d_6).

Owing to the increased hydrophobicity of the C_{3u} extender, the diol formed a precipitate which was collected *via* vacuum filtration and washed with diethyl ether to yield the C_{3u} extender with no further purification needed.

In the case of both C_{3c} and C_{3u} extenders, complete functionalisation was confirmed by ^{1}H NMR spectroscopy by the presence of a triplet attributed to the –CH_3 (C_{3c}: δ = 1.15 ppm, C_{3u}: δ = 0.97 ppm) and a quartet attributed to the –CH_2– protons (C_{3c}: δ = 3.97 ppm, C_{3c}: δ = 2.99 ppm) of the ethyl side chain, while retaining the triplet attributed to the protons of the dihydroxy functionality (C_{3c}: δ = 4.54 ppm, C_{3u}: δ = 4.64 ppm). Furthermore, in the ^{1}H NMR spectrum of the C_{3c} extender, the appearance of a doublet attributed to the presence of a secondary amine proton adjacent to the serinol methine (δ = 6.62 ppm) is indicative of successful functionalisation. The appearance of this doublet

is also observed in the C_{3u} ^{1}H NMR spectrum (δ = 5.64 ppm), in conjunction with a triplet (δ = 5.98 ppm) attributed to the additional secondary amine of the urea functionality, adjacent to the ethyl –CH_2– protons (Figure 5.2).

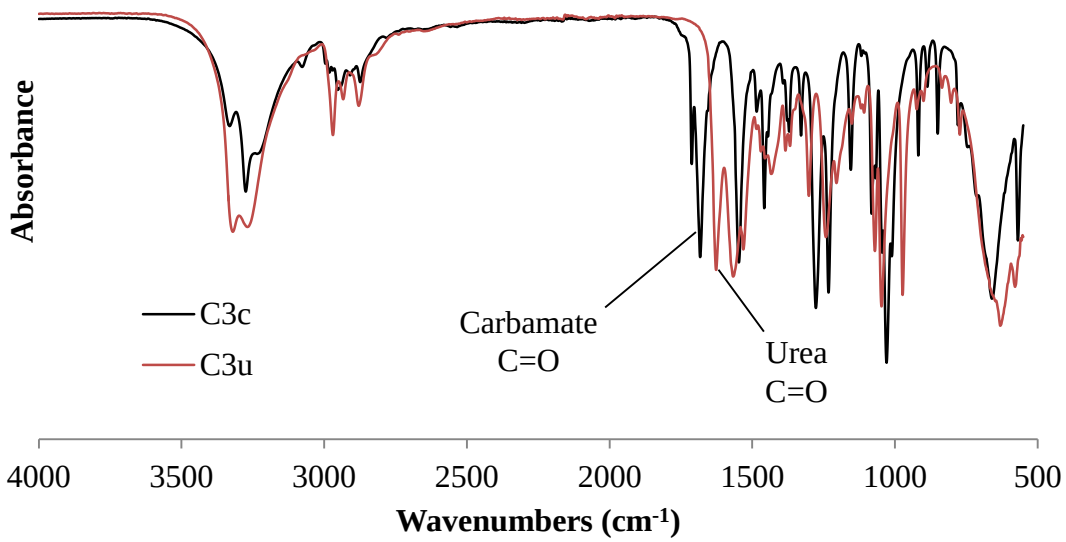

Figure 5.3. FT-IR spectrum of C_{3c} and C_{3u} with the stretching frequencies attributed to the carbonyl of the carbamate and urea functionality highlighted.

The modification of serinol could also be characterised by Fourier-transform infrared spectroscopy (FT-IR). The absorption band attributed to the stretching frequency of the carbamate carbonyl can be seen at ~ 1700 cm^{-1} and of the urea at ~ 1660 cm^{-1}, while a characteristic increase in the absorption band attributed to the N-H stretching frequency of a secondary amine (~ 3400 cm^{-1}) can be observed when changing from the carbamate to urea functionality (Figure 5.3).

5.2.2 Synthesis of extenders derived from L-aspartic acid (C_{4u}) and L-glutamic acid (C_{5u})

Unlike serine, the amino diol derivatives of L-aspartic acid and L-glutamic are not commercially available, and were therefore synthesised by methylation and subsequent reduction of the amino dimethyl esters as described in literature.[13] L-Aspartic acid and L-glutamic acid were methylated by the acid catalysed esterification of the carboxylic acid in methanol, yielding the pure dimethyl ester analogues in good quantities (80-90%) and were used in the subsequent reduction without any further purification.

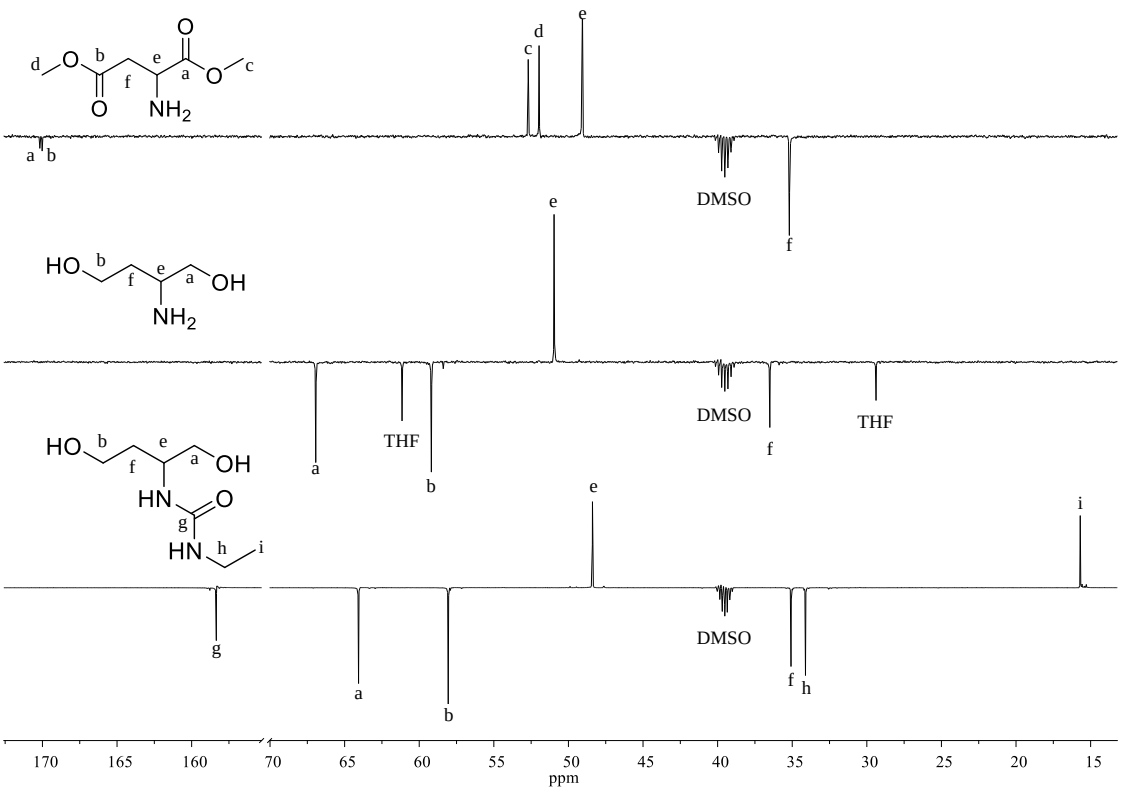

Figure 5.4. ^{13}C APT NMR spectrum of dimethyl aspartate, corressponding amino diol and ethyl-urea diol. (125 MHz, 298 K, DMSO-d_6).

The use of lithium aluminium hydride as the reducing agent allowed for the complete conversion of the aspartate and glutamate dimethyl esters to the corresponding C_4 and C_5 amino diols respectively. This was verified by ^{13}C APT NMR spectroscopy through the loss of two singlets between δ = 165-175 ppm which corresponds to the carbonyl carbons of the methyl esters and the appearance two singlets which corresponds to the -**C**H_2-OH carbons of the diol (δ = 60 ppm and 66 ppm, Figure 5.4). The complete reduction of the amino acids was further verified by FT-IR spectroscopy by the complete loss of the carbonyl stretching frequency attributed to the di-methyl esters (~ 1750 cm^{-1}) and the appearance of a broad signal (~ 3300 cm^{-1}) which corresponds to the alcohol –OH stretch (Figure 5.5).

Although the use of lithium aluminium hydride allowed for the complete conversion of the amino dimethyl esters to the corresponding amino diols, yields were found to be quite low (<40 %) as a consequence of the difficulties associated with handling the aluminium-based salts produced during the reaction. As such, the amino diols were extracted from the lithium and aluminium-based salt residues *via* Soxhlet extraction with hot THF to produce the amino diols in good yields (> 70%). The amino diols were used in the subsequent functionalisation without any further purification.

Utilising the method employed in the synthesis of the C_{3u} extender, 2-amino-1,4-butanediol (C_4) and 2-amino-1,5-pentanediol (C_5) precursors were functionalised with ethyl isocyanate to yield the urea-protected C_4 (C_{4u}) and C_5 (C_{5u}) extenders (yield: >80%). However, as a consequence of the increased solubility of the C_4 and C_5 amino diols in organic solvents in comparison to serinol, the reaction was conducted in THF alone. As with the C_{3u} extender, the successful modification of the C_4 and C_5 amino diols could be verified by FT-IR (Figure 5.5), ^1H and ^{13}C APT NMR spectroscopy (Figure 5.6-5.7).

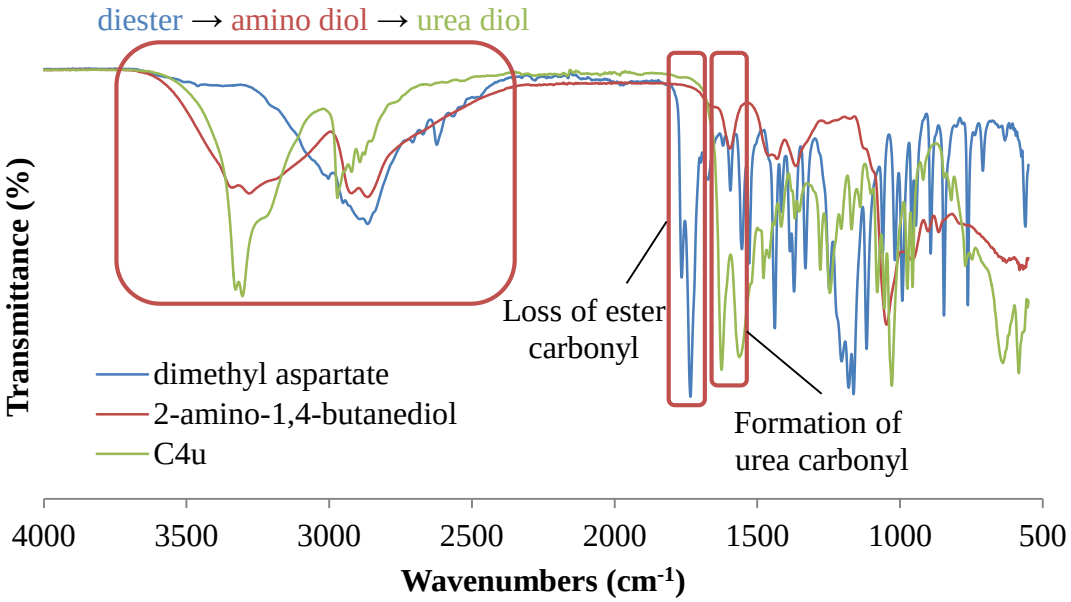

Figure 5.5. FT-IR spectrum of dimethyl aspartate, corresponding amino diol (after $LiAlH_4$ reduction) and ethyl-urea diol.

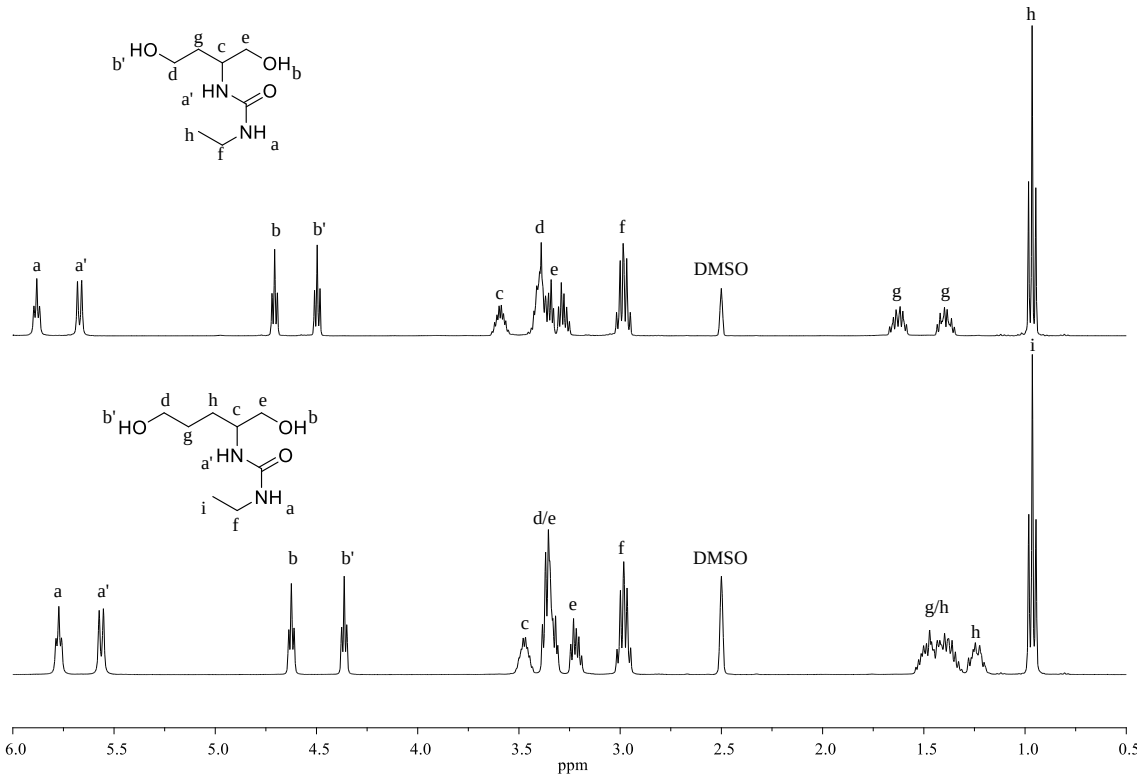

Figure 5.6. ^{1}H NMR spectrum of C_{4u} (*top*) and C_{5u} (*bottom*) extender. (400 MHz, 298 K, DMSO-d_6).

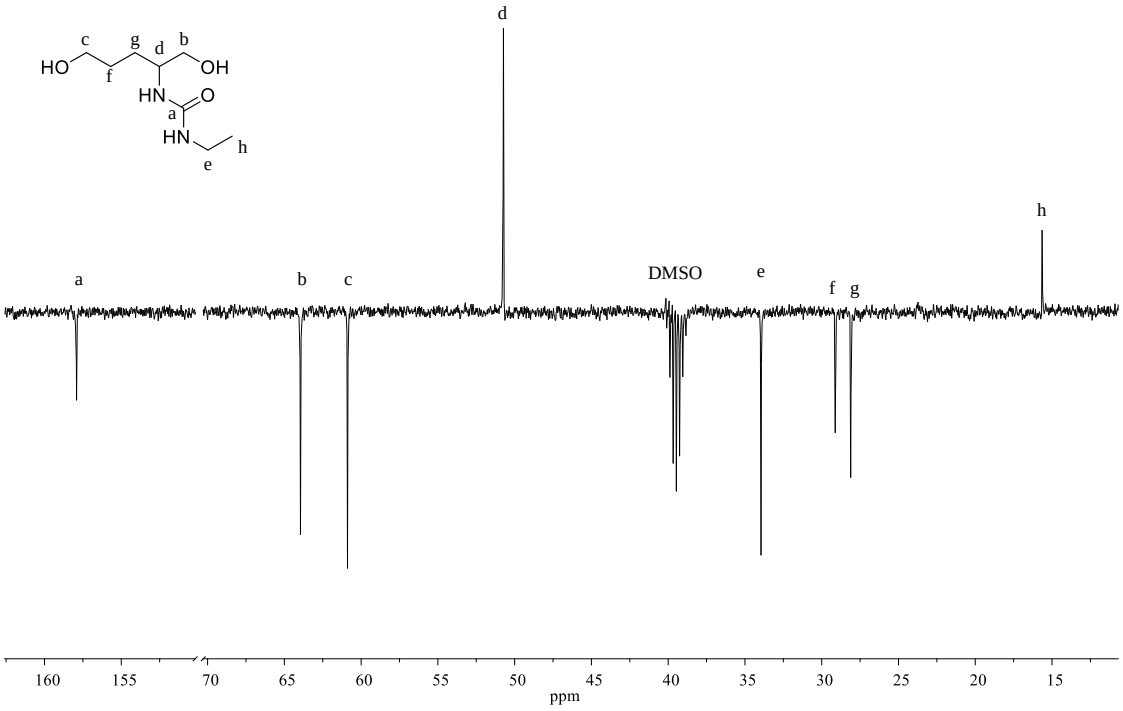

Figure 5.7. ^{13}C APT NMR spectrum of C_{5u} extender. (125 MHz, 298 K, DMSO-d_6).

5.2.3 Synthesis of TPEUs from C_{3c} and C_{3u} extenders; a comparison of the effects of side group functionality.

As mentioned in chapter 4, owing to its ability to form highly segmented polyurethanes (PUs), the most common method employed in the synthesis of TPEUs is the '2-shot' method.[14] As such this method was employed in the synthesis of all TPEUs herein in which poly(caprolactone) (PCL, M_W = 2000 g mol^{-1} as determined GPC) was chosen as the polyol and 1-isocyanato-4-[(4-isocyanatocyclohexyl)methyl] cyclohexane (H_{12}MDI) was chosen as the diisocyanates. The weight percentage of the overall TPEU that is 'hard segment' (%HS) was calculated based on the overall urethane content, as described in chapter 4 (eq. 4.1).

TPEUs with a varying %HS of 30, 45 and 60% were selected and the mole ratio of diisocyanate to polyol was calculated (Table 5.1). For reasons mentioned in chapter 4, 1,8-diazabicycloundec-7-ene (DBU) was employed as a catalyst for the step-growth polymerisation (5 mol% of polyol content).

For comparative ease, the weight average molecular weights (M_W) of the polymers were targeted at ~100 kg mol^{-1} and were analysed by GPC using triple detection. The GPC chromatograms showed that the C_{3c} and C_{3u}-based TPEUs had a unimodal distribution with polydispersities ($Đ_M$) close to 2 ($Đ_M \approx 2.0$-2.5). (Table 5.1, Figure 5.8).[15] It was found, similar to the results observed in chapter 4, that the disperities of the TPEUs increased, while the M_W decreased, with increasing %HS. Also as previously mentioned, this is a consequence of the increased viscosity of the polymerisation reaction with higher molar ratios of diisocyanate/extender to polyol, reducing the availability of reactive chain ends.

Table 5.1. Composition and molecular weight comparison of C_{3c} and C_{3u} based TPEUs.

Polymer	wt % 'hard block' (%HS)	H_{12}MDI/polyol ratio (R) [a]	M_W (kg mol^{-1})[b]	$Đ_M$[b]
30C_{3c}	30	3.28	110.5	1.98
45C_{3c}	45	5.35	97.8	2.20
60C_{3c}	60	8.98	91.9	2.41
30C_{3u}	30	3.28	100.9	2.10
45C_{3u}	45	5.36	96.5	2.23
60C_{3u}	60	9.12	89.7	2.26

[a] Determined by eq 4.1. [b] Determined by GPC analysis in DMF against poly(methyl methacrylate) (PMMA) standards.

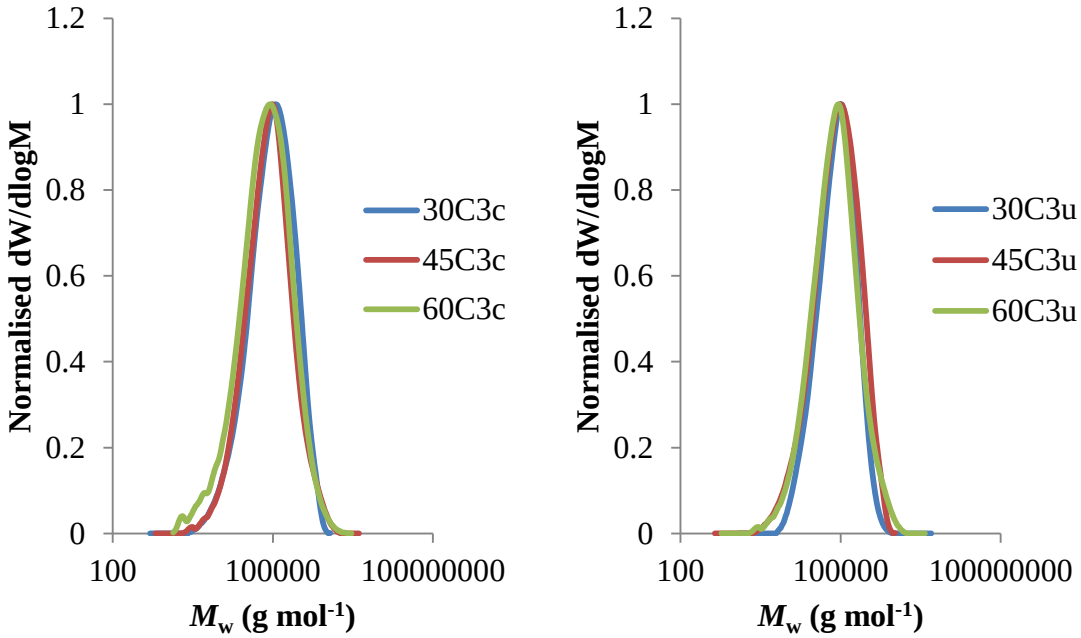

Figure 5.8. RI GPC chromatograms of C_{3c} (*left*) and C_{3u} (*right*)-based TPEUs in DMF against PMMA standards (Table 5.1).

The final composition of the C_{3c} and C_{3u}-based TPEUs, as calculated by equation 4.1, was verified by ^{1}H NMR and FT-IR spectroscopy. It was found by ^{1}H NMR spectroscopy, for C_{3c}-based TPEUs, that the signals attributed to PCL (δ = 3.98, 2.27, 1.52 and 1.29 ppm, Figure 5.9) reduced with increasing hard block content as expected from the ratios calculated. Furthermore, it was found by FT-IR spectroscopy, that an absorption band which corresponds to the stretching frequency of a urethane carbonyl (~ 1700 cm^{-1}) increased proportionally with the increase in %HS, as expected owing to the higher urethane content (Figure 5.10, Amide I). This was further confirmed by the presence of a second absorption band which corresponds to a urethane carbonyl bearing a mono-substituted secondary amide (~ 1550 cm^{-1}) indicative of both the higher urethane content but also of the retention of the side group functionality (Figure 5.10, Amide II).

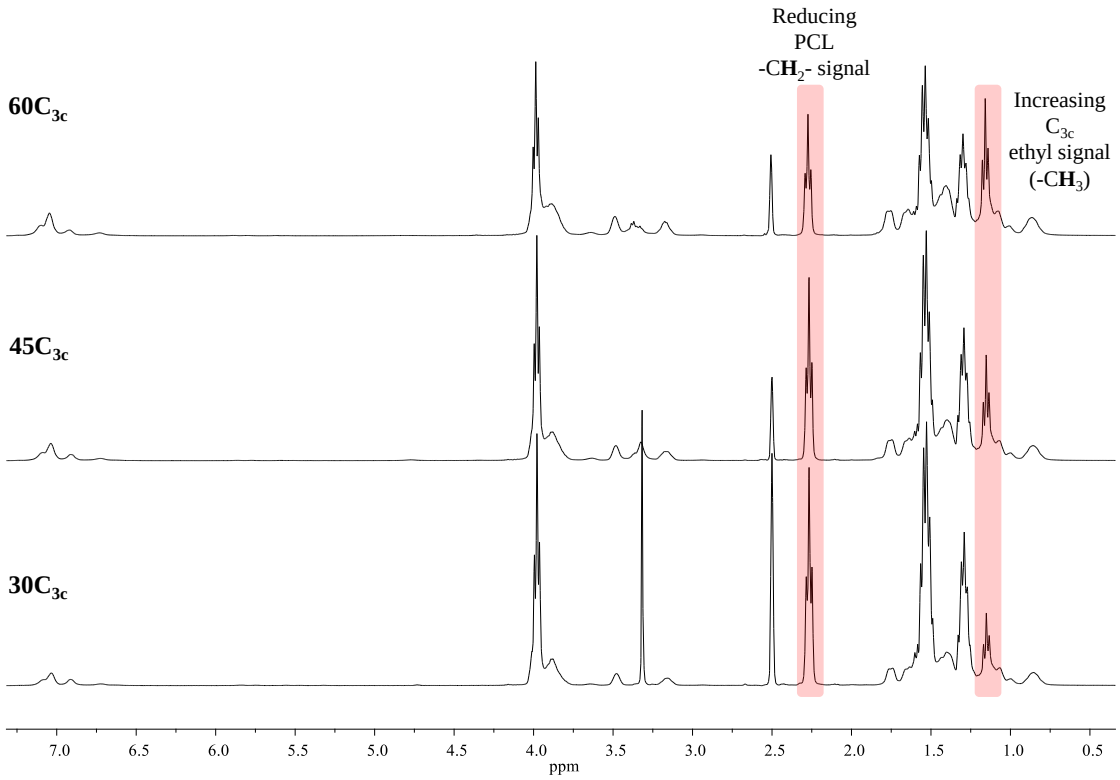

Figure 5.9. ^{1}H NMR spectra of C_{3c}-based TPEUs (Table 5.1). (400 MHz, 298 K, DMSO-d_6).

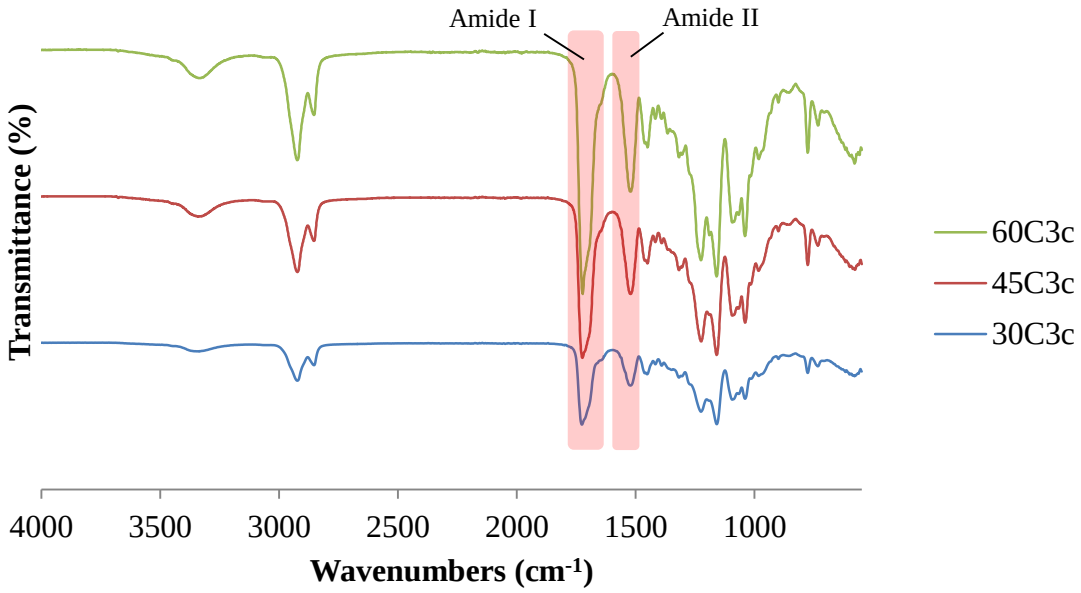

Figure 5.10. FT-IR spectra of C_{3c}-based TPEUs.

This trend was also observed for the C_{3u}-based TPEUs, however additional peaks in the ^{1}H NMR spectrum at δ = 5.83 ppm and 5.99 ppm which corresponds to the C_{3u} urea protons were also found to increase with increasing hard segment. Using the integration of these urea protons and the PCL protons α to the carbonyl (δ = 2.27 ppm), the ratio of extender to polyol could be determined and was found to be in agreement with the ratios calculated (eq 4.1) (Fiqure 5.11). Furthermore, the FT-IR spectrum of the C_{3u}-based TPEUs displayed a second carbonyl stretching frequency (~ 1660 cm^{-1}), which corresponds to the urea carbonyl, was present in conjuntion with the urethane carbonyl stretching frequency. This band was also found to increase with increasing hard segment indicative of retention of side group functionality with varying compositions.

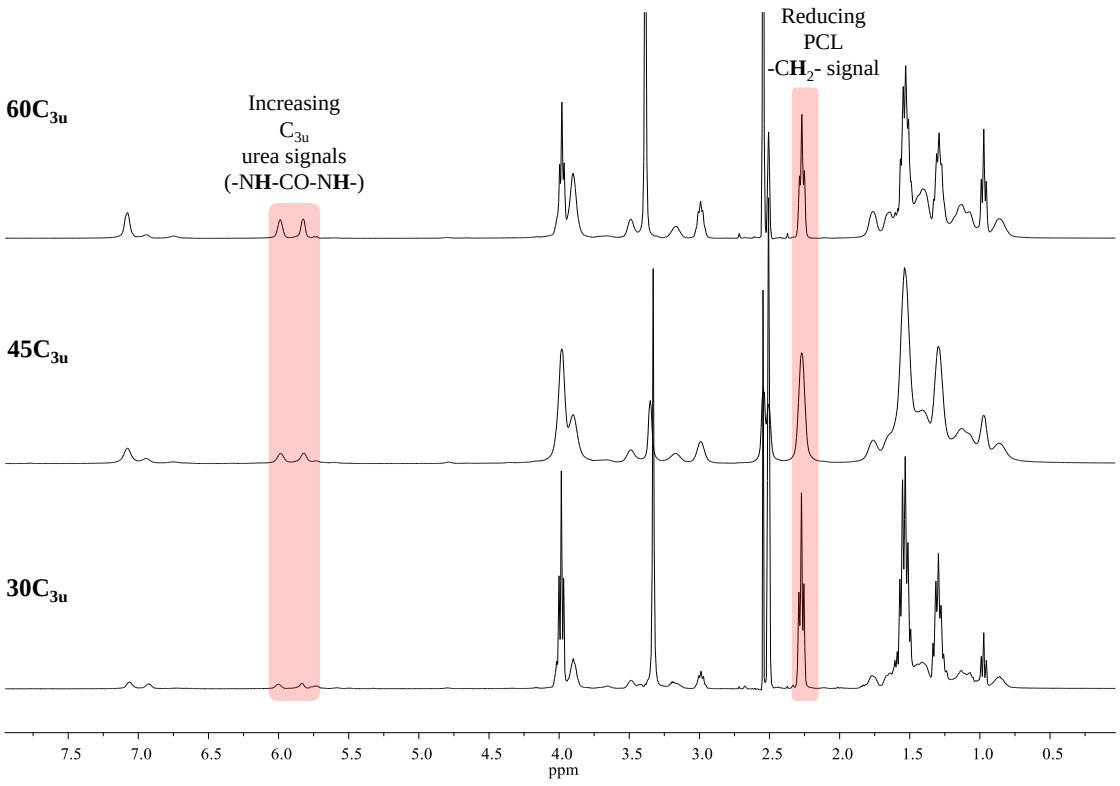

Figure 5.11. ^{1}H NMR spectra of C_{3u}-based TPEUs (Table 5.1). (400 MHz, 298 K, DMSO-d_6).

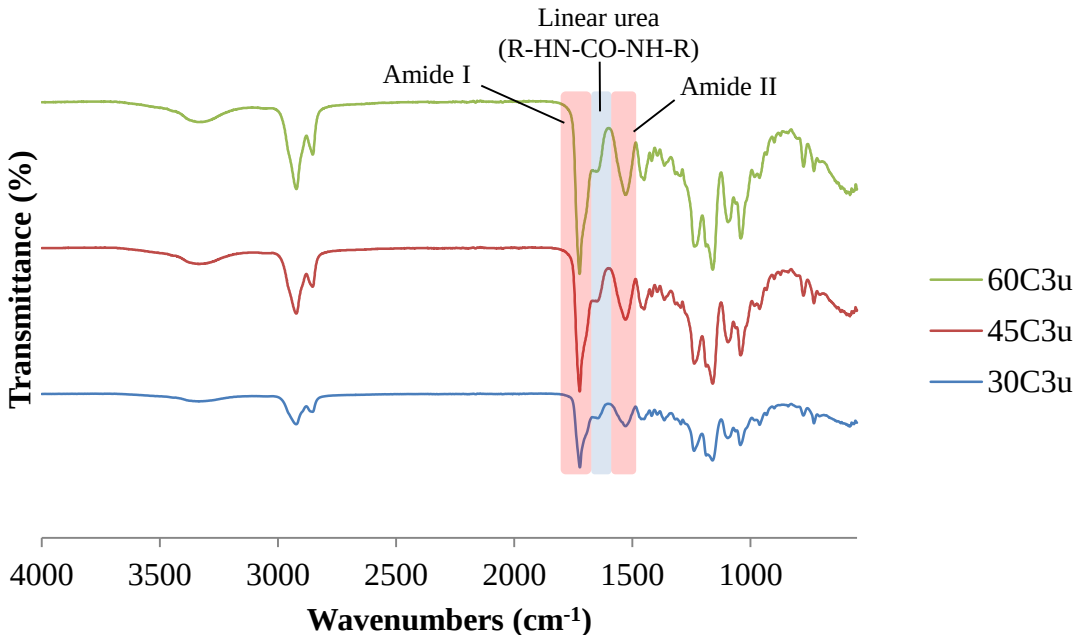

Figure 5.12. FT-IR spectra of C_{3u} TPEUs (Table 5.1).

In the case of both the C_{3c} and C_{3u}-based TPEUs, the complete consumption of the H_{12}MDI was confirmed by FT-IR spectroscopy by the absence of an absorption band between 2275-2250 cm^{-1} which corresponds to the absorption frequency of the diisocyanates cumulated double bonds.

In order to deduce the effect of side group functionality on the mechanical properties of the C_{3c} and C_{3u}-based TPEUs, the tensile properties of the materials were investigated by tensiometric analysis, analogous to previous chapters. For comparative reasons, each TPEU was annealed at 25 °C in an incubator for 5 days before in order to promote phase separation of the 'hard' and 'soft' segments. The TPEUs were subsequently subjected to axial loading at a constant crosshead speed, or rate of elongation, (5 mm min^{-1}) until failure. From an average of 10 comparable samples, the Young's modulus (E), elongation at break (ε_{break}) and ultimate tensile strength (UTS) of the materials were determined (Table 5.2).

Table 5.2. Comparison of tensile properties of C_{3c} and C_{3u}-based TPEUs.

Polymer	*E* (MPa)[a]	ε_{break} (%)[a]	UTS (MPa)[a]
$30C_{3c}$	8.6 ± 0.20	1050 ± 31	10.1 ± 0.19
$45C_{3c}$	37.2 ± 0.81	561 ± 11	12.2 ± 0.51
$60C_{3c}$	156.2 ± 2.3	39 ± 5	15.4 ± 0.91
$30C_{3u}$	13.0 ± 0.39	619 ± 19	10.4 ± 0.33
$45C_{3u}$	60.5 ± 0.98	309 ± 13	21.7 ± 0.29
$60C_{3u}$	167.5 ± 1.95	85 ± 6	26.5 ± 0.15

[a] Determined by tensiometric analysis (average of 10 samples, Figure 5.13-5.14)

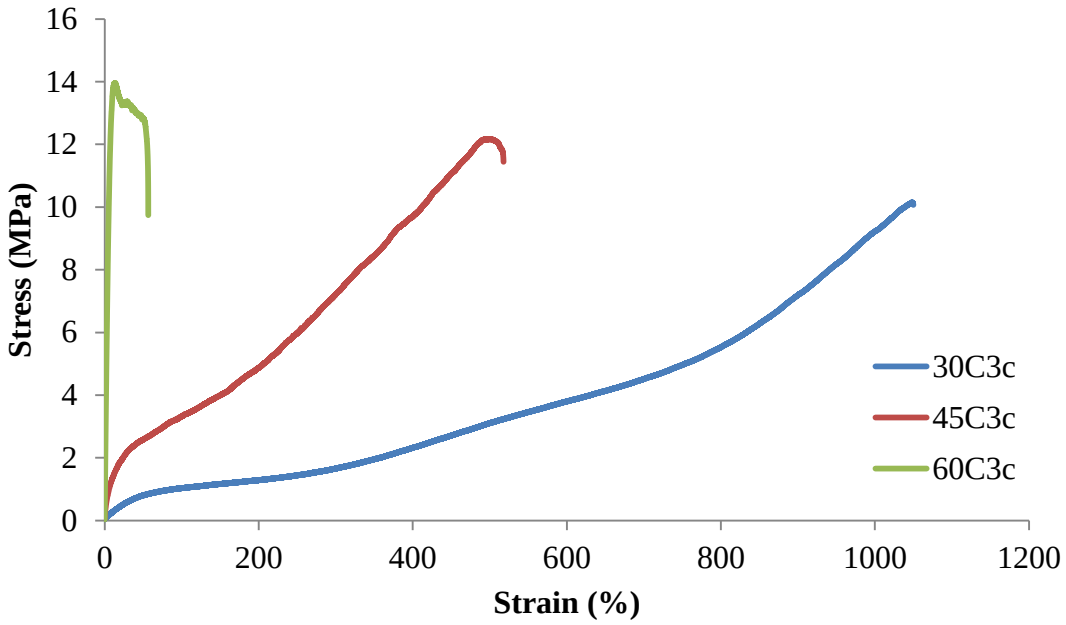

Figure 5.13. Exemplar stress-strain curves of C_{3c}-based TPEUs (Table 5.2). Experiments were conducted at ambient temperature (~ 25 °C) at an elongation rate of 5 mm min^{-1} until failure.

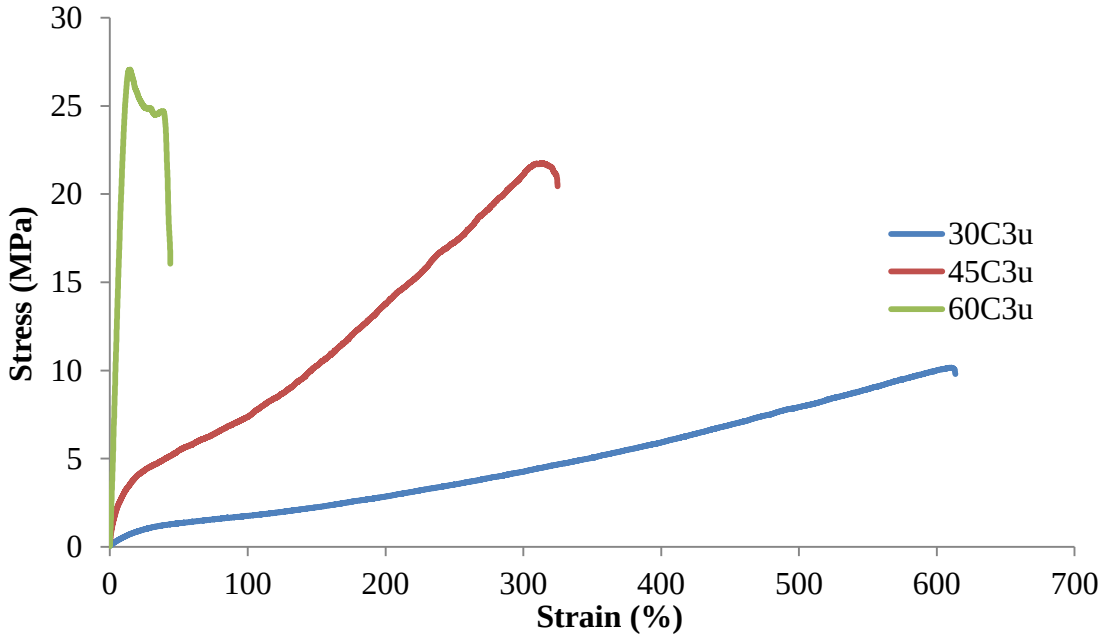

Figure 5.14. Exemplar stress-strain curves of C_{3u}-based TPEUs (Table 5.2). Experiments were conducted at ambient temperature (~ 25 °C) at an elongation rate of 5 mm min^{-1} until failure.

For both C_{3c} and C_{3u}-based TPEUs, it was found that both *E* and UTS increased proportionately with increasing %HS, however, elongation at break was found to be inversely proportionate. As described in chapter 4, this is owed to the increased brittle nature of the materials as the PU 'hard' segments becomes the major component of the bulk material and therefore dictating the mechanical properties. Furthermore, it was found that at higher %HS (*e.g.* 60%) both the carbamate and urea functional materials underwent severe plastic deformation at relatively low strains (<20%) before mechanical failure. Conversely, low %HS (30-45%) led to materials which displayed a nonlinear viscoelastic behaviour with a recoverable deformation at 40-50% strain (Figure 5.13-5.14).

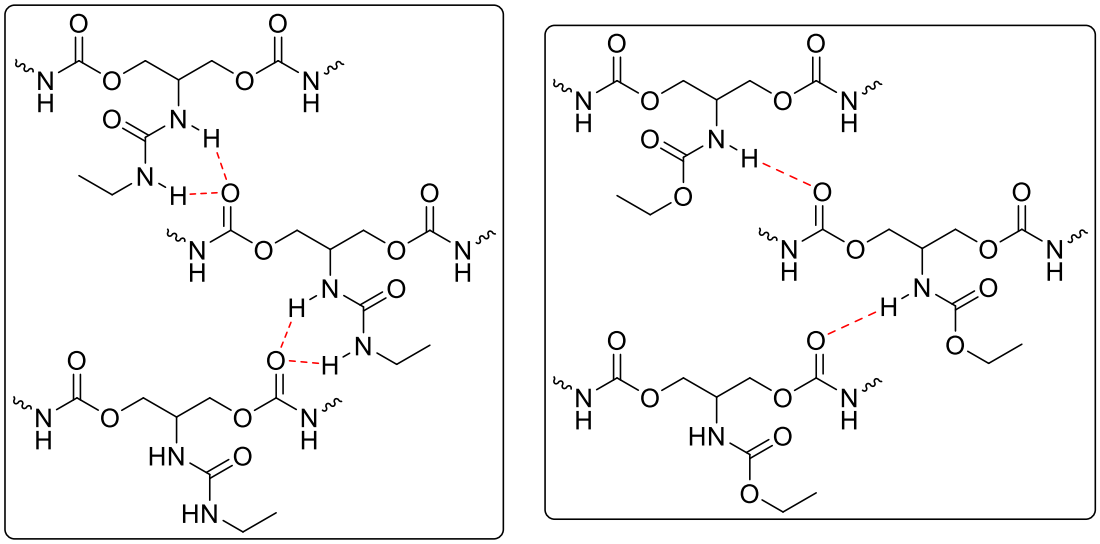

Urea functionality Carbamate functionality

Figure 5.15. Hydrogen bonding between C_{3u}-based hard segments (*left*) and C_{3c}-based hard segments (*right*).

In comparison, it was found that the C_{3u}-based TPEUs exhibited a reduced ε_{break} than the equivalent %HS C_{3c}-based TPEUs. It is hypothesised that this is owed to the increased uniform organisation of the hard segments as a consequence of the improved hydrogen bonding through the side groups when moving from the carbamate to the urea functionality (Figure 5.15). This enhanced hydrogen bonding led to the improved phase separation of the segmented C_{3u}-based TPEUs and consequently led to the stiffening of the materials. In turn, this stiffening not only reduced the ε_{break}, but produced materials with superior Young's moduli and UTS.

In order to verify this hypothesis, the extenders and TPEUs were analysed using wide-angle x-ray diffraction (WAXD), allowing for the visualisation of the phase separated domains. All diffraction patterns were plotted as a function of Bragg's angle (2θ) (Figure 5.16).

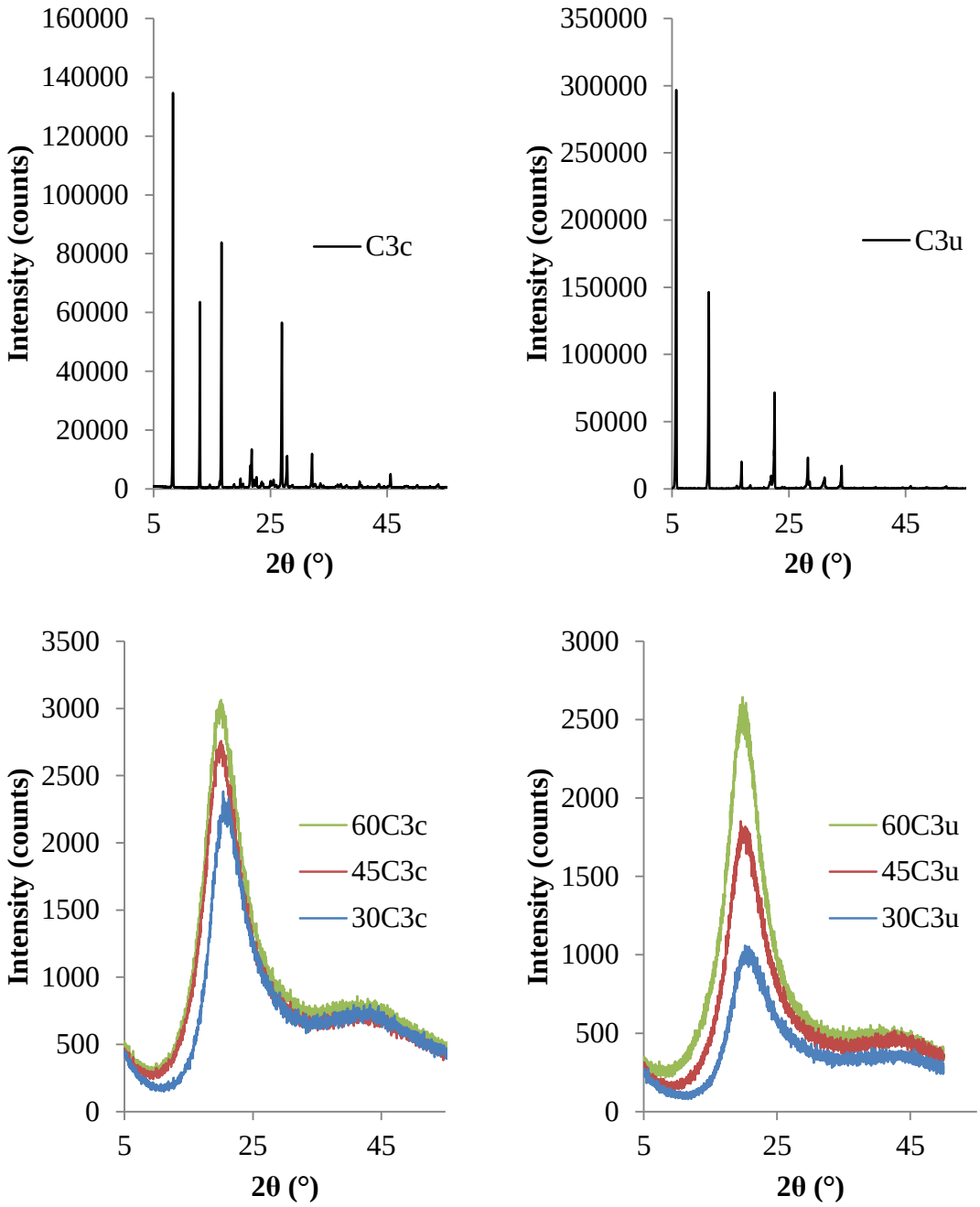

Figure 5.16. WAXD patterns for C_{3c} extender and TPEUs (*left*) and C_{3u} extender and TPEUs (*right*).

For both C_{3c} and C_{3u} extenders, it was found that the x-ray diffraction patterns displayed a series of sharp crystalline peaks with a Bragg's angle (2θ) between 5-30°, however,

the resultant TPEUs were found to display two broad undefined peaks at 2θ ≈ 19° and 2θ ≈ 44°, indicative of phase separated amorphous domains attributed to the 'hard' polyurethane segment and the 'soft' PCL segment respectively.

As has been described in literature, the deconvolution of broad amorphous peaks allows for the differentiation of minor from major phase and therefore provides information on the statistical organisation of the mesoscopic structure.[16,17] Using a Gaussian peak-fit on the baseline-corrected peaks attributed to the functionalised polyurethane 'hard' segment, the amorphous regions were deconvoluted, using the OriginPro 8 software, until the adjusted R^2 value was > 0.99. It was found that when the side group functionality of the C_3 extenders was altered from the carbamate to the urea, there was a decrease in the number of deconvoluted peaks (Figure 517-5.18).

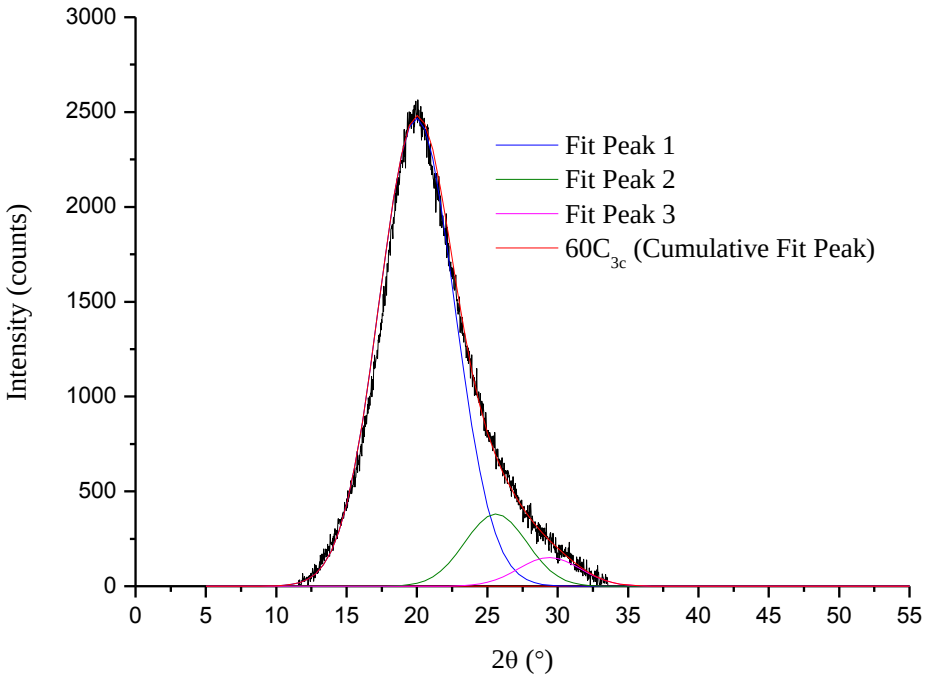

Figure 5.17. Deconvoluted baseline-corrected WAXD pattern of the 'hard' PU segment of the $60C_{3c}$ TPEU.

The reduction in the number of deconvoluted peaks observed in the C_{3u}-based TPEUs is indicative of a reduction of the number of minor phases, and therefore, an increased uniformity of the C_{3u}-based 'hard' segments in comparison with the C_{3c}-based TPEUs.

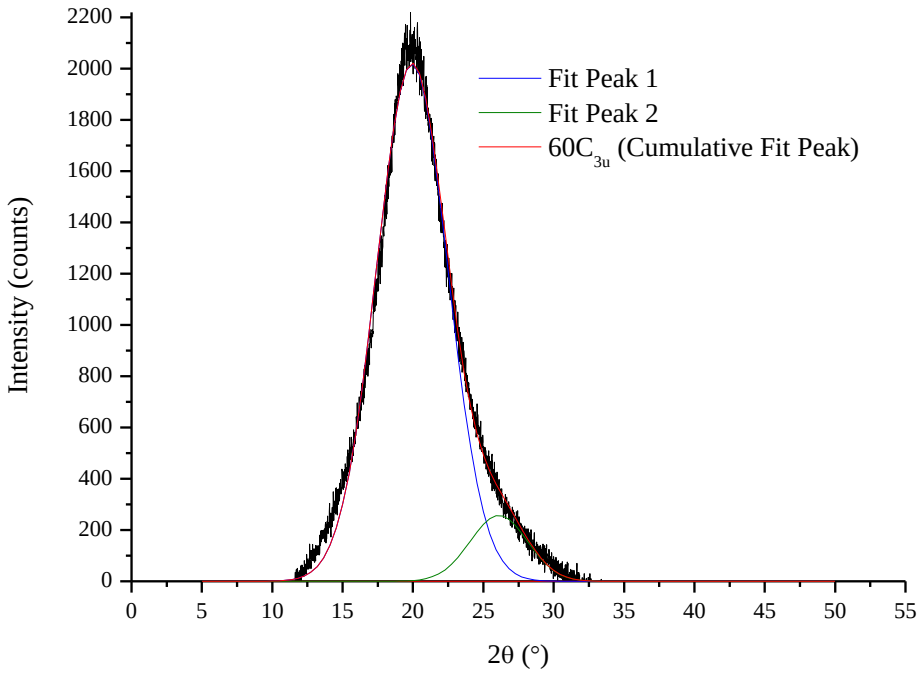

Figure 5.18. Deconvoluted baseline-corrected WAXD pattern of the 'hard' PU segment of the $60C_{3u}$ TPEU.

As has been extensively reported in literature, copolymers composing of immiscible blocks can form discrete domains through phase separation, which exhibit independent thermally-induced phase transitions (*i.e.* glass transitions, melt transitions, crystallisation *etc*.). As such, dynamic mechanical thermal analysis (DMTA) was employed to further verify the synthesis of phase separated segmented TPEUs, by the measurement of glass transition temperatures (T_g) of both the 'hard' PU and 'soft' PCL segments.

DMTA was selected as it offers a more sensitive measurement of thermal transitions of segmented multi-block copolymers than other thermal analysis (differential scanning calorimetry (DSC)). Thermal transitions, such as the glass transition of a material, are characterised by a decrease in the elastic, or storage, modulus of a material, while a maximum in the non-elastic, or loss, modulus is reached. The T_g of a material can therefore be defined in terms of the tangent function of the ratio of the storage and loss modulus, given as the equation 5.2 (eq. 5.2);

$$\tan \delta = \frac{E''}{E'} \qquad (\mathbf{5.2})$$

Where δ is the phase angle, E'' is the loss modulus and E' is the storage modulus. As has been previously described, the T_g of a polymer is defined as the peak maxima of tan δ.

Furthermore, DMTA was selected owing also to its ability to determine the storage modulus (E') of viscoelastic materials at given temperatures. The storage modulus is defined as the modulus of the 'in-phase' or elastic region of a material and is calculated using equation 5.3 (eq.5.3);

$$E' = \frac{\sigma}{\varepsilon} \cos \delta \qquad (\mathbf{5.3})$$

Where σ is the bending stress, ε is the strain and δ is the phase angle.

In a similar manner to the preparation of samples for tensile analysis, each TPEU was compression moulded into beams and annealed at 25 °C in an incubator for 5 days. The TPEUs were subsequently subjected to transverse loading through single cantilever bending at a constant displacement (100 mm). The storage modulus (*E*') at 37 °C and T_g, defined by the peak maxima of tan δ, of the materials were determined (Table 5.3).

Table 5.3. Comparison of thermal mechanical properties of C_{3c} and C_{3u}-based TPEUs.

Polymer	*E*' at 37 °C (MPa)[a]	T_g of PCL 'soft' segment (°)[b]	T_g of PU 'hard' segment (°)[b]
$30C_{3c}$	4.01	-45.7	36.5
$45C_{3c}$	4.63	-38.1	37.1
$60C_{3c}$	5.21	-36.8	37.9
$30C_{3u}$	15.4	-52.3	88.1
$45C_{3u}$	77.8	-50.9	88.0
$60C_{3u}$	183.9	-47.8	87.8

[a]Determined by DMTA using eq 5.2, [b]determined by DMTA, value taken as the peak maximum of tan δ.

As predicted, it was found that the tan δ curves displays two peaks which corresponds to the T_g of the PCL 'soft' segment and the PU 'hard' segment (Table 5.3). The T_g of the PCL segments was found to be between -40 and -50 °C, consistent with previous literature results.[18] The C_{3c}-based TPEUs displayed a second T_g at ~ 37 °C which corresponds to the PU 'hard' segment, while the second T_g for the C_{3u}-based TPEUs were displayed at ~ 88 °C (Figure 5.19-5.20). As mentioned previously, the presence of

two T_g's this is indicative of, and further verifies, the formation of a phase separated material.

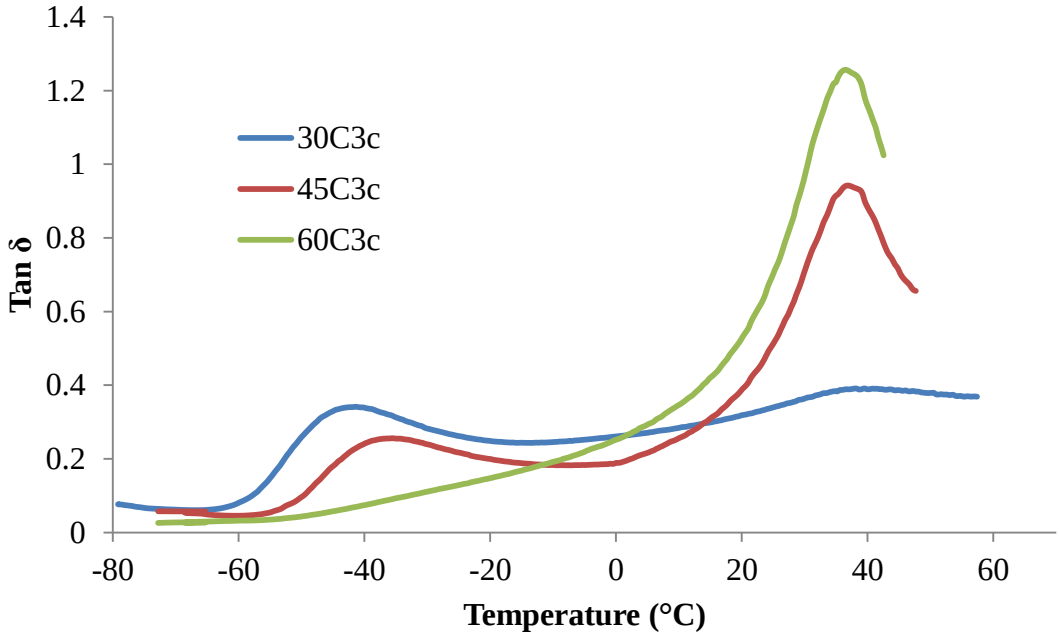

Figure 5.19. Tan δ vs temperature curves for C_{3c}-based TPEUs

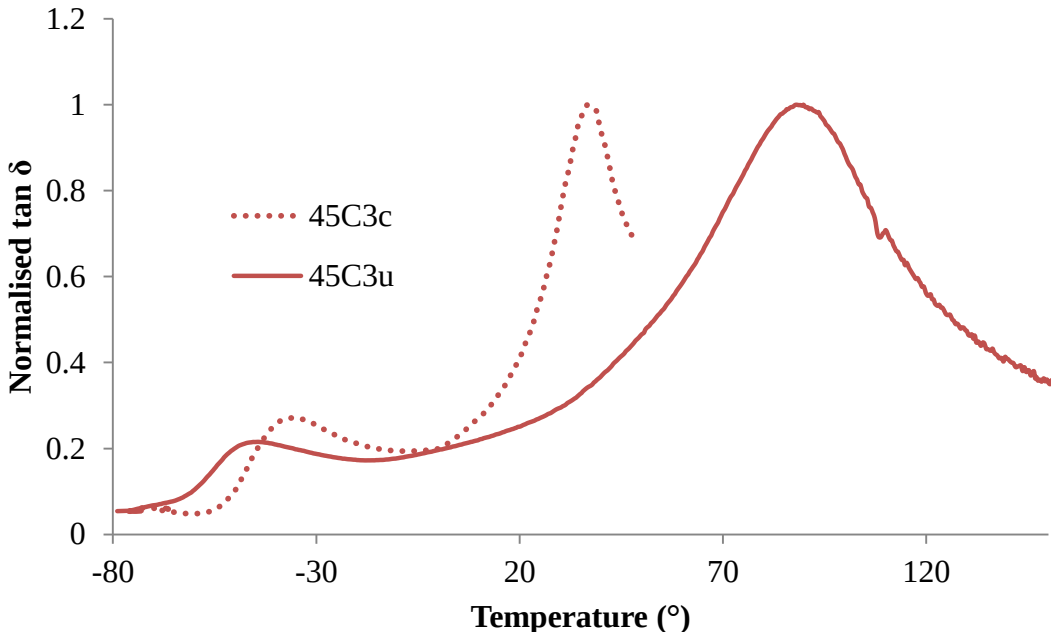

Figure 5.20. Normalised tan δ vs temperature curves; comparison of $45C_{3c}$ and $45C_{3u}$ TPEUs.

The materials were also analysed in order to determine their storage modulus (E') at body temperature (37 °C). It was found that for the C_{3u}-based TPEUs, the E' was found to be higher than the Young's modulus (E) determined by tensile analysis. Although both E and E' are defined as the modulus of a material for the elastic region, E is determined by applying an axial load on a material creating tensile strain. Conversely, during the application of a transverse load on a material in a bending mode, both tensile and compressive strains are observable (Scheme 5.3). As has been extensively reported, the compressive strength of bulk polymeric materials tends to be significantly higher than the tensile strength.[19] Therefore, E', determined by DMTA, appears higher than E but lower than the compressive modulus of the material. Interestingly the C_{3c}-based TPEUs did not exhibit this apparent compressive stiffening, owing to the low T_g of the TPEU 'hard' segments. This led to the softening of the C_{3c}-TPEUs and therefore the loss of mechanical rigidity.

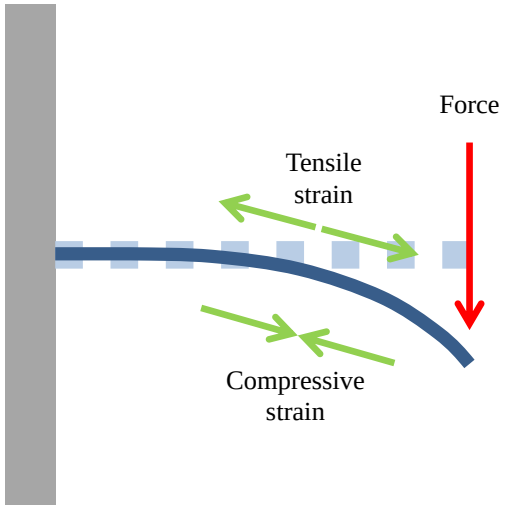

Scheme 5.3. Application of a transverse load in a single cantilever bending experiment exhibiting both tensile and compressive strain.

In order to assess the hydrolytic degradability of the C_{3c} and C_{3u}-based TPEUs, in conjunction with the effect of side-group functionality on the degradation and swelling rates, the materials were subjected to accelerated degradation conditions. Each of the TPEUs was compression moulded into degradation 'disks' and placed into individual vials before being submerged in basic aqueous media (5 M aq. NaOH). The degradation samples were stored at 37 °C with constant agitation at 60 rpm and the weights of the dried disks were measured periodically with an analytical balance until they were unretrievable from the degradation media. This method was chosen to exhibit the hydrolytic degradation of the TPEUs as it allowed for the most rapid analysis and comparison of the degradation properties of the materials. The accelerated degradation was performed in triplicate and all results were reported as an average.

As has been described in Chapter 1, the most common mode of degradation exhibited by polyester-urethanes (PEUs) is bulk erosion. Bulk erosion is characterised by a higher rate of water ingression into the polymer network than of hydrolysis of susceptible bonds. As such, the percentage of water uptake or 'swelling' of the C_{3c} and C_{3u}-based TPEUs, in comparison to starting weight, was determined. Furthermore, as the rate of water uptake is, amongst other factors, dependant on hydrophilicity of the material, static contact angle measurements were also made on solvent cast thin films of the materials in order to characterise this property. It was found that for both the C_{3c} and C_{3u}-based TPEUs, that percentage swelling increased proportionately with %HS. Conjointly, a decrease in the contact angle with increasing %HS was also observed (contact angle 30>45>60 %HS, Figure 5.21). This is indicative of an increased hydrophilicity of the material obtained with increasing extender content. This increased hydrophilicity allows for a greater totally percentage ingression of degradation media and also a greater degree of wettability as seen by static contact angle.

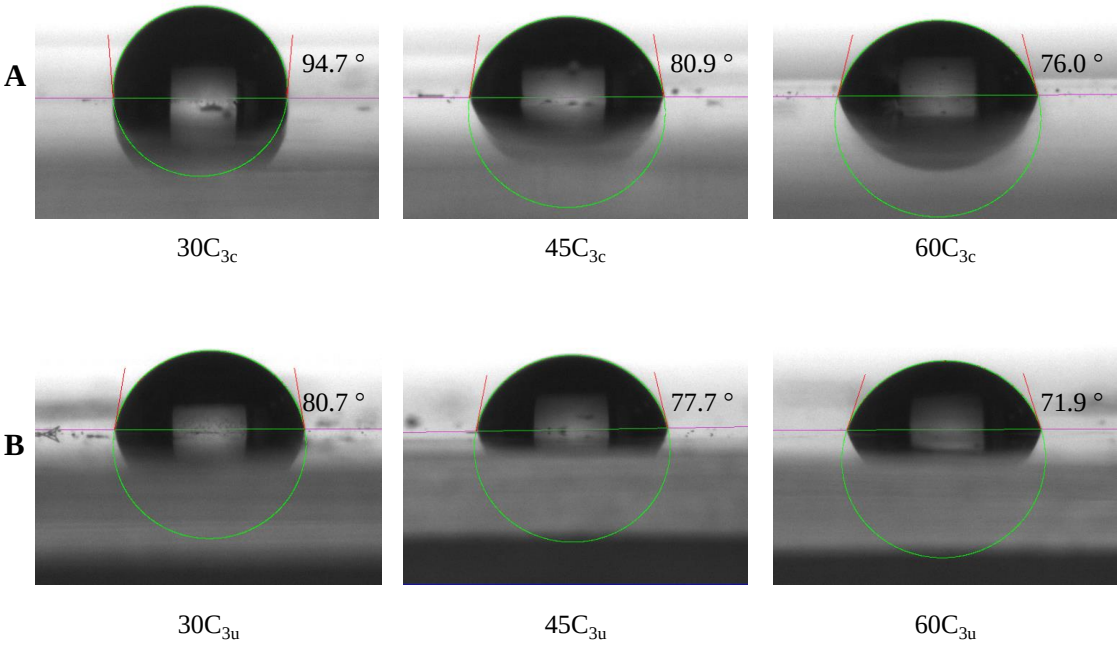

Figure 5.21. Static contact angle measurements for (A) C_{3c} and (B) C_{3u}-based TPEUs. Contact angle increases with increasing %HS (30>45>60 %HS).

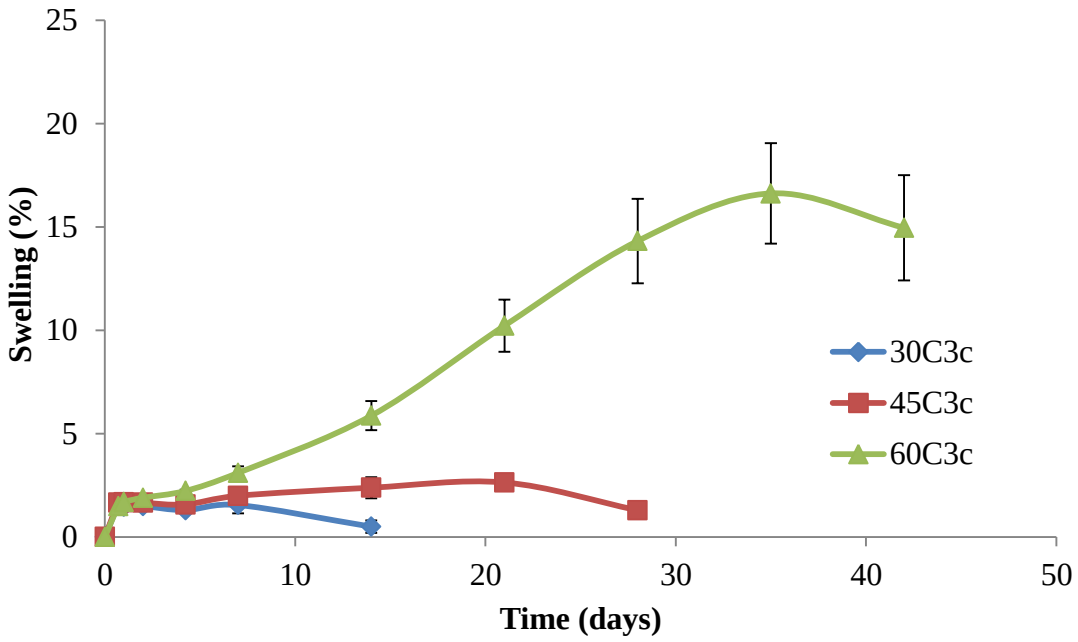

Figure 5.22. Percentage swelling for C_{3c}-based TPEUs, average of 3 samples.

Furthermore, it was noted that the rate of swelling was also dependant on side-group functionality. It was found that when transitioning from the carbamate- to the urea-functional extender, a dramatic increase in the initial percentage swelling is observed. In the case of the 60 %HS materials, the C_{3c}-based TPEU ($60C_{3c}$) exhibited a maximum swelling of 16.6 % after 35 days. Similarly, the $60C_{3u}$ material exhibited a maximum swelling of 15.9 %. Conversely, however, the $60C_{3u}$ material exhibited 13.2 % of its swelling within in the first 5 days, in comparison to the 2.2 % swelling of the $60C_{3c}$ material in the same time (Figure 5.22-5.23). This trend held true for both 30 and 45 %HS materials also. It is important to note, although swelling is not independent of network degradation, it offers a good comparative model for the hydrophilicity of a series of materials.

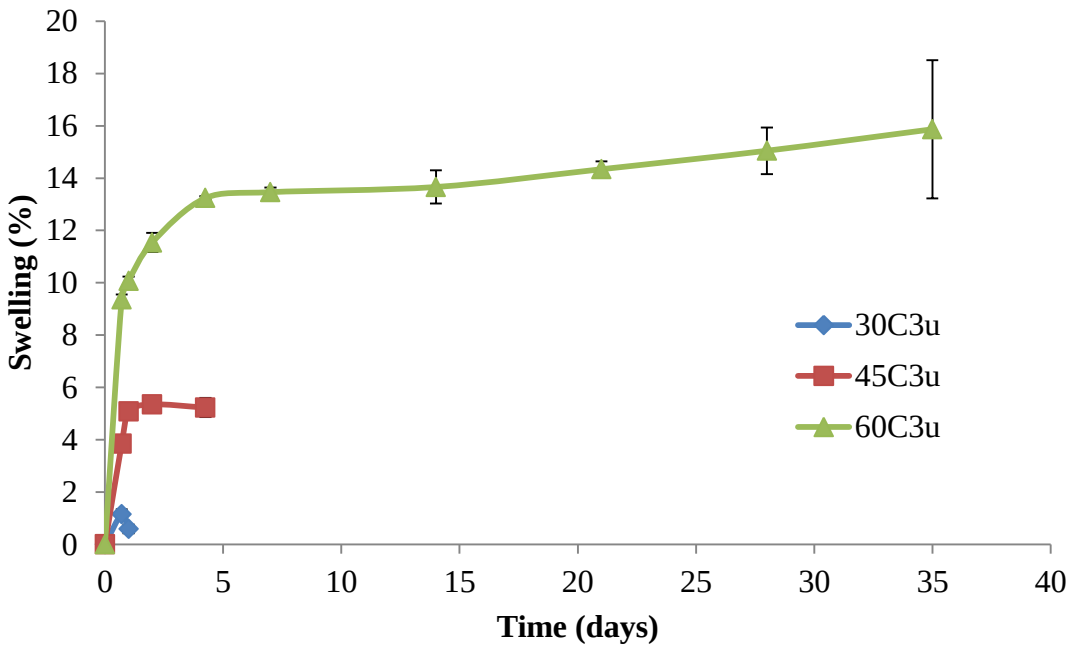

Figure 5.23. Percentage swelling for C_{3u}-based TPEUs, average of 3 samples.

For both the C_{3c} and C_{3u}-based TPEUs, it was observed that the rate of degradation to increase with %HS. This is partly owed to the increased hydrophilicity observed allowing for a higher concentration of degradation medium to ingress into the polymer network, consistent with the swelling and contact angle results previously described.

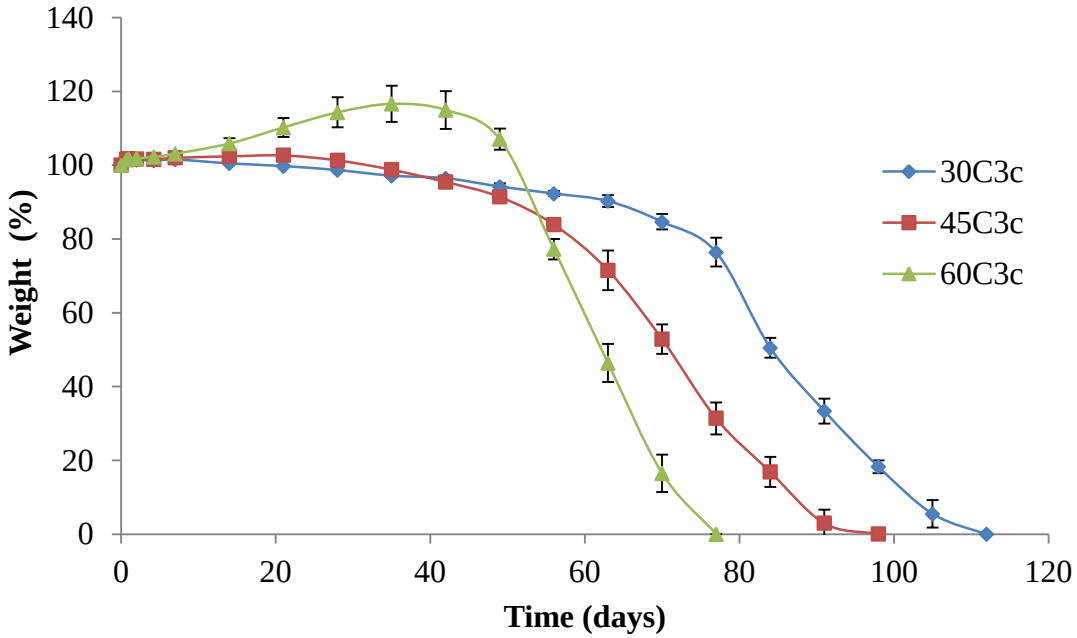

Figure 5.24. Percentage weight for C_{3c}-based TPEUs, average of 3 samples.

Furthermore, from the degradation profiles of the C_{3c} and C_{3u}-based TPEUs, it is noted that a higher rate of degradation is observed for the urea-functional materials in comparison to the carbamate-functional materials (Figure 5.24-5.25). This is partly owed to the increased rate of water uptake into the more hydrophilic C_{3u}-based TPEUs allowing for an increased rate of hydrolysis. In addition to this, ethylamine released upon the degradation of the urea side groups of the C_{3u} moiety, can go on to further catalyse the hydrolysis process. This process of auto-catalysis allows for the efficient

degradation of the polymer network which allows further ingression of the degradation media.

Although, the degradation of the carbamate side groups of the C_{3c} moiety produces a carbamic acid analogue, also observed in the urea degradation, this is only present on the polymer backbone and is therefore less able to infiltrate and aide degradation throughout the polymer network. The presence of this carbamic acid analogue however, may in conjunction with network swelling, elucidate the secondary swelling process observed in both the C_{3c} and C_{3u}-based TPEUs.

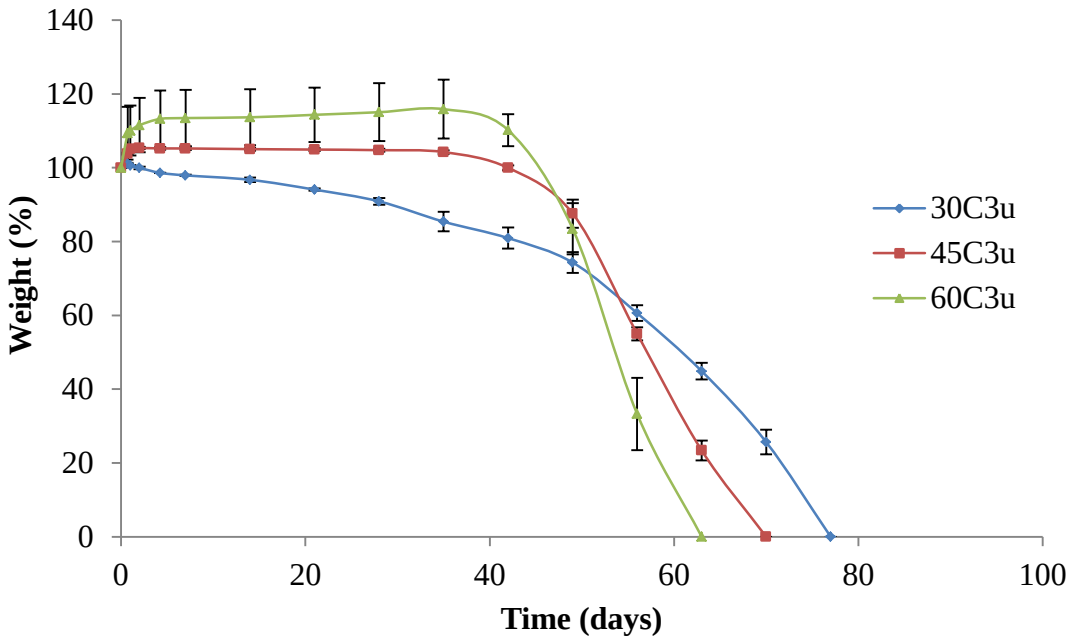

Figure 5.25. Percentage weight for C_{3u}-based TPEUs, average of 3 samples.

5.2.4 Synthesis of TPEUs from C_{4u} and C_{5u} extenders; a comparison of the effects of chain length.

In order to investigate the effect of chain length, TPEUs were made as previously described in the synthesis of the C_{3u}-based TPEUs. As with the C_{3u}-based TPEUs, it was found that C_{4u} and C_{5u}-based TPEUs exhibited a unimodal distribution with a $Đ_M$ between 2.1-.2.4 characteristic of step-growth polymerisations. Furthermore, synonymously to the C_{3u}-based TPEUs, the successful incorporation of the C_{4u} and C_{5u} extenders, at the ratios calculated by eq. 5.1, could be confirmed by ^{1}H NMR and FTIR spectroscopy (Figure 5.26-5.28).

Table 5.4. Composition and molecular weight comparison of C_{4u} and C_{5u}-based TPEUs.

Polymer	wt % 'hard block' (%HS)	H_{12}MDI/polyol ratio (R) [a]	M_W (kg mol^{-1})[b]	$Đ_M$[b]
30C_{4u}	30	3.21	119.0	2.14
45C_{4u}	45	5.22	97.0	2.19
60C_{4u}	60	8.74	88.4	2.31
30C_{5u}	30	3.14	94.9	2.11
45C_{5u}	45	5.09	91.8	2.10
60C_{5u}	60	8.50	108.7	2.46

[a] Determined by eq 5.1. [b] Determined by GPC analysis in DMF against poly PMMA standards.

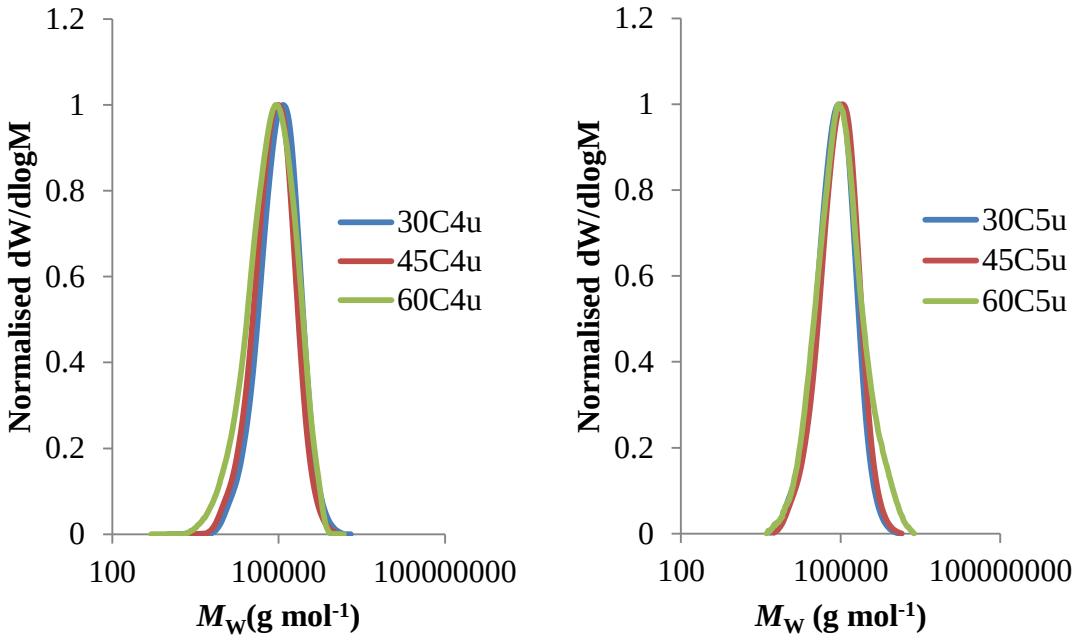

Figure 5.26. RI GPC chromatograms of C_{4u} (left) and C_{5u} (right)-based TPEUs in DMF against PMMA standards. (Table 5.4).

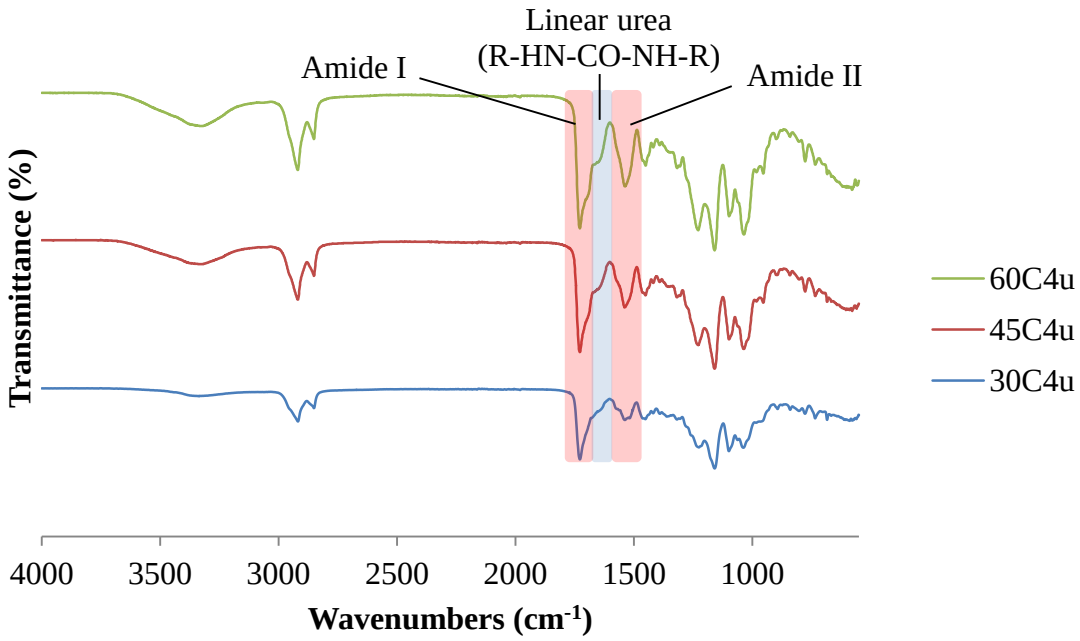

Figure 5.27. FT-IR spectra of C_{4u} TPEUs (Table 5.4).

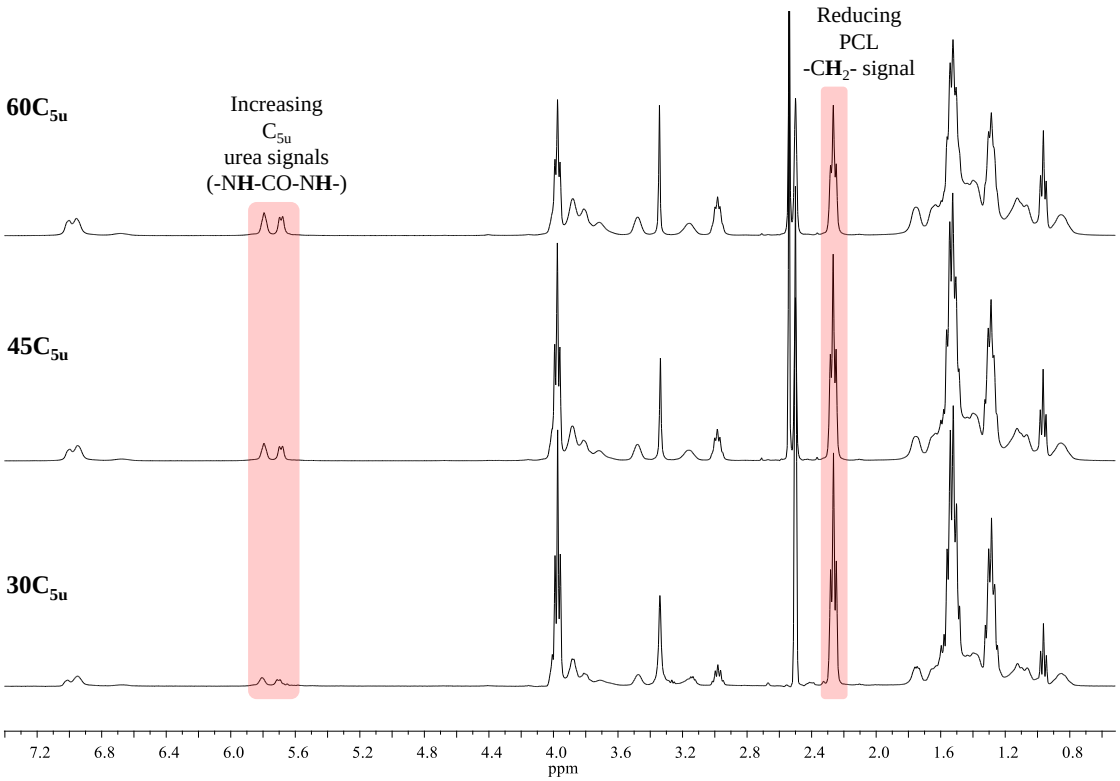

Figure 5.28. ^{1}H NMR spectra of C_{5u}-based TPEUs (Table 5.4). (400 MHz, 298 K, DMSO-d_6).

It was also found that both the C_{4u} and C_{5u}-based TPEUs, prepared as previously described, exhibited tensile properties similar to their C_3 analogues *e.g.* a proportionate increase in *E* and inversely proportionate decrease in ε_{break} with increasing %HS.

Table 5.5. Comparison of tensile properties of C_{4u} and C_{5u}-based TPEUs.

Polymer	*E* (MPa)[a]	ε_{break} (%)[a]	UTS (MPa)[a]
$30C_{3u}$	13.0 ± 0.39	619 ± 19	10.4 ± 0.33
$45C_{3u}$	60.5 ± 0.98	309 ± 13	21.7 ± 0.29
$60C_{3u}$	167.5 ± 1.95	85 ± 6	26.5 ± 0.15
$30C_{4u}$	12.8 ± 0.40	755 ± 20	13.0 ± 0.34
$45C_{4u}$	57.9 ± 0.77	470 ± 11	21.6 ± 0.19
$60C_{4u}$	151.8 ± 1.64	56 ± 5	24.8 ± 0.08
$30C_{5u}$	32.8 ± 0.28	600 ± 14	14.3 ± 0.45
$45C_{5u}$	94.2 ± 0.82	335 ± 8	24.7 ± 0.35
$60C_{5u}$	170.4 ± 1.79	47 ± 3	29.9 ± 0.20

[a] Determined by tensiometric analysis (average of 10 samples, Figure 5.30-5.31).

Furthermore, it was noted that the TPEUs based on the urea-functional extenders exhibited an increase in UTS and a decrease in ε_{break} with increasing chain length, however, in the case of the C_{3u} and C_{4u}-based TPEUs *E* remained comparable while increasing for the C_{5u}-based materials. It is hypothesised that this may be a consequence of a higher degree of flexibility within the 'hard' segment leading to more complex secondary structures and producing more rigid materials.

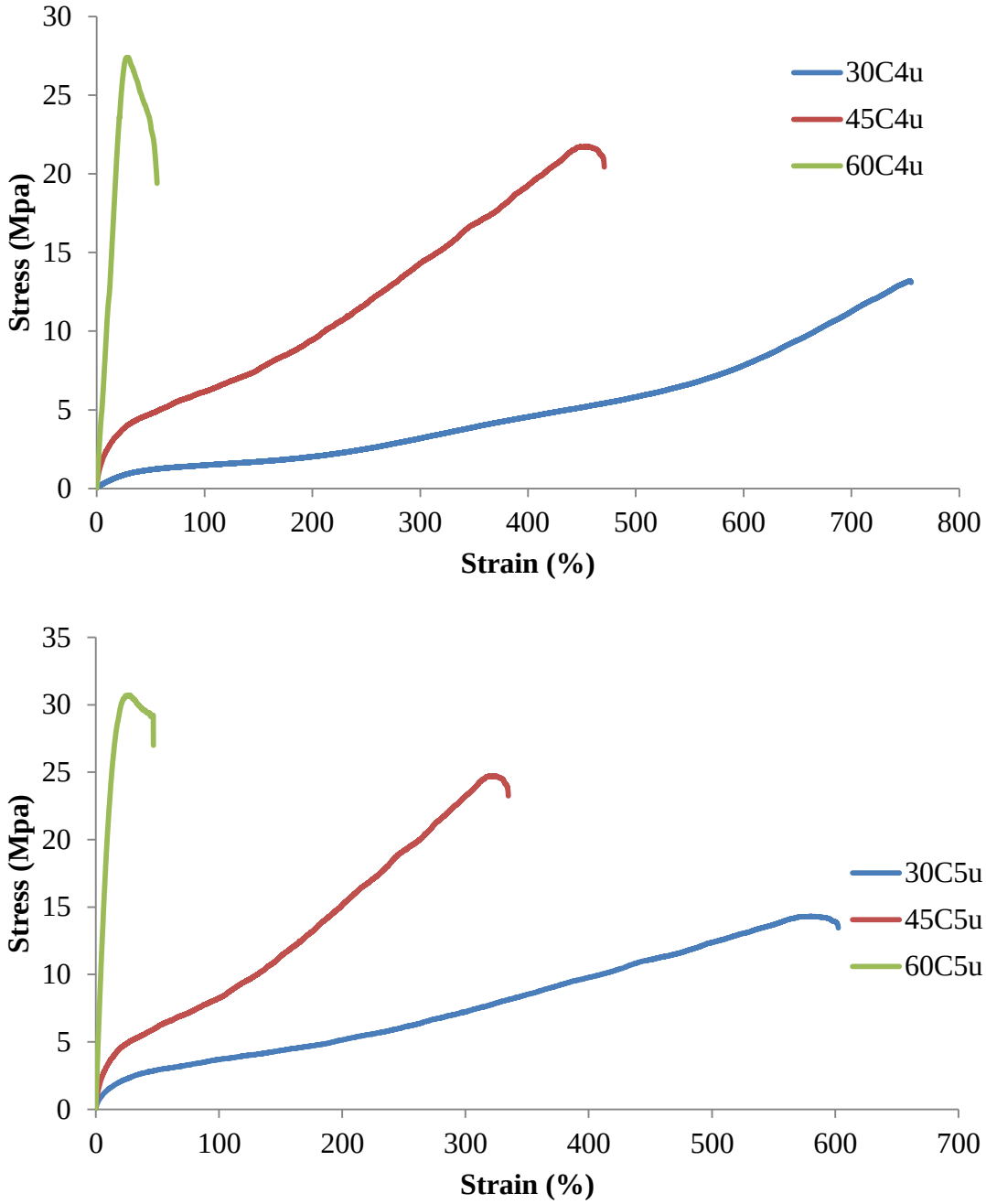

Figure 5.29. Exemplar stress-strain curves of C_{4u}- (*top*) and C_{5u}-based TPEUs (*bottom*).

As with the C_{3u}-based TPEUs, the phase separation of the the C_4 and C_{5u} materials were analysed using WAXD. Similarly, both extenders were found to exhibit diffration pattern with several sharp crystalline peaks between $2\theta \approx 5\text{-}40°$, however, it was noted that the C_{4u} extender displayed some peak broadening indicative of amorphous or imperfectly crystalline regions (Figure 5.30). The WAXD patterns of the resultant

materials were found to exhibit two broad undefined peaks at 2θ ≈ 20 and 43° which corresponds to the PU 'hard' segment and the PCL 'soft' segment respectively

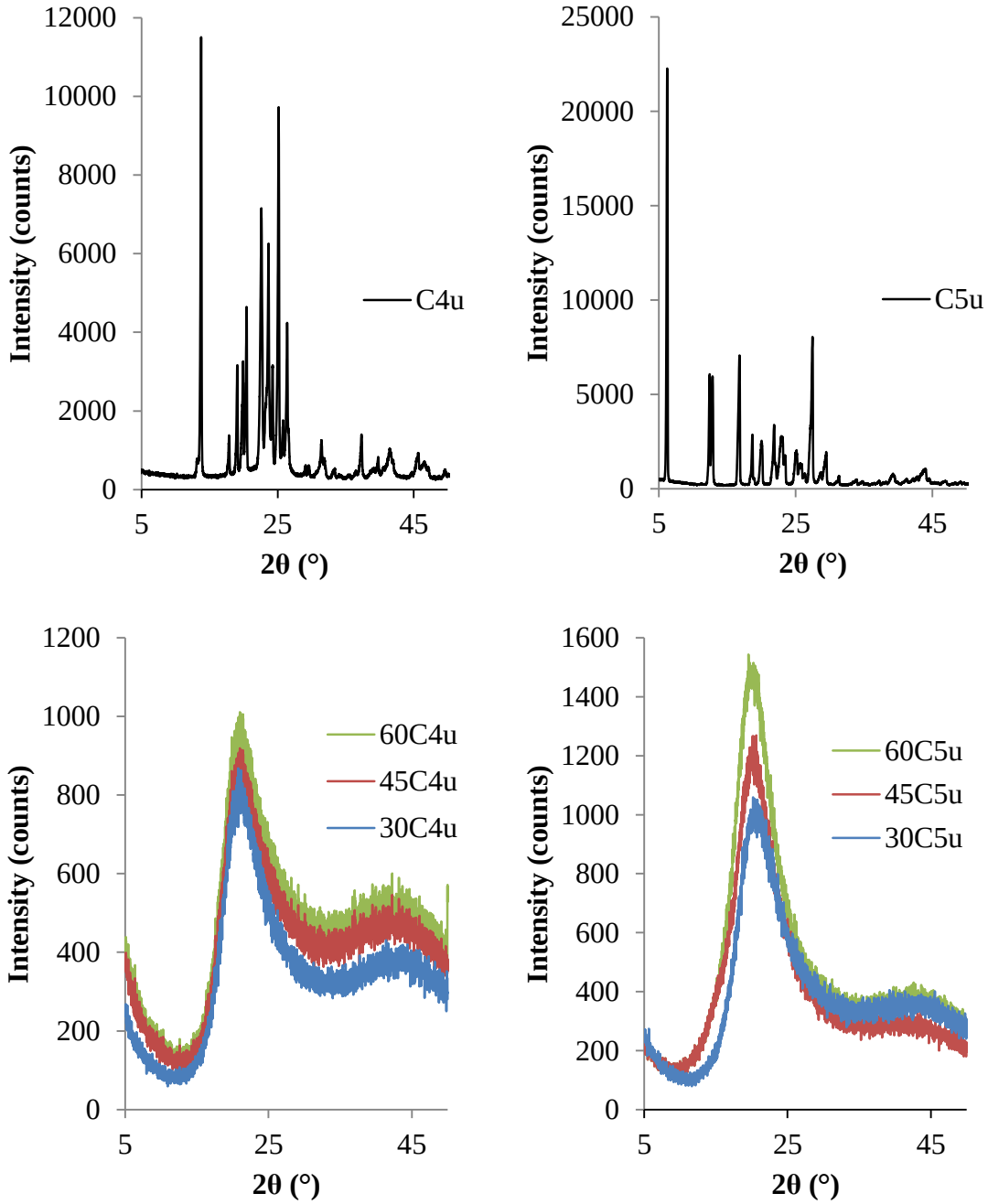

Figure 5.30. WAXD patterns for C_{4u} extender and TPEUs (*left*) and C_{5u} extender and TPEUs (*right*).

Using a Gaussian peak-fit on the baseline-corrected peaks attributed to the functionalised PU 'hard' segment as previously described for the C_{3u}-based TPEUs, the amorphous regions were deconvoluted. It was found that when moving from the C_{3u} to the C_{4u}-based TPEUs that there was an increase in number of deconvoluted peaks, however, when examining the C_{5u} analogues it was noted that the number of deconvoluted peaks decreased. It is believed that owing to steric hindrances, that the C_{3u}-based 'hard' segments are locked in a uniform arrangement, however as a consequence of increased mobility, the C_{4u}-based TPEUs are able to actualise more complex secondary structures with imperfect regularity. Furthermore, it is thought that owing to an even more increased flexibility, the C_{5u}-based TPEUs are able to permit secondary structures with a higher degree of regularity. (Figure 5.31-5.32)

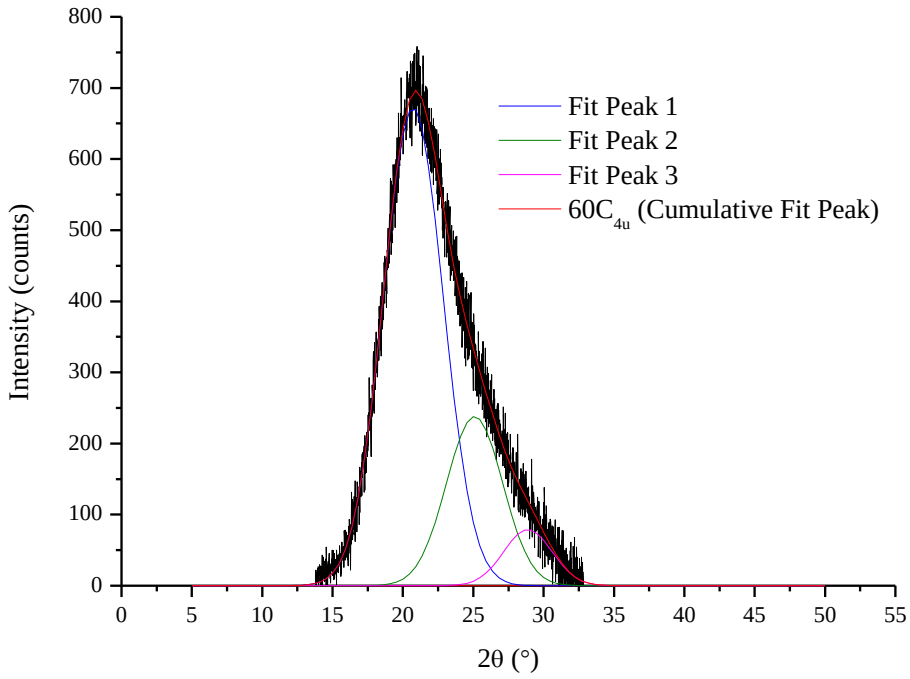

Figure 5.31. Deconvoluted baseline-corrected WAXD pattern of the 'hard' PU segment of the $60C_{4u}$ TPEU.

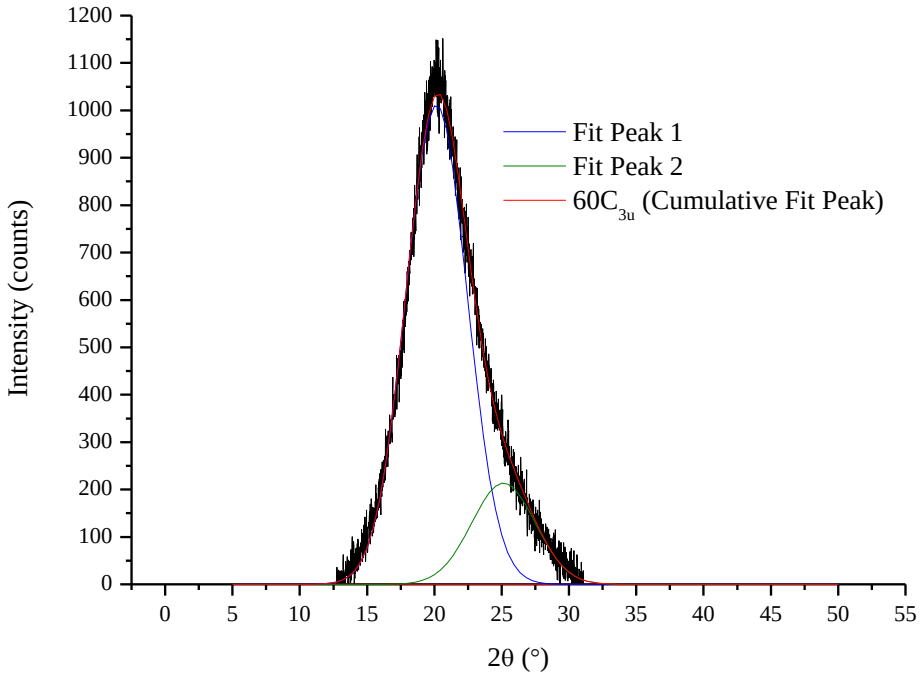

Figure 5.32. Deconvoluted baseline-corrected WAXD pattern of the 'hard' PU segment of the $60C_{5u}$ TPEU.

To further investigate the phase separation of the C_{4u} and C_{5u}-based TPEUs, the materials were subjected to dynamic mechanical and thermal analysis as per the previously described preparation and method. It was found, as predicted, that the tan δ curves exhibited two peak maxima, indicative of a phase separated material (Table 5.6). In agreement with the previous results, the T_g which corresponds to the PCL 'soft' segment was detected between -45 and -55 °C while the C_{4u}- and C_{5u}-based TPEUs exhibited a second T_g at ~ 80 and ~ 61 °C respectively, which corresponds to the PU 'hard' segment (Figure 5.33).

Table 5.6. Comparison of thermal mechanical properties of C_{4u} and C_{5u}-based TPEUs.

Polymer	E' at 37 °C (MPa)[a]	T_g of PCL 'soft' segment (°)[b]	T_g of PU 'hard' segment (°)[b]
$30C_{3u}$	15.4	-52.3	88.1
$45C_{3u}$	77.8	-50.9	88.0
$60C_{3u}$	183.9	-47.8	87.8
$30C_{4u}$	15.8	-55.0	80.0
$45C_{4u}$	61.3	-54.7	80.2
$60C_{4u}$	179.4	-49.0	79.9
$30C_{5u}$	69.4	-48.6	61.1
$45C_{5u}$	104.3	-47.1	61.0
$60C_{5u}$	201.1	-46.6	61.8

[a]Determined by DMTA using eq 5.2, [b]determined by DMTA, value taken as the peak maximum of tan δ.

In agreement with the tensile analysis, E' increased proportionately with increasing %HS. Conjointly, C_{3u} and C_{4u}-based TPEUs had comparable E' while the C_{5u}-based TPEUs exhibited a higher E'. It was also noted that E' was higher than E as a consequence of the compressive stiffening previously described.

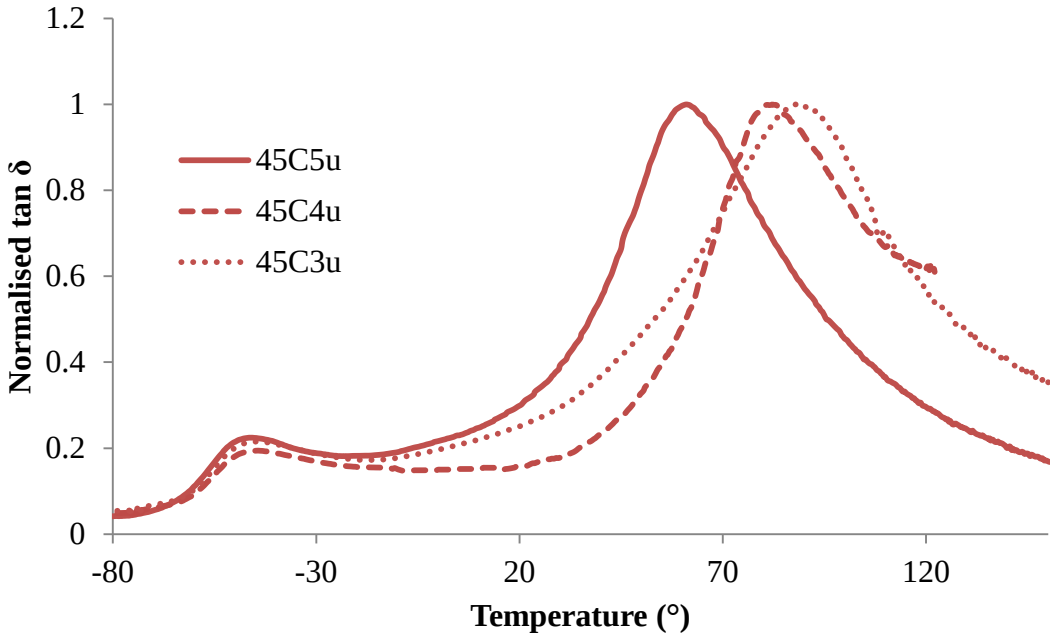

Figure 5.33. Normalised tan δ vs temperature curves; comparison of $45C_{3u}$, $45C_{4u}$ and $45C_{5u}$ TPEUs.

In order to determine the effect of extender chain length on the swelling behaviour and degradation profile of the materials, the C_{4u} and C_{5u}-based TPEUs were analysed by static contact angle and subjected to accelerated degradation as previously described. In the case of the C_{4u}-based TPEUs it was found, as with the C_{3u}-based TPEUs, that both percentage swelling and rate of swelling increased proportionately with %HS. Notably, it was found that although the percentage swelling of the C_{5u}-based TPEUs followed the same trend, the initial rate of swelling decreased with increasing %HS. Furthermore, the overall percentage swelling decreased significantly with increasing extender chain length (Figure 5.35-5.36). It is believed that this trend is owed to the increased hydrophobicity of the TPEU 'hard' segments with increasing extender chain lengths and therefore hydrocarbon content.

The increased hydrophobicity of the materials was verified by the increase in the static contact angle measurement when moving from the C_{3u} extender to the C_{4u} and C_{5u} extenders (Figure 5.34).

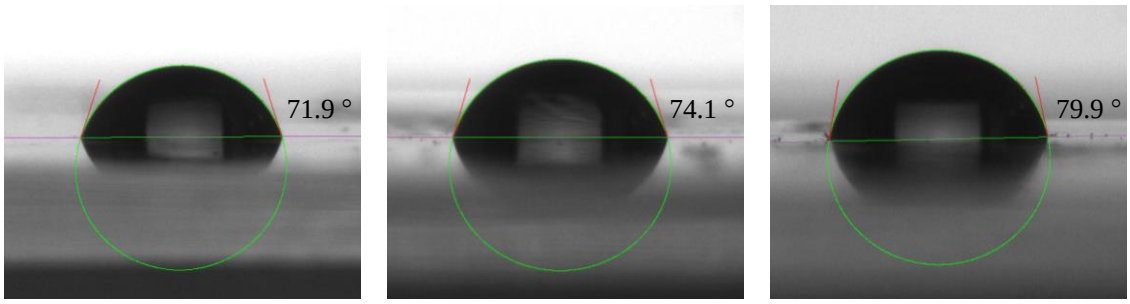

$60C_{3u}$ $60C_{4u}$ $60C_{5u}$

Figure 5.34. Comparison of static contact angle measurement of $60C_{3u}$, $60C_{4u}$ and $60C_{5u}$ TPEUs.

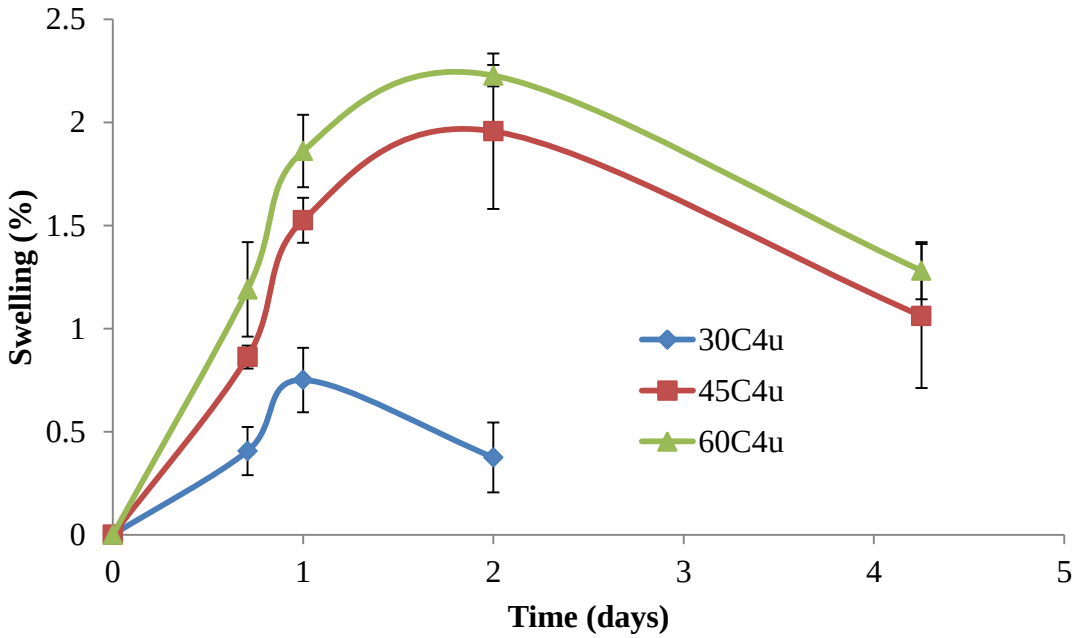

Figure 5.35. Percentage weight for C_{4u}-based TPEUs, average of 3 samples.

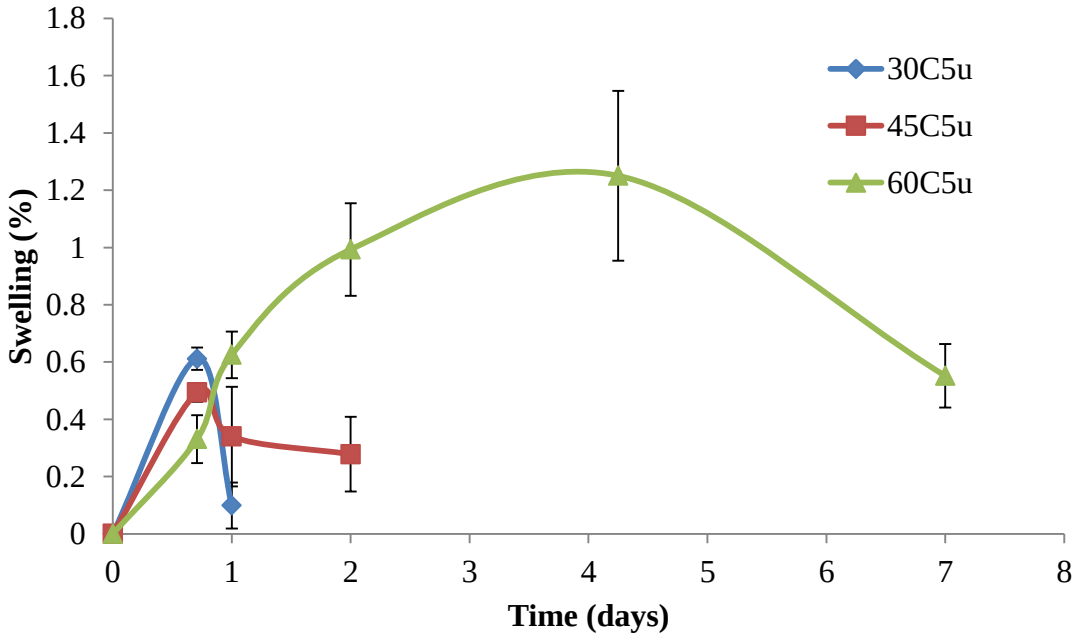

Figure 5.36. Percentage weight for C_{5u}-based TPEUs, average of 3 samples.

From the degradation profiles of the C_{4u} and C_{5u}-based TPEUs, it was found that the degradation rate of these materials was considerably slower than the degradation of the C_{3u}-based TPEUs (Figure 5.37-5.38). Furthermore, it was noted that with increasing extender chain length, the degradation profile of the materials became more linear. It is believed, in conjunction with the swelling and static contact angle data, that this is owed to the increased hydrophobicity of the TPEUs. This progression toward a more linear degradation profile, alongside the decrease in percentage swelling, is suggestive that the mode of degradation is shifting from bulk degradation to a more surface erosion-type mechanism (Figure 5.39-5.40).

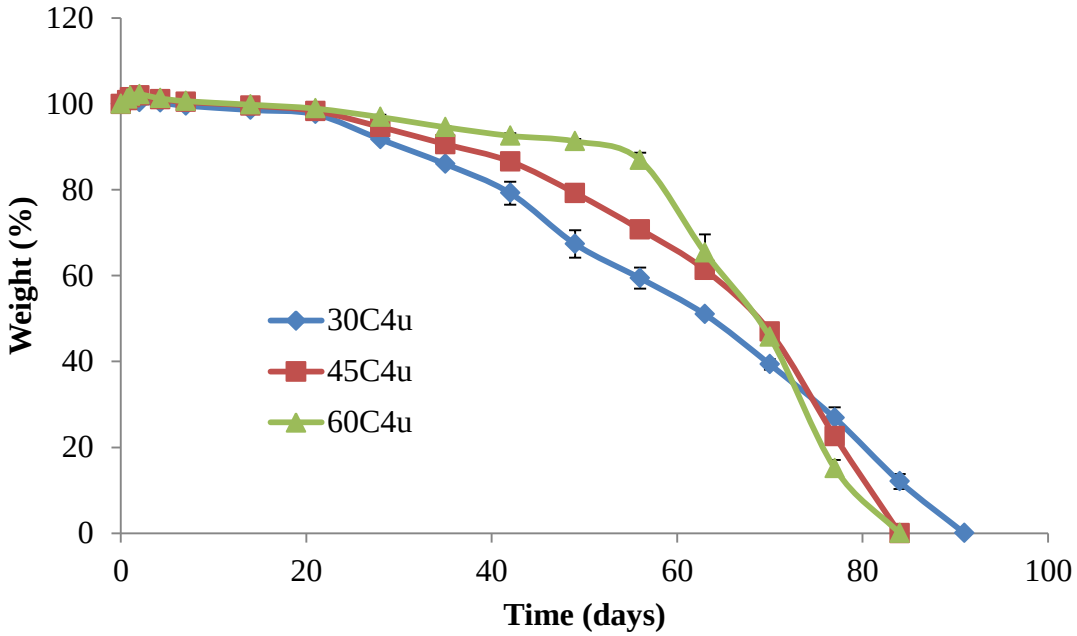

Figure 5.37. Percentage weight for C_{4u}-based TPEUs, average of 3 samples.

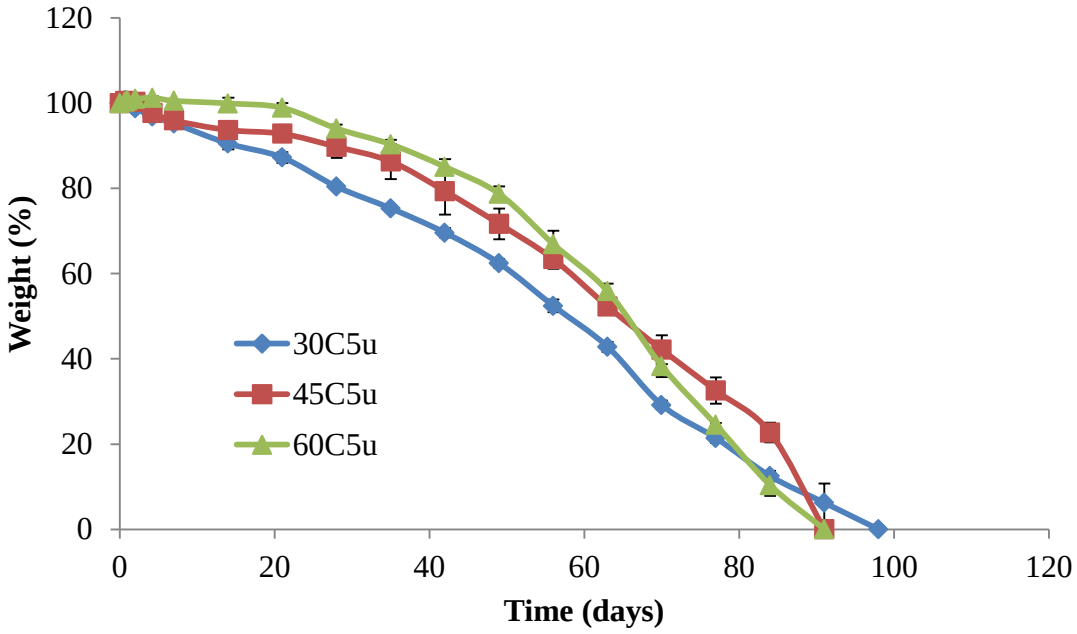

Figure 5.38. Percentage weight for C_{5u}-based TPEUs, average of 3 samples.

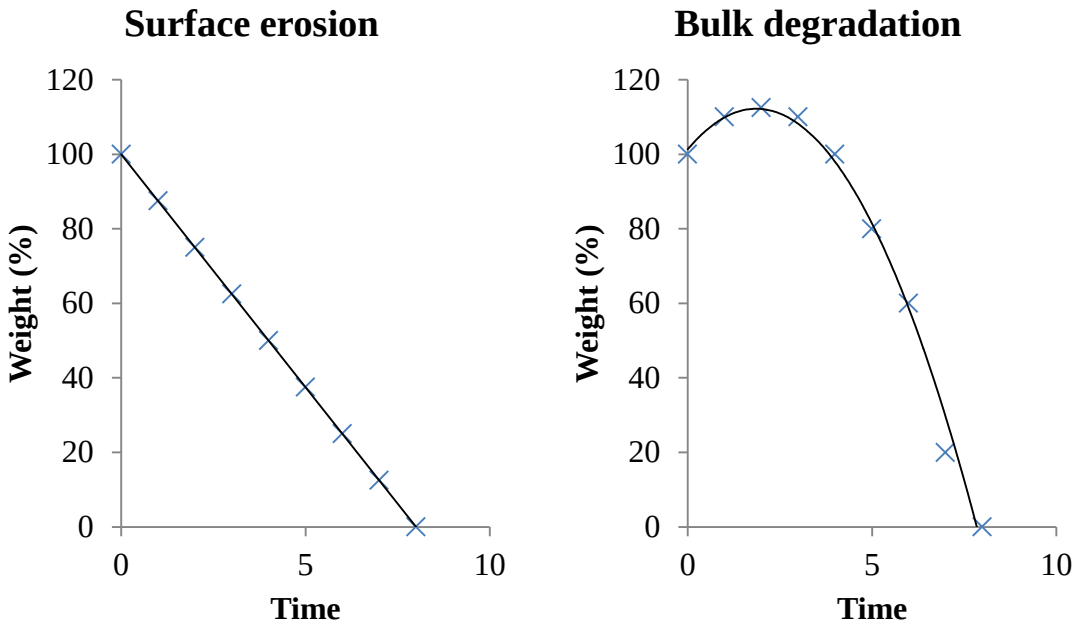

Figure 5.39. Example of a degradatioin profile exhibiting surface erosion (*left*) and bulk degradation (*right*).

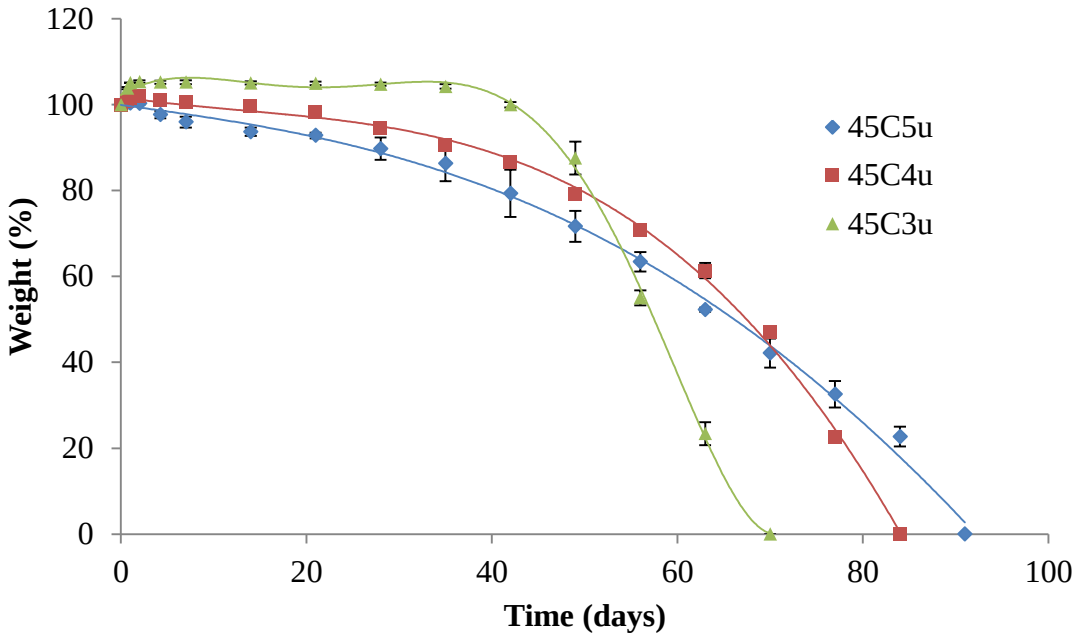

Figure 5.40. Comparison of degradation profiles of $45C_{3u}$, $45C_{4u}$ and C_{5u} TPEUs with polynomial best fit lines.

5.3 Conclusion

In conclusion, it has been demonstrated that hydroxyl and carboxylic acid functional amino acids, such as L-serine, L-aspartic acid and L-glutamic acid, offer a unique and facile route to modifiable extenders for the synthesis of thermoplastic polyurethanes. It was found that the composition %HS of these materials could be accurately calculated and utilised to determine the mechanical rigidity of the resultant polymers. Furthermore, through alterations of the extender chain length and side group functionality it was possible to tailor both the thermal and mechanical properties of the TPEUs.

Finally, it was demonstrated, through extender selection, that the hydrophilicity and swelling capabilities of the materials could be determined. Moreover, it was shown that the dominant mode of degradation of the materials could be shifted from bulk degradation to a surface erosion-type mechanism, and *vice versa*, through selection of extender chain length.

5.4 References

1. B. D. Ratner and S. J. Bryant, *Annu. Rev. Biomed. Eng.*, 2004, 6, 41-75.
2. M. Okada, *Prog. Polym. Sci.*, 2002, 27, 87-113.
3. L. S. Nair and C. T. Laurencin, *Prog. Polym. Sci.*, 2007, 32, 762-798.
4. J. F. Mano, G. A. Silva, H. S. Azevedo, P. B. Malafaya, R. A. Sousa, S. S. Silva, L. F. Boesel, J. M. Oliveira, T. C. Santos, A. P. Marques, N. M. Neves and R. L. Reis, *J. R. Soc. Interface*, 2007, 4, 999-1030.
5. I. Engelberg and J. Kohn, *Biomaterials*, 1990, 12, 292-304.
6. J. Kylma and J. V. Seppala, *Macromolecules*, 1997, 30, 2876-2882.
7. A. Asefnejad, M. T. Khorasani, A. Behnamghader, B. Farsadzadeh and S. Bonakdar, *Int. J. Nanomed.*, 2011, 6, 2375-2384.
8. H. S. Park, M. S. Gong and J. C. Knowles, *J. Mater. Sci.: Mater. Med.*, 2013, 24, 281-294.
9. L. H. Chan-Chan, C. Tkaczyk, R. F. Vargas-Coronado, J. M. Cervantes-Uc, M. Tabrizian and J. V. Cauich-Rodriguez, *J. Mater. Sci.: Mater. Med.*, 2013, 24, 1733-1744.
10. R. F. Storey, J. S. Wiggins and K. A. Mauritz, *Polym. Compos.*, 1993, 14, 17-25.
11. S. Venkataraman, N. Veronica, Z. X. Voo, J. L. Hedrick and Y. Y. Yang, *Polym. Chem.*, 2013, 4, 2945-2948.
12. J. Oble, B. Riflade, A. Noel, M. Malacria, S. Thorimbert, B. Hasenknopf and E. Lacote, *Org. Lett.*, 2011, 13, 5990-5993.
13. Y. C. Jung, C. H. Yoon, E. Turos, K. S. Yoo and K. W. Jung, *J. Org. Chem.*, 2007, 72, 10114-10122.
14. M. J. O'Sickey, B. D. Lawrey and G. L. Wilkes, *J. Appl. Polym. Sci.*, 2002, 84, 229-243.

15. G. Odian, *Principles of Polymerization*, *Fourth Edition*, John Wiley & Sons, Inc., 2004.

16. V. Pistor, D. de Conto, F. G. Ornaghi and A. J. Zattera, *J. Nanomater.*, 2012, 2012, 1-8.

17. G. Trovati, E. A. Sanches, S. C. Neto, Y. P. Mascarenhas and G. O. Chierice, *J. Appl. Polym. Sci.*, 2010, 115, 263-268.

18. K. S. Lee and Y.-W. Chang, *Polym. Int.*, 2013, 62, 64-70.

19. H. F. Brinson and L. C. Brinson, *Polymer Engineering Science and Viscoelasticity*, Springer, 2008.

6 Conclusions

In conclusion, pentaerythritol, through the acid catalysed acetal formation and subsequent ring closure reaction with ethyl chloroformate, was shown to be an excellent platform in the synthesis of novel functional spirocyclic carbonate monomers. Furthermore, the binary organocatalyst system of DBU/TU could be employed in the ROP of these monomers to produce well-defined poly(carbonate)s with no adverse side reactions. As is clear from the study, grafted copolymers of PNTC offer a facile method to produce nano-structure with possible triggered release applications. In Chapter 3, it was found that the utilisation DBU/TU in the ROP of PTO could be used in the synthesis of A-B-A triblock co-polymers, in which PTO was initiated from PCL macro-initiators. The ROP of pentaerythritol-based cyclic carbonates offers a simple synthetic route into degradable high T_g polymers for utilisation in improving the tensile properties of low T_g polyesters, yielding a thermoplastic 'hard-soft' materials, through micro-phase separation.

The versatility of pentaerythritol was realised by the application of the modified pentaerythritol diol precursors, synthesised in Chapter 2, as an excellent chain extender in the synthesis of novel functional thermoplastic polyester-urethanes with a range of mechanical properties which were determined by extender content. As is also evident from the study, norbornene-functional TPEUs (CNb) offer a unique route to decorated elastomeric materials which may be employed to control the hydrophilicity and degradation rate of the materials with minimal effect on the mechanical properties through post-polymerisation modifications.

Finally, utilising the concept side group influence on extender properties realised in Chapter 4, it was demonstrated that hydroxyl and carboxylic acid functional amino acids, such as L-serine, L-aspartic acid and L-glutamic acid, offer a unique and facile route to side group modifiable extenders for the synthesis of thermoplastic

polyurethanes. It was demonstrated, through side selection, that the hydrophilicity and swelling capabilities of the materials could be dictated. Moreover, it was shown that the dominant mode of degradation of the materials could be shifted from bulk degradation to a surface erosion-type mechanism, and *vice versa*, through selection of extender chain length. Furthermore, it was found that the %HS composition of these materials could be accurately calculated and utilised to dictate the mechanical rigidity of the resultant polymers. Furthermore, through alterations of the extender chain length and side group functionality it was possible to tailor both the thermal and mechanical properties of the TPEUs.

7 Experimental

7.1 Materials

Pentaerythritol 98% and 2,2-dimethoxy-2-phenylacetophenone were purchased from Acros Chemicals. Amberlyst A21 free base resin, ethyl chloroformate, ethyl isocyanate, benzaldehyde, 5-norbornene-2-carboxaldehyde (endo/exo), thionyl chloride, lithium aluminium hydride, L-aspartic acid and 1,8-diazabicyclo[5.4.0]undec-7-ene (DBU, subsequently dried over CaH_2) were purchased from Sigma Aldrich. 1-(3,5-bis(trifluoromethyl)phenyl)-3-cyclohexylthiourea (TU) was synthesised as previously reported and was solubilised in dry CH_2Cl_2 before being dried over CaH_2 before filtration and solvent removal *via* standard Schlenk techniques to yield dry TU.[1] Diphenylphosphate (subsequently dried over phosphorous pentoxide (P_2O_5) in a vacuum desiccator) 2-amino-1,3-propanediol, deuterated chloroform ($CDCl_3$) (subsequently dried over activated 3Å molecular sieves) and deuterated dimethyl sulfoxide ($(CD_3)_2SO_4$) were purchased from Apollo Scientific Ltd. Poly(caprolactone) M_W = 2,000 g·mol^{-1} (PCL_{2k}) was received from Perstorp UK Ltd. L-glutamic acid and propionyl chloride were purchased from Alfa Aesar. 4,4′-diisocyanato dicyclohexylmethane (H_{12}MDI) was purchased from Tokyo Chemical Industry (TCI) UK Ltd. Sodium carbonate, sodium hydrogen carbonate, magnesium sulfate, methanol (MeOH), ethanol (EtOH), diethyl ether (Et_2O), dimethyl sulfoxide (DMSO), dichloromethane (CH_2Cl_2), hydrochloric acid (HCl 37%), ethyl acetate (EtOAc), toluene and tetrahydrofuran (THF) were purchased from Fisher Scientific. All chemicals were used as received from the suppliers unless otherwise stated.

7.2 Instrumental methods

7.2.1 NMR spectroscopy and gel permeation chromatography (GPC)

^{1}H and ^{13}C NMR spectra were obtained on a Bruker DPX-400 spectrometer (400 MHz) at 293 K. All chemical shifts were reported as δ in parts per million (ppm) and referenced to the residual solvent signal ($CDCl_3$: ^{1}H, δ = 7.26 ppm; ^{13}C, δ = 77.16 ppm; $(CD_3)SO$: ^{1}H, δ = 2.50 ppm; ^{13}C, δ = 39.52). Gel permeation chromatography (GPC) was used to determine the dispersities ($Đ_M$) and molecular weights of synthesised polymers. GPC was conducted in dimethylformamide (DMF), with 0.1% (w/v) LiBr salt, or chloroform ($CHCl_3$), with 0.1% (v/v) trimethylamine, using an Varian PL-GPC 50 system equipped with 2 × PLgel 5 μM MIXED-D columns in series and a differential refractive index (RI) detector at a flow rate of 1.0 mL min^{-1}. The systems were calibrated against Varian Polymer Laboratories Easi-Vial linear poly(methyl methacrylate) (PMMA) and poly(styrene) (PS) standards respectively and analysed by the software package Cirrus v3.3.

7.2.2 Thermal analysis

Differential scanning calorimetry (DSC) and thermogravametric analysis (TGA) data was obtained using a Mettler Toledo DSC1 star and a TGA/DSC star system and was analysed using the software package STARe V12.0. DSC heating and cooling cycles were run in triplicate in series under a nitrogen atmosphere at a heating rate of +/- 10 °C min^{-1} in a 40 μL aluminium crucible. TGA was conducted between 20 °C and 400 °C at a heating rate of 10 °C min^{-1} in a 40 μL aluminium crucible.

7.2.3 Tensile analysis

Tensile data was obtained at ambient temperature by axially loading 'dog-bones' in a Tensiometric M100-1CT system with a load cell capacity of 1 kN and crosshead speed of 5 mm min^{-1} with a premeasured grip-to-grip separation All values reported were obtained from an average of 10 repeat specimens and the results were recorded using winTest v4.3.2 software. Molten polymer samples were moulded into 'dog-bones' via compression moulding using a PTFE mould and allowed to cool to ambient temperature.

7.2.4 Dynamic mechanical thermal analysis (DMTA)

Dynamic mechanical thermal analysis (DMTA) data was obtained using a Mettler Toledo DMA 1 star system and was analysed using the software package STARe V13.00a (build 6917). DMTA samples were analysed by single cantilever bending, oscillating at a frequency of 5.0 and 0.5 MHz with a displacement of 10 mm between -80 and 180 °C at a heating rate of 2 °C min^{-1}. All polymers were analysed using a Mettler Toledo DMA 1 Star system to determine the thermo-mechanical properties and glass transitions of the materials. Molten polymer samples were moulded into 'bars' *via* compression moulding using a PTFE mould and allowed to cool to ambient temperature. All TPEUs were annealed for 5 days in an incubator at 25 °C.

7.2.5 Wide angle x-ray diffraction (WAXD)

Wide angle x-ray diffraction data was obtained using a Panalytical X'Pert Pro MPD equipped with a Cu Kα_1 hybrid monochromator (λ = 0.154 nm) as the incident beam optics and PiXcel detector was processed using OriginPro 8 software. All UV

irradiation was conducted using a Primotech Metalight Classic UV box equipped with a twelve UV light 360° array (ultimate light power within the spectrum of 320-400nm). Each polymer was compression moulded into discs and allowed to anneal for 5 days in an incubator at 25 °C before standard "powder" 2θ-θ diffraction scans were carried out at room temperature in the angular range between 5° and 60° 2θ.

7.2.6 Static contact angle measurements

Static contact angle measurements were obtained using a KRUSS DSA10 drop shape analyser and were processed using the software package DSA3 1.72b IEEE1394b. Each polymer was dissolved in minimal DMSO before being deposited as a thin film on a glass slide. The solvent was allowed to evaporate overnight before trace solvent was removed *in vacuo*. TPEU samples were allowed to anneal at 25 °C in an incubator for 5 days prior to analysis. Using a KRUSS DSA100 a 100 μL droplet of DI H_2O was deposited onto the surface of the film and the measurement was taken immediately and analysed using a sessile drop type with a polynomial (tangent 2) computational method.

7.2.7 Laser light scattering measurements

Laser light scattering measurements were performed at angles of observation ranging from 50° up to 130° with an ALV CGS3 setup operating at λ_0 = 632 nm and at 20 °C ± 1 °C. Data were collected in duplicate with 100 s run times. Calibration was achieved with filtered toluene and the background was measured with filtered solvent. Values of M_w were obtained after extrapolation to zero concentration and angle was determined classically and used to derive the aggregation number of the micellar aggregates N_{agg} = $M_{w,aggregate}/M_{w,unimers}$. The normalised intensity autocorrelation functions $g_2(t)$ obtained

from dynamic light scattering were related to $g_1(t)$ (the normalised electric field autocorrelation functions) via the Siegert relation. Then $g_1(t)$ were analysed in terms of a continuous distribution of relaxation times using the REPES routine without assuming a specific mathematical shape for the distribution of the relaxation times. The diffusion coefficient *D* was calculated from the average relaxation times of the scatterers given that they were q^2-dependent. The diffusion coefficient was then used for computing the hydrodynamic radius (R_h) of the scatterers according to the Stokes-Einstein equation:

$$D_0 = \frac{kT}{6\pi\eta R_h}$$

With η the solvent viscosity, k Boltzmann's constant and T the absolute temperature. Values of R_h given in the following are then obtained after extrapolation to zero concentration.

7.2.8 Degradation study

Accelerated degradation studies were conducted under conditions previously reported by C X F Lam *et al*.[2] All polymers which could form 'degradation disks' were subjected to accelerated degradation studies (5M aq. NaOH). Molten polymer samples were moulded into disks *via* compression moulding at 100 °C using a PTFE mould and allowed to cool to ambient temperature. The disks were placed in individual vials containing 20 mL of 5M NaOH solution and incubated at 37 °C. The weight of the air dried disks was measured periodically using an analytical balance.

7.3 Experimental for Chapter 2

7.3.1 2-phenyl-5,5-bis(hydroxymethyl)-1,3-dioxane (PHD) synthesis:

The benzylidene acetal-functionalised pentaerythritol-based diol was synthesised *via* the acid-catalysed acetal formation from benzaldehyde, modified from previous reports.[3] In a clean round bottom flask, pentaerythritol (50 g, 36.7×10^{-2} mol) was suspended in 400 mL of deionised water and heated to 80 ^{o}C with stirring until all the solid had dissolved. The pentaerythritol solution was allowed to cool to ambient temperature before the addition of conc. HCl (1.5 mL, 14.8 mmol, HCl 36 wt% in H_2O) with continual stirring for 15 min. Benzaldehyde (42.87 g, 40.4×10^{-2} mol) was added drop-wise to the acidified solution over 20 min and allowed to stir for a further 2 hours. The mono-functionalised product formed a white crystalline precipitate which was collected *via* vacuum filtration before being purified by re-crystallisation from hot toluene to yield white crystals. Analysis was consistent with previous reports.[3] (36.5 g, yield: 44%) ^{1}H NMR (400 MHz, DMSO-d_6) δ 7.50 – 7.29 (m, 5H), 5.41 (s, 1H), 4.67 (t, $^{3}J_{H\text{-}H}$ = 5.3 Hz, 1H), 4.58 (t, $^{3}J_{H\text{-}H}$ = 5.1 Hz, 1H), 3.93 (d, $^{2}J_{H\text{-}H}$ = 11.2 Hz, 2H), 3.80 (d, $^{2}J_{H\text{-}H}$ = 11.2 Hz, 2H), 3.69 (d, $^{3}J_{H\text{-}H}$ = 5.2 Hz, 2H), 3.26 (d, $^{3}J_{H\text{-}H}$ = 5.0 Hz, 2H). ^{13}C NMR (101 MHz, DMSO-d_6) δ 138.76 (s, C), 128.59 (s, CH), 127.95 (s, 2(CH)), 126.14 (s, 2(CH)), 100.66 (s, CH), 69.06 (s, 2(CH_2)), 60.97 (s, CH_2), 59.48 (s, CH_2).

7.3.2 9-phenyl-2,4,8,10-tetaoxaspiro-[5,5]-undec-3-one (PTO) synthesis:

The synthesis of PTO was conducted *via* the procedure outlined below, modified from previous reports.[3] In a clean dry 2-necked round bottom flask, mono benzylidene protected pentaerythritol (17 g, 76 mmol) was dissolved in 800 mL of THF and cooled to 0 ^{o}C using an ice-bath. Under an N_2 blanket, ethyl chloroformate (21.8 mL, 228

mmol) was slowly added to the diol solution and stirred for 30 min. Triethylamine (23.1 mL, 228 mmol) was added to drop-wise to the cooled solution over a 45 min period and the reaction was allowed to stir for 3 hours while being allowed to warm to ambient temperature. The resultant salt formed during the reaction was removed *via* vacuum filtration and was further rinsed with THF. The filtrate and washings were combined and solvent was removed *in vacuo* to yield off-white crystals. The crude carbonate-monomer was purified by re-crystallisation from hot toluene to yield white crystals. The monomer was dissolved in dry CH_2Cl_2 and dried over activated 3Å molecular sieves using standard Schlenk-line techniques. The solvent was removed under reduced pressure and the dry monomer stored in the glovebox. Analysis was consistent with previous reports.[3] (9.88 g, yield: 52%). ^{1}H NMR (400 MHz, DMSO-d_6) δ 7.48 – 7.35 (m, 5H), 5.55 (s, 1H), 4.65 (s, 2H), 4.18 (s, 2H), 3.99 (dd, $^4J_{H\text{-}H}$ = 47.0, 11.8 Hz, 4H). ^{13}C NMR (101 MHz, DMSO-d_6) δ 147.63 (s, C=O), 137.81 (s, C), 129.00 (s, CH), 128.10 (s, 2(CH)), 126.21 (s, 2(CH)), 101.22 (s, CH), 70.61 (s, CH_2), 69.88 (s, CH_2), 68.25 (s, 2(CH_2)).

7.3.3 General procedure for the organocatalysed ROP of PTO:

All polymerisations were carried out using standard glovebox and Schlenk-line techniques. The ROP of PTO using 1 mol% 1,8-diazabicyclo[5.4.0]undec-7-ene (DBU) and 5 mol% 1-(3,5-bis(trifluoromethyl)phenyl)-3-cyclohexylthiourea (TU) was carried out in dry $CDCl_3$ at ambient temperature using 1,4-butanediol (1,4-BDO) as the initiator. In a clean dry vial, PTO (50 mg, 2 mmol) was dissolved in 500 µL of $CDCl_3$ before the addition of freshly prepared stock solutions of DBU (30.4 µL, 2×10^{-2} mmol, 0.1 mg µL^{-1} $CDCl_3$ stock), TU (740 µL, 1×10^{-1} mmol, 50 mg mL^{-1} $CDCl_3$ stock) and

1,4-BDO (29.5 μL, 16 mmol, 0.1 mg μL^{-1} $CDCl_3$ stock). The polymerisation was stopped by precipitation into hexanes and the polymer recovered *via* a silica plug. Silica plug conditions; the crude material was loaded onto the silica plug in CH_2Cl_2. The residual monomer and TU co-catalysts were eluted using CH_2Cl_2 (R_f = 0.9 and R_f = 0.8 respectively) before a direct solvent switch to ethyl acetate was employed to elute the pure polymer (R_f = 0.9), with the DBU catalyst remaining on the silica (R_f = 0). DP50 homopolymer; ^{1}H NMR (250 MHz, $CDCl_3$) δ 7.58 – 7.30 (m, 250H), 5.43 (s, 50H), 4.57 (s, 100H), 4.24 – 3.79 (m, all other H), 3.25 (t, $^2J_{H\text{-}H}$ = 5.9 Hz, 4H), 1.87 – 1.79 (m, 4H). M_n = 11.7 kg·mol^{-1}, $Đ_M$ = 1.12 (RI detection, $CHCl_3$ GPC).

7.3.4 2-norbornene-5,5-bis(hydroxymethyl)-1,3-dioxane (NHD) Synthesis:

The norbornene-functionalised pentaerythritol-based diol was synthesised *via* the acid catalysed acetal formation. In a clean round bottom flask, pentaerythritol (13.5 g, 99.2 mmol) was suspended in 100 mL of deionised water and heated to 80^{o}C with stirring until all the solid had dissolved. The pentaerythritol solution was allowed to cool to ambient temperature before the addition of conc. HCl (330 μL, 3.26 mmol) with continual stirring for a further 15 min. 5-Norbornene-2-carboxaldehyde (10 g, 89.2 mmol) was added drop-wise to the acidified solution over 20 min and allowed to stir for a further 2 hours. The mono-functionalised product formed an orange precipitate which was collected *via* vacuum filtration before further purification by silica plug, ethyl acetate as the eluent, and re-crystallisation from hot toluene to yield white crystals (10.8 g, yield: 51 %). ^{1}H NMR (400 MHz, DMSO-d_6) δ 6.15 (dd, $^3J_{H\text{-}H}$ = 5.7, 3.0 Hz, 1H), 5.90 (dd, $^3J_{H\text{-}H}$ = 5.7, 3.0 Hz, 1H), 4.52 (t, $^3J_{H\text{-}H}$ = 5.4 Hz, 1H), 4.40 (t, $^3J_{H\text{-}H}$ = 5.2 Hz, 1H), 3.76 – 3.66 (m, 3H), 3.54 (d, $^3J_{H\text{-}H}$ = 5.2 Hz, 2H), 3.42 (m, 2H), 3.13 (d, $^3J_{H\text{-}H}$ = 5.2

Hz, 2H), 2.83 (s, 1H), 2.76 (s, 1H), 2.16 (ddd, $^{3}J_{H\text{-}H}$ = 12.8, 8.5, 4.0 Hz, 1H), 1.72 (ddd, $^{3}J_{H\text{-}H}$ = 12.8, 9.3, 3.8 Hz, 1H), 1.30 – 1.14 (m, 2H), 0.72 (ddd, $^{3}J_{H\text{-}H}$ = 11.9, 4.1, 2.6 Hz, 1H). ^{13}C NMR (101 MHz, DMSO-d_6) δ 137.26 (s, CH), 132.58 (s, CH), 105.41 (s, CH), 68.64 (s, CH_2), 68.46 (s, CH_2), 61.02 (s, CH_2), 59.57 (s, CH_2), 48.71 (s, CH_2), 43.19 (s, CH), 43.11 (s, CH), 41.62 (s, CH), 28.21 (s, CH_2).

7.3.5 2-norbornene-5,5-bis(hydroxymethyl) trimethylene carbonate (NTC) synthesis:

In a clean dry 2-necked round bottom flask, NHD (4 g, 16.7 mmol) was dissolved in 400 mL of THF and cooled to 0^{o}C using an ice-bath. Under an N_2 blanket, ethyl chloroformate (4.78 mL, 49.9 mmol) was slowly added to the NHD solution and stirred for 30 min. Triethylamine (6.95 mL, 49.9 mmol) was added to drop-wise to the cooled solution over a 45 min period and the reaction was allowed to stir for 3 hours while being allowed to warm to ambient temperature. The resultant salt formed during the reaction was removed *via* vacuum filtration and was further rinsed with THF. The filtrate and washings were combined and solvent was removed *in vacuo* to yield off-white crystals. The crude carbonate-monomer was purified by re-crystallisation from hot cyclohexane/THF to yield white crystals. The monomer was dried over activated 3Å molecular sieves using standard Schlenk-line techniques and stored in the glovebox.(2.6 g, yield: 59 %) ^{1}H NMR (400 MHz, DMSO-d_6) δ 6.17 (dd, $^{3}J_{H\text{-}H}$ = 5.7, 3.0 Hz, 1H), 5.93 (dd, $^{3}J_{H\text{-}H}$ = 5.7, 2.8 Hz, 1H), 4.51 (s, 2H), 4.06 (s, 2H), 3.89 – 3.83 (m, 3H), 3.61 – 3.58 (m, 2H), 2.85 (s, 1H), 2.78 (s, 1H), 2.22 (ddd, $^{3}J_{H\text{-}H}$ = 12.8, 8.6, 3.9 Hz, 1H), 1.75 (ddd, $^{3}J_{H\text{-}H}$ = 12.8, 9.3, 3.8 Hz, 1H), 1.31 – 1.17 (m, 2H), 0.74 (ddd, $^{3}J_{H\text{-}H}$ = 11.9, 4.1, 2.6 Hz, 1H). ^{13}C NMR (101 MHz, DMSO-d_6) δ 147.59 (s, C=O), 137.51 (s, CH),

132.45 (s, CH), 105.96 (s, CH), 70.70 (s, CH_2), 69.86 (s, CH_2), 67.79 (s, CH_2), 67.68 (s, CH_2), 48.70 (s, CH_2), 43.07 (s, CH), 42.97 (s, CH), 41.61 (s, CH), 28.11 (s, CH_2). Elemental analysis; anal. calcd for $C_{14}H_{18}O_5$: C 63.15; H 6.18; N 0 %. Found: C 63.15, H 6.81, N 0.01 %. Mass spectrometry (ESI +ve); m/z = 267.12 (M^+).

7.3.6 General procedure for the organocatalysed ROP of NTC:

All polymerisations were carried out using standard glovebox and Schlenk-line techniques. The ROP of NTC using 1 mol% DBU and was carried out in dry $CDCl_3$ at ambient temperature using benzyl alcohol (BnOH) as the initiator. In a clean dry vial, NTC (66.5 mg, 2.5×10^{-2} mmol) was dissolved in 500 µL of $CDCl_3$ before the addition of freshly prepared stock solutions of DBU (4 µL, 2.5×10^{-3} mmol, 1 µL/10 µL $CDCl_3$ stock), TU (188 µL, 1.25×10^{-2} mmol, 5 mg/200 µL $CDCl_3$ stock) and BnOH (dependant on target chain length). The polymerisation was stopped by precipitation into hexanes and the polymer recovered *via* a silica plug. Silica plug conditions; the crude material was loaded onto the silica plug in CH_2Cl_2. The residual monomer and TU co-catalysts were eluted using CH_2Cl_2 (R_f = 0.9 and R_f = 0.8 respectively) before a direct solvent switch to ethyl acetate was employed to elute the pure polymer (R_f = 0.9), with the DBU catalyst remaining on the silica (R_f = 0). DP50 homopolymer; ^{1}H NMR (400 MHz, DMSO-d_6) δ 7.36 (m, 5H), 6.15 (m, 50H), 5.93 (m, 50H), 5.15 (s, 2H) 4.54 – 4.33 (m, 100H), 4.08 – 3.71 (m, 250H), 3.66 – 3.42 (m, 100H), 2.92 (s, 50H), 2.81 (s, 50H), 2.30 (m, 50H), 1.81 (m, 50H), 1.44 – 1.15 (m, 100H), 0.82 (m, 50H). ^{13}C NMR (101 MHz, DMSO-d_6) δ 147.59 (s, C=O), 137.51 (s, CH), 132.45 (s, CH), 105.96 (s, CH), 70.70 (s, CH_2), 69.86 (s, CH_2), 67.79 (s, CH_2), 67.68 (s, CH_2), 48.70 (s, CH_2), 43.07 (s, CH), 42.97 (s, CH), 41.61 (s, CH), 28.11 (s, CH_2). M_n = 11.5 kg·mol^{-1}, $Đ_M$ = 1.10 (RI detection, $CHCl_3$ GPC).

7.3.7 Functionalisation and cleavage of Poly(NTC) (PNTC)

7.3.7.1 Benzyl azide:

In a clean dry vial fitted with a stirrer bar, $PNTC_{DP10}$ (50 mg, 2.11×10^{-5} mol) was dissolved in 500 μL of 1,4-dioxane. Benzyl azide (28 μL, 2.11×10^{-4} mol) was added to the solution before being sealed and heated to 90 °C for 12 hours with stirring. The functionalised polymer was recovered by precipitation into cold methanol before being filtered and dried *in vacuo*. ^{1}H NMR (400 MHz, CDCl3) δ 7.45 – 7.16 (m, 62H), 5.13 (m, 2H), 4.91 (t, m, 10H), 4.69 – 2.99 (m, 223H), 2.82 – 2.51 (m, 17H), 2.39 – 0.66 (m, 116H). M_n = 6.5 kg·mol^{-1}, $Đ_M$ = 1.14 (RI detection, $CHCl_3$ GPC).

7.3.7.2 Dodecanethiol:

In a clean dry vial fitted with a stirrer bar, $PNTC_{DP10}$ (50 mg, 2.11×10^{-5} mol) was dissolved in 500 μL of $CHCl_3$. Dodecanethiol (50 μL, 2.11×10^{-4} mol) and 2,2-dimethoxy-2-phenylacetophenone photoinitiator (54 mg, 2.11×10^{-4} mol) were added to the solution before being sealed and UV irradiated for 30 min. The functionalised polymer was recovered by precipitation into cold methanol before being filtered and dried *in vacuo*. ^{1}H NMR (400 MHz, CDCl3) δ 7.35 (m, 5H), 5.14 (s, 2H), 4.58 – 4.05 (m, 34H), 4.05 – 3.23 (m, 100H), 2.86 (d, J = 48.9 Hz, 22H), 2.66 – 1.05 (m, 194H), 0.97 – 0.67 (m, 28H). M_n = 7.3 kg·mol^{-1}, $Đ_M$ = 1.12 (RI detection, $CHCl_3$ GPC).

7.3.7.3 PEG_{550} thiol

In a clean dry vial fitted with a stirrer bar, $PNTC_{DP20}$ (100 mg, 2.11×10^{-5} mol) was dissolved in 500 μL of THF. PEG_{550} thiol (232 mg, 4.22×10^{-4} mol) and 2,2-dimethoxy-2-phenylacetophenone photoinitiator (106 mg, 4.22×10^{-4} mol) were added to the solution before being sealed and UV irradiated for 30 min. The functionalised polymer was recovered by precipitation into cold methanol before being filtered and dried *in*

vacuo. ^{1}H NMR (400 MHz, DMSO) δ 7.38 (s, 9H), 5.13 (s, 3H), 4.68 – 3.58 (m, 460H), 3.55 – 3.30 (m, 1449H), 3.23 (s, 91H), 2.61 (m, 142H), 2.37 – 0.71 (m, 299H). M_n = 13.3 kg·mol^{-1}, $Đ_M$ = 1.10 (RI detection, $CHCl_3$ GPC).

7.3.7.4 Tetrazine:

In a clean dry vial fitted with a stirrer bar, $PNTC_{DP10}$ (50 mg, 2.11 × 10^{-5} mol) was dissolved in 500 μL of 1,4-dioxane. 2,5-Dioxopyrrolidin-1-yl 6-(6-(pyrimidin-2-yl)-1,2,4,5-tetrazin-3-yl)benzoate (76.6 mg, 2.11 × 10^{-4} mol) was added to the solution before being stirred at room temperature for 1 hour. The functionalised polymer was recovered by precipitation into cold methanol before being filtered and dried *in vacuo*. ^{1}H NMR (400 MHz, CDCl3) δ 9.49 – 6.89 (m, 66H), 5.27 (s, 2H), 4.75 – 0.59 (m, 206H). M_n = 6.9 kg·mol^{-1}, $Đ_M$ = 1.13 (RI detection, $CHCl_3$ GPC).

7.3.7.5 Cleavage of acetals:

In a clean dry vial fitted with a stirrer bar, $PNTC_{DP10}$ (50 mg, 2.11 × 10^{-5} mol) was suspended in 1 mL of methanol. 0.01M HCl was added to the solution before being sealed and stirred for 12 h. The cleaved polymer was recovered by precipitation into hexanes before being filtered and dried *in vacuo*. M_n = 4.2 kg·mol^{-1}, $Đ_M$ = 1.32 (RI detection, $CHCl_3$ GPC, with 5 wt% NEt_3).

7.3.8 Self-assembly and multi-angle light scattering analysis

PNTC-*g*-PEG_{550} polymers were self-assembled by direct dissolution of the graft copolymer in DI H_2O at a concentration of 1 mg mL^{-1}. Polymer solutions were stirred at room temperature overnight before being filtered using a 2 μm PTFE filter and analysed *via* SLS and DLS at room temperature.

7.4 Experimental for Chapter 3

7.4.1 General procedure for the organocatalysed ROP of ε-caprolactone

All polymerisations were carried out using standard glovebox and Schlenk-line techniques. Using the method previously reported by Kakuchi *et al*.[4] The ROP of ε-caprolactone (ε-CL) catalysed by di-phenyl phosphate (DPP) (1 mol% with respect to monomer) was carried out in dry toluene at ambient temperature using 1,4-BDO as the initiator. In the glovebox in a clean dry Schlenk flask fitted with a stirrer bar, ε-CL (10 g, 87.6 mmol) was dissolved in 100 mL of dry toluene before the addition of neat 1,4-BDO (77.6 μL, 8.76×10^{-1} mmol) and a freshly prepared stock solution of DPP (219 μL, 8.76×10^{-1} mmol, 1 mg μL^{-1} dry toluene stock). The Schlenk flask was sealed and removed from the glovebox and the polymerisation was allowed to proceed with stirring until completion. The reaction was quenched and the catalyst removed with washed basic amberlyst resin. The resin was removed *via* gravity filtration and the poly(caprolactone) (PCL) was recovered *via* precipitation from hexane before being filtered and dried in vacuo. The macro-initiator was dissolved in CH_2Cl_2 and dried over activated 3 Å molecular sieves using standard Schlenk-line techniques. The solvent was removed under reduced pressure and the dry macro-initiator was stored in the glovebox. Analysis was consistent with previous reports.[4] (8.8 g, yield: 88%) ^{1}H NMR (400 MHz, $CDCl_3$) δ 4.07 (t, $^3J_{H\text{-}H}$ = 6.7 Hz, 2H), 2.32 (t, $^3J_{H\text{-}H}$ = 7.5 Hz, 2H), 1.76 – 1.59 (m, 4H), 1.46 – 1.34 (m, 2H). ^{13}C NMR (101 MHz, $CDCl_3$) δ 173.54 (s, C=O), 64.14 (s, CH_2), 34.12 (s, CH_2), 28.35 (s, CH_2), 25.53 (s, CH_2), 24.57 (s, CH_2). M_n = 24.2 kg·mol^{-1}, $Đ_M$ = 1.10 (RI detection, $CHCl_3$ GPC).

7.4.2 General synthesis of A-B-A triblock copolymers:

All polymerisations were carried out using standard glovebox and Schlenk-line techniques. The ROP of PTO using 1 mol% 1,8-diazabicyclo[5.4.0]undec-7-ene (DBU) and 5 mol% 1-(3,5-bis(trifluoromethyl)phenyl)-3-cyclohexylthiourea (TU) was carried out in dry CH_2Cl_2 at ambient temperature using α,ω-dihydroxy PCL ranging in molecular weights (M_n NMR = 14 kg·mol^{-1} – 30 kg·mol^{-1}) as the macro-initiator. In a clean dry vial, PTO (2 g, 8 mmol) was dissolved in 20 mL of CH_2Cl_2 before the addition of freshly prepared stock solutions of DBU (121.6 µL, 8 × 10^{-2} mmol, 0.1 mg µL^{-1} CH_2Cl_2 stock), TU (2.96 mL, 4 × 10^{-1} mmol, 50 mg mL^{-1} CH_2Cl_2 stock) and PCL (Varying dependant on target degree of polymerisation (DP)). The polymerisation was stopped by precipitation into hexanes and the polymer recovered via a silica plug. Silica plug conditions; the crude material was loaded onto the silica plug in CH_2Cl_2. The residual monomer and TU co-catalysts were eluted using CH_2Cl_2 (Rf = 0.9 and Rf = 0.8 respectively) before a direct solvent switch to ethyl acetate was employed to elute the pure triblock copolymer (Rf = 0.9), with the DBU catalyst remaining on the silica (Rf = 0). ^{1}H NMR (400 MHz, CDCl3) δ 7.55 – 7.31 (m, 5H), 5.46 (m, 1H), 4.56 (s, 2H), 4.26 – 3.65 (m, 10H), 2.31 (m, 4H), 1.76 – 1.19 (m, 13H). M_n = 68.9 kg·mol^{-1}, $Đ_M$ = 1.14 (RI detection, $CHCl_3$ GPC).

7.5 Experimental for Chapter 4

7.5.1 General synthesis of pentaerythritol-derived diol extenders

2-norbornene-5,5-bis(hydroxymethyl)-1,3-dioxane (NHD, C_{Nb} extender) and 2-phenyl-5,5-bis(hydroxymethyl)-1,3-dioxane (PHD, C_{Ph} extender) were synthesised as previously reported in the experimental for Chapter 2.

7.5.2 General synthesis of TPEUs from pentaerythritol-derived extenders

The TPEU synthesis described is based on the synthesis of a poly(urethane) with a 30% hard-block composition using the C_{Nb} extender.

In a clean and dry vial fitted with a magnetic stirrer bar, poly(caprolactone) with a M_W = 2,000 g·mol^{-1} (PCL_{2k}) (1 g, 5 × 10^{-4} mol) and DBU (3.73 μL, 6.9 × 10^{-6} mol) were heated to 100 °C under a flow N_2 for 20 min to aid the reduction of water within the system. The molten mixture was cooled to 80 °C before the addition of H_{12}MDI (359 μL, 1.47 ×10^{-3} mol). The reaction mixture was allowed to stir under N_2 for 40 min to allow for prepolymer formation before the addition of a solution of C_{Nb} extender (232 mg, 9.65 × 10^{-4} mol) dissolved in 100 μL of DMSO. The polymerisation was allowed to proceed for 2h before being removed from the heat to retard further reaction. The molecular weight was analysed *via* GPC and any unreacted isocyanate, *via* IR spectroscopy, was quenched by washing the TPEU in 50 mL of methanol before being dried *in vacuo*. ^{1}H NMR (400 MHz, DMSO-d_6) δ 6.97 (m, 3H), 5.99 (m, 3H), 4.34 – 2.97 (m, 51H), 2.89 – 0.50 (m, 90H). M_n = 99.0 kg·mol^{-1}, $Đ_M$ = 2.19 (RI detection, DMF GPC).

7.5.3 Functionalisation and cleavage of C_{Nb}-based TPEUs

7.5.3.1 TEG-azide

In a clean dry vial fitted with a stirrer bar, $30C_{Nb}$ (1.5 g, 1.5×10^{-5} mol) was dissolved in 1 mL of DMSO. TEG-azide (223 μL, 9.65×10^{-4} mol) was added to the solution before being sealed and heated at 90 °C for 12 hours. The functionalised polymer was recovered by precipitation into cold methanol before being filtered and dried *in vacuo*.

7.5.3.2 Thioglycerol

In a clean dry vial fitted with a stirrer bar, $30C_{Nb}$ (1.5 g, 1.50×10^{-5} mol) was dissolved in 1 mL of DMSO. Thioglycerol (104 mg, 9.65×10^{-4} mol) and 2,2-dimethoxy-2-phenylacetophenone photoinitiator (247 mg, 9.63×10^{-4} mol) were added to the solution before being sealed and UV irradiated for 30 min. The functionalised polymer was recovered by precipitation into cold methanol before being filtered and dried *in vacuo*.

7.5.3.3 7-Mercapto-4-methylcoumarin

In a clean dry vial fitted with a stirrer bar, $30C_{Nb}$ (1.5 g, 1.5×10^{-5} mol) was dissolved in 1 mL of DMSO. 7-Mercapto-4-methylcoumarin (186 mg, 9.63×10^{-4} mol) and 2,2-dimethoxy-2-phenylacetophenone photoinitiator (247 mg, 9.63×10^{-4} mol) were added to the solution before being sealed and UV irradiated for 30 min. The functionalised polymer was recovered by precipitation into cold methanol before being filtered and dried *in vacuo*.

7.6 Experimental for Chapter 5

7.6.1 General synthesis of 2-amino-diol extenders derived from amino acids

The synthesis of amino-diol extenders were synthesised according to literature.[5,6,7] In a 1 L round bottom flask fitted with a magnetic stirrer bar, L-glutamic acid (100 g, 6.80×10^{-1} mol) was suspended in 700 mL of methanol before being cooled on an ice-bath. Thionyl chloride (100 mL, 1.40 mol) was added dropwise to the cooled suspension over 30min with stirring after which the reaction was removed from the ice-bath and allowed to warm to ambient temperature. The reaction was allowed to proceed overnight (~ 12h) before the reaction mixture was concentrated *in vacuo* and diluted in 300 mL of fresh methanol. The acidic solution was neutralised to pH 7 by addition of solid sodium hydrogen carbonate and the resultant suspension was filtered. The solvent was removed from the filtrate *in vacuo* before the addition 300 mL of CH_2Cl_2 to precipitate any remaining salts. The suspension was filtered and the solvent was removed *in vacuo* to yield the dimethyl L-glutamate as a colourless oil which was used without any further purification. Analysis was consistent with previous reports.[7] ^{1}H NMR (400 MHz, DMSO-d_6) δ 3.96 (t, $^3J_{H\text{-}H}$ = 6.6 Hz, 1H), 3.70 (s, 3H), 3.59 (s, 3H), 2.63 – 2.41 (m, 2H), 2.06 (m, 2H). ^{13}C NMR (101 MHz, DMSO-d_6) δ 172.22 (s, C=O), 169.84 (s, C=O), 52.62 (s, CH_3), 51.46 (s, CH_3), 51.32 (CH), 28.92 (s, CH_2), 25.32 (s, CH_2).

To a 3-necked round bottom flask fitted with a magnetic stirrer bar and an N_2 inlet, dimethyl L-glutamate (25 g, 1.40×10^{-1} mol) was dissolved in 500 mL of dry THF and cooled on an ice-bath. Under an N_2 flow and vigorous stirring lithium aluminium hydride was slowly in small aliquots over a 30min period. After complete addition, the reaction mixture was removed from the ice-bath and allowed to stir overnight (~ 10h) at ambient temperature. The reaction suspension was cooled on an ice and the unreacted

LiAlH was quenched by subsequent and slow addition of 20 mL DI.H_2O, 20 mL 1 M NaOH and 20 mL DI.H_2O. The quenched suspension was allowed to warm to ambient temperature and stir for 30 min before the addition of $MgSO_4$ and subsequent vacuum filtration. The solvent was removed from the filterate *in vacuo* to yield the crude amino diol. Analysis was consistent with previous reports.[7] ^{1}H NMR (400 MHz, DMSO-d_6) δ 3.37 (m, 2H), 3.29 – 3.06 (m, 2H), 2.55 (m, 1H), 1.54 – 1.37 (m, 1H), 1.18 – 0.99 (m, 1H). ^{13}C NMR (101 MHz, DMSO-d_6) δ 66.79 (s, CH_2), 61.13 (s, CH_2), 52.73 (s, CH), 30.50 (s, CH_2), 29.45 (s, CH_2).

The solids filtered from the reaction were collected and any remaining product was recovered *via* Soxhlet extraction using THF as the solvent. The solvent was removed *in vacuo* and the fractions of amino diol were combined.

This method was applied in the synthesis of 2-amino-1,4-butanediol (C_4) from aspartic acid.

Aspartate dimethyl ester: ^{1}H NMR (400 MHz, DMSO-d_6) δ 7.58 (s, 1H), 4.13 (t, $^{3}J_{H\text{-}H}$ = 5.8 Hz, 1H), 3.69 (s, 1H), 3.62 (s, 1H), 2.94 (d, $^{3}J_{H\text{-}H}$ = 5.8 Hz, 1H). ^{13}C NMR (101 MHz, DMSO-d_6) δ 170.10 (s, C=O), 169.95 (s, C=O), 52.62 (s, CH_3), 51.89 (s, CH_3), 48.99 (s, CH), 35.12 (s, CH_2).

2-amino-1,4-butanediol: ^{1}H NMR (400 MHz, DMSO-d_6) δ 3.46 (m, 1H), 3.31 – 3.09 (m, 1H), 2.76 – 2.66 (m, 1H), 1.58 – 1.19 (m, 1H). ^{13}C NMR (101 MHz, DMSO-d_6) δ 66.48 (s, CH_2), 58.73 (s, CH_2), 50.50 (s, CH), 36.05 (s, CH_2).

7.6.2 General synthesis of protected 2-amino-diol extenders

7.6.2.1 Carbamate-protected (C_{3c})

The carbamate-protected 2-amino-1,3-propanediol extender (C_{3c}) was synthesised according to literature.[5] In a 1 L round bottom flask fitted with a magnetic stirrer bar, 2-amino-1,3-propanediol (10 g, 1.10×10^{-1} mol) and Na_2CO_3 (25 g, 2.36×10^{-1} mol) were dissolved in a mixture of deionised H_2O:THF (500 mL, 2:1 respectively). The solution was cooled on an ice-bath for 20 min before the addition of ethyl chloroformate (10.25 mL, 1.07×10^{-1} mol) and allowed to stir for 2 h. The reaction mixture was removed from the ice-bath and allowed to warm to room temperature and was stirred overnight (~ 12 h). The desired product was extracted with ethyl acetate (6 × 300 mL), dried over $MgSO_4$ and filtered before all volatiles were removed *in vacuo* to yield an off white crystalline solid. The solid was sublimed to yield the pure product as a white crystalline solid. Analysis was consistent with previous reports.[5] (15.07 g, yield 84%). ^{1}H NMR (400 MHz, DMSO-d_6) δ 6.62 (d, $^3J_{H\text{-}H}$ = 7.1 Hz, 1H), 4.54 (t, $^3J_{H\text{-}H}$ = 5.3 Hz, 2H), 3.97 (q, $^3J_{H\text{-}H}$ = 7.0 Hz, 2H), 3.50 – 3.28 (m, 6H), 1.15 (t, $^3J_{H\text{-}H}$ = 7.1 Hz, 3H). ^{13}C NMR (101 MHz, DMSO-d_6): δ 157.34 (s, C=O), 62.10 (s, CH_2), 61.60 (s, CH), 54.1 (s, CH_2), 14.60 (s, CH_3).

7.6.2.2 Urea-protected

The urea-protected 2-amino-1,3-propanediol extender (C_{3u}) was synthesised according to literature.[6] In a 1 L round bottom flask fitted with a magnetic stirrer bar, 2-amino-1,3-propanediol (10 g, 1.10×10^{-1} mol) was dissolved in a mixture of methanol:THF (500 mL, 1:2 respectively). The solution was cooled on an ice-bath for 20 min before the addition of ethyl isocyanate (8.69 mL, 1.10×10^{-1} mol) and allowed to stir for 15min. The reaction mixture was removed from the ice-bath and allowed to warm to room

temperature and was stirred for 4 h. The solvent was removed *in vacuo* and the white off-white solid was suspended and stirred in 400 mL of diethyl for 20min before being collected by filtration. The white crystalline solid was dried *in vacuo* to yield the pure urea-protected extender as a fluffy white solid. (16.04 g, yield 90%). Analysis was consistent with previous reports.[6] ^{1}H NMR (400 MHz, DMSO-d_6) δ 5.98 (t, $^{3}J_{H\text{-}H}$ = 5.5 Hz, 1H), 5.64 (d, $^{3}J_{H\text{-}H}$ = 7.8 Hz, 1H), 4.64 (t, $^{3}J_{H\text{-}H}$ = 5.3 Hz, 2H), 3.55 – 3.45 (m, 1H), 3.44 – 3.27 (m, 4H), 3.05 – 2.93 (m, 2H), 0.97 (t, $^{3}J_{H\text{-}H}$ = 7.2 Hz, 3H). ^{13}C NMR (101 MHz, DMSO-d_6) δ 157.85 (s, C=O), 60.47 (s, CH_2), 52.64 (s, CH), 33.92 (s, CH_2), 15.63 (s, CH_3).

This method was applied in the synthesis of urea-protected 2-amino-1,4-butanediol (C_{4u}) and 2-amino-1,5-pentanediol (C_{5u}) extenders.

C_{4u}: ^{1}H NMR (400 MHz, DMSO-d_6) δ 5.88 (t, $^{3}J_{H\text{-}H}$ = 5.4 Hz, 1H), 5.67 (d, $^{3}J_{H\text{-}H}$ = 8.3 Hz, 1H), 4.71 (t, $^{3}J_{H\text{-}H}$ = 5.2 Hz, 1H), 4.50 (t, $^{3}J_{H\text{-}H}$ = 5.4 Hz, 1H), 3.63 – 3.51 (m, 1H), 3.43 – 3.21 (m, 4H), 3.03 – 2.93 (m, 2H), 1.68 – 1.32 (m, 2H), 0.96 (t, $^{3}J_{H\text{-}H}$ = 7.2 Hz, 3H). ^{13}C NMR (126 MHz, DMSO-d_{6l}) δ 158.56 (s, C=O), 64.07 (s, CH_2), 57.98 (s, CH_2), 48.39 (s, CH), 35.03 (s, CH_2), 34.16 (s, CH_2), 15.79 (s, CH_3). Elemental analysis; anal. calcd for $C_7H_{16}N_2O_3$: C 47.71; H 9.15; N 15.90 %. Found: C 47.70, H 9.15, N 15.91 %.

C_{5u}: ^{1}H NMR (400 MHz, DMSO-d_6) δ 5.77 (t, $^{3}J_{H\text{-}H}$ = 5.4 Hz, 1H), 5.56 (d, $^{3}J_{H\text{-}H}$ = 8.4 Hz, 1H), 4.62 (t, $^{3}J_{H\text{-}H}$ = 5.2 Hz, 1H), 4.36 (t, $^{3}J_{H\text{-}H}$ = 5.1 Hz, 1H), 3.53 – 3.41 (m, 1H), 3.40 – 3.28 (m, 3H), 3.28 – 3.16 (m, 1H), 3.03 – 2.92 (m, 2H), 1.58 – 1.16 (m, 4H), 0.96 (t, $^{3}J_{H\text{-}H}$ = 7.2 Hz, 3H). ^{13}C NMR (101 MHz, DMSO-d_6) δ 157.91 (s, C=O), 63.95 (s, CH_2), 60.89 (s, CH_2), 50.73 (s, CH), 33.96 (s, CH_2), 29.12 (s, CH_2), 28.11 (s, CH_2),

15.64 (s, CH_3). Elemental analysis; anal. calcd for $C_8H_{18}N_2O_3$: C 50.51; H 9.54; N 14.73 %. Found: C 5.51, H 9.54, N 14.73 %.

7.6.3 General synthesis of TPEUs from carbamate-protected extenders

The TPEU synthesis described is based on the synthesis of a poly(urethane) with a 30% hard-block composition using the C_{3c} extender.

In a clean and dry vial fitted with a magnetic stirrer bar, poly(caprolactone) with a M_n = 2,000 g·mol^{-1} (PCL_{2k}) (1 g, 5 × 10^{-4} mol) and DBU (3.73 μL, 6.9 × 10^{-6} mol) were heated to 100 °C under a flow N_2 for 20min to aid the reduction of water within the system. The molten mixture was cooled to 80 °C before the addition of H_{12}MDI (402 μL, 1.64 ×10^{-3} mol). The reaction mixture was allowed to stir under N_2 for 40min to allow for prepolymer formation before the addition of the C_{3c} extender (186 mg, 1.14 × 10^{-3} mol). The polymerisation was allowed to proceed for 2h before being removed from the heat to retard further reaction. The molecular weight was analysed *via* GPC and the unreacted isocyanate was quenched by washing the TPEU in methanol before being dried *in vacuo*. ^{1}H NMR (400 MHz, DMSO-d_6) δ 7.22 – 6.64 (m, 1H), 4.08 – 3.72 (m, 8H), 3.55 – 3.01 (m, 3H), 2.27 (t, J = 7.2 Hz, 5H), 1.92 – 0.66 (m, 27H). M_n = 110.5 kg·mol^{-1}, $Đ_M$ = 1.98 (RI detection, DMF GPC).

7.6.4 General synthesis of TPEUs from urea-protected extenders

The TPEU synthesis described is based on the synthesis of a poly(urethane) with a 30% hard-block composition using the C_{3u} extender.

In a clean and dry vial fitted with a magnetic stirrer bar, poly(caprolactone) with a M_n = 2,000 g·mol^{-1} (PCL_{2k}) (1 g, 5 × 10^{-4} mol) and DBU (3.73 μL, 6.9 × 10^{-6} mol) were heated to 100 °C under a flow N_2 for 20min to aid the reduction of water within the system. The molten mixture was cooled to 80 °C before the addition of H_{12}MDI (402 μL, 1.64 ×10^{-3} mol). The reaction mixture was allowed to stir under N_2 for 40min to allow for prepolymer formation before the addition of a solution of C_{3u} extender (185 mg, 1.14 × 10^{-3} mol) dissolved in 150 μL of DMSO. The polymerisation was allowed to proceed for 2h before being removed from the heat to retard further reaction. The molecular weight was analysed *via* GPC and any unreacted isocyanate, *via* IR spectroscopy, was quenched by washing the TPEU in 50 mL of methanol before being dried *in vacuo*. ^{1}H NMR (400 MHz, DMSO-d_6) δ 6.04 – 5.67 (m, 2H), 4.11 – 3.80 (m, 19H), 3.53 – 2.89 (m, 23H), 2.27 (m, 14H), 1.91 – 0.69 (m, 79H). M_n = 100.9 kg·mol^{-1}, $Đ_M$ = 2.10 (RI detection, DMF GPC).

7.7 References

1. A. P. Dove, R. C. Pratt, B. G. G. Lohmeijer, R. M. Waymouth and J. L. Hedrick, *J. Am. Chem. Soc.*, 2005, 127, 13798-13799.
2. C. X. F. Lam, M. M. Savalani, S.-H. Teoh and D. W. Hutmacher, *Biomed. Mater.*, 2008, 3, 1-15.
3. J. Xu, Z.-L. Liu and R.-X. Zhuo, *J. Appl. Polym. Sci.*, 2006, 101, 1988-1994.
4. K. Makiguchi, T. Satoh and T. Kakuchi, *Macromolecules*, 2011, 44, 1999-2005.
5. S. Venkataraman, N. Veronica, Z. X. Voo, J. L. Hedrick and Y. Y. Yang, *Polym. Chem.*, 2013, 4, 2945-2948.
6. J. Oble, B. Riflade, A. Noel, M. Malacria, S. Thorimbert, B. Hasenknopf and E. Lacote, *Org. Lett.*, 2011, 13, 5990-5993.
7. M. Hudlicky, *Reductions in Organic Chemistry*, Ellis Horwood Limited, 1984.